Polar phytoplankton dynamics in relation to virus and zooplankton predators

Tristan Euan George Biggs

Cover page rear

Polar phytoplankton dynamics in relation to virus and zooplankton predators

Tristan Euan George Biggs

Polar phytoplankton dynamics in relation to virus and zooplankton predators

PhD thesis, Universiteit van Amsterdam, IBED, The Netherlands

Polar phytoplankton dynamics in relation to virus and zooplankton predators

ACADEMISCH PROEFSCHRIFT

ter verkrijging van de graad van doctor

aan de Universiteit van Amsterdam

op gezag van de Rector Magnificus

prof. dr. ir. K.I.J. Maex

ten overstaan van een door het College voor Promoties ingestelde commissie,

in het openbaar te verdedigen in de Agnietenkapel

op dinsdag 8 december 2020, te 12 uur

door

Tristan Euan George Biggs

geboren te Leicester

This thesis is dedicated to my wife Maram Ghadban, my daughters Mireia and Marella, and my mum Linda Biggs.

Contents

Chapter 1

General Introduction

Due to their small size but numerical dominance, marine microbes contribute > 70% to total living biomass in the ocean (Bar-On et al. 2018) and the unicellular photosynthetic organisms (phytoplankton) fraction is responsible for roughly half of global net primary production (Field et al. 1998). Phytoplankton serve as the foundation of most ocean food webs, fuelling the flow of energy and matter to higher trophic levels, as well as carbon sequestration to the deep ocean (i.e. process of capturing and storing atmospheric carbon dioxide). Primary production is controlled by 'bottom-up' factors such as light, nutrients and temperature, and the accumulation of phytoplankton biomass (standing stock) is regulated by so called 'top-down' predation factors (traditionally zooplankton grazing). Not only the sum, but also the timing of primary (and secondary) production determines food availability for consumers and influences the ecosystem carrying capacity. As an alternative loss factor to zooplankton grazing, viral lysis of phytoplankton has been shown quantitatively (mortality rates) and qualitatively (selective infection) important in temperate and (sub)tropical oceans and coastal seas (Wilson et al. 2002; Brussaard 2004; Baudoux et al. 2007; Brussaard and Martínez 2008; Mojica 2015). The ecological importance of viral lysis is, however, highly understudied in cold polar waters. Even the environmental variables underlying phytoplankton dynamics are still not fully understood. An improved insight into the regulatory factors of polar phytoplankton production, as well as the most dominant type of mortality factor, is highly relevant as these processes affect trophic transfer efficiency and consequently biogoechemical cycling very differently. The low temperature polar waters are particularly sensitive to global warming (Montes-Hugo et al. 2009; Stammerjohn et al. 2012; Constable et al. 2014) and as such it is utterly warranted to obtain a better understanding of the functioning of the lower food web to predict more accurately how the oceans will respond to environmental change (Dinasquet et al. 2018).

This introductory chapter provides a brief overview of the key players of the polar marine environment and their ecological roles, while providing knowledge gaps that underlie the research questions of the current thesis.

1

1.1 Phytoplankton

Phytoplankton rely on light for photosynthesis and as such seasonality in phytoplankton production is observed in temperate and especially high latitude regions (Ma et al. 2014). Environmental drivers of net primary production such as light, nutrients and temperature are, in turn, influenced by oceanic and atmospheric processes such as cloud cover, wind speed, vertical stratification strength and, in polar seas, also ice (Boyd et al. 2014). In polar oceans, phytoplankton inevitably experience extremely low to zero light availability during winter and accumulation of phytoplankton biomass only begins as light returns (Venables and Moore 2010; Venables et al. 2013). The mixed layer is still deep and average light levels are low (~ 1 µmol quanta m^{-2} s^{-1}; Venables et al. 2013). As day length rises after winter (and wind speeds decline), the annual onset of vertical stratification resulting from seasonal warming and fresh water input (ice melt), further improves light conditions and generally initiates the (highly productive) phytoplankton Spring bloom (Thomalla et al. 2011; Venables et al. 2013; Llort et al. 2015; Eveleth et al. 2017). Phytoplankton can experience low light intensities again during high biomass phytoplankton blooms as a result of self-shading (Vernet et al. 2008). In response to seasonal and weather-induced light variability, phytoplankton have to adapt their photosynthetic efficiency and light saturation point (MacIntyre et al. 2002), a process of photoacclimation. Overall, the phytoplankton community response to light could be due to physiological changes within cells and populations, a shift in community or size composition (Timmermans et al. 2001; Moore et al. 2006; Arrigo et al. 2010; Alderkamp et al. 2012). Still, the mechanisms that regulate peak phytoplankton biomass and seasonal carbon flow, especially after periods of low light and in the more productive coastal regions of the Southern Ocean, are not fully understood and require further investigation. As it is the sum of production and losses over an annual cycle that determines the ecosystem carrying capacity (Sarker and Wiltshire 2017), studies that span entire productive seasons have the potential to vastly improve our understanding of phytoplankton dynamics.

Polar phytoplankton are strongly linked to the dynamics of sea ice (Garibotti et al. 2003; Arrigo et al. 2008b; Leu et al. 2015; Moreau et al. 2015) as it not only influences light availability but also acts as a vector for seeding phytoplankton cells into the water column (Tison et al. 2010). Rapid warming in recent decades has increased ice melt (a faster retreat and melting of glaciers and ice sheets) and freshwater input as well as a decline in sea ice (Cook 2005; Vaughan 2006; Stammerjohn et al. 2012; Depoorter et al. 2013; Rignot et al. 2013) that has resulted in an earlier spring retreat and a later autumn advance, increasing the ice-free period (with high light availability) and consequently the length of the productive season (Arrigo et al. 2008b; Stammerjohn et al. 2008). Furthermore, the period of solar heating is extended (due to less sea ice) and leads to an increase in polar surface water temperatures (Meredith and King 2005; Perovich et al. 2007). Temperature imposes a fundamental control on phytoplankton metabolic processes (Raven and Geider 1988; Moisan et al. 2002) and can impose biogeographic boundaries for major taxonomic groups e.g. the absence of cyanobacteria from polar waters could be explained by a higher optimum temperature for growth than other groups of algae (Thomas 2013).

The oceans serve as one of the largest natural CO_2 reservoirs on earth and especially important are the cold polar oceans that take up relatively large amounts of anthropogenic CO_2 (Bates et al. 2006; Arrigo et al. 2008a). Carbon dioxide generated by anthropogenic activities is one of the main drivers of global warming (Lam et al. 2012) and the global ocean heat content has been rising since the early 90s (Cheng et al. 2017, 2018), with the most rapid warming observed in polar regions (Vaughan et al. 2003; Screen and Simmonds 2010; Bromwich et al. 2013). Ocean climate models predict that warming of ocean surface waters (due to global warming) combined with increased fresh water input at high latitudes (due to increased precipitation and ice melt) will strengthen vertical stratification (Sarmiento et al. 2004; Toggweiler and Russell 2008). In the Arctic this may reduce the input of dissolved inorganic nutrients from the deep to the surface ocean, increasing the share of small-sized phytoplankton (Li et al. 2009; Tremblay and Gagnon 2009; Ardyna

et al. 2011). Predictions for coastal waters of the Antarctic Peninsula are that the phytoplankton community will also change with fewer micro-sized diatoms in favour of smaller-sized cells, impacting overall phytoplankton abundance, size class and taxonomic structure (Garibotti et al. 2005; Hilligsøe et al. 2011; Doney et al. 2012; Mendes et al. 2017; Rozema et al. 2017). These changes will alter the structure and functioning of the polar marine pelagic food webs, carbon cycling and ultimately carbon sequestration to the deep ocean (biological pump) (Hoegh-Guldberg and Bruno 2010). Cell size is an important functional trait that influences almost every aspect of phytoplankton biology such as physiological rates (growth, photosynthesis, respiration) and ecological function such as grazing (Finkel et al. 2010; Key et al. 2010; Marañón 2015). Smaller cells have a larger surface to volume ratio which typically gives them a competitive advantage in oligotrophic waters with relatively low nutrient availability, whilst larger cells dominate under eutrophic conditions where nutrient concentrations are higher (Marañón et al. 2001; Hirata et al. 2011). The smaller size classes are represented by cyanobacteria, prasinophytes, prymnesiophytes and cryptophytes whilst the largest cells are mostly composed of diatoms (Bacillariophyceae) and dinoflagellates (Klaveness 1988; Not et al. 2012). The size scaling exponent of metabolism (or chlorophyll content per cell) suggests that larger cells have a relatively lower Chl-*a* content than smaller cells (Álvarez et al. 2017), related to the potential for intracellular self-shading (the 'package effect'; Finkel et al. 2004). Biomass estimates based on Chl-*a* concentrations could thus, underestimate carbon content and the nutritional value of production. The size structure and elemental composition of phytoplankton can affect both the quality and quantity of carbon and nutrients available to higher trophic levels and are key factors determining food web structure besides the efficiency of carbon sequestration (Arrigo 2005; Finkel et al. 2010; Marañón 2015).
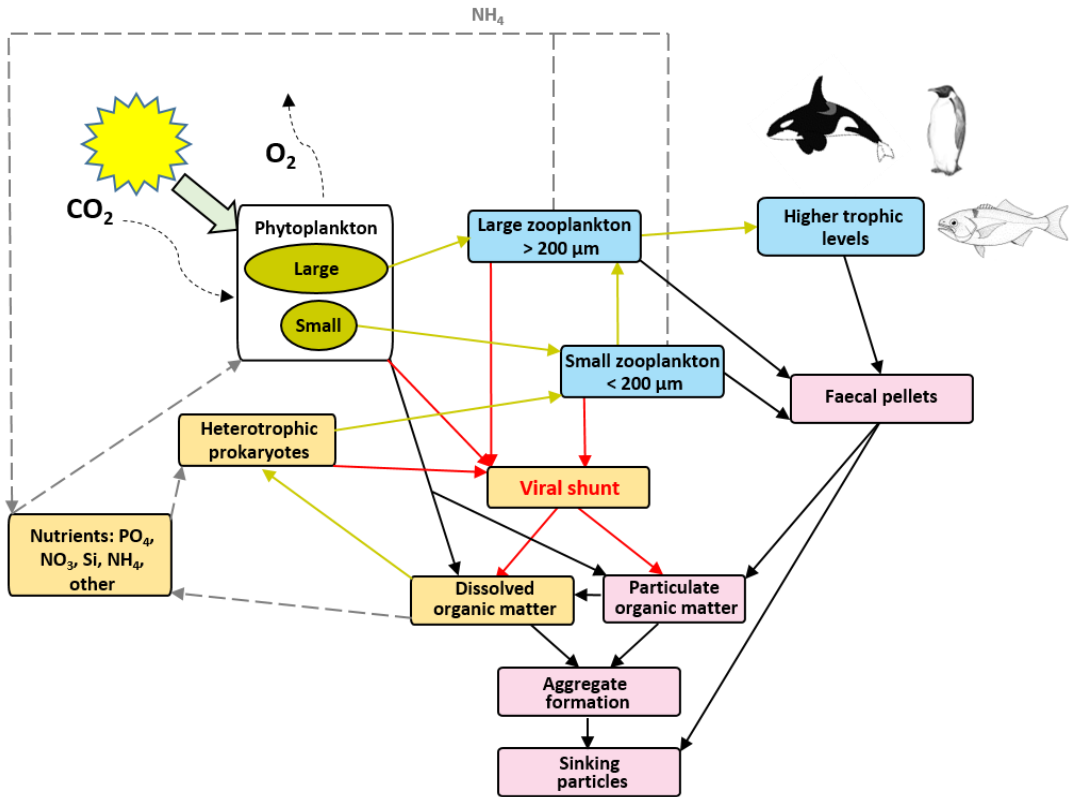
Fig. 1. Simplified schematic representation of the polar pelagic food web. The olive arrows represent the flow of photosynthetically fixed carbon (PFC) to higher trophic levels; black arrows represent the 'traditional' flow of PFC to dead (particulate and dissolved) organic matter pools; dashed grey arrows represent flows of inorganic nutrients; red arrows represent the flow of PFC related to the viral shunt. Blue boxes represent grazers, yellow the microbial loop and pink the sedimentation aspect of the biological carbon pump. CO_2 stands for carbon dioxide, PO_4, NO_3, Si, NH_4 and other, for dissolved inorganic phosphate, nitrate, silicate, ammonium and other nutrients such as dissolved iron. For clarity, organic nutrient uptake, respiration, grazing on aggregates, mixotrophy and allochthonous inputs are excluded from this diagram. Antarctic Butterfish drawing by Dr Tony Ayling – Guide to the Sea Fishes of New Zealand, CC BY-SA 1.0, https://commons.wikimedia.org/w/index.php?curid=934897.

1.2 Zooplankton

1.2.1 Large zooplankton

In the marine food web, phytoplankton are the primary source of essential fatty acids that are deemed critical for the health and stability of marine systems (Parrish 2013). Large zooplankton (>200 µm), such as herbivorous copepods, are an important

1

trophic link in polar marine pelagic ecosystems as they efficiently transfer photosynthetically fixed carbon (including the essential fatty acids) and nutrients from larger-sized phytoplankton (> ~ 10 µm) to higher trophic predators (Fig. 1) (Voronina 1998; Falk-Petersen et al. 2009). Copepods dominate the mesozooplankton community across most of the Arctic and Southern Ocean (Atkinson et al. 2012) and their life cycles are strongly affected by the distinct seasonality of their phytoplankton prey (Ma et al. 2014). Several species, particularly those in the Calanidae and Eucalanidae families (Baumgartner and Tarrant 2017), undergo ontogenetic vertical migration from shallow to deep water where they spend a large proportion of their life cycle in dormancy (Hagen et al. 1993; Sartoris et al. 2010), a resting stage with reduced metabolism and swimming activity (Maps *et al.*, 2014). During the productive polar summer months, dormancy inducing copepods feed on phytoplankton and accumulate large stores of lipid as wax ester (a fatty acid esterified to a long chain alcohol) that serve as an energy store for use in the long winter period (Lee et al. 2006). Fatty acid profiles of storage lipids indicate the importance of diatoms and dinoflagellates in the zooplankton diet (Graeve et al. 1994; Falk-Petersen et al. 2000; Budge et al. 2006).

Although potential triggers involved in dormancy initiation and termination have been identified, our perception of how they combine to influence behaviour is still limited. Lipid accumulation above a threshold level and utilisation during dormancy could be involved as well as the composition of storage lipids (Rey-Rassat et al. 2002; Johnson et al. 2008; Maps et al. 2012). A highly unsaturated lipid store possesses the ability to shift from a liquid to solid state (at pressures and temperatures typical of overwintering depths), allowing dormant copepods to become neutrally buoyant in cold deep water and conserve energy (Visser and Jónasdóttir 1999; Lee et al. 2006; Pond and Tarling 2011). Following the development of a population over an entire lifecycle is likely to provide a better understanding how these factors influence behaviour. However, the lifespan of these large copepod species can show considerable plasticity (for example 1-5 years for *Calanus hyperboreus* in the Arctic and 1-2 years for *Calanoides acutus* in the Southern Ocean (Marin 1988; Drits et al.

1994; Hagen and Schnack-Schiel 1996; Atkinson et al. 1997; Falk-Petersen et al. 2009), and the mechanisms involved in its regulation remain largely unknown. *Calanoides acutus* is an important species in the Southern Ocean, yet there are very few studies of copepods that repeatedly sample the same population over time scales relevant to their lifespan. Furthermore, the timing and duration of phytoplankton blooms vary spatially and temporally, as a result of physicochemical factors, and could help explain why the timing of descent in dormancy inducing copepods can be so variable between regions and between years (Heath et al. 2004; Johnson et al. 2008; Pepin and Head 2009).

More research is required to better describe the trophic transfer of lipids, particularly in a time of global climate change shown to affect the composition, timing and magnitude of phytoplankton blooms (Smetacek and Nicol 2005; Sommer and Lengfellner 2008; Rozema et al. 2017). As smaller phytoplankton cells are inefficiently grazed by larger zooplankton (Saba et al. 2014), understanding population dynamics is fundamental to predict how copepods might respond to future climate change. Cold polar ecosystems have relatively short food chains and alterations in copepod community dynamics can be expected to rapidly feed through to higher trophic levels (Steinberg et al. 2015), with direct consequences for the lipid pump (Jónasdóttir et al. 2015) as well as the biological carbon pump (Turner 2015). The biological pump in polar regions plays a crucial role in long term climate regulation (Ducklow et al. 2001; DeVries et al. 2012) and the larger-sized zooplankton faecal pellets produced rapidly sink (especially when ballasted with biogenic silica from diatom prey; Voss 1991) to the deep ocean compared to those produced by microzooplankton (Liszka et al. 2019).

1.2.2 Small zooplankton

Although larger-sized diatoms often dominate polar phytoplankton biomass (due to their larger cell size; von Quillfeldt 2000; Ducklow et al. 2012), the nano- (>3 µm) and pico-sized (≤ 3 µm) phytoplankton fraction is often overlooked (Leblanc et al. 2018). These smaller-sized phytoplankton are increasingly being recognised as

important contributors, accounting for as much as 20 to 90% of primary production in Arctic and Antarctic waters (Ducklow et al. 2013; Metfies et al. 2016; Sadanandan Bhavya et al. 2018). Pelagic ecosystems are highly size-structured (Sommer et al. 2018) and small phytoplankton are more efficiently grazed by smaller zooplankton (<200 µm) than by meso- and macro-sized copepods (Stibor et al. 2019). Microzooplankton and protozoans account for the majority of primary production consumed in much of the global ocean (Calbet and Landry 2004; Atkinson et al. 2012; Schmoker et al. 2013), however, there are relatively few microzooplankton grazing rate studies in polar (compared to lower latitude) regions and none that span complete productive seasons. Feeding on small-sized prey, and producing smaller faecal pellets, microzooplankton contribute less to the process of carbon sequestration (biological pump) compared to larger zooplankton (Fig. 1; Turner 2015; Liszka et al. 2019). Although sedimentation rates may be relatively low, the generation times of microzooplankton (Finkel et al. 2010) are much faster and closer to their phytoplankton prey (Banse 1982; Strom and Morello 1998). Slower sedimentation of smaller faecal pellets promotes the rapid recycling of organic matter by the microbial loop (Pomeroy et al. 2007). Global warming combined with a greater input of freshwater (from ice melt) may increase the importance of microzooplankton grazing as a result of a greater contribution of small algal prey (Moline and Prezelin 1996; Montes-Hugo et al. 2009).

1.3 Viruses

Viruses are the most abundant entities in marine ecosystems (Breitbart 2012) and have been found to infect all major phytoplankton taxonomic groups (Brussaard et al. 2004; Nagasaki 2008; Nagasaki et al. 2009; Martínez Martínez et al. 2015). Once viral infection has been established, the lytic cycle results in immediate virus replication followed by host cell lysis (mortality) and the release of progeny, as well as the content of the host cell into the surrounding water. Through host specificity and the ultimate action of host cell lysis, lytic viruses have a regulatory influence on phytoplankton population dynamics, species succession and community

composition (Brussaard et al. 2008b; Nagasaki 2008; Weitz and Wilhelm 2012). Not all viruses undergo lytic replication, latent viruses insert their genetic material into the hosts genome and replicate along with the host. Induction of the lytic cycle triggers excision of the viral genome followed by host cell lysis. Although lysogeny is likely to exist in eukaryotic phytoplankton, lysogenic hosts identified are typically prokaryotes (bacteria and archaea).

No detailed studies on polar phytoplankton virus-host systems have yet been reported in the literature, especially in relation to relevant environmental variables. Changes in environmental conditions may directly impact virus infectivity, e.g. temperature or light in combination with nutrient stress (Baudoux and Brussaard 2005; Tomaru et al. 2005; Maat et al. 2016; Horas et al. 2018 and references within). As obligate parasites, however, viruses are completely reliant on host cell machinery for replication. Studies have shown that phytoplankton virus production is shaped by temperature, nutrients and light availability (Baudoux and Brussaard 2005; Maat 2016; Maat and Brussaard 2016; Demory et al. 2017; Gann et al. 2020), all key factors for phytoplankton growth (see also review by Mojica and Brussaard 2014). Considering sea surface temperatures are expected to (further) increase during the next century (by $1 - 3$ °C; Collins et al. 2013), it seems opportune to try and isolate new polar phytoplankton virus-host model systems and examine the effect of temperature on virus-host interactions.

Viral lysis is recognized as a significant loss factor of phytoplankton cells (Brussaard and Martínez 2008) and there are reports of specific viral lysis rates being considerably larger than losses due to grazing (Baudoux et al. 2007, 2008; Mojica et al. 2016). The so called 'viral shunt' (Wilhelm and Suttle 1999) represents the transfer of particulate organic matter to the dissolved organic phase through viral induced mortality of host cells. It consequently reduces food availability for herbivorous zooplankton and enhances heterotrophic recycling of released organic carbon and nutrients and may increase community respiration due to bacterial activity, directly influencing biogeochemical cycling and food web structure (Brussaard et al. 2008; Weitz and Wilhelm 2012). Whilst grazing channels organic

1

carbon and nutrients to higher trophic levels, and facilitates sedimentation of zooplankton faecal pellets (containing the remains of their phytoplankton prey to be transfered to the deep ocean), lysed cellular material fuels the microbial loop and is largely recycled in the ocean surface layer (Brussaard et al. 2005; Suttle 2007). Temporal differences in the share of viral lysis, in comparison to grazing, could impact food availability for grazers and therefore alter food web dynamics. Our understanding of the temporal importance and share of viral lysis over seasonal time scales is, however, limited and no temporal studies have thus far been performed in polar waters. The few geographic studies on virus mortality rates of Antarctic phytoplankton are not representative of the more productive coastal waters with strong seasonal variation in primary production (Brussaard et al. 2008a, 2013; Evans and Brussaard 2012). Quantitative estimates of viral lysis, and subsequent carbon flux, are critically needed to provide 'baseline' estimates in these globally important ecosystems. A more complete understanding of top-down control is essential for carbon cycling models that aim to incorporate phytoplankton standing stocks and production rates, as well as the fate of fixed carbon.

Outline of thesis

The overall aim of this thesis is to investigate polar phytoplankton dynamics in relation to viruses and zooplankton predators. As such it is important to assess the environmental drivers of phytoplankton communities and how these factors affect virus-host interactions as well as grazers. Seasonal data sets are essential to the understanding of carbon and nutrient flow as it is the sum of seasonal variation in phytoplankton growth (and standing stock) that serves as the foundation for productive ecosystems.

This thesis specifically aims to:

(1) Investigate the environmental factors responsible for structuring the seasonal dynamics of polar phytoplankton communities

(2) Determine specific phytoplankton mortality rates due to viral lysis and grazing and how inter-annual differences relate to environmental variables and seasonal mass balance

(3) Examine how changing environmental factors, such as light and temperature, affect natural phytoplankton population dynamics and more specifically polar virus-host interactions

(4) Study how phytoplankton dynamics influence lipid accumulation and dormancy behaviour of key copepod grazers.

In **Chapter 2,** we investigated the relative importance of environmental drivers in the cold productive coastal waters of the Western Antarctic Peninsula (WAP). Phytoplankton data obtained from the Rothera Time Series (RaTS) site (Northern Marguerite Bay) was collected over two consecutive productive seasons. Multivariate analysis of the phytoplankton community, including the chemical and physical data, identified ice type, temperature and light as key factors driving the distribution and abundance of key phytoplankton taxa and size classes. Combining methods for this type of study was important, i.e., flow cytometry, pigment analysis and size fractionation, as it allowed a better discrimination of phytoplankton groups and improve the variance explained by multivariate analysis.

In **Chapter 3**, we examined the temporal importance and share of viral lysis and grazing for phytoplankton groups of varied taxonomy and size over a full productive season. Viral lysis was responsible for roughly half of total phytoplankton losses and, in combination with grazing, explained the temporal dynamics of phytoplankton standing stock. Viral lysis appears to be an essential loss factor at all times and critically important for obtaining a complete seasonal mass balance of phytoplankton. Variation in the susceptibility to viral lysis, by different taxonomic groups and size classes is discussed and the necessity of including viral lysis for a more accurate prediction of climate change induced shifts in trophic transfer efficiency.

In **Chapter 4**, we investigated inter-annual variation of apparent growth, grazing, and viral lysis rates of phytoplankton. We compared data from a second productive season (S2) to that in chapter 3 (S1), to determine if growth, as well as the share of viral lysis and grazing, differs between productive seasons and how this is related to environment conditions. It is vital to understand if variation of environmental factors leads to changes in the importance of losses as this directly influences biogeochemical cycles. Whilst temperature was linked to differences between seasons, a shift in the share of mortality factors was observed in both S1 and S2, between phases of phytoplankton accumulation and decline.

In **Chapter 5**, we study the impact of light intensity on the natural phytoplankton community using growth bioassays with 3 ecologically relevant light levels as treatment variables. The results show that the light exposure prior to the experiments largely regulates community dynamics. The low light levels used in this study could represent an important boundary concentration where phytoplankton blooms either develop or decline. The combination of flow cytometry, size fractionation and pigment based taxonomic analysis provided enhanced insight into growth and light acclimation strategies of the different phytoplankton populations identified.

In **Chapter 6**, we describe the characterization of novel polar phytoplankton viruses and explore how temperature influences Artic phytoplankton host-virus interactions. No polar phytoplankton-virus model system yet existed in culture, despite the need for controlled experimental studies examining the impact of changing environmental conditions on virus proliferation. Differences in the response to temperature of the various virus and host strains assessed, implies that polar phytoplankton and virus community structure will be strongly influenced by temperature, over short term seasonal cycles as well as longer time periods relevant to global warming.

In **Chapter 7**, we explore potential mechanisms that may influence the dormancy behaviour of *Calanoides acutus*, a major contributor to zooplankton biomass in the Southern Ocean. So far few studies have repeatedly sampled polar copepods throughout a summer-winter-summer cycle, a time period relevant to their (currently debated) lifespan. Novel plasticity in dormancy behaviour is described and linked to

phytoplankton dynamics, predator pressure and lipid composition that combine to ultimately determine their lifecycle and lifespan. The flexibility of copepods to modulate their life-cycle strategy in response to bottom-up and top-down conditions enables individuals to optimise their probability of reproductive success in the very variable environment prevalent in the Southern Ocean.

In **Chapter 8,** the results presented in this thesis are discussed in relation to what is known; how they contribute to a greater understanding of polar food web dynamics and how they can be used for predictions of ecological processes under altered environmental states.

References

Alderkamp AC, Kulk G, Buma AGJ, et al (2012) The effect of iron limitation on the photophysiology of *Phaeocystis antarctica* (Prymnesiophyceae) and *Fragilariopsis cylindrus* (Bacillariophyceae) under dynamic irradiance. J Phycol 48:45–59. doi: 10.1111/j.1529-8817.2011.01098.x

Álvarez E, Nogueira E, López-Urrutia Á (2017) In vivo single-cell fluorescence and size scaling of phytoplankton chlorophyll content. Appl Environ Microbiol 83:1–16. doi: 10.1128/aem.03317-16

Ardyna M, Gosselin M, Michel C, et al (2011) Environmental forcing of phytoplankton community structure and function in the Canadian high Arctic: Contrasting oligotrophic and eutrophic regions. Mar Ecol Prog Ser 442:37–57. doi: 10.3354/meps09378

Arrigo KR (2005) Marine microorgansisms and global nutrient cycles. Nature 437:349–355. doi: 10.1038/nature0415

Arrigo KR, Mills MM, Kropuenske LR, et al (2010) Photophysiology in two major southern ocean phytoplankton taxa: Photosynthesis and growth of *Phaeocystis antarctica* and *Fragilariopsis cylindrus* under different irradiance levels. Integr Comp Biol 50:950–966. doi: 10.1093/icb/icq021

Arrigo KR, van Dijken G, Long M (2008a) Coastal Southern Ocean: A strong anthropogenic CO_2 sink. Geophys Res Lett 35:L21602. doi: 10.1029/2008GL035624

Arrigo KR, van Dijken G, Pabi S (2008b) Impact of a shrinking Arctic ice cover on marine primary production. Geophys Res Lett 35:1–6. doi: 10.1029/2008GL035028

Atkinson A, Schnack-Schiel S, Ward P, Marin V (1997) Regional differences in the life cycle of *Calanoides acutus* (Copepoda: Calanoida) within the Atlantic sector of the Southern Ocean. Mar Ecol Prog Ser 150:99–111. doi: 10.3354/meps150099

Atkinson A, Ward P, Hunt BP V., et al (2012) An overview of Southern Ocean zooplankton data: Abundance, biomass, feeding and functional relationships. CCAMLR Sci 19:171–218

Banse K (1982) Cell volumes, maximal growth rates of unicellular algae and ciliates, and the role of ciliates in the marine pelagial,. Limnol Oceanogr 27:1059–1071. doi: 10.4319/lo.1982.27.6.1059

Bar-On YM, Phillips R, Milo R (2018) The biomass distribution on Earth. Proc Natl Acad Sci U S A 115:6506–6511. doi: 10.1073/pnas.1711842115

Bates NR, Moran SB, Hansell DA, Mathis JT (2006) An increasing CO_2 sink in the Arctic Ocean due to sea-ice loss. Geophys Res Lett 33:1–7. doi: 10.1029/2006GL027028

Baudoux A-C, Brussaard CPD (2005) Characterization of different viruses infecting the marine harmful algal bloom species *Phaeocystis globosa*. Virology 341:80–90. doi: 10.1016/j.virol.2005.07.002

Baudoux A-C, Veldhuis MJW, Noordeloos AAM, et al (2008) Estimates of virus- vs. grazing induced mortality of picophytoplankton in the North Sea during summer. Aquat Microb Ecol 52:69–82. doi: 10.3354/ame01207

Baudoux A-C, Veldhuis MJW, Witte HJ, Brussaard CPD (2007) Viruses as mortality agents of picophytoplankton in the deep chlorophyll maximum layer during IRONAGES III. Limnol Oceanogr 52:2519–2529. doi: 10.4319/lo.2007.52.6.2519

Baumgartner MF, Tarrant AM (2017) The physiology and ecology of diapause in marine copepods. Ann Rev Mar Sci 9:387–411. doi: 10.1146/annurev-marine-010816-060505

Boyd PW, Sundby S, Pörtner H-O (2014) Net Primary Production in the Ocean. In: Field CB, Barros VR, Dokken DJ, et al (eds) In: Climate Change 2014: Impacts, Adaptation, and Vulnerability. Part A: Global and Sectoral Aspects. Contribution of Working Group II to the Fifth Assessment Report of the Intergovernmental Panel on Climate Change. Cambridge University Press, United Kingdom and New York, NY, USA, Cambridge, pp 133–136

Breitbart M (2012) Marine viruses: Truth or dare. Ann Rev Mar Sci 4:425–448. doi: 10.1146/annurev-marine-120709-142805

Bromwich DH, Nicolas JP, Monaghan AJ, et al (2013) Central West Antarctica among the most rapidly warming regions on Earth. Nat Geosci 6:139–145. doi: 10.1038/ngeo1671

Brussaard CPD (2004) Viral control of phytoplankton populations-A review. J Eukaryot Microbiol 51:125–138. doi: 10.1111/j.1550-7408.2004.tb00537.x

Brussaard CPD, Mari X, Bleijswijk JDL Van, Veldhuis MJW (2005) A mesocosm study of *Phaeocystis globosa* (Prymnesiophyceae) population dynamics II. Significance for the microbial community. Harmful Algae 4:875–893. doi: 10.1016/j.hal.2004.12.012

Brussaard CPD, Martínez J (2008) Algal bloom viruses. Plant Viruses 2:1–13

Brussaard CPD, Noordeloos AAM, Witte H, et al (2013) Arctic microbial community dynamics influenced by elevated CO_2 levels. Biogeosciences 10:719–731. doi: 10.5194/bg-10-719-2013

Brussaard CPD, Short SM, Frederickson CM, Suttle CA (2004) Isolation and Phylogenetic Analysis of Novel Viruses Infecting the Phytoplankton. Society 70:3700–3705. doi: 10.1128/AEM.70.6.3700

Brussaard CPD, Timmermans KR, Uitz J, Veldhuis MJW (2008a) Virioplankton dynamics and virally induced phytoplankton lysis versus microzooplankton grazing southeast of the Kerguelen (Southern Ocean). Deep Sea Res Part II Top Stud Oceanogr 55:752–765. doi: 10.1016/j.dsr2.2007.12.034

Brussaard CPD, Wilhelm SW, Thingstad F, et al (2008b) Global-scale processes with a nanoscale drive: The role of marine viruses. ISME J 2:575–578. doi: 10.1038/ismej.2008.31

Budge SM, Iverson SJ, Koopman HN (2006) Studying trophic ecology in marine ecosystems using fatty acids: A primer on analysis and interpretation. Mar Mammal Sci 22:759–801. doi: 10.1111/j.1748-7692.2006.00079.x

Calbet A, Landry MR (2004) Phytoplankton growth, microzooplankton grazing, and carbon cycling in marine systems. Limnol Oceanogr 49:51–57. doi: 10.4319/lo.2004.49.1.0051

Cheng L, Trenberth KE, Fasullo J, et al (2017) Improved estimates of ocean heat content from 1960 to 2015. Sci Adv 3:e1601545. doi: 10.1126/sciadv.1601545

Cheng L, Wang G, Abraham J, Huang G (2018) Decadal Ocean Heat Redistribution Since the Late 1990s and Its Association with Key Climate Modes. Climate 6:91. doi: 10.3390/cli6040091

Collins M, Knutti R, Arblaster J, et al (2013) Long-term climate change: Projections, commitments, and irreversibility. Cambridge University Press, United Kingdom and New York, NY, USA,

Constable AJ, Melbourne-Thomas J, Corney SP, et al (2014) Climate change and Southern Ocean ecosystems I: How changes in physical habitats directly affect marine biota. Glob Chang Biol 20:3004–3025. doi: 10.1111/gcb.12623

Cook AJ (2005) Retreating Glacier Fronts on the Antarctic Peninsula over the Past Half-Century Retreating Glacier Fronts on the Antarctic Peninsula over the Past Half-Century. 541:. doi: 10.1126/science.1104235

Demory D, Arsenieff L, Simon N, et al (2017) Temperature is a key factor in *Micromonas*–virus interactions. ISME J 11:601–612. doi: 10.1038/ismej.2016.160

Depoorter MA, Bamber JL, Griggs JA, et al (2013) Calving fluxes and basal melt rates of Antarctic ice shelves. Nature 502:89–92. doi: 10.1038/nature12567

DeVries T, Primeau F, Deutsch C (2012) The sequestration efficiency of the biological pump. Geophys Res Lett 39:L13601. doi: 10.1029/2012GL051963

Dinasquet J, Ortega-Retuerta E, Lovejoy C, Obernosterer I (2018) Editorial: Microbiology of the rapidly changing polar environments. Front Mar Sci 5:. doi: 10.3389/fmars.2018.00154

Doney SC, Ruckelshaus M, Emmett Duffy J, et al (2012) Climate change impacts on marine

ecosystems. Ann Rev Mar Sci 4:11–37. doi: 10.1146/annurev-marine-041911-111611

Drits A V., Pasternak AF, Kosobokova KN (1994) Physiological characteristics of the antarctic copepod *Calanoides acutus* during late summer in the Weddell Sea. Hydrobiologia 292–293:201–207. doi: 10.1007/BF00229942

Ducklow H, Clarke A, Dickhut R, et al (2012) The marine system of the Western Antarctic Peninsula. In: Rogers AD, Johnston NM, Murphy EJ, Clarke A (eds) Antarctic Ecosystems: An Extreme Environment in a Changing World. Blackwell Publishing Ltd., pp 121–159

Ducklow H, Steinberg D, Buesseler K (2001) Upper ocean carbon export and the biological pump. Oceanography 14:50–58. doi: 10.5670/oceanog.2001.06

Ducklow HW, Fraser W, Meredith M, et al (2013) West Antarctic Peninsula: An ice-dependent coastal marine ecosystem in transition. Oceanography 26:190–203. doi: 10.5670/oceanog.2013.62

Evans C, Brussaard CPD (2012) Viral lysis and microzooplankton grazing of phytoplankton throughout the Southern Ocean. Limnol Oceanogr 57:1826–1837. doi: 10.4319/lo.2012.57.6.1826

Eveleth R, Cassar N, Sherrell RM, et al (2017) Ice melt influence on summertime net community production along the Western Antarctic Peninsula. Deep Res Part II Top Stud Oceanogr 139:89–102. doi: 10.1016/j.dsr2.2016.07.016

Falk-Petersen S, Hagen W, Kattner G, et al (2000) Lipids, trophic relationships, and biodiversity in Arctic and Antarctic krill. Can J Fish Aquat Sci 57:178–191. doi: 10.1139/f00-194

Falk-Petersen S, Mayzaud P, Kattner G, Sargent JR (2009) Lipids and life strategy of Arctic *Calanus*. Mar Biol Res 5:18–39. doi: 10.1080/17451000802512267

Field CB, Behrenfeld MJ, Randerson JT, Falkowski P (1998) Primary production of the biosphere: Integrating terrestrial and oceanic components. Science (80-) 281:237–240. doi: 10.1126/science.281.5374.237

Finkel Z V., Beardall J, Flynn KJ, et al (2010) Phytoplankton in a changing world: Cell size and elemental stoichiometry. J Plankton Res 32:119–137. doi: 10.1093/plankt/fbp098

Finkel Z, Irwin A, Schofield O (2004) Resource limitation alters the 3/4 size scaling of metabolic rates in phytoplankton. Mar Ecol Prog Ser 273:269–279. doi: 10.3354/meps273269

Gann ER, Gainer PJ, Reynolds TB, Wilhelm SW (2020) Influence of light on the infection of *Aureococcus anophagefferens* CCMP 1984 by a "giant virus." PLoS One 15:e0226758. doi: 10.1371/journal.pone.0226758

Garibotti I, Vernet M, Ferrario M, et al (2003) Phytoplankton spatial distribution patterns along the western Antarctic Peninsula (Southern Ocean). Mar Ecol Prog Ser 261:21–39. doi: 10.3354/meps261021

Garibotti IA, Vernet MM, Ferrario ME, et al (2005) Annually recurrent phytoplanktonic assemblages during summer in the seasonal ice zone west of the Antarctic Peninsula (Southern Ocean). Deep Res Part I Oceanogr Res Pap 52:1823–1841. doi: 10.1016/j.dsr.2005.05.003

Graeve M, Kattner G, Hagen W (1994) Diet-induced changes in the fatty acid composition of Arctic herbivorous copepods: Experimental evidence of trophic markers. J Exp Mar Bio Ecol 182:97–110. doi: 10.1016/0022-0981(94)90213-5

Hagen W, Kattner G, Graeve M (1993) *Calanoides acutus* and *Calanus propinquus*, Antarctic copepods with different lipid storage modes via wax esters or triacylglycerols. Mar Ecol Prog Ser 97:135–142. doi: 10.3354/meps097135

Hagen W, Schnack-Schiel SB (1996) Seasonal lipid dynamics in dominant Antarctic copepods: Energy for overwintering or reproduction? Deep Res Part I Oceanogr Res Pap 43:139–158. doi: 10.1016/0967-0637(96)00001-5

Heath MR, Boyle PR, Gislason A, et al (2004) Comparative ecology of over-wintering *Calanus finmarchicus* in the northern North Atlantic, and implications for life-cycle patterns. ICES J Mar Sci 61:698–708. doi: 10.1016/j.icesjms.2004.03.013

Hilligsøe KM, Richardson K, Bendtsen J, et al (2011) Linking phytoplankton community size composition with temperature, plankton food web structure and sea–air CO_2 flux. Deep Sea Res Part I Oceanogr Res Pap 58:826–838. doi: 10.1016/j.dsr.2011.06.004

Hirata T, Hardman-Mountford NJ, Brewin RJW, et al (2011) Synoptic relationships between surface Chlorophyll-*a* and diagnostic pigments specific to phytoplankton functional types. Biogeosciences 8:311–327. doi: 10.5194/bg-8-311-2011

Hoegh-Guldberg O, Bruno JF (2010) The impact of climate change on the world's marine ecosystems. Science (80-) 328:1523–1528. doi: 10.1126/science.1189930

Horas EL, Theodosiou L, Becks L (2018) Why are algal viruses not always successful? Viruses 10:19–27. doi: 10.3390/v10090474

Johnson CL, Leising AW, Runge JA, et al (2008) Characteristics of *Calanus finmarchicus* dormancy patterns in the Northwest Atlantic. ICES J Mar Sci 65:339–350. doi: 10.1093/icesjms/fsm171

Jónasdóttir SH, Visser AW, Richardson K, Heath MR (2015) Seasonal copepod lipid pump promotes carbon sequestration in the deep North Atlantic. Proc Natl Acad Sci 112:12122–12126. doi: 10.1073/pnas.1512110112

Key T, McCarthy A, Campbell DA, et al (2010) Cell size trade-offs govern light exploitation strategies in marine phytoplankton. Environ Microbiol 12:95–104. doi: 10.1111/j.1462-2920.2009.02046.x

Klaveness D (1988) Biology and ecology of the Cryptophyceae: status and challenges. Biol Oceanogr 6:257–270. doi: 10.1080/01965581.1988.10749530

Lam MK, Lee KT, Mohamed AR (2012) Current status and challenges on microalgae-based carbon capture. Int J Greenh Gas Control 10:456–469. doi: 10.1016/j.ijggc.2012.07.010

Leblanc K, Quéguiner B, Diaz F, et al (2018) Nanoplanktonic diatoms are globally overlooked but play a role in spring blooms and carbon export. Nat Commun 9:1–12. doi: 10.1038/s41467-018-03376-9

Lee RF, Hagen W, Kattner G (2006) Lipid storage in marine zooplankton. Mar Ecol Prog Ser 307:273–306. doi: 10.3354/Meps307273

Leu E, Mundy CJ, Assmy P, et al (2015) Arctic spring awakening - Steering principles behind the phenology of vernal ice algal blooms. Prog Oceanogr 139:151–170. doi: 10.1016/j.pocean.2015.07.012

Li WKW, McLaughlin FA, Lovejoy C, Carmack EC (2009) Smallest algae thrive as the arctic ocean freshens. Science (80-) 326:539. doi: 10.1126/science.1179798

Liszka CM, Manno C, Stowasser G, et al (2019) Mesozooplankton community composition controls fecal pellet flux and remineralization depth in the Southern Ocean. Front Mar Sci 6:230: doi: 10.3389/fmars.2019.00230

Llort J, Lévy M, Sallée J-B, Tagliabue A (2015) Onset, intensification, and decline of phytoplankton blooms in the Southern Ocean. ICES J Mar Sci J du Cons 72:1971–1984. doi: 10.1093/icesjms/fsv053

Ma S, Tao Z, Yang X, et al (2014) Estimation of marine primary productivity from satellite-derived phytoplankton absorption data. IEEE J Sel Top Appl Earth Obs Remote Sens 7:3084–3092. doi: 10.1109/JSTARS.2014.2298863

Maat DS (2016) Ecophysiological aspects of algal host - virus interactions in a changing ocean. University of Amsterdam

Maat DS, Brussaard CPD (2016) Both phosphorus- and nitrogen limitation constrain viral proliferation in marine phytoplankton. Aquat Microb Ecol 77:87–97. doi: 10.3354/ame01791

Maat DS, de Blok R, Brussaard CPD (2016) Combined phosphorus limitation and light stress prevent viral proliferation in the phytoplankton species *Phaeocystis globosa*, but not in *Micromonas pusilla*. Front Mar Sci. doi: 10.3389/fmars.2016.00160

MacIntyre HL, Kana TM, Anning T, Geider RJ (2002) Photoacclimation of photosynthesis irradiance response curves and photosynthetic pigments in microalgae and cyanobacteria. J Phycol 38:17–38. doi: 10.1046/j.1529-8817.2002.00094.x

Maps F, Record NR, Pershing AJ (2014) A metabolic approach to dormancy in pelagic copepods helps explaining inter- and intra-specific variability in life-history strategies. J Plankton Res 36:18–30. doi: 10.1093/plankt/fbt100

Maps F, Runge JA, Leising A, et al (2012) Modelling the timing and duration of dormancy in populations of *Calanus finmarchicus* from the Northwest Atlantic shelf. J Plankton Res 34:36–54. doi: 10.1093/plankt/fbr088

Marañón E (2015) Cell size as a key determinant of phytoplankton metabolism and community structure. Ann Rev Mar Sci 7:241–64. doi: 10.1146/annurev-marine-010814-015955

Marañón E, Holligan P, Barciela R, et al (2001) Patterns of phytoplankton size structure and productivity in contrasting open-ocean environments. Mar Ecol Prog Ser 216:43–56. doi: 10.3354/meps216043

Marin V (1988) Qualitative models of the life cycles of *Calanoides acutus, Calanus propinquus*, and *Rhincalanus gigas*. Polar Biol 8:439–446. doi: 10.1007/BF00264720

Martínez Martínez J, Boere A, Gilg I, et al (2015) New lipid envelope-containing dsDNA virus isolates

infecting *Micromonas pusilla* reveal a separate phylogenetic group. Aquat Microb Ecol 74:17–28. doi: 10.3354/ame01723

Mendes CRB, Tavano VM, Dotto TS, et al (2017) New insights on the dominance of cryptophytes in Antarctic coastal waters: A case study in Gerlache Strait. Deep Sea Res Part II Top Stud Oceanogr 149:161–170. doi: 10.1016/j.dsr2.2017.02.010

Meredith MP, King JC (2005) Rapid climate change in the ocean west of the Antarctic Peninsula during the second half of the 20th century. Geophys Res Lett 32:1–5. doi: 10.1029/2005GL024042

Metfies K, Von Appen WJ, Kilias E, et al (2016) Biogeography and photosynthetic biomass of arctic marine pico-eukaroytes during summer of the record sea ice minimum 2012. PLoS One 11:1–20. doi: 10.1371/journal.pone.0148512

Moisan JR, Moisan TA, Abbott MR (2002) Modelling the effect of temperature on the maximum growth rates of phytoplankton populations. Ecol Modell 153:197–215. doi: 10.1016/S0304-3800(02)00008-X

Mojica KDA (2015) Viral lysis of marine microbes in relation to vertical stratification. University of Amsterdam

Mojica KDA, Brussaard CPD (2014) Factors affecting virus dynamics and microbial host - virus interactions in marine environments. FEMS Microbiol Ecol 89:495–515. doi: 10.1111/1574-6941.12343

Mojica KDA, Huisman J, Wilhelm SW, Brussaard CPD (2016) Latitudinal variation in virus-induced mortality of phytoplankton across the North Atlantic Ocean. ISME J 10:500–513. doi: 10.1038/ismej.2015.130

Moline M a, Prezelin BB (1996) Long-term monitoring and analyses of physical factors regulating variability in coastal Antarctic phytoplankton composition over seasonal and interannual timescales. Mar Ecol Prog Ser 145:143–160. doi: 10.3354/Meps145143

Montes-Hugo M, Doney SC, Ducklow HW, et al (2009) Recent changes in phytoplankton communities associated with rapid regional climate change along the western Antarctic Peninsula. Science (80-) 323:1470–1473. doi: 10.1126/science.1164533

Moore CM, Suggett DJ, Hickman AE, et al (2006) Phytoplankton photoacclimation and photoadaptation in response to environmental gradients in a shelf sea. Limnol Oceanogr 51:936–949. doi: 10.4319/lo.2006.51.2.0936

Moreau S, Mostajir B, Bélanger S, et al (2015) Climate change enhances primary production in the western Antarctic Peninsula. Glob Chang Biol 21:2191–2205. doi: 10.1111/gcb.12878

Nagasaki K (2008) Dinoflagellates, diatoms, and their viruses. J Microbiol 46:235–243. doi: 10.1007/s12275-008-0098-y

Nagasaki K, Kim J-J, Tomaru Y, et al (2009) Isolation and characterization of a novel virus infecting *Teleaulax amphioxeia* (Cryptophyceae). Plankt Benthos Res 4:122–124. doi: 10.3800/pbr.4.122

Not F, Siano R, Kooistra WHCF, et al (2012) Diversity and ecology of eukaryotic marine phytoplankton. In: Advances in Botanical Research. pp 1–53

Parrish CC (2013) Lipids in Marine Ecosystems. ISRN Oceanogr 2013:1–16. doi: 10.5402/2013/604045

Pepin P, Head EJH (2009) Seasonal and depth-dependent variations in the size and lipid contents of stage 5 copepodites of *Calanus finmarchicus* in the waters of the Newfoundland Shelf and the Labrador Sea. Deep Res Part I Oceanogr Res Pap 56:989–1002. doi: 10.1016/j.dsr.2009.01.005

Perovich DK, Light B, Eicken H, et al (2007) Increasing solar heating of the Arctic Ocean and adjacent seas, 1979-2005: Attribution and role in the ice-albedo feedback. Geophys Res Lett 34:1–5. doi: 10.1029/2007GL031480

Pomeroy L, leB. Williams P, Azam F, Hobbie J (2007) The Microbial Loop. Oceanography 20:28–33. doi: 10.5670/oceanog.2007.45

Pond DW, Tarling G a. (2011) Phase transitions of wax esters adjust buoyancy in diapausing *Calanoides acutus*. Limnol Oceanogr 56:1310–1318. doi: 10.4319/lo.2011.56.4.1310

Raven JA, Geider RJ (1988) Temperature and algal growth. New Phytol 110:441–461. doi: 10.1111/j.1469-8137.1988.tb00282.x

Rey-Rassat C, Irigoien X, Harris R, Carlotti F (2002) Energetic cost of gonad development in *Calanus finmarchicus* and *C. helgolandicus*. Mar Ecol Prog Ser 238:301–306. doi: 10.3354/meps238301

Rignot E, Jacobs S, Mouginot J, Scheuchl B (2013) Ice-shelf melting around Antarctica. Science (80-) 341:266–70. doi: 10.1126/science.1235798

Rozema PD, Venables HJ, van de Poll WH, et al (2017) Interannual variability in phytoplankton biomass and species composition in northern Marguerite Bay (West Antarctic Peninsula) is governed by both winter sea ice cover and summer stratification. Limnol Oceanogr 62:235–252. doi: 10.1002/lno.10391

Saba GK, Fraser WR, Saba VS, et al (2014) Winter and spring controls on the summer food web of the coastal West Antarctic Peninsula. Nat Commun 5:4318. doi: 10.1038/ncomms5318

Sadanandan Bhavya P, Han Lee J, Won Lee H, et al (2018) First in situ estimations of small phytoplankton carbon and nitrogen uptake rates in the Kara, Laptev, and East Siberian seas. Biogeosciences 15:5503–5517. doi: 10.5194/bg-15-5503-2018

Sarker S, Wiltshire KH (2017) Phytoplankton carrying capacity: Is this a viable concept for coastal seas? Ocean Coast Manag 148:1–8. doi: 10.1016/j.ocecoaman.2017.07.015

Sarmiento JL, Slater R, Barber R, et al (2004) Response of ocean ecosystems to climate warming. Global Biogeochem Cycles 18:. doi: 10.1029/2003GB002134

Sartoris FJ, Thomas DN, Cornils A, Schnack-Schiel SB (2010) Buoyancy and diapause in Antarctic copepods: The role of ammonium accumulation. Limnol Oceanogr 55:1860–1864. doi: 10.4319/lo.2010.55.5.1860

Schmoker C, Hernández-León S, Calbet A (2013) Microzooplankton grazing in the oceans: Impacts, data variability, knowledge gaps and future directions. J Plankton Res 35:691–706. doi: 10.1093/plankt/fbt023

Screen JA, Simmonds I (2010) The central role of diminishing sea ice in recent Arctic temperature amplification. Nature 464:1334–1337. doi: 10.1038/nature09051

Smetacek V, Nicol S (2005) Polar ocean ecosystems in a changing world. Nature 437:362–368. doi: 10.1038/nature04161

Sommer U, Charalampous E, Scotti M, Moustaka-Gouni M (2018) Big fish eat small fish: Implications for food chain length? Community Ecol 19:107–115. doi: 10.1556/168.2018.19.2.2

Sommer U, Lengfellner K (2008) Climate change and the timing, magnitude, and composition of the phytoplankton spring bloom. Glob Chang Biol 14:1199–1208. doi: 10.1111/j.1365-2486.2008.01571.x

Stammerjohn S, Massom R, Rind D, Martinson D (2012) Regions of rapid sea ice change: An inter-hemispheric seasonal comparison. Geophys Res Lett 39:1–8. doi: 10.1029/2012GL050874

Stammerjohn SE, Martinson DG, Smith RC, et al (2008) Trends in Antarctic annual sea ice retreat and advance and their relation to El Niño–Southern Oscillation and Southern Annular Mode variability. J Geophys Res 113:C03S90. doi: 10.1029/2007JC004269

Steinberg DK, Ruck KE, Gleiber MR, et al (2015) Long-term (1993-2013) changes in macrozooplankton off the Western Antarctic Peninsula. Deep Res Part I Oceanogr Res Pap 101:54–70. doi: 10.1016/j.dsr.2015.02.009

Stibor H, Stockenreiter M, Nejstgaard JC, et al (2019) Trophic switches in pelagic systems. Curr Opin Syst Biol 13:108–114. doi: 10.1016/j.coisb.2018.11.006

Strom SL, Morello TA (1998) Comparative growth rates and yields of ciliates and heterotrophic dinoflagellates. J Plankton Res 20:571–584. doi: 10.1093/plankt/20.3.571

Suttle CA (2007) Marine viruses — major players in the global ecosystem. Nat Rev Microbiol 5:801–812. doi: 10.1038/nrmicro1750

Thomalla SJ, Fauchereau N, Swart S, Monteiro PMS (2011) Regional scale characteristics of the seasonal cycle of chlorophyll in the Southern Ocean. Biogeosciences 8:2849–2866. doi: 10.5194/bg-8-2849-2011

Thomas MK (2013) The effect of temperature on the ecology, evolution and biogeography of phytoplankton. Michigan State University

Timmermans KR, Davey MS, Van der Wagt B, et al (2001) Co-limitation by iron and light of *Chaetoceros brevis, C. dichaeta and C. calcitrans* (Bacillariophyceae). Mar Ecol Prog Ser 217:287–297. doi: 10.3354/meps217287

Tison J-L, Brabant F, Dumont I, Stefels J (2010) High-resolution dimethyl sulfide and dimethylsulfoniopropionate time series profiles in decaying summer first-year sea ice at Ice Station Polarstern, western Weddell Sea, Antarctica. J Geophys Res 115:G04044. doi: 10.1029/2010JG001427

Toggweiler JR, Russell J (2008) Ocean circulation in a warming climate. Nature 451:286–288. doi: 10.1038/nature06590

Tomaru Y, Tanabe H, Yamanaka S, Nagasaki K (2005) Effects of temperature and light on stability of microalgal viruses, HaV, HcV and HcRNAV. Plankt Biol Ecol 52:1–6

Tremblay J-É, Gagnon J (2009) The effects of irradiance and nutrient supply on the productivity of Arctic waters: A perspective on climate change. In: Nihoul JCJ, Kostianoy AG (eds) Influence of Climate Change on the Changing Arctic and Sub-Arctic Conditions. Springer Netherlands, Dordrecht, pp 73–93

Turner JT (2015) Zooplankton fecal pellets, marine snow, phytodetritus and the ocean's biological pump. Prog Oceanogr 130:205–248. doi: 10.1016/j.pocean.2014.08.005

Vaughan DG (2006) Recent trends in melting conditions on the Antarctic Peninsula and their implications for ice-sheet mass balance and sea level. Arctic, Antarct Alp Res 38:147–152. doi: 10.1657/1523-0430(2006)038[0147:RTIMCO]2.0.CO;2

Vaughan DG, Marshall GJ, Connolley WM, et al (2003) Recent rapid climate change warming on the Antarctic Peninsula. Clim Change 60:243–274. doi: 10.1023/A:1026021217991

Venables H, Moore CM (2010) Phytoplankton and light limitation in the Southern Ocean: Learning from high-nutrient, high-chlorophyll areas. J Geophys Res 115:C02015. doi: 10.1029/2009JC005361

Venables HJ, Clarke A, Meredith MP (2013) Wintertime controls on summer stratification and productivity at the western Antarctic Peninsula. Limnol Oceanogr 58:1035–1047. doi: 10.4319/lo.2013.58.3.1035

Vernet M, Martinson D, Iannuzzi R, et al (2008) Primary production within the sea-ice zone west of the Antarctic Peninsula: I—Sea ice, summer mixed layer, and irradiance. Deep Sea Res Part II Top Stud Oceanogr 55:2068–2085. doi: 10.1016/j.dsr2.2008.05.021

Visser AW, Jónasdóttir SH (1999) Lipids, buoyancy and the seasonal vertical migration of *Calanus finmarchicus*. Fish Oceanogr 8:100–106. doi: 10.1046/j.1365-2419.1999.00001.x

von Quillfeldt CH (2000) Common diatom species in Arctic spring blooms: Their distribution and abundance. Bot Mar 43:499–516. doi: 10.1515/BOT.2000.050

Voronina N. (1998) Comparative abundance and distribution of major filter-feeders in the Antarctic pelagic zone. J Mar Syst 17:375–390. doi: 10.1016/S0924-7963(98)00050-5

Voss M (1991) Content of copepod faecal pellets in relation to food supply in Kiel Bight and its effect on sedimentation rate. Mar Ecol Prog Ser 75:217–225. doi: 10.3354/meps075217

Weitz JS, Wilhelm SW (2012) Ocean viruses and their effects on microbial communities and biogeochemical cycles. F1000 Biol Rep 4:2–9. doi: 10.3410/B4-17

Wilhelm SW, Suttle CA (1999) Viruses and nutrient cycles in the sea. Bioscience 49:781–788. doi: 10.2307/1313569

Wilson WH, Tarran GA, Schroeder D, et al (2002) Isolation of viruses responsible for the demise of an *Emiliania huxleyi* bloom in the English Channel. J Mar Biol Assoc United Kingdom 82:369–377. doi: 10.1017/S002531540200560X

Chapter 2

Antarctic phytoplankton community composition and size structure: Importance of ice type and temperature as regulatory factors

Antarctic phytoplankton community composition and size structure: Importance of ice type and temperature as regulatory factors

Tristan E.G. Biggs[1,2]; Santiago Alvarez-Fernandez[3]; Claire Evans[4]; Kristina D.A. Mojica[5]; Patrick D. Rozema[6]; Hugh J. Venables[7]; David W. Pond[8] and Corina P.D. Brussaard[1,2]

[1] Department of Marine Microbiology and Biogeochemistry, NIOZ Royal Netherlands Institute for Sea Research, and University of Utrecht, Texel, The Netherlands.
[2] Department of Freshwater and Marine Ecology, Institute for Biodiversity and Ecosystem Dynamics (IBED), University of Amsterdam, Amsterdam, The Netherlands.
[3] Alfred Wegener Institut Helmholtz Zentrum für Polar und Meeresforschung, Biologische Anstalt Helgoland, Helgoland, Germany.
[4] Ocean Biogeochemistry & Ecosystems Research Group, National Oceanography Centre, Southampton, UK.
[5] Department of Botany and Plant Pathology, Cordley Hall 2082, Oregon State University, Corvallis, Oregon, USA.
[6] Department of Ocean Ecosystems, Energy and Sustainability Research Institute Groningen, University of Groningen, Groningen, The Netherlands
[7] British Antarctic Survey, Natural Environmental Research Council, Cambridge, UK.
[8] Institute of Aquaculture, University of Stirling, Stirling, Scotland UK.

Abstract

Climate change at the Western Antarctic Peninsula (WAP) is predicted to cause major changes in phytoplankton community composition, however, detailed seasonal field data remain limited and it is largely unknown how (changes in) environmental factors influence cell size and ecosystem function. Physicochemical drivers of phytoplankton community abundance, taxonomic composition and size class were studied over two productive austral seasons in the coastal waters of the climatically sensitive WAP. Ice type (fast, grease, pack or brash ice) was important in structuring the pre-bloom phytoplankton community as well as cell size of the summer phytoplankton bloom. Maximum biomass accumulation was regulated by light and nutrient availability, which in turn were regulated by wind driven mixing events. The proportion of larger-sized (>20 µm) diatoms increased under prolonged summer stratification in combination with frequent and moderate-strength wind-induced mixing. Canonical correspondence analysis showed that relatively high temperature was correlated with nano-sized cryptophytes, whereas prymnesiophytes (*Phaeocystis antarctica*) increased in association with high irradiance and low salinities. During autumn of Season 1, a large bloom of 4.5 µm sized diatoms occurred under conditions of seawater temperature >0°C and relatively high light and phosphate concentrations. This bloom was followed by a succession of larger nano-sized diatoms (11.4 µm) related to reductions in phosphate and light availability. Our results demonstrate that flow cytometry in combination with chemotaxonomy and size-fractionation provides a powerful approach to monitor phytoplankton community dynamics in the rapidly warming Antarctic coastal waters.

2

Introduction

Global climate change will have consequences for marine ecosystems throughout the world's oceans (Boyce et al. 2010; Hallegraeff 2010). In polar marine ecosystems, the impact of a warming climate is magnified because a relatively small change in temperature can have a large impact on sea ice melt and ice cover (Smetacek and Nicol 2005; Schofield et al. 2010). In the Antarctic, declines in sea ice have been associated with a longer growing season and consequently, higher annual net production (Moreau et al. 2015). However, the influence of sea ice is complicated by variability in relation to the extent as well as the timing of advance and retreat which may be largely influenced by local-scale, rather than large-scale, forcing (Kim et al. 2018). Decreased ice cover has been associated with a reduction in photosynthetic efficiency (Schofield et al. 2018) and several studies have described a reduction in overall phytoplankton biomass and a shift from large phytoplankton (diatoms) to smaller flagellated species. These shifts have been associated with reduced salinities, higher temperatures and stronger vertical stratification (Moline and Prezelin 1996; Moline et al. 2004; Montes-Hugo et al. 2009; Venables et al. 2013; Mendes et al. 2017; Rozema et al. 2017c). However, the physicochemical drivers behind community shifts towards flagellated phytoplankton remain unclear, likely due to the diversity among flagellated phytoplankton spanning different taxonomic groups and cell sizes, and each may interact differently with the physicochemical environment. Our current understanding of the drivers associated with the seasonal progression within the phytoplankton community (Henley et al. 2019), particularly the pico- ($\leq$3 µm) and nano-sized (> 3-20 µm) phytoplankton, limits our ability to accurately predict how polar marine systems will respond to future climate change with implications for food web dynamics and the marine carbon cycle (e.g. Pinhassi et al. 2004; Conan et al. 2007; Christaki et al. 2008; Obernosterer et al. 2008; Agustí and Duarte 2013; Evans et al. 2017).

Cell size is an important functional trait that influences almost every aspect of phytoplankton biology (Marañón 2015). Phytoplankton community size structure is therefore a key factor regulating food-web dynamics, biogeochemical cycling and

trophic carbon transfer in the marine environment (Finkel et al. 2010; Marañón 2015). Shifts in the size class of primary producers in productive regions may also affect ocean carbon sequestration (the biological pump) as the larger phytoplankton (e.g. diatoms) are typically grazed by large copepods and krill (Quetin and Ross 1985; Jacques and Panouse 1991; Kopczynska 1992; Granéli et al. 1993) whereas the smaller-sized cells (flagellates) are grazed by salps, small copepods and protozoans (Harbison et al. 1986; Riegman et al. 1993; Froneman and Perissinotto 1996; Perissinotto and A. Pakhomov 1998). As a result, obtaining a mechanistic understanding of the factors that control the variability of phytoplankton community size structure remains a central goal in biological oceanography (Marañón 2015).

The Western Antarctic Peninsula (WAP) has experienced rapid climate change (Saba et al. 2014) resulting in alterations in phytoplankton community structure (Beardall and Stojkovic 2006; Rozema et al. 2017c; Deppeler and Davidson 2017) which are evident at higher trophic levels, with shifts in the grazer community from krill to the nutritionally poorer salps (Loeb et al. 1997; Atkinson et al. 2004; Saba et al. 2014; Steinberg et al. 2015). Moreover, reduced viral activity predicted due to changes in host population dynamics (Evans et al. 2017), may exacerbate impacts on community structure due to reduced substrate availability for microbial loop processes. Although the WAP area has been studied in quite some detail over the past 20 years, to our knowledge no studies have simultaneously investigated the size class distribution of Antarctic phytoplankton abundances using flow cytometry (FCM) and chemotaxonomy (CHEMTAX). Thus far, WAP phytoplankton communities have been examined using mostly light microscopy and/or pigment-based taxonomic analysis (Garibotti et al. 2003, 2005; Rozema et al. 2017c). Studies using flow cytometry (FCM) to investigate phytoplankton community composition and examine environmental drivers are still lacking. Furthermore, fractionated Chlorophyll-*a* (Chl-*a*) studies did not include taxonomic distinction of the different size classes and investigated long-term trends and inter-seasonal differences rather than intra-seasonal variation (Clarke et al. 2008; Rozema et al. 2017c). Here we describe phytoplankton community dynamics (abundances, taxonomic composition

and size of single cells) over two consecutive productive seasons. The combination of FCM and CHEMTAX, with size-fractionation, potentially represents a powerful approach to uncover physicochemical factors structuring phytoplankton community size structure, particularly the pico- and nano-size classes.
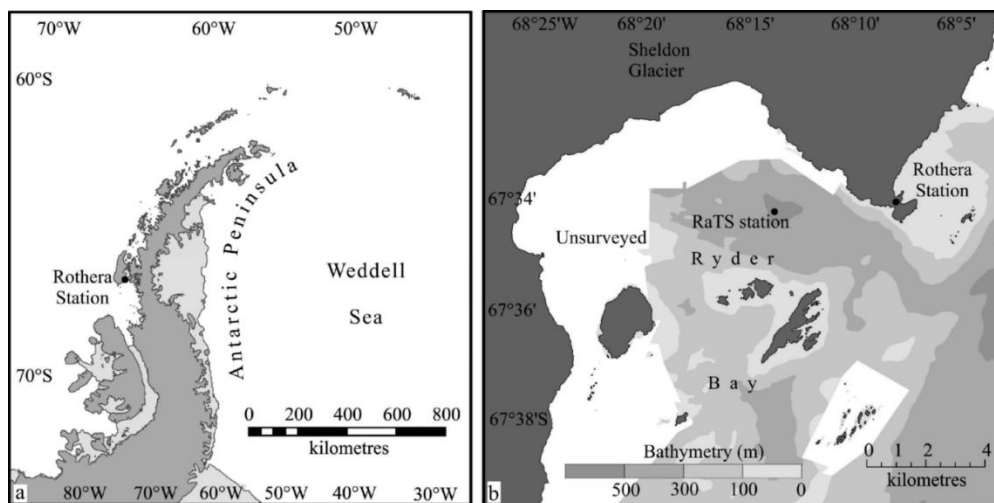
Fig. 1. Map of the sampling area: (a) location of Rothera station on the northern tip of Marguerite Bay along the Western Antarctic Peninsula (b) large scale map of the sampling site within Ryder Bay and close to Rothera station.

Methods

Study area and sampling

Data for this study was obtained at the Rothera time series site (RaTS, latitude 67.572°S; longitude 68.231°W; Clarke et al. 2008) located in Ryder Bay on the WAP (Fig. 1). Samples were taken over two consecutive austral productive seasons designated S1 (November 2012 to April 2013) and S2 (November 2013 to April 2014). Discrete seawater samples were collected from 15 m depth by a 12 L Niskin bottle deployed from a small boat. Full water column profiles were obtained using a SeaBird 19+ conductivity temperature depth instrument (CTD) supplemented with a flat LiCor sensor to measure photosynthetically available radiation (PAR) and an in-line fluorescence sensor (WetLabs). Calibration of the CTDs between years is discussed in Venables et al (2013). Sampling for physicochemical variables, FCM

abundances and phytoplankton pigments was conducted approximately twice weekly. Water samples were shielded from the light and processed as soon as possible in a temperature-controlled lab maintained at c.a. 0.5 - 1°C.

Physicochemical variables

Density, temperature, salinity and PAR were obtained from the CTD. Sampling was conducted when the study site was ice free and accessible by boat (i.e. no CTD casts were performed under sea ice). Euphotic zone depth (Z_{eu}) was calculated as the depth at which PAR was 1% of surface (1m) PAR. As an index to determine possible light limitation at the sampling depth, Z_{eu} was divided by 15 m ($Z_{eu}/15m$), whereby a score <1 indicates possible light limitation (phytoplankton are below the euphotic zone) and >1 no (or reducing probability of) light limitation. Stratification was quantified as the potential energy required to homogenize the water column from the surface to 40m depth (J m^{-2}) according to Venables et al. (2013). MLD was defined as a 0.05 kg m^{-3} difference in density relative to the surface (Venables et al. 2013). Sea ice type and coverage (%) was determined routinely every day in Ryder Bay by visual observation by Rothera base staff, with the Rothera records agreeing well with wider scale satellite derived trends (see Venables et al. 2013). Definitions for ice type (as defined by the British Antarctic Survey) were as follows: fast ice is a solid sheet of ice attached to the land, pack ice is a large area of sea ice that is not land fast, brash ice is small fragments of floating ice, grease ice is a very thin layer of frazil ice (ice crystals formed in water that is too turbulent to freeze solid) and pancake ice is round pieces of newly formed ice (from grease ice). Discrete water samples (6 mL) for dissolved inorganic phosphate, nitrate, nitrite, and silicate, were gently filtered through 0.2 µm pore-size Supor membrane Acrodisk filters (25 mm diameter, Pall, Port Washington, NY11050, USA). Ammonium samples were collected and analysed as in Clarke et al. (2008). Silicate samples were stored at 4°C and those for nitrogen and phosphorus at -20°C until analysis according to procedures described in detail by Bown et al. (2017).

Phytoplankton data

For phytoplankton enumeration (of single cells), fixed samples were counted during S1 and fresh (live) samples during S2. Technical problems with the flow cytometer during S1 prohibited live counts of phytoplankton abundances. No significant difference was found in phytoplankton population counts between live and fixed samples (Mann-Whitney Rank Sum Test: $p = 0.24$, $n = 44$). For S1, 3.5 mL subsamples were fixed with 100 µl formaldehyde-hexamine (18% v/v:10% w/v) at 4°C for 15-30 minutes, after which they were snap-frozen in liquid nitrogen and stored at -80°C until analysis. Samples were analysed according to Marie et al (1999) using a Becton Dickinson FACSCalibur FCM equipped with an air-cooled Argon laser with an excitation wavelength of 488nm (15mW) and the trigger was set on red fluorescence. Phytoplankton populations were distinguished using bivariate scatter plots of red Chlorophyll-*a* (Chl-*a*) autofluorescence versus side scatter. Cryptophytes were discriminated based on their orange phycoerythrin autofluorescence. The FCM data files were analysed using the freeware CYTOWIN (Vaulot 1989). No indications of chains or colonies were found in FCM cytograms. During the summer months, approximately weekly size fractionations were performed to determine the average cell size of the different phytoplankton populations distinguished using FCM. A whole water sample (5-10 mL) was gently filtered through either a 50, 20, 10, 8, 5, 3, 2, 1, 0.65 or 0.4 µm pore-size filters. The filtrates were then analysed by FCM as described previously. Mean cell size was calculated as the size corresponding to a 50% retention of cells based on the fit of an S-shaped plot (i.e., number of cells retained versus the pore size; Veldhuis and Kraay 2004). Over the course of both seasons, a total of 10 phytoplankton populations were distinguished, referred to as Phyto I to Phyto X according to increasing average cell diameter (Table 1). Vertical profiles (published in Bown et al. 2017; Rozema et al. 2017b) indicate that fluorescence based Chl-*a* concentrations at 15 m were most often comparable to subsurface Chlorophyll maximum (SCM). For Chl-*a* concentration and taxonomic composition, 1-8 L of whole seawater was filtered over GF/F glass fiber filters (47 mm, Whatman, The Netherlands). Filters were wrapped

Table 1. Average cell diameter (with standard deviation, $n = 15$) of the different phytoplankton groups identified by flow cytometry.

Name	Diameter (µm)
Phyto I	0.9 ± 0.1
Phyto II	1.8 ± 0.6
Phyto III	3.1 ± 0.5
Phyto IV	4 ± 0.6
Phyto V	4.5 ± 0.7
Phyto VI	4.5 ± 0.7
Phyto VII	7.4 ± 1.7
Phyto VIII	8.1 ± 1.8
Phyto IX	11.5 ± 3.0
Phyto X	20.4 ± 2.2

2

in aluminium-foil, snap-frozen in liquid nitrogen and stored at -80°C until analysis. For the majority of samples, phytoplankton pigments were analysed by high performance liquid chromatography (HPLC) according to Brussaard et al (2016). Three phytoplankton samples in S1 and 8 phytoplankton samples in S2 were analysed by HPLC according to Rozema et al. (2017a), as these samples were part of the BAS monitoring project. The pigment concentrations extracted and detected by the two separate approaches were not significantly different ($p < 0.0001$; $R^2 = 0.99$, $n = 39$) for natural samples collected *in situ* (Fig. S1). In both cases, pigment quantification was performed using standards (DHI, Hørsholm, Denmark) for Chlorophyll c_3, Peridinin, 19'-Butanoyloxyfucoxanthin, Fucoxanthin, Neoxanthin, 19'-Hexa-fucoxanthin, Alloxanthin, Lutein, Chlorophyll *b*, Chl-*a*, and identified peaks were manually checked for quality assessment. Phytoplankton class abundances were calculated using pigment data from HPLC by CHEMTAX v1.95 (Mackey et al. 1996). This programme uses a factor analysis and steepest decent algorithm to find the best fit based on a pigment ratio matrix. Six different taxonomic phytoplankton classes were chosen to represent the WAP marine ecosystem, identical to those used previously for the RaTS time series (Rozema et al. 2017a) and confirmed by microscopy

observations (unpublished data): Prasinophyceae, Chlorophyceae, Dinophyceae, Cryptophyceae, Prymnesiophyceae and Bacillariophyceae (diatoms). Unfractionated pigment concentration data were sorted into two bins depending on season (S1 and S2). Additionally, size-fractionated samples were also binned per season. CHEMTAX was run 60 times per bin with randomized (+-35%) pigment ratios to minimize the root mean square error (RMSE) using settings recommended in Kozlowski et al. (2011). The run with the lowest RMSE was deemed final with initial and final ratios shown in Table S1.

Within each season (S1 and S2), four distinct periods were identified based on the temporal dynamics of Chl-*a* concentration: no bloom (NB) from 1-29 November, and bloom 1-3 (B1-3) from 30 November to 8/9 January, 9/10 January to 10/14 February, and 11/15 February to 15 April, respectively.

In general size-fractionation of whole water for pigment analysis was performed once a week during the summer months. Between 1-5 L of whole seawater was pre-sieved through different filters (20 and 5 µm) and then filtered over a 47 mm GF/F glass fiber filter (Whatman, 0.7 µm nominal pore size) to obtain size fractions >20, 5-20 and <5 µm. Filters were subsequently snap-frozen in liquid nitrogen wrapped in aluminium foil and stored at -80°C until analysis.

Carbon conversion

To allow for a better comparison between FCM and CHEMTAX data, phytoplankton abundances and taxon- specific Chl-*a* concentrations were converted to cellular carbon (C). The C content of each phytoplankton population identified by FCM (FCM-C) was estimated from the average cell diameter (assuming cells to be spherical) using conversion factors of 196.5 and 237 fg C $µm^{-3}$ for nano- and pico-sized phytoplankton populations, respectively (Garrison et al. 2000; Worden et al. 2004). Carbon conversion factors may vary, depending on taxonomy, cell size and growth-regulating factors such as light and nutrient availability; (Geider 1987; Álvarez et al. 2017). Cell size variation was taken into account by using size-dependent conversion factors for the various FCM phytoplankton clusters (Phyto I-

X). To accommodate for taxonomic variations in cellular Chl-*a* concentrations (Geider 1987; Álvarez et al. 2017), we used different conversion factors (also reflecting cell size) for the classified groups (e.g. diatoms and cryptophytes). Carbon estimates for the different phytoplankton taxonomic groups were thus obtained from taxon-specific Chl-*a* concentration multiplied by taxon-specific conversion factors according to Garibotti et al. (2003), with the exception of Dinophyceae for which an average of ratios by Llewellyn et al. (2005) and Agirbas et al. (2015) were used. Moreover, for the dominating diatoms and cryptophytes it was possible to refine carbon estimates based on Chl-*a* (named Chl-C) using published conversion factors specific for different biomass concentrations (according to Garibotti et al. 2003a); i.e., low <1, medium 1-4 and high >4 µg Chl-*a* L^{-1} dominated by small-, nano- and micro-sized phytoplankton, respectively. The only exception was during B3 of S1, where the medium biomass C:Chl-*a* ratio was used due to the dominance of total Chl-*a* by nano-sized phytoplankton (Fig. S3) despite high Chl-*a* concentrations. For the majority of both seasons, Chl-*a* cell^{-1} ($\leq$ 20 µm) ranged between 0.1 – 0.8 pg.

The C to Chl-*a* ratios used in this study originate from Garibotti et al. (2003; with reference to Montagnes and Franklin 2001 and Montagnes et al. 1994) who used different taxonomic groups and cell sizes with culture light conditions below light saturation (50 µmol photons m^{-2} s^{-1}), more representative of natural conditions. However, it is difficult to correct for potential seasonal variability of (natural variation in) carbon conversion factors (not already covered by us). Chl-*a* (< 20 µm) varied between 0.1 and 4.1 pg cell^{-1} and was within range of experimental values (Álvarez et al. 2017). Cellular Chl-*a* content was only higher (i.e. > 0.8 pg cell^{-1}) during the B3 bloom of S1 when PAR reduced to very low levels, indicating possible photoacclimation. However, increased Chl-*a* cell^{-1} was most likely the result of a change in community composition as larger cells (from Phyto VI to Phyto IX) increasingly dominated Chl-*a* (< 20 µm). Furthermore, size fractionation on 13th March indicated that the average diameter of Phyto IX had also increased from 11 to 12 - 15 µm.

Statistical analysis

To check for potential differences in FCM abundances between fresh and fixed phytoplankton samples, a Mann-Whitney Rank Sum Test (SigmaPlot 14.0) was performed on 44 population counts from 8 samples spread over S2.

Canonical correspondence analysis (CCA) was performed on measured data using the R statistical software (R Development Core Team 2012) supplemented with Vegan (Oksanen et al. 2013). Data exploration was carried out following the protocol described in Zuur et al. (2010). A combined forward-backward selection procedure was applied to select only those explanatory variables that contributed significantly to the CCA model, while removing non-significant terms. Significance was assessed by a permutation test, using the multivariate pseudo-F-value as the test statistic (Zuur et al. 2009). A total of 999 permutations were used to estimate p-values associated with the Pseudo-F statistic. To identify and remove any collinearity from final models, variance inflation factors (VIF) were calculated. Sequentially, explanatory variables with the largest VIF were removed until all variables resulted in VIF<10 (Zuur et al. 2009). The environmental variables (after VIF selection) included as constraining variables in the multivariate analysis were: temperature, salinity, PAR, MLD, Z_{eu}/15m, stratification (Strat), phosphate, nitrate, silicate, wind speed and ice cover. Additionally, ice type (levels) and season (S1 and S2) were added as factors to see how they relate to phytoplankton abundance and taxonomic composition. PAR, MLD, Z_{eu}/15m, phosphate and nitrate data were log transformed due to their non-linear relationship to total biomass, and to reduce the effects of outliers. CTD casts were absent for 13 phytoplankton abundance samples and 17 pigment samples from S1, and 9 from both sample types of S2. To overcome this limitation and permit data to be included into the CCA, the time series data (temperature, salinity, PAR, MLD, Z_{eu}/15m and Strat) were linearly interpolated. For most of those samples (80%), CTD casts were taken within 1 day (and often 1 day before and 1 day after) of biological samples and the remaining were taken within 2 days (apart from 1 sample taken 3 days apart). Five data points (spread evenly over the season) in S1

and 1 data point in S2 were missing nutrient data and so interpolated data were also used for these 6 time points.

The analysis of biological variables consisted of phytoplankton abundance (FCM) and carbon biomass (converted from FCM), and pigment-based phytoplankton taxonomic community composition (in Chl-*a*) and taxon-specific carbon biomass (converted from Chl-*a*). Note: for Chl-*a* data 'season' did not contribute significantly to the model, allowing combined analysis of both seasons. For FCM data, season was a significant factor and subsequently S1 and S2 data sets were ran separately.

When interpreting CCA correlation triplots, arrow lengths represent the covariates and their correlation with the axis (CCA1 horizontal axis and CCA2 vertical axis). The correlation between response variables is reflected in the angles between lines. Wherein, a small angle between two lines represents a high positive correlation, a 90° angle represents no correlation and 180° a strong negative correlation.

Results

Physicochemical data

At the beginning of November in S1, Ryder Bay was completely covered by fast ice which rapidly declined to 10% by mid-December (Fig. 2a). For the remainder of S1, brash ice was the main ice type with gradual declining cover (from 80 to 10%) until mid-January after which it remained relatively low but with considerable variability. At the beginning of S2, grease ice was the dominated ice type (up to 100% cover) but ice cover rapidly changed to pack ice and declined in extent to 10% by 17th November. Following this, brash ice took over and cover increased to 100% (Fig. 2b). A short period of pack ice cover was observed in mid-December, returning into brash ice as ice cover rapidly declined during the second half of December. For the remainder of the season, brash ice remained generally low but variable (10 to 80%). Stratification increased steadily at the beginning of December in both seasons (Fig. 2c) accompanied by a shallowing of the MLD (Fig. 2d). Stratification peaked at the end of December (1544 in S1 and 1264 J m^{-2} in S2) and then declined during the first half of January in both seasons. In S2 stratification increased again and remained
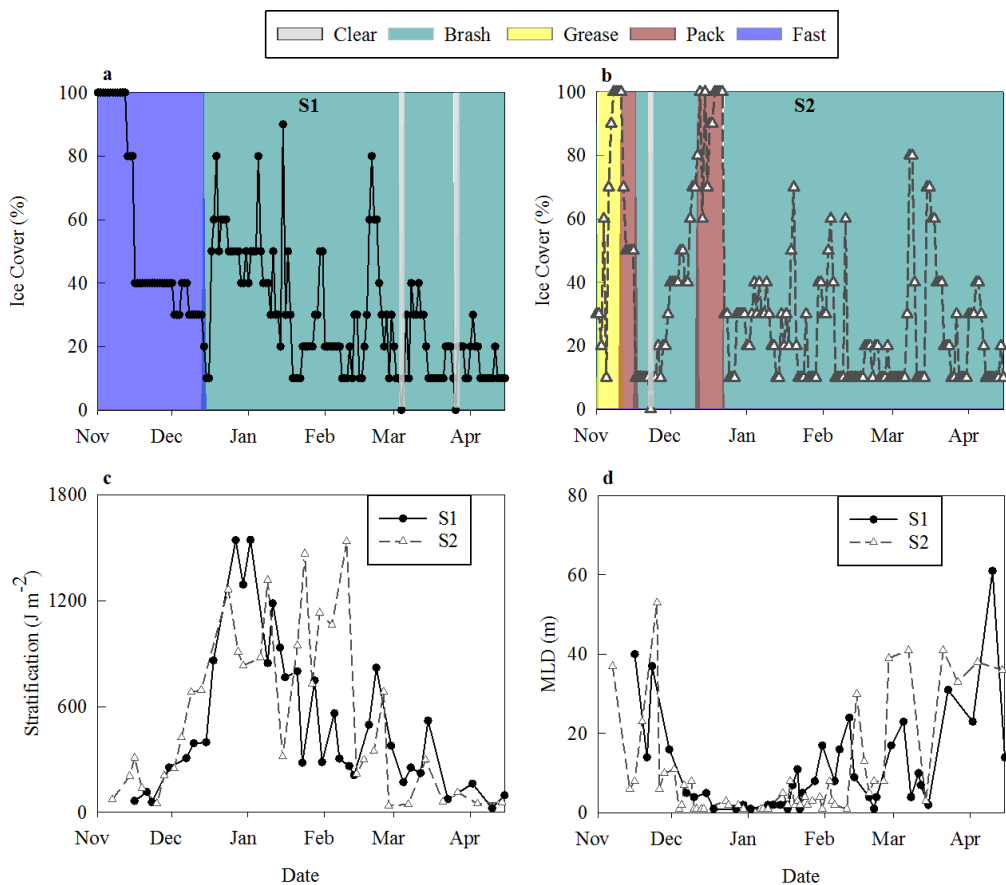
Fig. 2. Temporal dynamics of environmental conditions at the RaTS monitoring site (15 m depth) in Ryder Bay, Antarctica, from November to April during two consecutive years, S1 (circles, solid line) and S2 (triangles, dotted line). Ice cover and ice type (Clear = no ice, Brash = Brash ice, Grease = Grease ice, Pack = Pack ice and Fast = Fast ice) in (a) S1 and (b) S2, (c) vertical stratification, and (d) mixed layer depth (MLD).

high until 10th February. This difference in stratification between the two seasons was apparent in MLD which was deeper in S1 at 16 ± 8 m ($n = 3$) compared to 2 ± 1 m ($n = 3$) during the same period of S2. Stratification levels were weak for both seasons in March and April and MLD were relatively high ranging from 20 to 40 m. In both seasons, seawater temperature steadily increased from -1.7°C in November to 0°C during early January (Fig. 3a). Temperature during S1 peaked at 1.9°C on 16th January and remained around 1.2°C for 1 month before gradually declining to below 0°C in April. In S2, seawater temperature peaked later in the season (1.4°C on 5th February) and declined to < 0°C in early February, followed by a gradual
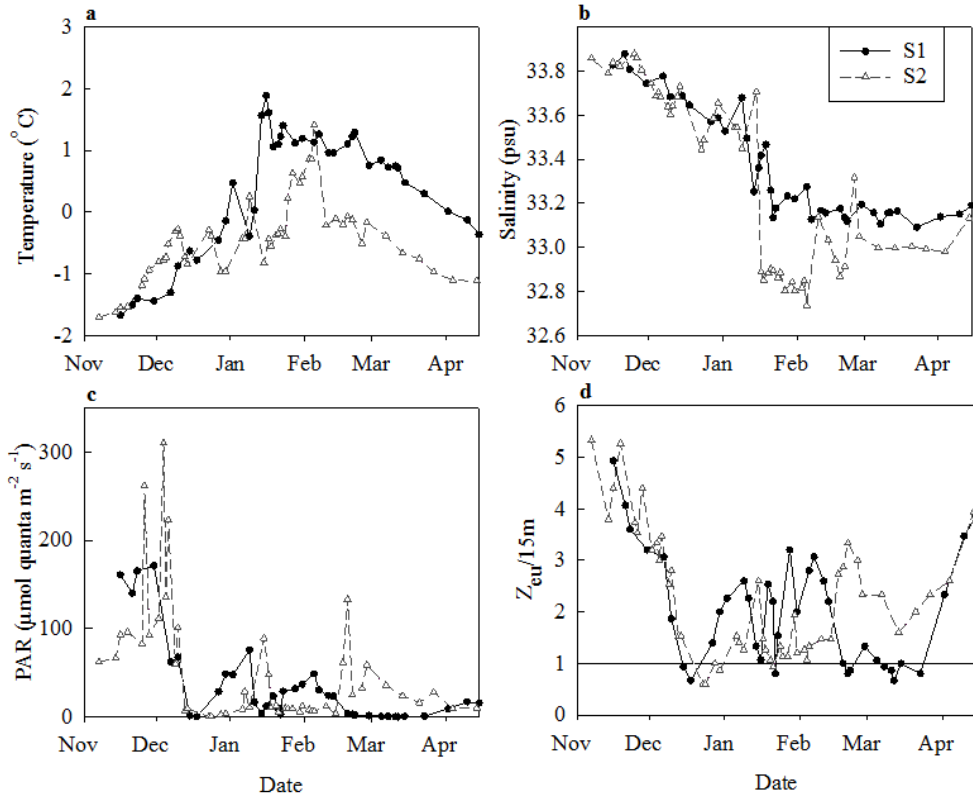
Fig. 3. Time series of (a) temperature, (b) salinity, (c) photosynthetic active radiation (PAR) and (d) the index of light limitation ($Z_{eu}/15m$), sampled at 15 m at RaTS in Ryder Bay during two consecutive years, S1 (circles, solid line) and S2 (triangles, dotted line). The reference line in subplot (d) indicates potential light limitation.

decrease to around -1.1°C in April. Compared to S1, average temperature during S2 was ~2.5-fold lower (0.36 ± 1 vs -0.45 ± 0.6°C, $n = 39$ and 50, respectively), with the strongest difference during bloom period B2 (1.09 ± 0.62 vs 0.09 ± 0.63°C, $n = 13$ and 16, respectively) and B3 (half February to April; 0.64 ± 0.49 vs -0.55 ± 0.40°C, $n = 15$ and 11, respectively). Salinity gradually declined until January during S1 (Fig. 3b), whereas in S2, a rapid drop was observed during January and values remained low for 3 weeks before stabilising at ~ 33.0 psu by March, slightly lower than the salinity of 33.2 psu in S1 over this period. PAR levels were highest at the start of both seasons (Fig. 3c), declining thereafter to potentially growth limiting levels (as indicated by $Z_{eu}/15m$; Fig 3d) and reaching values as low as $0.3 – 0.4 \, \mu mol$ quanta $m^{-2} \, s^{-1}$ by the second half of December. During the B2 bloom period of S2,

PAR was generally low (17 ± 23 µmol quanta m^{-2} s^{-1}, $n = 15$) and had a higher potential for light limitation compared to the same period in S1. Conversely, during the bloom period B3 of S1, PAR levels (<3 µmol quanta m^{-2} s^{-1}) were much lower compared to S2.

Phosphate and nitrate in S1 were drawn down from concentrations of 1.7 and 28 µM on 8th Dec to 0.17 and 1.3 µM, respectively, at the start of January, before rising again until mid-February (Fig. S2a, b). In S2, the initial drawdown of phosphate and nitrate was more gradual and variable than S1, lasting until the beginning of February and reaching 0.04 and 0.03 µM, respectively. A second large drawdown of phosphate was observed during S1, declining to 0.06 µM on 12th March. Ammonium concentrations were initially low in both seasons (~0.35 µM) and increased to 5 µM on 5th February in S1 and 2.6 µM on 17th February in S2 (Fig. S2c). Silicate concentrations remained replete over the observation period of both seasons (Fig. S2d), as were concentrations of dissolved iron (DFe, Bown et al. 2017).

Chlorophyll -*a* and taxonomic groups

The mean Chl-*a* concentration in S1 (4.3 ± 4.4 µg L^{-1}, $n = 51$) was 1.6-fold higher than in S2 (2.7 ± 2.2 µg L^{-1}, $n = 50$, Fig. 4). This was due to the S1 phytoplankton blooms (i.e. peaks in Chl-*a*) during Bloom periods B1 and B3 (12.3 and 16.1 µg Chl-*a* L^{-1}, respectively). In contrast, the B2 period in S2 displayed a higher mean Chl-*a* concentration than in S1, i.e. 4.6 ± 1.7 and 2.0 ± 1.5 µg L^{-1}, $n = 17$ and 16, respectively. Diatoms (Bacillariophyceae) often dominated total Chl-*a* both during S1 and S2 (Fig. 4c and d) but at the start of S2 (NB period) it was both Prymnesiophyceae and Prasinophyceae and during B2 in S1, Cryptophyceae contributed most to total Chl-*a* concentration. Furthermore, at the start of B3 (second half of February) for both S1 and S2 the Cryptophyceae and Prymnesiophyceae co-dominated, while towards the end of B3 in S2, Prasinophyceae were most important. Contributions to Chl-*a* by Chlorophyceae and Dinophyceae were marginal over both seasons of this study.
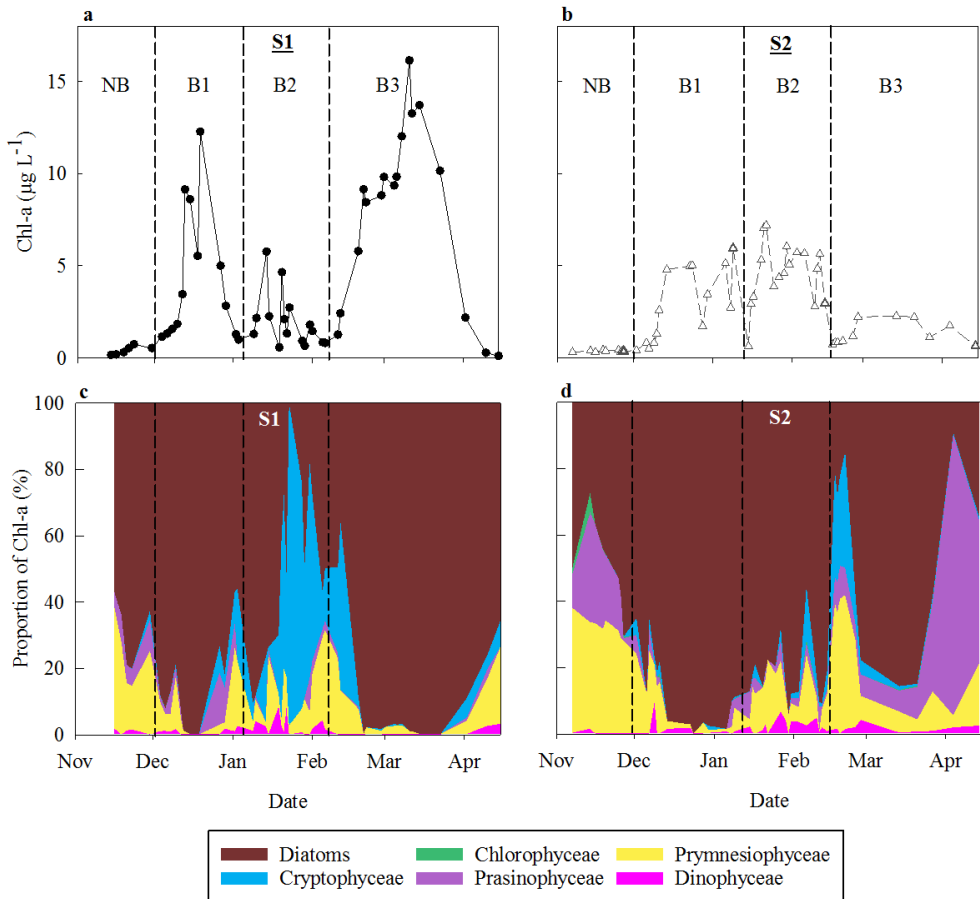
Fig. 4. Seasonal dynamics of total Chl-*a* concentration for (a) S1 and (b) S2. The relative proportions of each taxonomic group (identified through CHEMTAX) are shown over (c) S1 and (d) S2. NOTE: Vertical dotted lines separate bloom periods NB and B1-3.

Size fractionated Chl-*a* shows that initially during the NB period when total Chl-*a* concentrations were still low (Fig. 4), the phytoplankton community was mostly <20 µm (Fig. S3). Temporal Chl-*a* size fraction dynamics in S1 revealed a shift from larger-sized (>20 µm) phytoplankton during the first bloom period B1 to smaller-sized phytoplankton during the remainder of the season (up to 89% of total Chl-*a* in B3; Fig. S3a). In contrast, relatively smaller (< 20 µm) cells contributed most to phytoplankton biomass during the initial increase during B1 in S2 and larger cells dominating during B2 (Fig. S3b). Taxonomic analysis of fractionated Chl-*a* revealed

that diatoms and Cryptophyceae were present in all 3 size fractions. Prymnesiophyceae were present largely in the <5 µm fraction but were also observed in the >20 µm fraction, during March (B3) in S1 and late January to beginning of February in S2, presumably indicative for *P. antarctica* colonies (confirmed by light microscopy, data not shown).
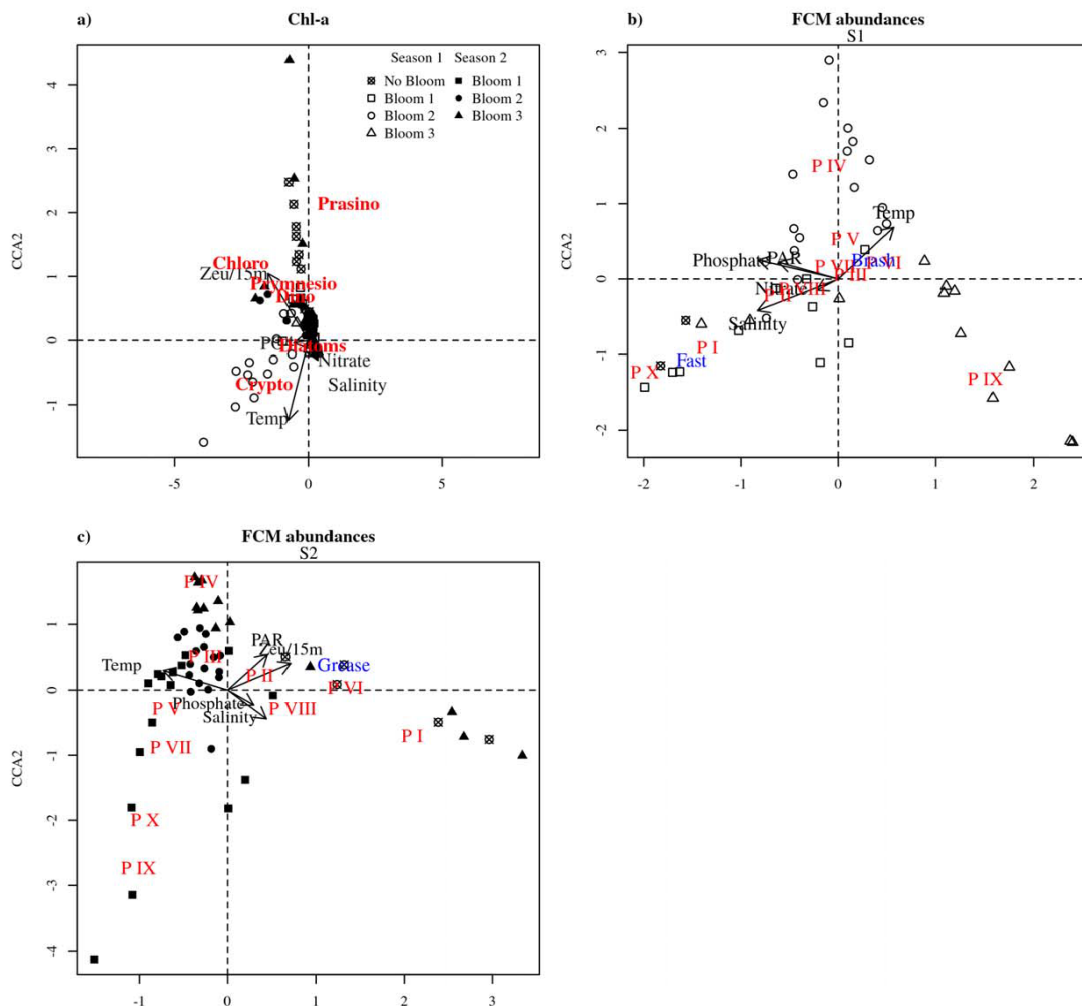
Fig. 5. Canonical Correspondence Analysis (CCA) of phytoplankton community composition (in red) in relation to environmental variables (in black). Ice type is represented in the CCA (in blue) where Fast = Fast ice, Brash = Brash ice etc. Subplots represent the community in terms of (a) Chl-*a* (with S1 and S2 combined), (b) FCM abundance in S1 and (c) FCM abundance in S2. Symbol shape represents bloom periods: No Bloom (NB) and Bloom 1-3 (B1-3), open symbols representing S1 Bloom 1-3 and filled symbols S2 Bloom 1-3. Abbreviations of response variables are as follows: Cryp = Cryptophyceae, Chlo = Chlorophyceae, Prymn = Prymnesiophyceae, Pras = Prasinophyceae, Dino = Dinophyceae, P I-X = Phytoplankton groups I-X.

Canonical correspondence analysis (CCA) was used to investigate the relationship between taxonomic composition (in Chl-*a* concentration) and the environmental variables with both S1 and S2 combined. The eigenvalues (obtained from the model output; Table S2) indicated that the main environmental variables contributing to the formation of the axes explained 35% of total variation in the dataset (23 and 11% for first and second axis, respectively). These variables were temperature ($p < 0.001$, $n = 101$), $Z_{eu}/15m$ ($p < 0.001$, $n = 101$), salinity ($p = 0.058$, $n = 101$), phosphate ($p = 0.005$, $n = 101$) and nitrate ($p = 0.039$, $n = 101$, Fig. 5a). Overall, higher concentrations of Cryptophyceae were associated with high temperature (>1°C) and Prymnesiophyceae with relatively high $Z_{eu}/15m$ and low salinity. More specifically, the B2 data points in S1 clustered with high temperature and Cryptophyceae Chl-*a*, which were both highest during this period.

Phytoplankton abundance (and taxonomy)

The 10 phytoplankton clusters distinguished by FCM (Fig. 6) could be partially characterized (taxonomically). Temporal dynamics of Phyto III matched well with the dynamics of Prymnesiophyceae and light microscopy confirmed co-occurrence of *P. antarctica* single cells at times of high Phyto III abundances. Phyto III cell size (range 2 – 5 µm in diameter) corresponds to that of solitary *P. antarctica* cells (between 2-6 µm, Schoemann et al. 2005; Lee et al. 2016). Phyto IV dynamics compared well to Cryptophyceae Chl-*a* (< 20 µm, Fig. S4) and was identified as a cryptophyte group based on high orange (phycoerythrin) autofluorescence (Li and Dickie 2001) in combination with microscopic identification during times of high abundance. Phyto V-X are most likely diatoms, based on the good comparison of relative carbon contribution of individual phytoplankton groups with CHEMTAX analysis of specific Chl-*a* size fractions (at times when large group specific carbon contributions were observed). The picoeukaryotes (Phyto I and II) could not be classified due to their small cell size and limited contribution to FCM-C.

Similar to the average Chl-*a* concentration, mean phytoplankton abundance in S1 was higher than in S2 (5.5 ± 3.0 vs 3.7 ± 2.2 x 10^3 cells mL^{-1}, $n = 40$ and 51,
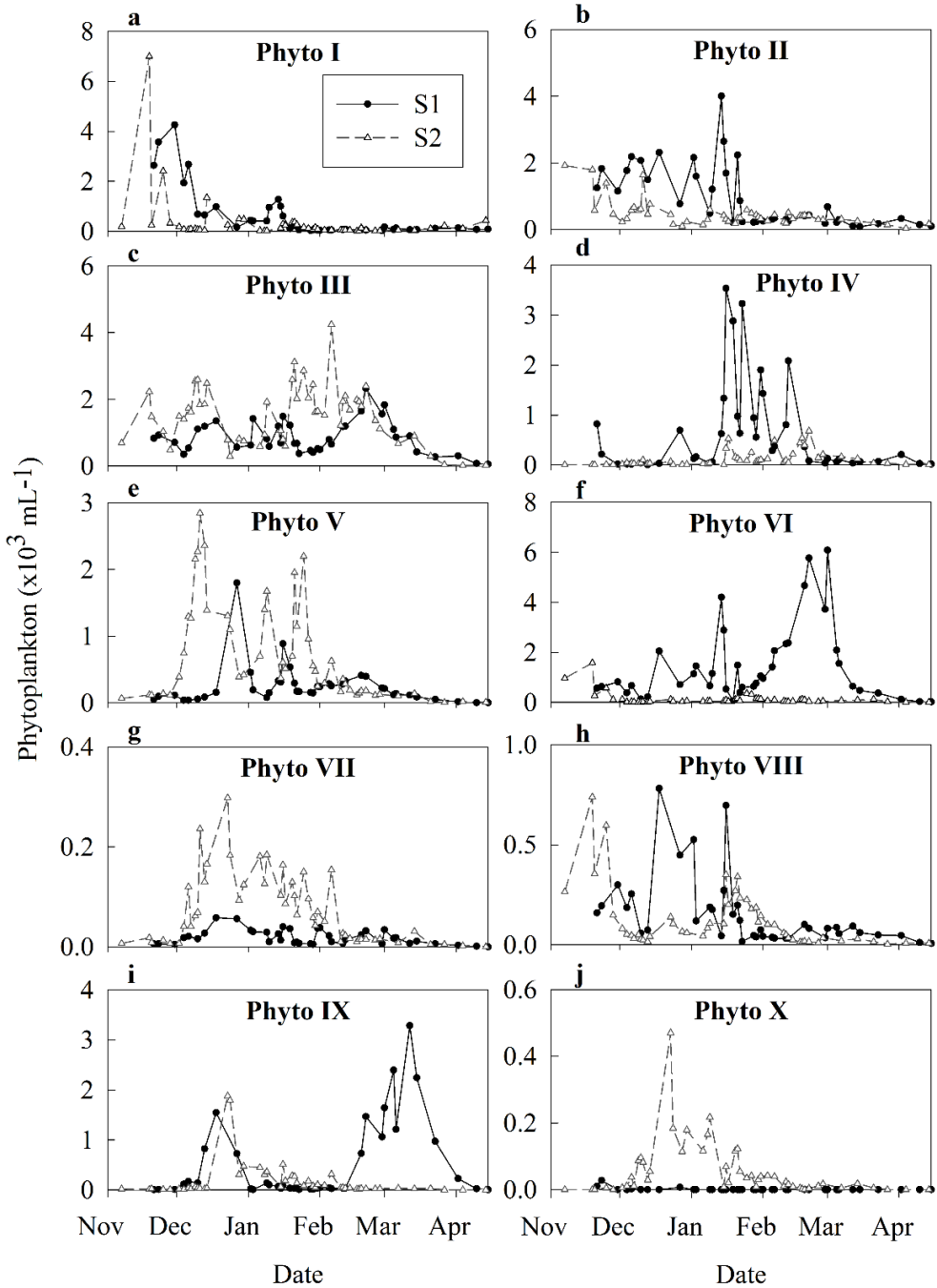
Fig. 6. Temporal dynamics of phytoplankton abundance over S1 (circles, solid line) and S2 (triangles, dotted line) whereby 10 distinct populations could be discriminated (using FCM): Phyto I – X (a – f). Note the different scales for abundances.

respectively, Fig. S5). Overall, the contribution of nano-sized phytoplankton (Phyto IV – X) was 1.5 times higher in S1 compared to S2 (53 ± 24 and $35 \pm 16\%$, $n = 40$ and 51, respectively), with Phyto IV, VI and IX dominating in S1 (13 ± 17, 24 ± 16 and $9 \pm 16\%$, $n = 40$, respectively) and Phyto V in S2 ($17 \pm 13\%$, $n = 51$). All 10 phytoplankton clusters distinguished by FCM showed strong temporal dynamics with distinct differences between seasons (Fig. 6). At the start of the season during the NB period, the picoeukaryotic phytoplankton Phyto I and II were most abundant in S1 ($45 \pm 4\%$ and $22 \pm 3\%$, $n = 3$; Fig. 6a-c) and equally abundant to *Phaeocystis* Phyto III in S2 (25 ± 20, 26 ± 13, and $25 \pm 14\%$, respectively, $n = 5$; Fig. S6). Phyto I-III persisted during B1 in S1 (24 ± 19, 31 ± 11 and $15 \pm 8\%$, respectively, $n = 9$), while diatom Phyto V bloomed during this period in S2 ($30 \pm 10\%$, $n = 15$; Fig. 6e). Phyto IX (diatom) became also abundant during B1 of both seasons, contributing up to 18% in S1 and 45% in S2 (Fig. 6i and Fig. S6). The B2 period of S1 was dominated by cryptophytes (Phyto IV $26 \pm 21\%$, $n = 16$; Fig. 6d and Fig. S6) and diatom Phyto VI ($26 \pm 14\%$, $n = 16$; Fig. 6f), whereas *Phaeocystis* Phyto III and diatom Phyto V had the largest share in S2 ($51 \pm 14\%$ and $16 \pm 7\%$, respectively, $n = 17$; Fig. 6c, e). During the initial stage of the large phytoplankton bloom in B3 of S1 (Fig. 4a), *P. antarctica* and diatom group Phyto VI were most abundant (contributing up to 23 and 56% of total abundances, respectively; Fig. 6c, f, and Fig. S6). The larger diatom group Phyto IX (11.5 ± 3 µm, $n = 15$) succeeded, making up to 64% of total abundance (Fig. 6i). Unlike S1, total phytoplankton abundances during B3 in S2 were relatively low (mean 5.1 ± 3.4 and 1.9 ± 1.2 $\times 10^3$ mL^{-1}, $n = 40$ and 51, respectively) and mostly dominated by Phyto III ($44 \pm 24\%$, $n = 51$).

The CCA of FCM abundances revealed that the models shown in Fig. 5 (b and c) explained 66% of the variation in the dataset of S1 (33% and 25% by first two axes) and 71% of S2 (35 and 22% by first two axes explained). Contributing to the formation of both axes during both seasons were ice type (S1 $p < 0.001$, $n = 40$; S2 $p = 0.010$, $n = 51$), temperature (S1 $p < 0.001$, $n = 40$; S2 $p < 0.001$, $n = 51$), PAR (S1 $p < 0.001$, $n = 40$; S2 $p = 0.008$, $n = 51$) and salinity (S1 $p < 0.001$, $n = 40$; S2 p

< 0.001, $n = 51$), followed by phosphate (S1 $p < 0.001$, $n = 40$; S2 $p < 0.001$, $n = 51$), and also for S1 nitrate (S1 $p < 0.001$, $n = 40$) and S2 $Z_{eu}/15m$ (S2 $p < 0.001$, $n = 51$). Phyto I, II, VIII and X in S1 were associated with fast ice, as well as high salinity and low temperature. In S2, ice type (grease ice) was again associated with Phyto I and II, but also diatoms Phyto VI and VIII. Additionally (in S2), these phytoplankton clusters were associated with high salinity, PAR, $Z_{eu}/15m$ and phosphate. Phyto X in S2 was, together with other diatom clusters, Phyto V, VII and IX, associated with low PAR and low $Z_{eu}/15m$ conditions (Fig. 5c). Phyto IX in S1 was also correlated with low PAR and low phosphate concentrations, the predominant environmental conditions during B3 in S1 (open triangles in Fig. 5b). Phyto IV (cryptophytes) in S1 was associated with high temperature, PAR and phosphate conditions (as for example found during B2 in S1; open circles Fig. 5b). In S2, these cryptophytes, as well as *Phaeocystis* (Phyto III), were similarly associated with high temperature and high PAR, but also low salinity and low phosphate (Fig. 5c).

Phytoplankton carbon

Considering the variation in cell sizes, we converted both phytoplankton abundances and Chl-*a* to cellular carbon for a more detailed comparison (Fig. 7a, b). As to be expected, the larger-sized phytoplankton clusters made up most of the cellular carbon (FCM-C) during both seasons (Fig. 8a, b), despite occasional low abundances (e.g. diatom Phyto X during March in S2; Fig. 6j). Due to size restrictions of FCM analysis (reliable acquisition is limited to cells around 20 µm in diameter, based on the laser beam width), we focused our comparison of FCM-C with CHEMTAX-C on the ≤20 µm size fraction. The <5 µm and 5 - 20 µm fractions showed generally good agreement for both seasons (Fig. 7c-f). The few discrepancies were related to FCM population-specific variations in cell diameter over time, whereby the actual diameter of the dominant population, at that specific moment in time, was larger than the mean. A larger diameter (compared to the mean) combined with high abundance resulted in observably lower FCM carbon estimations when using mean cell size compared to the actual cell size at the time.
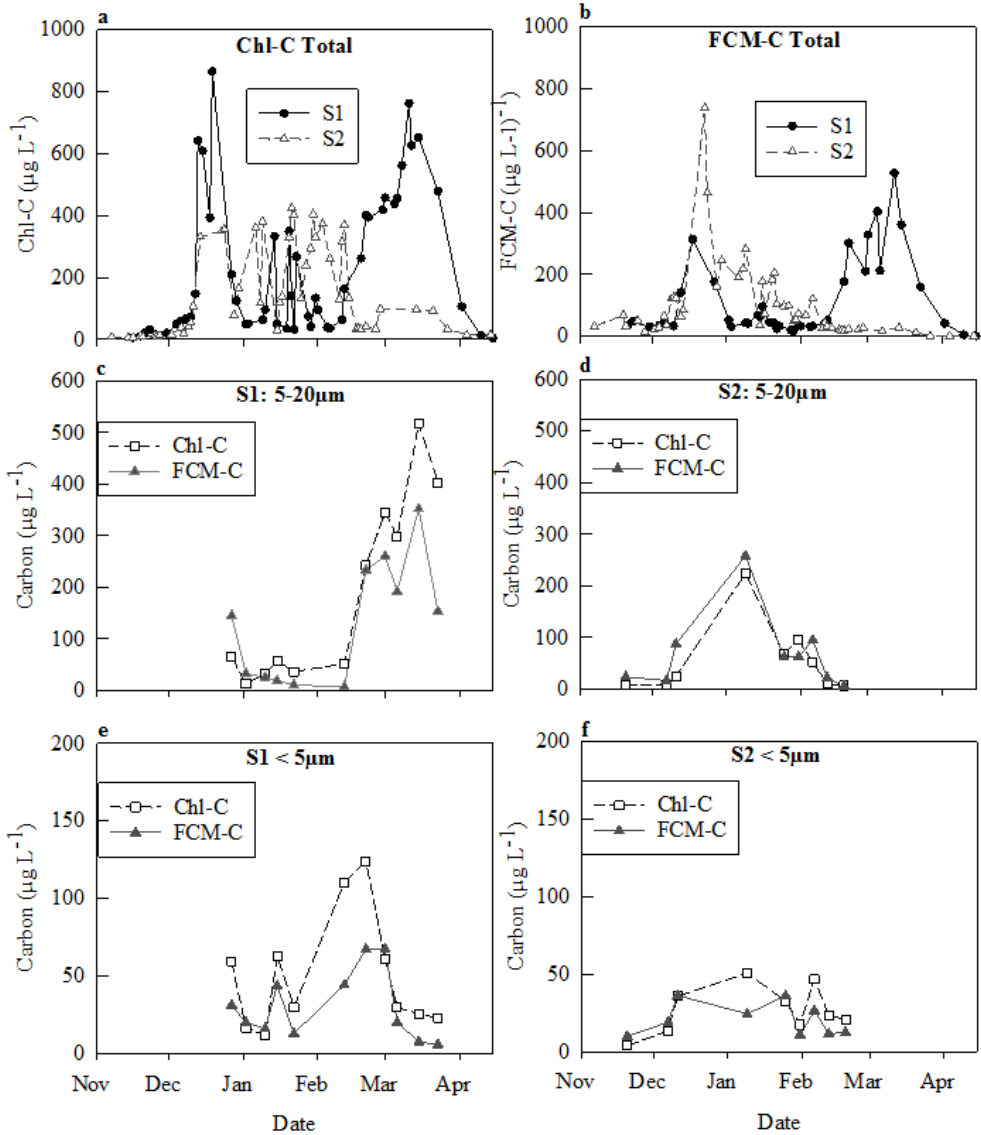
Fig. 7. Time series of phytoplankton cellular carbon where (a) represents total Chl-C and (b) total FCM-C, over S1 and S2. Fractionated Chl-C is compared to FCM-C for the 5-20µm fraction in (c) over S1 and (d) over S2, whilst the <5µm fraction is shown in (e) over S1 and (f) over S2. Note the different Y-axis scales.
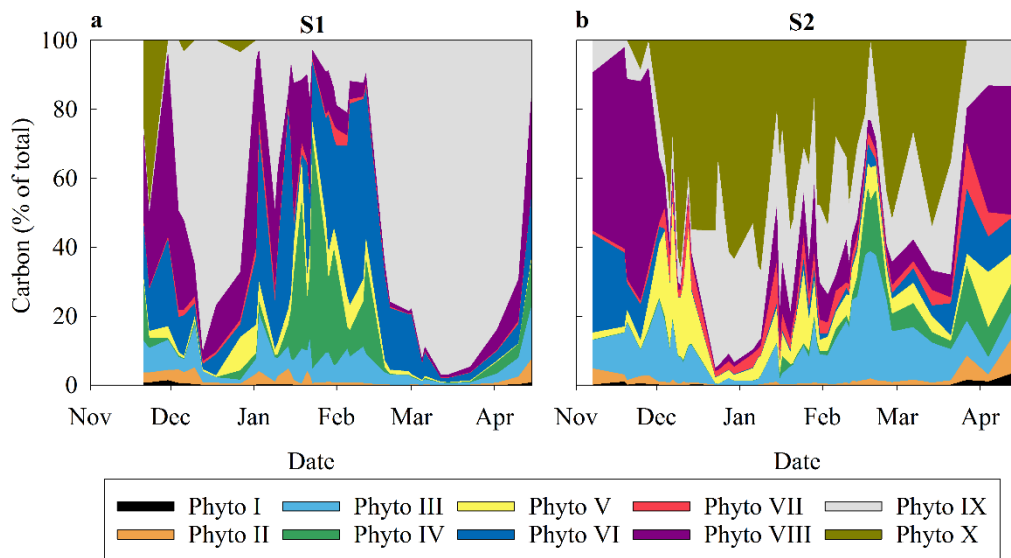
Fig. 8. Seasonal dynamics in the relative contribution of each phytoplankton group to total FCM-C over (a) S1 and (b) S2

When taxonomic composition was expressed in Chl-C, 42% of variation was explained by the CCA model shown in Fig. 9a (40 and 1% by first 2 axes). In particular, Cryptophyceae were associated with the main environmental variables contributing to the formation of the 2 primary axes, i.e. higher temperature ($p <$ 0.001, $n = 101$), a reduced potential for light limitation (higher $Z_{eu}/15m$, ($p < 0.001$, $n = 101$) and higher phosphate concentrations ($p = 0.002$, $n = 101$). The CCA based on FCM-C in S1 showed similar clear clustering of cryptophytes Phyto IV with B2 environmental data points when temperature was highest (Fig. 9b). Besides temperature, Phyto IV also correlated with higher PAR in both S1 and S2 (Fig. 9b, c). The FCM-C based CCA showed that the prymnesiophytes Phyto III also related strongly to higher PAR in S1 and high PAR, high $Z_{eu}/15m$, and relatively low salinity in S2. The different diatoms did not display similar relationships based on FCM-C. Phyto V, VII, and VIII were all associated with high PAR in S1, and ice type especially in S2 (Phyto VI and VIII with grease and Phyto V and VII with pack ice; Fig. 9b, c). With the FCM-C based CCA model, 42% of variation in the dataset of S1 was explained by the environmental variables with the first 2 axes explaining 31 and 9%, respectively. During S2, the CCA model explained even more, i.e. 65% of

total variation in FCM-C with the first 2 axes explaining 40 and 16% of variation, respectively.
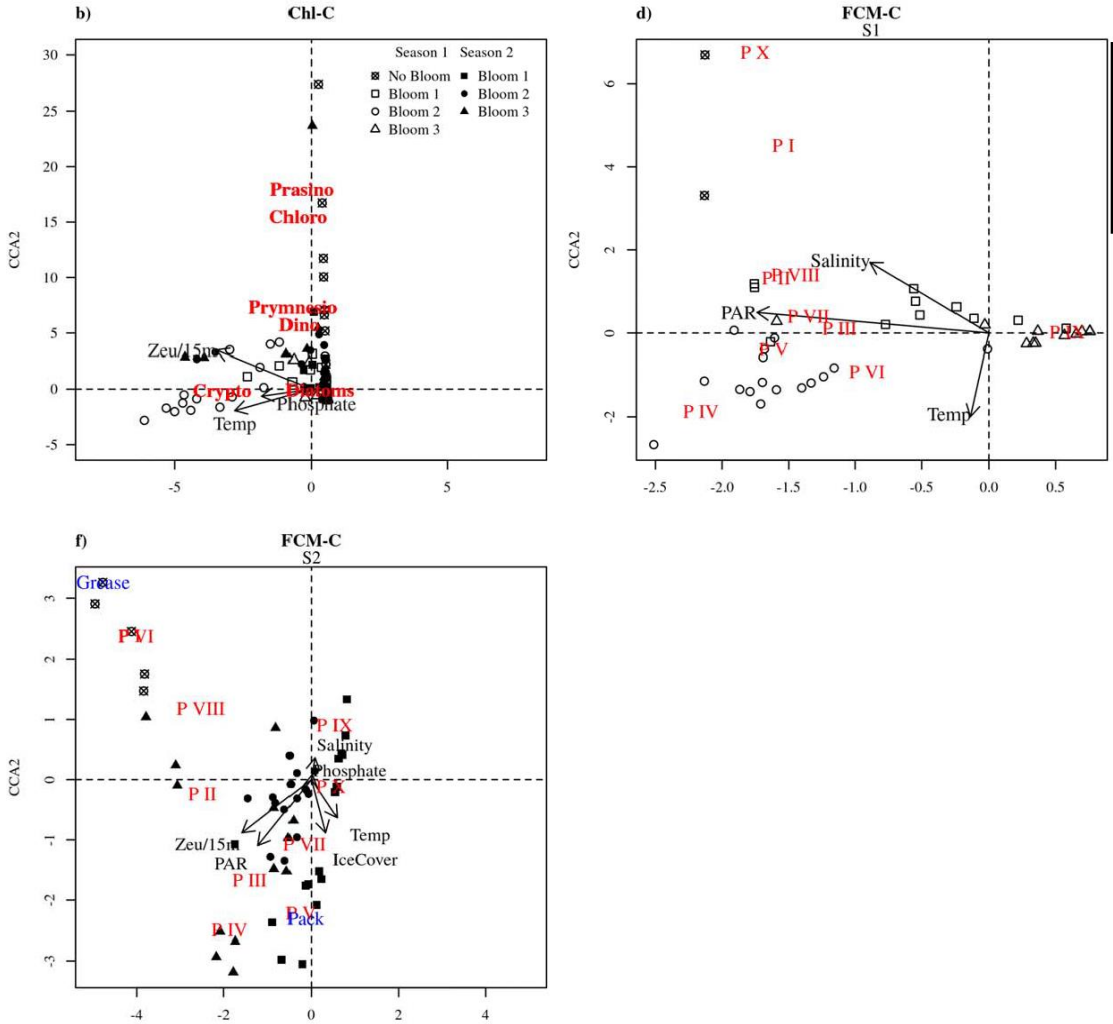
Fig. 9. Canonical Correspondence Analysis (CCA) of phytoplankton community composition (in red) in relation to environmental variables (in black). Ice type is represented in the CCA (in blue) where Fast = Fast ice, Brash = Brash ice etc. Subplots represent the community in terms of (a) Chl-C concentration (with S1 and S2 combined), (b) FCM-C in S1 and (c) FCM-C in S2. Symbol shape represents bloom periods: No Bloom (NB) and Bloom 1-3 (B1-3), open symbols representing S1 Bloom 1-3 and filled symbols S2 Bloom 1-3. Abbreviations of response variables are as follows: Cryp = Cryptophyceae, Chlo = Chlorophyceae, Prymn = Prymnesiophyceae, Pras = Prasinophyceae, Dino = Dinophyceae, P I-X = Phytoplankton groups I-X. Note: in FCM-C S2 (subplot c), Phyto groups I and VI are located directly on top of each other.

Discussion

Ice type and early season phytoplankton dynamics.

Previous studies have shown that melting sea-ice can seed the surrounding waters with phytoplankton cells (e.g. Garrison et al. 1987; Arrigo 2003; Jin et al. 2007), however, there is currently a limited understanding how ice type can structure phytoplankton community dynamics. Our data indicate that ice type (fast, grease, pack or brash ice) was an important factor structuring the pre-bloom phytoplankton community and the cell size structure of the early summer phytoplankton bloom community (Fig. 5 and 9). During the pre-season (August to October, data not shown) ice cover was similar between the two years, however, the pre-bloom phytoplankton community of S1 was associated with fast ice whilst grease ice was important during S2 (Fig 5 and 8). Ice type rather than ice cover seemed the most influential factor establishing the seed population for the productive season. The initial summer phytoplankton bloom (B1) during both seasons (Fig. 4) coincided with the period of greatest increase in vertical stratification (Eveleth et al. 2017). Nevertheless, decreasing fast ice cover in S1 (Fig. 2) coincided with a bloom of large diatoms (>20 µm) while in S2 the B1 bloom consisted of diatoms mostly ≤ 20 µm (Fig. S3) which corresponded to an increase in brash ice (turning into pack ice). Distinct differences in the pigment to Chl-*a* ratios during S1 and S2 are indicative of dissimilar phytoplankton seeding from ice. The relatively low ratios of Chl-c2, fucoxanthin and diadinoxanthin+diatoxanthin [Dd+Dt] to Chl-*a* (0.1, 0.5 and 0.1, respectively; Fig. S7a) during B1 in S1 indicate the larger diatoms were the result of marginal ice edge algal blooms (Rodriguez et al. 2002; Wulff and Wängberg 2004; Hashihama et al. 2008; Kozlowski et al. 2011). In contrast, the higher Chl-c2 and fucoxanthin to Chl-*a* ratios (1.4 and 2.5, respectively, Fig. S7b) during the initial phytoplankton biomass rise in S2 suggests the smaller-sized diatoms had higher light absorption efficiencies in the blue spectrum (characteristic of ice-associated algae; Robinson et al. 1995). Furthermore, the higher Dd+Dt to Chl-*a* ratio of 1.2 indicates these diatoms were recently released from the photo-protective effect of ice and

became exposed to high surface light (Robinson et al. 1997; Petrou et al. 2011; Van De Poll et al. 2011).

Summer phytoplankton dynamics.

The increased Chl-*a* concentrations during B1 in both seasons coincided with rapid declines in PAR (to potentially limiting levels; Fig. 3d) most likely due to increasing light attenuation (community shading). The low light availability was associated with a shift towards smaller-sized diatoms (Timmermans et al. 2001), particularly Phyto IX (Fig. 6i). Whereas additional nutrient depletion may have caused the decline of the B1 bloom in S1, a short-lived moderate mixing event end of December of S2 (Fig. S8) resulted in elevated nutrient concentrations and sustained phytoplankton standing stock during the low salinity-induced highly stratified (Gonçalves-Araujo et al. 2015; Rozema et al. 2017b) B2 period (Fig. S2, Fig. 3b and Fig. 2c). Subsequently, rapid nutrient drawdown may have caused growth-limiting conditions during early February (0.04 and 0.03 µM, for phosphate and nitrate respectively), however, a mixing event around that time (represented here for example by increased salinity, Fig. 3b) quickly reintroduced nutrients into the euphotic zone and sustained high proportions of large diatoms (Fig. 4b and Fig. S3b: data on 12 Feb).

In contrast to S2, the B2 period in S1 was largely dominated by Cryptophyceae (Fig. 4), which were found to be associated with high temperature and light availability (Fig. 5 and 9). Temperature and light have previously been reported as the most likely factors promoting Cryptophyceae in the WAP (Kopczynska 1992) and Buma and coworkers (1993) reported maximum division rates of Antarctic cryptophytes at $1°C$ and 50 µmol quanta m^{-2} s^{-1}, similar to B2 in S1 of this study. Mendes et al. (2017) also described strong positive correlations between cryptophytes and temperature in WAP waters. Although some studies linked reduced salinity with cryptophytes (Buma et al. 1992; Moline et al. 1997, 2004; Mendes et al. 2013), our study displays only a weak association with salinity (Fig. 5 and 9). It may be that previous associations of cryptophytes with salinity were largely driven by

collinearity between salinity and temperature. Alternatively, differences in species-specific responses to environmental variables could also be responsible for the variances observed (Henley et al. 2019).

Phaeocystis (Phyto III) was one of the most abundant FCM groups consistently present during both seasons (Fig. 6c). Phyto III dynamics were largely associated with light availability (PAR and $Z_{eu}/15m$) and salinity, factors also important for Prymnesiophyceae (Fig. 5 and 9), with highest abundances occurring during a period of relatively low salinity (B2 in S2; Fig. 6c and 3b). *Phaeocystis antarctica* has been reported to tolerate low salinity better than high salinity (Bates and Cota 1986; Van Leeuwe et al. 2014) and display decreased photosynthetic activity in response to higher salinity and lower temperatures (Kennedy et al. 2012). Additionally, *P. antarctica* appears to have an efficient photosystem and photo-damage repair mechanisms, enabling it to grow at higher PAR and well-mixed waters (Kropuenske et al. 2009; Alderkamp et al. 2012). Finally, *P. antarctica* growth rate has been reported to increase with temperature (Schoemann et al. 2005; Rose et al. 2009; Lee et al. 2016), supporting our finding that Phyto III is also associated with increasing temperature.

Towards the end of the productive season (B3 period), a large and prolonged bloom of nano-sized diatoms (Phyto VI and IX; Fig. 6f, i) was observed in S1 but not present in S2. Phyto VI correlated with relatively high temperature, PAR and phosphate (sustained by deeper mixing; Fig. 2d, 5 and 9). As Phyto VI peaked in abundance, PAR declined, light became potentially limiting and the shallowed MLD resulted in a rapid decrease in phosphate. Subsequently, Phyto IX bloomed under conditions of reduced phosphate (however sustained by regular mixing) and low light availability (<3 µmol quanta m^{-2} s^{-1}). Blooms of Phyto IX only occurred when biomass accumulation reduced light to potentially limiting levels. Conversely, light conditions may have restricted Phyto IX bloom development in S2 when PAR and $Z_{eu}/15m$ were higher (Fig. 2c, d). Specifically during B3 in S2, low temperature may have restricted the accumulation of Phyto VI (Suzuki and Takahashi 1995; Montagnes and Franklin 2001) and consequently the relatively reduced light

attenuation (lack of community-shading) would have prevented Phyto IX to bloom and increase Chl-*a* concentrations further.

Losses

The environmental variables were unable to explain all of the variability in phytoplankton abundance and community composition in Ryder Bay. The remaining variation is likely an indication for the importance of loss factors in structuring phytoplankton communities (Mojica et al. 2016; Yang et al. 2016). Biomass accumulation is after all the net result of production (regulated by physical and chemical variables) and loss rates such as grazing and viral lysis. The decline in phytoplankton biomass in S2 mid-February (end of B2) and the reduced Chl-*a* concentrations during B3 (compared to S1) may have been, at least partly, due to relatively high grazing pressure. Meso-zooplankton numbers peaked just before the start of the B3 period in S2 whereas numbers were declining at the same time in S1 (Fig. S9). For both seasons, the period with enhanced zooplankton standing stock coincided with a distinct rise in ammonium concentrations. Although the temporal dynamics of ammonium seems related to mixing events, similar to the other macronutrients (Fig. S2), micro- and meso-zooplankton are known to excrete ammonium (Goeyens 1991; Brussaard et al. 1996; Atkinson and Whitehouse 2000). The B2 period in S1 was cryptophytes-dominated with relatively low abundances of diatoms. Krill have been shown to selectively graze diatoms, rather than cryptophytes or prymnesiophytes, even when diatoms were rare (Verity and Smayda 1989; Head and Harris 1994; Haberman et al. 2003). Furthermorere, Kopczynska (1992) showed that in WAP coastal waters, low biomass areas dominated by flagellates also host dense krill swarms. This suggests that water column stability and zooplankton grazing act together to regulate phytoplankton community structure by reducing the biomass of diatoms and may suppress the development of a phytoplankton bloom. Besides grazing, viral lysis may contribute to the selective removal of phytoplankton (Brussaard 2004), influencing both species and strain diversity. Furthermore, high temperatures during B2 of S1 may have promoted

phytoplankton losses due to viral lysis, related to a shorter virus latent period and increased burst size (Maat et al. 2017; Piedade et al. 2018).

Combining methods.

The combined approach of using FCM (abundances), CHEMTAX (taxonomic composition) and size structure provides a more detailed understanding of the structure and composition of natural phytoplankton communities. Together with multivariate statistics, these methods increased the size spectrum of the study community and enabled the differentiation and comparison of individual size classes and chemotaxonomy within different bloom periods, as well as identifying physicochemical associations. This enabled predictions regarding the taxonomy of various phytoplankton groups identified by FCM (e.g. prymnesiophyte Phyto III) and allowed for a better discrimination within an individual taxonomic group (i.e., diatom populations Phyto V – X). Diatoms dominated the biomass generally throughout both seasons and in all size classes, however, Chl-*a* based CCAs could not assign strong drivers to this group. It can be expected that each size class (and each population within that size class) is driven by different environmental variables, preventing the assignment of reliable associations to this diverse taxonomic group. This oversimplification was avoided by defining populations via FCM which provided the greater resolution needed to understand the relationship between populations and environmental factors.

Conclusions

The current study provides a high-resolution temporal description of phytoplankton, particularly the pico- and nano-size fractions, and the physical and chemical characteristics over two distinct productive seasons. Multivariate analysis revealed that ice type was the most influential differential factor on phytoplankton community composition during spring and early summer, whereas temperature, light, phosphate and salinity played a more influential role during late summer and autumn. Ice type rather than ice cover structured the pre-bloom phytoplankton community as well as

the size class of the summer phytoplankton bloom. Maximum biomass accumulation was regulated by light and nutrient (mainly phosphate) availability which in turn were regulated by wind driven mixing events. Prolonged salinity driven stratification combined with moderate mixing and seawater temperature >0°C (supplying DFe from ice melt) coincided with the development of a large (>20 µm) diatom dominated phytoplankton community. Flagellates were associated with late summer conditions of high temperature (Cryptophyceae), low salinity and high light availability (Prymnesiophyceae) and would likely be more dominant under a warmer future climate with earlier and prolonged stratification (Falkowski and Oliver 2007). In a future 'warmer' autumn, that follows on from a 'warmer' summer, we would expect to see an increased frequency of large and prolonged nano-sized diatom blooms as observed during B3 in S1. To improve the variance explained by Chl-*a* based CCAs, we recommend performing frequent Chl-*a* fractionations. One caveat is that multiple FCM groups can fall into the same Chl-*a* size fraction and if driven by different factors this would lead to confounding results. FCM, however, provides fundamental information (for the ≤ 20 µm size fraction) on the abundances of the various populations while enhancing the ability to differentiate important physicochemical correlations with phytoplankton community structure and thus provides a vital tool for studying phytoplankton dynamics. The addition of large cell flow cytometry and high through-put sequencing of sorted phytoplankton populations (Eiler et al. 2013; Johnson and Martiny 2015; Massana et al. 2015; Visco et al. 2015), would enhance analysis of the phytoplankton community.

Acknowledgements

as well as Swier Oosterhuis and Anna Noordeloos for their technical support at the Royal Netherlands Institute for Sea Research (NIOZ).

Conflict of Interest: The authors declare that they have no conflict of interest.

References

Agirbas E, Feyzioglu AM, Kopuz U, Llewellyn CA (2015) Phytoplankton community composition in the south-eastern Black Sea determined with pigments measured by HPLC-CHEMTAX analyses and microscopy cell counts. J Mar Biol Assoc United Kingdom 95:35–52. doi: 10.1017/S0025315414001040

Agustí S, Duarte CM (2013) Phytoplankton lysis predicts dissolved organic carbon release in marine plankton communities. Biogeosciences 10:1259–1264. doi: 10.5194/bg-10-1259-2013

Alderkamp AC, Mills MM, van Dijken GL, et al (2012) Iron from melting glaciers fuels phytoplankton blooms in the Amundsen Sea (Southern Ocean): Phytoplankton characteristics and productivity. Deep Res Part II Top Stud Oceanogr 71–76:32–48. doi: 10.1016/j.dsr2.2012.03.005

Álvarez E, Nogueira E, López-Urrutia Á (2017) In vivo single-cell fluorescence and size scaling of phytoplankton chlorophyll content. Appl Environ Microbiol 83:1–16. doi: 10.1128/aem.03317-16

Annett AL, Carson DS, Crosta X, et al (2010) Seasonal progression of diatom assemblages in surface waters of Ryder Bay, Antarctica. Polar Biol 33:13–29. doi: 10.1007/s00300-009-0681-7

Arrigo KR (2003) Physical control of chlorophyll *a* , POC, and TPN distributions in the pack ice of the Ross Sea, Antarctica. J Geophys Res 108:3316. doi: 10.1029/2001JC001138

Atkinson A, Siegel V, Pakhomov EA, Rothery P (2004) Long-term decline in krill stock and increase in salps within the Southern Ocean. Nature 432:100–103. doi: 10.1038/nature02950.1.

Atkinson A, Whitehouse MJ (2000) Ammonium excretion by Antarctic krill *Euphausia superba* at South Georgia. Limnol Oceanogr 45:1012–1012. doi: 10.4319/lo.2000.45.4.1012

Bates SS, Cota GF (1986) Fluorescence induction and photosynthetic response of Arctic ice algae to sample treatment and salinity. J Phycol 22:421–429. doi: 10.1111/j.1529-8817.1986.tb02484.x

Beardall J, Stojkovic S (2006) Microalgae under global environmental change: Implications for growth and productivity, populations and trophic flow. ScienceAsia 32(s1):001. doi: 10.2306/scienceasia1513-1874.2006.32(s1).001

Bown J, Laan P, Ossebaar S, et al (2017) Bioactive trace metal time series during Austral summer in Ryder Bay, Western Antarctic Peninsula. Deep Sea Res Part II Top Stud Oceanogr 139:103–119. doi: 10.1016/j.dsr2.2016.07.004

Boyce DG, Lewis MR, Worm B (2010) Global phytoplankton decline over the past century. Nature 466:591–596. doi: 10.1038/nature09268

Brussaard CPD (2004) Viral control of phytoplankton populations-A review. J Eukaryot Microbiol 51:125–138. doi: 10.1111/j.1550-7408.2004.tb00537.x

Brussaard CPD, Gast GJ, Van Duyl FC, Riegman R (1996) Impact of phytoplankton bloom magnitude on a pelagic microbial food web. Mar Ecol Prog Ser 144:211–221. doi: 10.3354/meps144211

Brussaard CPD, Peperzak L, Beggah S, et al (2016) Immediate ecotoxicological effects of short-lived oil spills on marine biota. Nat Commun 7:1–11. doi: 10.1038/ncomms11206

Buma AGJ, Gieskes WWC, Thomsen HA (1992) Abundance of Cryptophyceae and chlorophyll b-containing organisms in the Weddell-Scotia Confluence area in the spring of 1988. Polar Biol 12:43–52. doi: 10.1007/BF00239964

Buma AGJ, Noordeloos AAM, Larsen J (1993) Strategies and kinetics of photoacclimation in three Antarctic nanophytoflagellates. J Phycol 29:407–417. doi: 10.1111/j.1529-8817.1993.tb00141.x

Christaki U, Obernosterer I, Van Wambeke F, et al (2008) Microbial food web structure in a naturally iron-fertilized area in the Southern Ocean (Kerguelen Plateau). Deep Res Part II Top Stud Oceanogr 55:706–719. doi: 10.1016/j.dsr2.2007.12.009

Clarke A, Meredith MP, Wallace MI, et al (2008) Seasonal and interannual variability in temperature, chlorophyll and macronutrients in northern Marguerite Bay, Antarctica. Deep Res Part II Top Stud Oceanogr 55:1988–2006. doi: 10.1016/j.dsr2.2008.04.035

Conan P, Søndergaard M, Kragh T, et al (2007) Partitioning of organic production in marine plankton communities: The effects of inorganic nutrient ratios and community composition on new dissolved organic matter. Limnol Oceanogr 52:753–765. doi: 10.4319/lo.2007.52.2.0753

Deppeler SL, Davidson AT (2017) Southern Ocean phytoplankton in a changing climate. Front Mar Sci 4:. doi: 10.3389/fmars.2017.00040

DiTullio GR, Garcia N, Riseman SF, Sedwick PN (2007) Effects of iron concentration on pigment composition in *Phaeocystis antarctica* grown at low irradiance. Biogeochemistry 83:71–81. doi: 10.1007/s10533-007-9080-8

Eiler A, Drakare S, Bertilsson S, et al (2013) Unveiling distribution patterns of freshwater phytoplankton by a next generation sequencing based approach. PLoS One 8:1–10. doi: 10.1371/journal.pone.0053516

Evans C, Brandsma J, Pond DW, et al (2017) Drivers of interannual variability in virioplankton abundance at the coastal western Antarctic peninsula and the potential effects of climate change. Environ Microbiol 19:740–755. doi: 10.1111/1462-2920.13627

Eveleth R, Cassar N, Sherrell RM, et al (2017) Ice melt influence on summertime net community production along the Western Antarctic Peninsula. Deep Res Part II Top Stud Oceanogr 139:89–102. doi: 10.1016/j.dsr2.2016.07.016

Falkowski PG, Oliver MJ (2007) Mix and match: How climate selects phytoplankton. Nat Rev Microbiol 5:966–966. doi: 10.1038/nrmicro1792

Finkel Z V., Beardall J, Flynn KJ, et al (2010) Phytoplankton in a changing world: Cell size and elemental stoichiometry. J Plankton Res 32:119–137. doi: 10.1093/plankt/fbp098

Froneman PW, Perissinotto R (1996) Microzooplankton grazing and protozooplankton community structure in the South Atlantic and in the Atlantic sector of the Southern Ocean. Deep Sea Res Part I Oceanogr Res Pap 43:703–721. doi: 10.1016/0967-0637(96)00010-6

Garibotti IA, Vernet M, Kozlowski WA, Ferrario ME (2003) Composition and biomass of phytoplankton assemblages in coastal Antarctic waters: A comparison of chemotaxonomic and microscopic analyses. Mar Ecol Prog Ser 247:27–42. doi: 10.3354/meps247027

Garibotti IA, Vernet M, Smith RC, Ferrario ME (2005) Interannual variability in the distribution of the phytoplankton standing stock across the seasonal sea-ice zone west of the Antarctic Peninsula. J Plankton Res 27:825–843. doi: 10.1093/plankt/fbi056

Garrison DL, Buck KR, Fryxell GA (1987) Algal assemblages in Antarctic pack ice and in ice-edge plankton. J Phycol 23:564–572. doi: 10.1111/j.1529-8817.1987.tb04206.x

Garrison DL, Gowing MM, Hughes MP, et al (2000) Microbial food web structure in the Arabian Sea: A US JGOFS study. Deep Sea Res Part II Top Stud Oceanogr 47:1387–1422. doi: 10.1016/S0967-0645(99)00148-4

Geider RJ (1987) Light and temperature dependence of the carbon to chlorophyll a ratio in microalgae and cyanobacteria: Implications for physiology and growth of phytoplankton. New Phytol 106:1–34. doi: 10.1111/j.1469-8137.1987.tb04788.x

Goeyens L (1991) Ammonium regeneration in the Scotia-Weddell Confluence area during spring 1988. Mar Ecol Prog Ser 78:241–252. doi: 10.3354/meps078241

Gonçalves-Araujo R, de Souza MS, Tavano VM, Garcia CAE (2015) Influence of oceanographic features on spatial and interannual variability of phytoplankton in the Bransfield Strait, Antarctica. J Mar Syst 142:1–15. doi: 10.1016/j.jmarsys.2014.09.007

Granéli E, Granéli W, Rabbani MM, et al (1993) The influence of copepod and krill grazing on the species composition of phytoplankton communities from the Scotia Weddell sea. Polar Biol 13:201–213. doi: 10.1007/BF00238930

Haberman KL, Quetin LB, Ross RM (2003) Diet of the Antarctic krill (*Euphausia superba* Dana). J Exp Mar Bio Ecol 283:79–95. doi: 10.1016/S0022-0981(02)00466-5

Hallegraeff GM (2010) Ocean climate change, phytoplankton community responses, and harmful algal blooms: A formidable predictive challenge. J Phycol 46:220–235. doi: 10.1111/j.1529-8817.2010.00815.x

Harbison GR, McAlister VL, Gilmer RW (1986) The response of the salp, *Pegea confoederata*, to high levels of particulate material: Starvation in the midst of plenty1. Limnol Oceanogr 31:371–382.

doi: 10.4319/lo.1986.31.2.0371

Hashihama F, Hirawake T, Kudoh S, et al (2008) Size fraction and class composition of phytoplankton in the Antarctic marginal ice zone along the 140°E meridian during February–March 2003. Polar Sci 2:109–120. doi: 10.1016/j.polar.2008.05.001

Head EJH, Harris LR (1994) Feeding selectivity by copepods grazing on natural mixtures of phytoplankton determined by HPLC analysis of pigments. Mar Ecol Prog Ser 110:75–84. doi: 10.3354/meps110075

Henley SF, Schofield OM, Hendry KR, et al (2019) Variability and change in the west Antarctic Peninsula marine system: Research priorities and opportunities. Prog Oceanogr 173:208–237. doi: 10.1016/j.pocean.2019.03.003

Jacques G, Panouse M (1991) Biomass and composition of size fractionated phytoplankton in the Weddell-Scotia confluence area. Polar Biol 11:315–328. doi: 10.1007/BF00239024

Jin M, Deal C, Wang J, et al (2007) Ice-associated phytoplankton blooms in the southeastern Bering Sea. Geophys Res Lett 34:1–6. doi: 10.1029/2006GL028849

Johnson ZI, Martiny AC (2015) Techniques for quantifying phytoplankton biodiversity. Ann Rev Mar Sci 7:299–324. doi: 10.1146/annurev-marine-010814-015902

Kennedy F, McMinn A, Martin A (2012) Effect of temperature on the photosynthetic efficiency and morphotype of *Phaeocystis antarctica*. J Exp Mar Bio Ecol 429:7–14. doi: 10.1016/j.jembe.2012.06.016

Kim H, Ducklow HW, Abele D, et al (2018) Correction to 'Inter-decadal variability of phytoplankton biomass along the coastal West Antarctic Peninsula.' Philos Trans R Soc A Math Phys Eng Sci 376:20180170. doi: 10.1098/rsta.2018.0170

Kopczynska EE (1992) Dominance of microflagellates over diatoms in the Antarctic areas of deep vertical mixing and krill concentrations. J Plankton Res 14:1031–1054. doi: 10.1093/plankt/14.8.1031

Kozlowski WA, Deutschman D, Garibotti I, et al (2011) An evaluation of the application of CHEMTAX to Antarctic coastal pigment data. Deep Res Part I Oceanogr Res Pap 58:350–364. doi: 10.1016/j.dsr.2011.01.008

Kropuenske LR, Mills MM, van Dijken GL, et al (2009) Photophysiology in two major Southern Ocean phytoplankton taxa: Photoprotection in *Phaeocystis antarctica* and *Fragilariopsis cylindrus*. Limnol Oceanogr 54:1176–1196. doi: 10.4319/lo.2009.54.4.1176

Lee Y, Yang EJ, Park J, et al (2016) Physical-biological coupling in the Amundsen Sea, Antarctica: Influence of physical factors on phytoplankton community structure and biomass. Deep Sea Res Part I Oceanogr Res Pap 117:51–60. doi: 10.1016/j.dsr.2016.10.001

Li WKW, Dickie PM (2001) Monitoring phytoplankton, bacterioplankton, and virioplankton in a coastal inlet (Bedford Basin) by flow cytometry. Cytometry 44:236–246. doi: 10.1002/1097-0320(20010701)44:3<236::AID-CYTO1116>3.0.CO;2-5

Llewellyn CA, Fishwick JR, Blackford JC (2005) Phytoplankton community assemblage in the English Channel: A comparison using chlorophyll *a* derived from HPLC-CHEMTAX and carbon derived from microscopy cell counts. J Plankton Res 27:103–119. doi: 10.1093/plankt/fbh158

Loeb VJ, Siegel V, Holm-Hansen O, et al (1997) Effects of sea-ice extent and krill or salp dominance on the Antarctic food web. Nature 387:879–900. doi: 10.1038/43174

Maat DS, Biggs TEG, Evans C, et al (2017) Characterization and temperature dependence of arctic *Micromonas polaris* viruses. Viruses 9:6–9. doi: 10.3390/v9060134

Mackey MD, Mackey DJ, Higgins HW, Wright SW (1996) CHEMTAX - A program for estimating class abundances from chemical markers: Application to HPLC measurements of phytoplankton. Mar Ecol Prog Ser 144:265–283. doi: 10.3354/meps144265

Marañón E (2015) Cell size as a key determinant of phytoplankton metabolism and community structure. Ann Rev Mar Sci 7:241–64. doi: 10.1146/annurev-marine-010814-015955

Marie D, Partensky F, Vaulot D, Brussaard CPD (2001) Enumeration of phytoplankton, bacteria, and viruses in marine samples. Curr Protoc Cytom 10:11.11.1-11.11.15. doi: 10.1002/0471142956.cy1111s10

Massana R, Gobet A, Audic S, et al (2015) Marine protist diversity in European coastal waters and sediments as revealed by high-throughput sequencing. Environ Microbiol 17:4035–4049. doi: 10.1111/1462-2920.12955

Mendes CRB, Tavano VM, Dotto TS, et al (2017) New insights on the dominance of cryptophytes in

Antarctic coastal waters: A case study in Gerlache Strait. Deep Sea Res Part II Top Stud Oceanogr 149:161–170. doi: 10.1016/j.dsr2.2017.02.010

Mendes CRB, Tavano VM, Leal MC, et al (2013) Shifts in the dominance between diatoms and cryptophytes during three late summers in the Bransfield Strait (Antarctic Peninsula). Polar Biol 36:537–547. doi: 10.1007/s00300-012-1282-4

Mojica KDA, Huisman J, Wilhelm SW, Brussaard CPD (2016) Latitudinal variation in virus-induced mortality of phytoplankton across the North Atlantic Ocean. ISME J 10:500–513. doi: 10.1038/ismej.2015.130

Moline M a, Prezelin BB (1996) Long-term monitoring and analyses of physical factors regulating variability in coastal Antarctic phytoplankton composition over seasonal and interannual timescales. Mar Ecol Prog Ser 145:143–160. doi: 10.3354/Meps145143

Moline MA, Claustre H, Frazer TK, et al (2004) Alteration of the food web along the Antarctic Peninsula in response to a regional warming trend. Glob Chang Biol 10:1973–1980. doi: 10.1111/j.1365-2486.2004.00825.x

Moline MA, Prezelin BB, Schofield OM, Smith RC (1997) Temporal dynamics of coastal Antarctic phytoplankton: Environmental driving forces and impact of a 1991/92 summer diatom bloom on the nutrient regimes. In: Battaglia B, Valencia H, Walton DWH (eds) Antarctic communities: Species, structure and survival. Cambridge University Press, pp 67–72

Montagnes DJS, Berges JA, Harrison PJ, Taylor FJR (1994) Estimating carbon, nitrogen, protein, and chlorophyll *a* from volume in marine phytoplankton. Limnol Oceanogr 39:1044–1060. doi: 10.4319/lo.1994.39.5.1044

Montagnes DJS, Franklin M (2001) Effect of temperature on diatom volume, growth rate, and carbon and nitrogen content: Reconsidering some paradigms. Limnol Oceanogr 46:2008–2018. doi: 10.4319/lo.2001.46.8.2008

Montes-Hugo M, Doney SC, Ducklow HW, et al (2009) Recent changes in phytoplankton communities associated with rapid regional climate change along the western Antarctic Peninsula. Science (80-) 323:1470–1473. doi: 10.1126/science.1164533

Moreau S, Mostajir B, Bélanger S, et al (2015) Climate change enhances primary production in the western Antarctic Peninsula. Glob Chang Biol 21:2191–2205. doi: 10.1111/gcb.12878

Obernosterer I, Christaki U, Lefèvre D, et al (2008) Rapid bacterial mineralization of organic carbon produced during a phytoplankton bloom induced by natural iron fertilization in the Southern Ocean. Deep Res Part II Top Stud Oceanogr 55:777–789. doi: 10.1016/j.dsr2.2007.12.005

Oksanen J, Blanchet FG, Friendly M, et al (2013) Vegan: Community ecology package. R Packag version 23-2 https://CRAN.R-project.org/package=vegan

Perissinotto R, A. Pakhomov E (1998) The trophic role of the tunicate *Salpa thompsoni* in the Antarctic marine ecosystem. J Mar Syst 17:361–374. doi: 10.1016/S0924-7963(98)00049-9

Petrou K, Hill R, Doblin MA, et al (2011) Photoprotection of sea-ice microalgal communities from the east antarctic pack ice. J Phycol 47:77–86. doi: 10.1111/j.1529-8817.2010.00944.x

Piedade GJ, Wesdorp EM, Borbolla EM, Maat DS (2018) Influence of irradiance and temperature on the virus MpoV-45T infecting the Arctic picophytoplankter *Micromonas polaris*. Viruses 1–17. doi: 10.3390/v10120676

Pinhassi J, Sala MM, Havskum H, et al (2004) Changes in bacterioplankton composition under different phytoplankton regimens. Appl Environ Microbiol 70:6753–6766. doi: 10.1128/AEM.70.11.6753-6766.2004

Quetin LB, Ross RM (1985) Feeding by Antarctic krill, *Euphausia superba*: Does size matter? In: W.R. S, P.R. C, R.M. L (eds) Antarctic Nutrient Cycles and Food Webs. Springer Berlin Heidelberg, pp 372–377

Riegman R, Kuipers BR, Noordeloos AAM, Witte HJ (1993) Size-differential control of phytoplankton and the structure of plankton communities. Netherlands J Sea Res 31:255–265. doi: 10.1016/0077-7579(93)90026-O

Robinson DH, Arrigo KR, Iturriaga R, Sullivan CW (1995) Microalgal light-harvesting in extreme low-light environments in McMurdo Sound, Antarctica. J Phycol 31:508–520. doi: 10.1111/j.1529-8817.1995.tb02544.x

Robinson DH, Kolber Z, Sullivan CW (1997) Photophysiology and photoacclimation in surface sea ice algae from McMurdo Sound, Antarctica. Mar Ecol Prog Ser 147:243–256. doi: 10.3354/meps147243

2

Rodriguez F, Varela M, Zapata M (2002) Phytoplankton assemblages in the Gerlache and Bransfield Straits (Antarctic Peninsula) determined by light microscopy and CHEMTAX analysis of HPLC pigment data. Deep Sea Res Part II Top Stud Oceanogr 49:723–747. doi: 10.1016/S0967-0645(01)00121-7

Rose JM, Feng Y, DiTullio GR, et al (2009) Synergistic effects of iron and temperature on Antarctic phytoplankton and microzooplankton assemblages. Biogeosciences 6:3131–3147. doi: 10.5194/bg-6-3131-2009

Rozema PD, Biggs T, Sprong PAA, et al (2017a) Summer microbial community composition governed by upper-ocean stratification and nutrient availability in northern Marguerite Bay, Antarctica. Deep Res Part II Top Stud Oceanogr 139:151–166. doi: 10.1016/j.dsr2.2016.11.016

Rozema PD, Kulk G, Veldhuis MP, et al (2017b) Assessing drivers of coastal primary production in northern Marguerite Bay, Antarctica. Front Mar Sci 4:1–20. doi: 10.3389/fmars.2017.00184

Rozema PD, Venables HJ, van de Poll WH, et al (2017c) Interannual variability in phytoplankton biomass and species composition in northern Marguerite Bay (West Antarctic Peninsula) is governed by both winter sea ice cover and summer stratification. Limnol Oceanogr 62:235–252. doi: 10.1002/lno.10391

Saba GK, Fraser WR, Saba VS, et al (2014) Winter and spring controls on the summer food web of the coastal West Antarctic Peninsula. Nat Commun 5:4318. doi: 10.1038/ncomms5318

Schoemann V, Becquevort S, Stefels J, et al (2005) *Phaeocystis* blooms in the global ocean and their controlling mechanisms: A review. J Sea Res 53:43–66. doi: 10.1016/j.seares.2004.01.008

Schofield O, Brown M, Kohut J, et al (2018) Changing upper ocean mixed layer depth and phytoplankton productivity along the West Antarctic Peninsula. Phil Trans R Soc A. doi: 10.1098/rsta.2017.0173

Schofield O, Ducklow HW, Martinson DG, et al (2010) How do polar marine ecosystems respond to rapid climate change? Science (80-) 328:1520–1523. doi: 10.1126/science.1185779

Smetacek V, Nicol S (2005) Polar ocean ecosystems in a changing world. Nature 437:362–368. doi: 10.1038/nature04161

Steinberg DK, Ruck KE, Gleiber MR, et al (2015) Long-term (1993-2013) changes in macrozooplankton off the Western Antarctic Peninsula. Deep Res Part I Oceanogr Res Pap 101:54–70. doi: 10.1016/j.dsr.2015.02.009

Suzuki Y, Takahashi M (1995) Growth responses of several diatom species isolated from various environments to temperature. J Phycol 31:880–888. doi: 10.1111/j.0022-3646.1995.00880.x

Timmermans KR, Davey MS, Van der Wagt B, et al (2001) Co-limitation by iron and light of *Chaetoceros brevis, C. dichaeta and C. calcitrans* (Bacillariophyceae). Mar Ecol Prog Ser 217:287–297. doi: 10.3354/meps217287

Van De Poll WH, Lagunas M, De Vries T, et al (2011) Non-photochemical quenching of chlorophyll fluorescence and xanthophyll cycle responses after excess PAR and UVR in *Chaetoceros brevis, Phaeocystis antarctica* and coastal Antarctic phytoplankton. Mar Ecol Prog Ser 426:119–131. doi: 10.3354/meps09000

Van Leeuwe MA, Visser RJW, Stefels J (2014) The pigment composition of *Phaeocystis antarctica* (Haptophyceae) under various conditions of light, temperature, salinity, and iron. J Phycol 50:1070–1080. doi: 10.1111/jpy.12238

Vaulot D (1989) CYTOPC: Processing software for flow cytometric data. Signal and Noise 2:8

Veldhuis MJW, Kraay GW (2004) Phytoplankton in the subtropical Atlantic Ocean: Towards a better assessment of biomass and composition. Deep Res Part I Oceanogr Res Pap 51:507–530. doi: 10.1016/j.dsr.2003.12.002

Venables HJ, Clarke A, Meredith MP (2013) Wintertime controls on summer stratification and productivity at the western Antarctic Peninsula. Limnol Oceanogr 58:1035–1047. doi: 10.4319/lo.2013.58.3.1035

Verity PG, Smayda TJ (1989) Nutritional value of *Phaeocystis pouchetii* (Prymnesiophyceae) and other phytoplankton for *Acartia* spp. (Copepoda): Ingestion, egg production, and growth of nauplii. Mar Biol 100:161–171. doi: 10.1007/BF00391955

Visco JA, Apothéloz-Perret-Gentil L, Cordonier A, et al (2015) Environmental monitoring: Inferring the diatom index from next-generation sequencing data. Environ Sci Technol 49:7597–7605. doi: 10.1021/es506158m

Worden AZ, Nolan JK, Palenik B (2004) Assessing the dynamics and ecology of marine

picophytoplankton: The importance of the eukaryotic component. Limnol Oceanogr 49:168–179. doi: 10.4319/lo.2004.49.1.0168

Wulff A, Wängberg S-Å (2004) Spatial and vertical distribution of phytoplankton pigments in the eastern Atlantic sector of the Southern Ocean. Deep Sea Res Part II Top Stud Oceanogr 51:2701–2713. doi: 10.1016/j.dsr2.2001.01.002

Yang EJ, Jiang Y, Lee SH (2016) Microzooplankton herbivory and community structure in the Amundsen Sea, Antarctica. Deep Res Part II Top Stud Oceanogr 123:58–68. doi: 10.1016/j.dsr2.2015.06.001

Zuur AF, Ieno EN, Elphick CS (2010) A protocol for data exploration to avoid common statistical problems. Methods Ecol Evol 1:3–14. doi: 10.1111/j.2041-210X.2009.00001.x

Zuur AF, Ieno EN, Walker N, et al (2009) Mixed effects models and extensions in ecology with R. Springer New York, New York, NY

2

Supplementary Figures
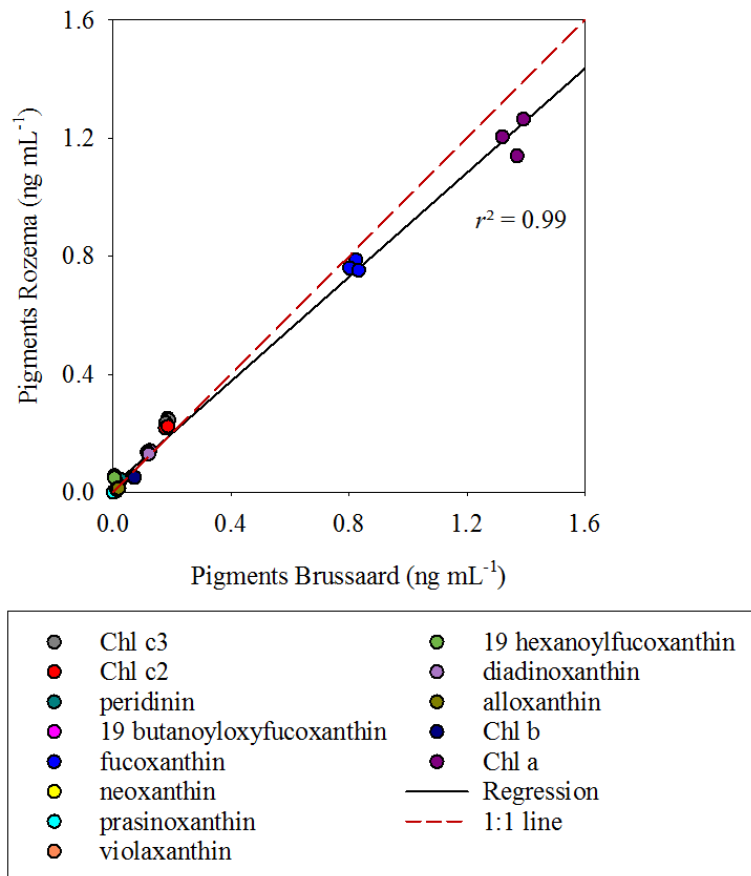
Fig. S1. Pigment extraction efficiency comparison between method of Brussaard et al 2016 (Pigments Brussaard) and method of Rozema et al 2017a (Pigments Rozema). 13 pigments, extracted from natural samples collected in situ, were compared in triplicate. Both linear regression line (solid black; $p < 0.0001$, $R^2 = 0.99$, $n = 39$) and 1:1 line (red dashed) are included.

2
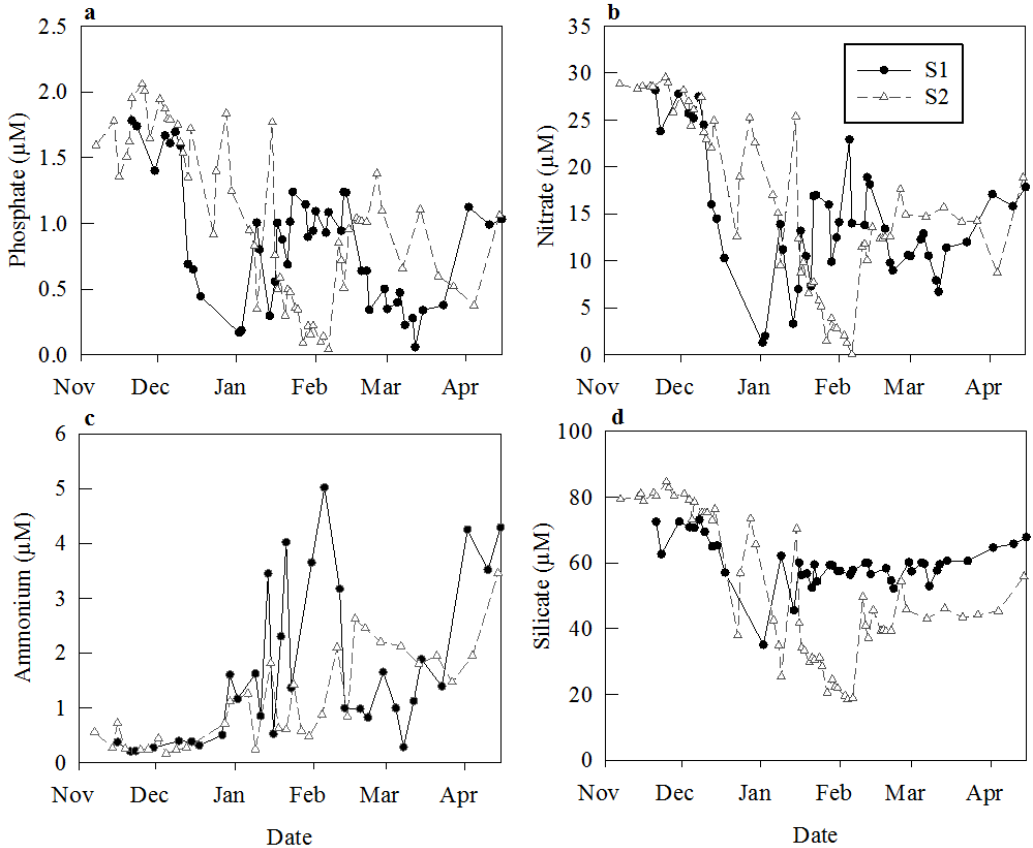
Fig. S2. Concentrations of dissolved inorganic nutrients (a) phosphate, (b) nitrate, (c) ammonium and (d) silicate at the RaTS monitoring site, Ryder Bay during two consecutive years, S1 (circles, solid line) and S2 (triangles, dotted line).
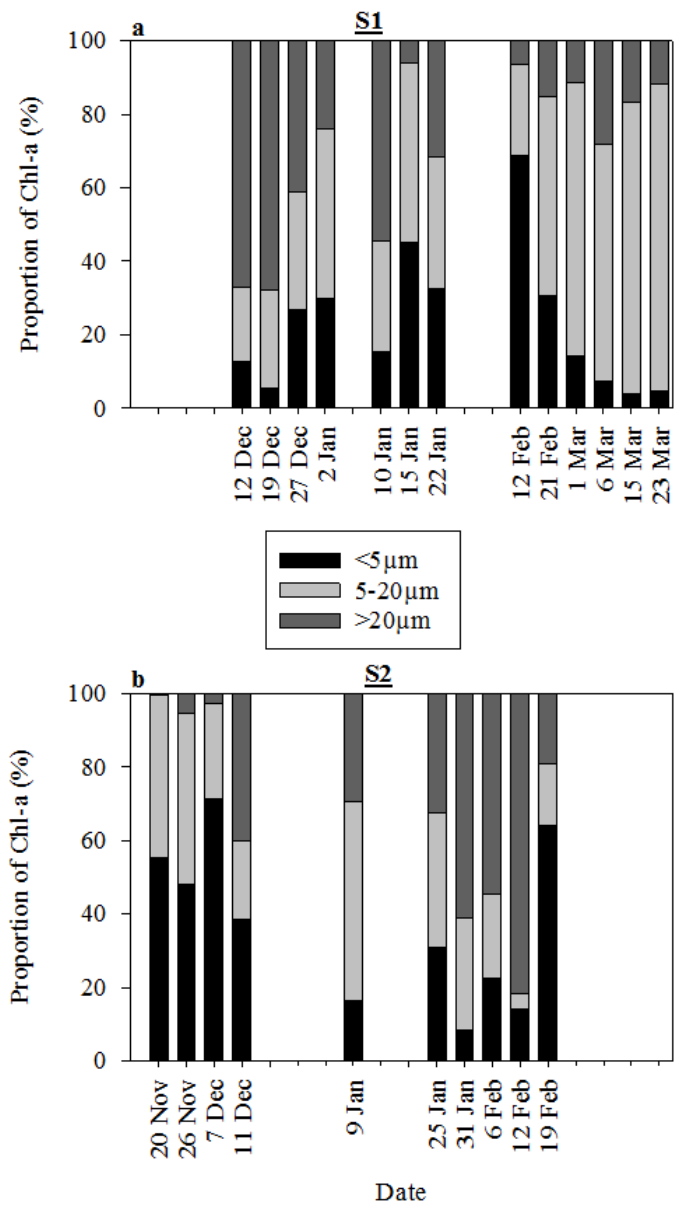
Fig. S3. Fractionated Chl-*a* concentration for size fractions <5 µm, 5-20 µm and >20 µm in (a) S1 and (b) S2.
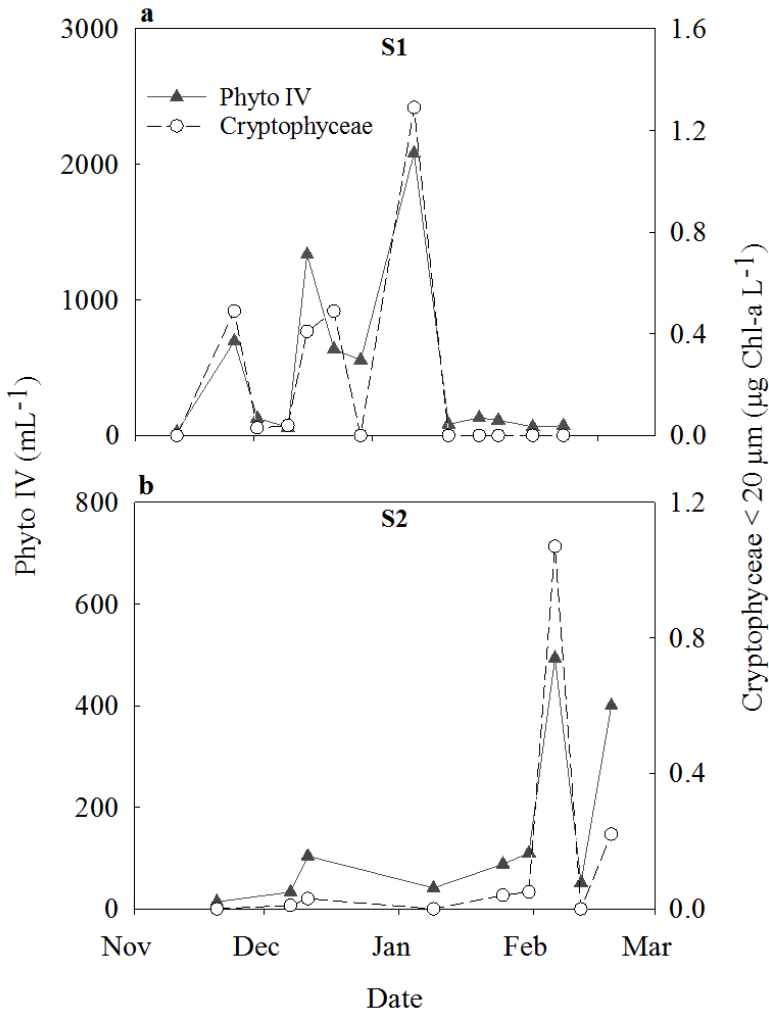
Fig. S4. Temporal variation in Phyto IV abundances (as measured by FCM) and <20 µm Cryptophyceae Chl-*a* (as measured by HPLC) in (a) S1 and (b) S2.
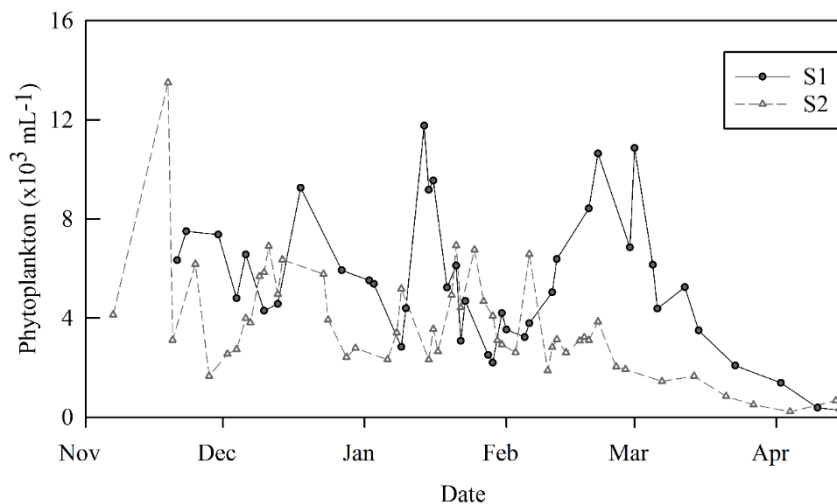
Fig. S5. Time series of total phytoplankton abundance during 2 consecutive years, S1 (circles, solid line) and S2 (triangles, dotted line) counted by flow cytometry (FCM).
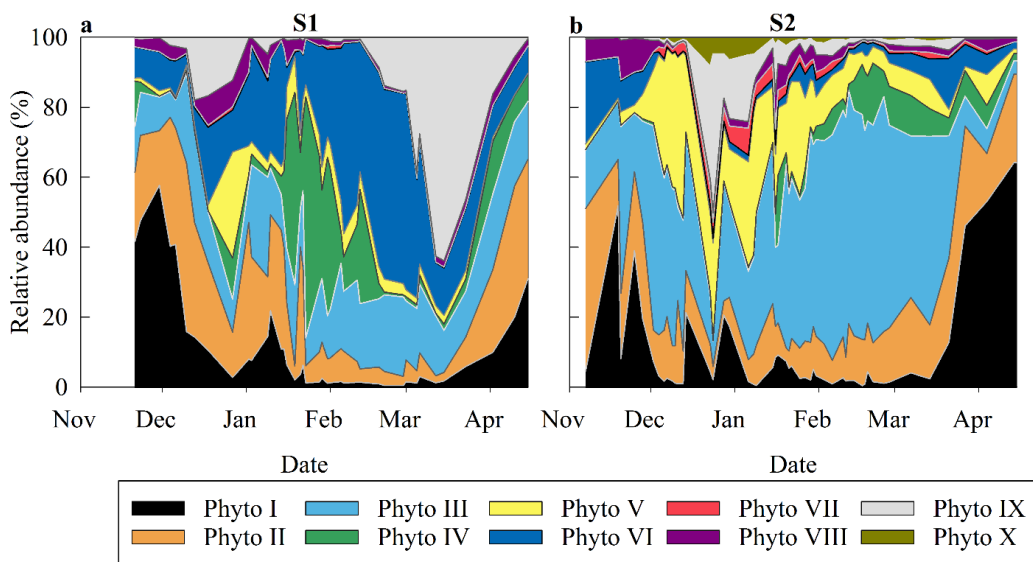
Fig. S6. Temporal variation in the relative proportion (%) of each flow cytometric phytoplankton group (Phyto I - X) in (a) S1 and (b) S2.
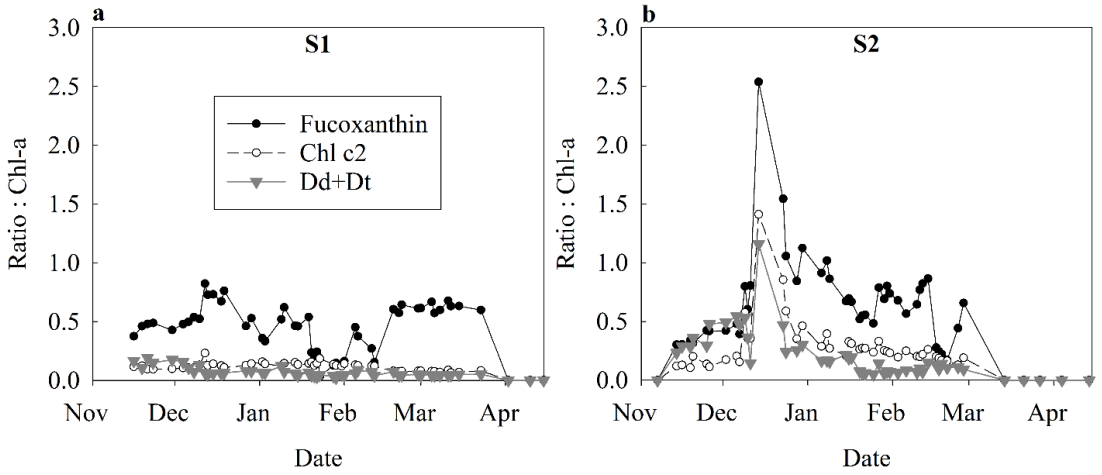
Fig. S7. Seasonal dynamics in the ratio of Fucoxanthin, Chlorophyll c2 (Chl c2) and Diadinoxanthin+Diatoxanthin (Dd+Dt) to Chl-*a* in (a) S1 and (b) S2.
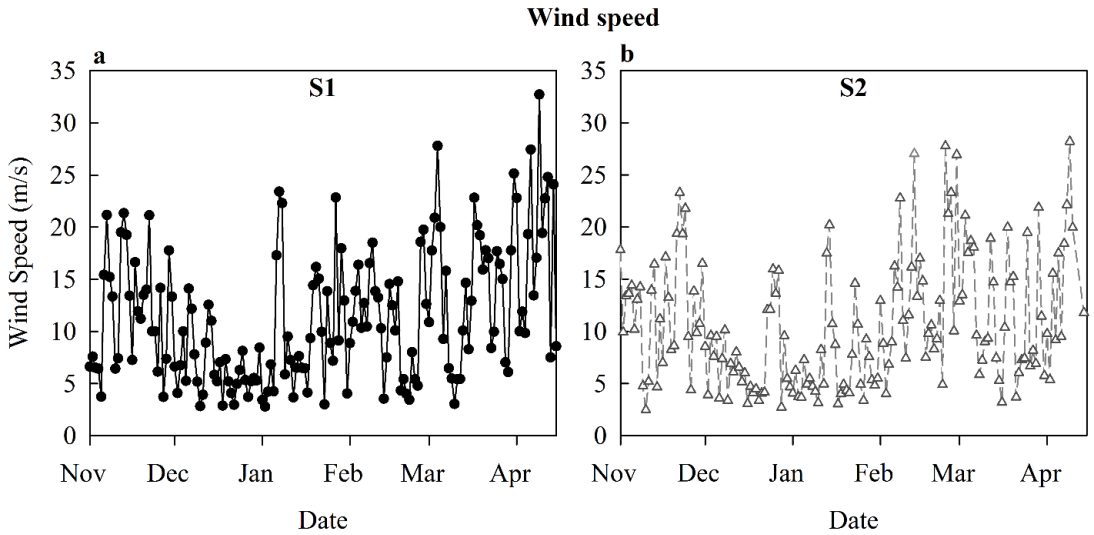
Fig. S8. Average (24h) daily wind speed measured at the weather station on Rothera base in (a) S1 and (b) S2.
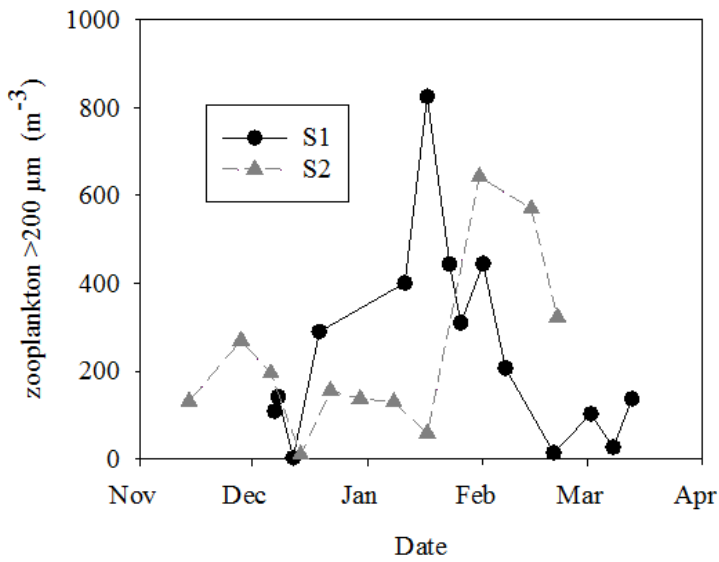
Fig. S9. Time series of total meso-zooplankton abundance (> 200 µm) at the sampling site from shallow water (200 – 0 m) net hauls for S1 (black circles and line) and S2 (grey triangle and dashed line).

Supplementary Tables

Table S1. Initial pigment ratio matrix (top, *n* = 101) included in the CHEMTAX analysis constructed using ratios taken from literature and a diatom (*Proboscia* sp.) isolate. Two types of Prymnesiophyceae were included to accommodate the high plasticity in pigment composition of *Phaeocystis* sp. under high light/low light and/or high/low iron conditions (DiTullio et al. 2007). Additionally, two types of diatoms were included due to the high abundances of *Pseudonitzschia* sp. and *Proboscia* sp. which both contain *Chlorophyll-c3 (Chl-c3;* unpublished data; Annett et al. 2010). The initial ratio matrix was based on [1]Wright et al. (2009), [2]Wright et al. (2010) and [3]unpublished culture data for Diatoms 2. The bottom section presents the averaged final summer ratios of fractionated and unfractionated samples. Pigment ratios were standardised to 1 unit Chlorophyll-*a* (Chl-*a*). Pigments used in the analysis were Chl-c3, peridinin (Per), 19-butanoyloxyfucoxanthin (19-But), fucoxanthin (Fuco), neoxanthin (Neo), 19-hexanoyloxyfucoxanthin (19-Hex), alloxanthin (Allo), lutein (Lut), chlorophyll b (Chl-b) and Chl-*a*.

2

Initial: Class / Pigment	Chl-c3	Per	19-Buta	Fuco	Neo	19-Hex	Allo	Lut	Chl-b	Chl-*a*
Prasinophyceae	-	-	-	-	0.030[2]	-	-	0.006[2]	0.620	1
Chlorophyceae	-	-	-	-	0.062[2]	-	-	0.220[2]	0.180	1
Dinophyceae	-	1.060[2]	-	-	-	-	-	-	-	1
Cryptophyceae	-	-	-	-	-	-	0.220[2]	-	-	1
Prymnesiophyceae 1	0.130[2]	-	0.120[1]	0.080[2]	-	0.400[2]	-	-	-	1
Prymnesiophyceae 2	0.270[2]	-	0.006[1]	0.010[2]	-	1.100[2]	-	-	-	1
Diatoms 1	-	-	-	0.520[2]	-	-	-	-	-	1
Diatoms 2	0.221[3]	-	-	0.864[2]	-	-	-	-	-	1
Averaged final ratio's										
Prasinophyceae	-	-	-	-	0.026	-	-	0.005	0.651	1
Chlorophyceae	-	-	-	-	0.059	-	-	0.212	0.157	1
Dinophyceae	-	1.089	-	-	-	-	-	-	-	1
Cryptophyceae	-	-	-	-	-	-	0.408	-	-	1
Prymnesiophyceae 1	0.085	-	0.281	0.079	-	0.165	-	-	-	1
Prymnesiophyceae 2	0.242	-	0.005	0.011	-	1.057	-	-	-	1
Diatoms 1	-	-	-	0.712	-	-	-	-	-	1
Diatoms 2	0.234	-	-	0.778	-	-	-	-	-	1

Table S2. Table of model outputs from Canonical Correspondence Analysis (CCA) of Chlorophyll data (Chl-*a*, Chl-C, *n* = 101) and flow cytometry (FCM) data (FCM abundance S1, S2 and FCM-C S1, *n* = 40, S2, *n* = 51). *p* values are shown for environmental variables within each model as well as for the model overall. Eigen values and % variation explained are also indicated for each CCA model.

	CCA / Variables	Chl-*a*	Chl-C	FCM abundance S1	FCM abundance S2	FCM-C S1	FCM-C S2
p values	Temp	<0.001	<0.001	<0.001	<0.001	<0.001	0.004
	Z_{eu}/15m	<0.001	<0.001		<0.001		<0.001
	Salinity	0.058		<0.001	<0.001	0.004	0.003
	PAR			<0.001	0.008	<0.001	<0.001
	Ice type			<0.001	0.010		0.058
	Phosphate	0.005	0.002	<0.001	<0.001		0.002
	Nitrate	0.039		<0.001			
	Ice cover				<0.001		<0.001
	Model	<0.001	<0.001	<0.001	<0.001	<0.001	<0.001
Eigen values	CCA1	0.191	0.286	0.331	0.275	0.350	0.276
	CCA2	0.093	0.010	0.250	0.175	0.103	0.113
	Total	0.826	0.716	1.011	0.792	1.120	0.690
	Constrained	0.292	0.297	0.672	0.566	0.469	0.448
Variation explained (%)	Constrained	35	41	66	71	42	65
	CCA1	23	40	33	35	31	40
	CCA2	11	1	25	22	9	16

Chapter 3

Viral lysis modifies seasonal phytoplankton dynamics and carbon flow in the Southern Ocean

Viral lysis modifies seasonal phytoplankton dynamics and carbon flow in the Southern Ocean

Tristan E.G. Biggs[1,2], Jef Huisman[2] and Corina P.D. Brussaard[1,2]

[1] Department of Marine Microbiology and Biogeochemistry, NIOZ Royal Netherlands Institute for Sea Research, and University of Utrecht, Texel, The Netherlands.
[2] Department of Freshwater and Marine Ecology, Institute for Biodiversity and Ecosystem Dynamics (IBED), University of Amsterdam, Amsterdam, The Netherlands.

Abstract

Phytoplankton form the base of marine food webs and are a primary conduit for carbon export in the Southern Ocean, a key area for global pCO_2 drawdown. Viral lysis and grazing have very different effects on microbial community dynamics and carbon export, yet, very little is known about the relative magnitude and ecological impact of viral lysis on natural phytoplankton communities, especially in Antarctic waters. Here, we report on the temporal dynamics and relative importance of viral lysis rates, in comparison to grazing, for Antarctic phytoplankton of varied taxonomy and size over a full productive season. Our results show that viral lysis is a major loss factor throughout the season, responsible for roughly half of total phytoplankton losses. Viral lysis appeared critically important for explaining temporal dynamics and for obtaining a complete seasonal mass balance of Antarctic phytoplankton. Group-specific responses indicated a negative correlation between grazing and viral losses in *Phaeocystis* and picoeukaryotes, while for other phytoplankton groups losses were more evenly spread throughout the season. Cryptophyte mortality was dominated by viral lysis, whereas small diatoms were mostly grazed. Larger diatoms dominated algal carbon flow and singular lysis events could direct as much as 18% of total seasonal carbon production away from higher trophic levels. This study highlights the need to consider viral lysis of key Antarctic phytoplankton for a better understanding of microbial community interactions and more accurate predictions of organic matter flux in this climate-sensitive region.

3

Introduction

Phytoplankton blooms are the net result of gross growth minus losses (Behrenfeld and Boss 2018) and the type of loss factor determines the flow of carbon and nutrients through the ecosystem (Suttle 2007). Hence, studies that quantify viral lysis and grazing rates, and their functional significance throughout the productive season are greatly warranted. Zooplankton grazing is traditionally viewed as the dominant loss factor of phytoplankton cells (Calbet and Landry 2004), however, phytoplankton are also prone to viral infection (Baudoux et al. 2006; Vardi et al. 2012; Mojica et al. 2016). Indeed, grazing rates do not always control primary production (Safi et al. 2007) and viral lysis may cause the collapse of phytoplankton populations (Bratbak et al. 1993; Brussaard et al. 2005a). In contrast to grazing, viral lysis predominantly channels particulate organic carbon and nutrients away from higher trophic levels (Brussaard et al. 2005b; Suttle 2007). The virus-induced release of host cellular content into surface waters fuels the so-called 'viral shunt' (Wilhelm and Suttle 1999), whereby microbial processing of the released cell material directly affects biogeochemical cycling (Brussaard et al. 2008; Weitz and Wilhelm 2012). All phytoplankton taxonomic groups are prone to infection by viruses (Brussaard and Martínez 2008; Nagasaki 2008; Coy et al. 2018) and the typically high host specificity of the lytic algal viruses can have a further regulatory influence on phytoplankton species succession (Bratbak et al. 1993; Brussaard 2004; Muhling et al. 2005; Haaber and Middelboe 2009). Although temporal variations in the relative magnitude of viral lysis and grazing could directly affect phytoplankton community composition and trophic transfer efficiency, studies on the seasonal dynamics of viral lysis rates in phytoplankton communities are scarce. Moreover, most knowledge on phytoplankton-virus interactions is from temperate oceans and coastal waters, whereas very little is known about the extent to which viral losses may affect phytoplankton populations in the cold, productive waters of the Antarctic (Brussaard et al. 2008, 2013; Evans and Brussaard 2012).

The Southern Ocean is one of the largest carbon sinks of the global ocean (Khatiwala et al. 2013; Frölicher et al. 2015). Its low temperatures are responsible for a relatively

high solubility of carbon dioxide (CO_2) and extensive phytoplankton blooms in the Southern Ocean absorb large amounts of CO_2 for photosynthesis and growth (Bakker et al. 1997; Moreau et al. 2012). Primary production in Antarctic waters directs ecosystem productivity (Ducklow et al. 2012) sustaining large populations of copepods and krill (Shreeve et al. 2002) that in turn provide food for higher trophic levels (marine fish, birds and mammals) (Barrera-Oro 2002; Ducklow et al. 2012; Belton and Thilsted 2014). Portions of primary and secondary production become stored in the ocean interior by the biological carbon pump (Turner 2015) and the formation of deep ocean water masses such as Antarctic Bottom Water and Antarctic Intermediate Water (Gordon 2001; Jacobs 2004). Ocean warming and acidification due to anthropogenic activities have been predicted to impact Antarctic phytoplankton species composition, i.e. by shifting from larger diatoms to smaller-sized flagellates (Moline et al. 2004; Sommer and Lengfellner 2008; Biggs et al. 2019; Petrou et al. 2019), which will directly impact food quality and availability for higher trophic levels in the Antarctic pelagic food web. If this shift in community composition coincides with changes in grazing and viral lysis rates, subsequent changes in the flux of organic matter and energy can be expected, with implications for the biological carbon pump. A detailed seasonal study is therefore required for a better understanding of the ecological role of viral lysis for Antarctic phytoplankton dynamics.

Here we report the seasonal dynamics of viral lysis rates of Antarctic phytoplankton groups, including picoeukaryotes, the prymnesiophyte *Phaeocystis* spp., cryptophytes and diatoms. Our results reveal that viruses not only exert a major control over the population dynamics of these key phytoplankton groups, but that viral lysis is also critically important for obtaining a complete seasonal mass balance. These findings call for a reconsideration of the microbial food web and the efficiency of the biological carbon pump in this climate-sensitive region.

Materials and Methods

Sampling site and procedure

This study was conducted at the Rothera time series site (RaTS, latitude 67.572°S; longitude 68.231°W; Clarke et al. 2008) located in Ryder Bay on the Western Antarctic Peninsula. Samples were taken over a productive season from December 2012 to March 2013. Discrete seawater samples were collected from 15 m depth by a 12 L Niskin bottle deployed from a small boat. Full water column profiles were obtained using a SeaBird 19+ conductivity temperature depth (CTD) instrument supplemented with a LiCor photosynthetically available radiation (PAR) and an in-line fluorescence sensor (WetLabs). Sampling was conducted approximately once per week and processed directly upon return to the research base in a temperature-controlled lab (~0.5-1°C).

Phytoplankton groups

Seawater samples (1-8L) were analysed for Chlorophyll *a* (Chl-*a*) concentration and for other pigments to determine taxonomic composition using high performance liquid chromatography (HPLC; see Biggs et al. 2019 for details).

For phytoplankton enumeration (of single cells), 3.5 mL sub-samples were fixed with 100 µL formaldehyde-hexamine (18v/v:10% w/v) at 4°C for 15-30 minutes, after which they were snap-frozen in liquid nitrogen and stored at -80°C until analysis. Samples were analysed according to Marie et al. (1999) using a Becton Dickinson FACSCalibur flow cytometer equipped with an air-cooled Argon laser with an excitation wavelength of 488 nm (15 mW) and the trigger was set on red fluorescence. Phytoplankton populations ($\leq$ 20 µm) were distinguished using bivariate scatter plots of red Chl-*a* auto-fluorescence versus side scatter. Cryptophytes were discriminated based on their orange phycoerythrin auto-fluorescence (Li and Dickie 2001). The flow cytometry data files were analysed using the freeware CYTOWIN (Vaulot 1989). No indications of chains or colonies were found in the cytograms and no significant difference was found in

phytoplankton population counts between live and fixed samples (Mann-Whitney Rank Sum Test: $n = 44$ and $p = 0.24$).

Over the course of the season 10 phytoplankton populations could be distinguished, Phyto I – X, with average cell diameters of 0.9, 1.8, 3.1, 4.0, 4.5, 4.5, 7.4, 8.1, 11.5 and 20.4 µm (Biggs et al. 2019). The Phyto III population was identified as *Phaeocystis* spp. (based on microscopic identification and resembling temporal dynamics with Prymnesiophyceae), Phyto IV as cryptophytes (based on phycoerythrin orange autofluoscence and microscopy), and Phyto V-X as diatoms (Biggs et al. 2019). The standing stock of Phyto VII and X were consistently low (< 50 mL^{-1}) and were not included for rate analysis.

To estimate phytoplankton carbon (C), phytoplankton rates were first converted into cells and then to cellular C. Cells produced after T days (X_T) and lost (C_T) were integrated using the formulas: $X_T = \frac{\mu_G}{\mu_G - M_T}\left(P_0\, e^{(\mu_G - M_T)T} - P_0\right)$ and $C_T = \frac{M_T}{\mu_G - M_T}\left(P_0\, e^{(\mu_G - M_T)T} - P_0\right)$ where μ_G = gross growth rate, M_T = total mortality rate, P_0 = phytoplankton abundance at time zero and e is the base of the natural logarithm. Virus mediated mortality (M_V) after T days is then $(M_V/M_T)C_T$ and grazing mortality (M_G) $(M_G/M_T)C_T$. The cellular C content of each phytoplankton population was estimated from the average cell diameter and using conversion factors of 237 and 196.5 fg C µm^{-3} for pico- (Phyto I-III) and nano-sized (Phyto IV-IX) phytoplankton populations (Garrison et al. 2000; Worden et al. 2004).

Growth and mortality rates

To determine viral lysis and grazing rates of the identified phytoplankton populations, the predation pressures by micro-zooplankton and viruses were reduced using the modified dilution assay (Mojica et al. 2016). In short, natural seawater was gently passed through a 200-µm mesh to remove larger-sized zooplankton and was then combined (by siphoning into 1L clear polycarbonate bottles) with either 0.45µm (grazer-free) or 30 kDa (grazer and virus-free) filtered seawater at four dilutions (100, 70, 40 and 20% whole water), in triplicate. The 0.45 µm filtrate was prepared by gravity filtration of natural seawater through a 0.45 µm Sartopore capsule filter

with a 0.8 µm pre-filter (Sartopore 2300, Sartorius Stedim Biotech, Göttingen, Germany). The 30-kDa ultra-filtrate was prepared by tangential flow filtration using a polyethersulfone membrane (Vivaflow 200, Sartorius Stedim Biotech, Göttingen, Germany). The dilutions were transferred in the dark to an outdoor flow-through incubator and incubated on a slow turning wheel (~ 0.5 rpm) at in-situ temperature and light conditions (using neutral -density screens) for 24h. Phytoplankton were enumerated at the start and end of the incubation using flow cytometry (see above) and the apparent growth rate was calculated based on the natural logarithm. By using flow cytometry, the loss rates could be specified for each phytoplankton group. The linear regression of the apparent growth rate versus the actual dilution factor provides both specific grazing (0.45 µm series) and grazing + viral lysis (30 kDa series) rates with viral lysis rates derived by subtraction. Actual dilution factors were determined by dividing the total phytoplankton count of the specific dilution (of the 0.45 µm or 30 kDa series) by the average total count of the 100% natural water. The y-axis intercept represented the gross growth rate (μ_{gross}), assuming the sum of grazing and viral lysis of these phytoplankton (≤ 20 µm) to equal total mortality (T_M).

Statistics

According to the modified dilution assay (Baudoux et al. 2006; Mojica et al. 2016), a significant difference from zero for the grazing regression coefficient (0.45 µm series) indicates significant grazing rates, whilst a significant difference between the regression coefficients of the 0.45 µm and 30 kDa series (as tested by analysis of covariance, $p < 0.05$, using R statistical software; R Development Core Team 2012) indicates significant viral lysis rates. A significant difference from zero for the regression coefficients of the 30 kDa series indicates significant gross growth. Throughout the text the plus-minus symbol ($\pm$) represents 1 standard deviation. Significant differences between viral lysis and grazing rates were tested using a two-tailed Student's t-test and a Mann-Whitney U test if data deviated from normality as assessed by the Shapiro-Wilk test (SigmaPlot v14, from Systat Software, Inc., San

Jose California, USA). The strength of the relationship between viral lysis and grazing rates was determined using Pearson's correlation (SigmaPlot v14).

Results and Discussion

Specific phytoplankton viral lysis rates

This study details the specific viral lysis rates for eight different Antarctic phytoplankton populations throughout the entire Austral productive season. To our knowledge, this is the first detailed viral lysis rate study of multiple phytoplankton species during major seasonal changes in plankton community composition and size distribution, not only for coastal waters of the Western Antarctic Peninsula (Fig. S1), but for the entire Southern Ocean.

The temporal dynamics of the different phytoplankton groups (Fig. 1) and total Chlorophyll *a* (Chl-*a*) concentration (Fig. S2) showed that at the start of the productive season (beginning of December) the smaller-sized Phyto I (average cell diameter of 0.9 µm), Phyto II (1.8 µm Ø), and *Phaeocystis antarctica* Phyto III (3.1 µm Ø, (Biggs et al. 2019) were numerically dominant (58, 16 and 10%, respectively). Thereafter, the abundance of the diatom groups (Phyto V, VI, VIII and IX, 4.5-11.5 µm Ø) increased during the 'spring' bloom in the second half of December. The 'spring' bloom was followed by dominance of smaller phytoplankton, particularly cryptophytes Phyto IV (4 µm Ø), driven by the relatively warm austral summer months (Biggs et al. 2019). Later in the productive season (February) when temperature was still relatively high, salinity had become relatively low due to melting ice and light was not yet limiting, *Phaeocystis* Phyto III and diatoms Phyto VI bloomed (Fig. 1). Finally, they were succeeded by diatoms Phyto IX during late summer and austral fall (mid-February to March) when light availability and nutrient (phosphate and nitrate) concentrations declined as a result of shorter daylengths, increased light attenuation and biological nutrient uptake (Biggs et al. 2019).

Overall, specific viral lysis rates were substantial for all phytoplankton groups (Fig. 1 and Table S1), with average lysis rates ranging between 0.23 ± 0.38 ($n = 13$, Phyto VI) and 0.42 ± 0.39 d^{-1} ($n = 9$, Phyto IV). Comparatively high rates of viral lysis
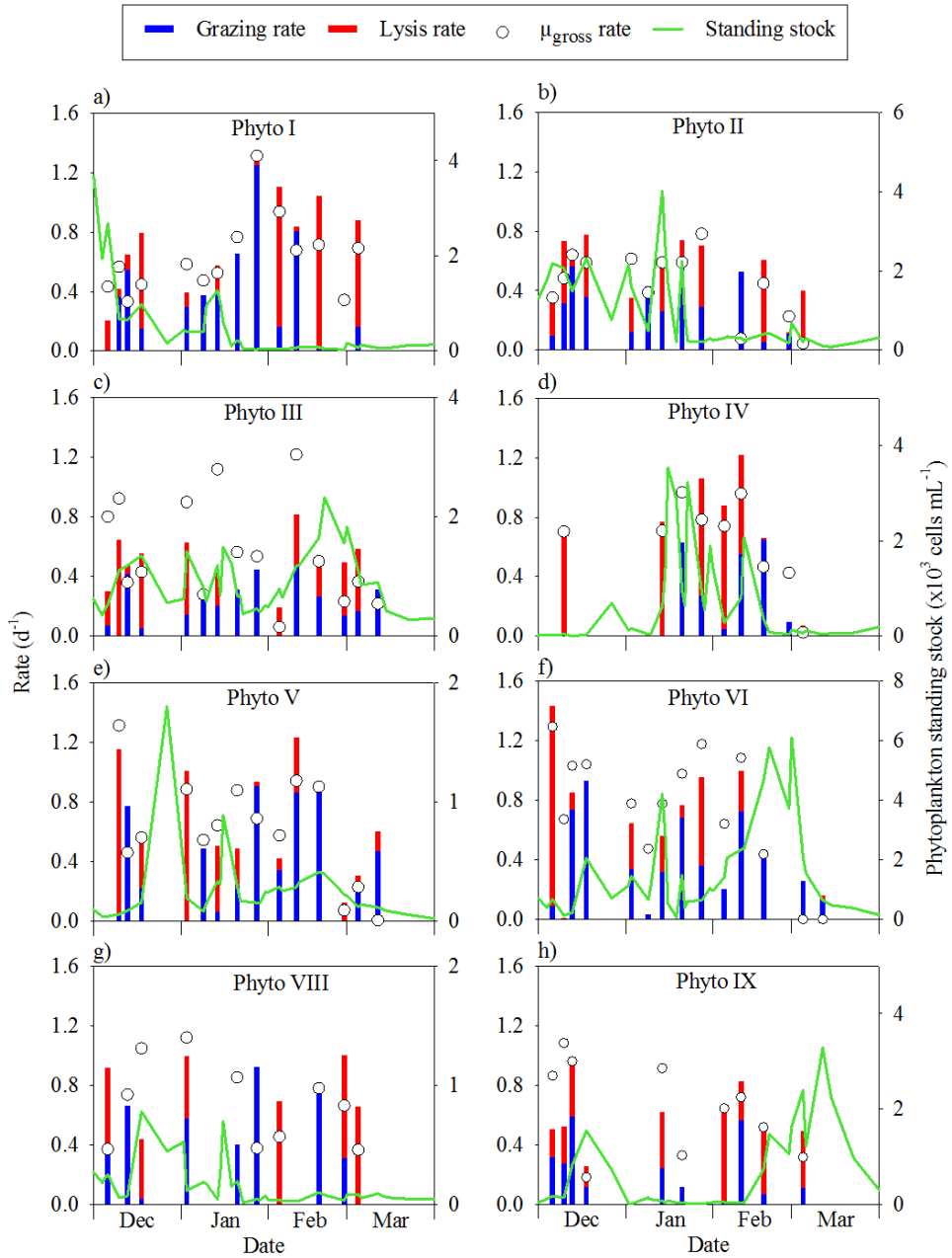
Fig. 1. Seasonal dynamics of phytoplankton standing stock (green line), specific gross growth rate (μ_{gross}; open circles), viral lysis rate (red bars) and grazing rate (blue bars) for different phytoplankton groups distinguished by flow cytometry. The phytoplankton groups include (a,b) picoeukaryotes (Phyto I and II), (c) *Phaeocystis* (Phyto III), (d) cryptophytes (Phyto IV), and (e-h) diatoms of different size classes (Phyto V, VI, VIII and IX). Note that the scale for standing stock (right y-axis) differs between the panels; standing stock data are composed of *n* = 41 data points.

have previously been reported for picoeukaryotic phytoplankton (0.23 to 0.81 d^{-1}) (Baudoux et al. 2007, 2008), for *Phaeocystis globosa* (0.35 d^{-1}) (Baudoux et al. 2006) and for nano-eukaryotes (up to 0.89 d^{-1}) (Mojica et al. 2016). Although diatom populations are known to be infected by viruses (Nagasaki 2008; Tomaru et al. 2009; Kranzler et al. 2019), specific viral lysis rates for natural diatom populations have not yet been reported in the literature. Our results demonstrate that viral lysis of diatoms (i.e., Phyto V, VI, VIII and IX) can be substantial (Fig. 1e-h). They displayed a seasonally average viral lysis rate of 0.29 ± 0.32 d^{-1}, which is almost of equal magnitude as their seasonally averaged grazing rate of 0.35 ± 0.27 d^{-1} (both n = 47; Table S1). Antarctic diatoms often dominate high-biomass phytoplankton blooms and are an important source of primary nutrition as they are major producers of long-chain polyunsaturated fatty acids (such as 20:5ω-3) (Kattner and Hagen 2009). The consumption of diatoms has been reported to increase the sedimentation speed of fecal pellets due to the ballasting effect of biogenic silica (Voss 1991; Ploug et al. 2008). Instead, viral lysis will promote the recycling of dying host cells in surface waters (Lønborg et al. 2013). Recent research, however, has shown that viral lysis may have the potential to also induce aggregate formation and potentially sedimentation (Yamada et al. 2018).

Ecological and seasonal importance of viral lysis

Viral lysis rates varied over the season (Fig. 1a), with Phyto I displaying significantly higher grazing than lysis rates during the first half of the season (average 0.45 ± 0.36 d^{-1} and 0.15 ± 0.20 d^{-1}, respectively; Mann-Whitney U test: $U = 16$, $n_1 = n_2 = 9$, $p = 0.034$). Nutrient depletion, as found at the end of December (Biggs et al. 2019), could have negatively impacted virus production (Maat et al. 2014; Maat and Brussaard 2016), however, nutrient stress was brief due to mixing at the beginning of January. During the second half of the season (February and March), viral lysis appeared to be the dominant loss factor for Phyto I (0.54 ± 0.50 d^{-1} compared to grazing 0.23 ± 0.33 d^{-1}, $n = 5$), which may have contributed to its reduced standing stock (Fig.1a). During the course of the blooms of *Phaeocystis*

Phyto III and cryptophytes Phyto IV, their viral lysis rates were substantial (0.30 ± 0.26 d^{-1} and 0.61 ± 0.35 d^{-1}, respectively; Fig. 1c, d). In contrast to Phyto I, Phyto V experienced high losses by viral lysis during the first half of the season (0.45 ± 0.44 d^{-1}, $n = 7$) whereas during the second half the share of grazing was significantly higher (0.53 ± 0.37 d^{-1} vs lysis 0.12 ± 0.12 d^{-1}; Student's *t*-test: $t_{12} = 2.787$, $n_1 = n_2 = 7$, $p = 0.0164$; Fig. 1e). Unlike Phyto III and IV, viral lysis rates were low for diatom Phyto VI (0.06 ± 0.12 d^{-1}; Fig. 1f) when they reached high abundances in February and March. Similar to Phyto I in the second half of the season, high lysis rates were measured for diatoms Phyto VIII and IX (0.51 ± 0.34 d^{-1} and 0.42 ± 0.14 d^{-1}, respectively; Fig. 1g and h). Temporally separated populations of phytoplankton may exhibit variability in the susceptibility to both viral lysis and grazing depending on the life history of both predator (viruses and grazers) and prey (phytoplankton).

Our results show that high viral lysis rates coincide with low grazing rates and vice versa (Pearson's r = -0.43, $n = 98$, $p < 0.0001$; Fig. 2a), in particular for
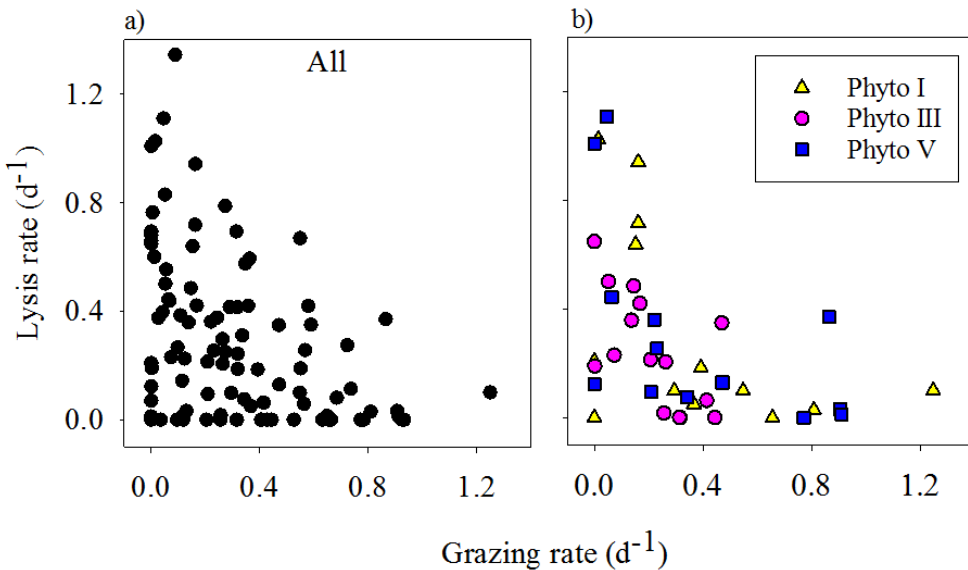
Fig. 2. Specific viral lysis rates are plotted against grazing rates for (a) all phytoplankton groups and (b) phytoplankton groups Phyto I, III and V only.

picoeukaryote Phyto I, *Phaeocystis* Phyto III and diatom Phyto V (Fig. 2b, Table S2). A negative correlation between viral lysis and grazing could arise from bottom-up control on algal host cell physiology but may also arise from direct or indirect interactions among grazers and viruses, such as preferential grazing on or avoidance of virally infected phytoplankton cells (Evans and Wilson 2008; Vermont et al. 2016), or grazing of (algal) viruses by heterotrophic nanoflagellates (González and Suttle 1993). The impact of larger-sized ($\geq$ 200 µm) zooplankton (Fig. S3) on microzooplankton could also influence the balance between the phytoplankton loss factors.

Net growth rates based on counts from the mortality assay (for distinct periods of abundance increase and decline, where experimental $n \geq 3$) aligned well with net growth rates obtained from *in situ* abundance dynamics (Fig. 3), indicating that the experimental rates (Table S1) provided a very good representation of actual growth
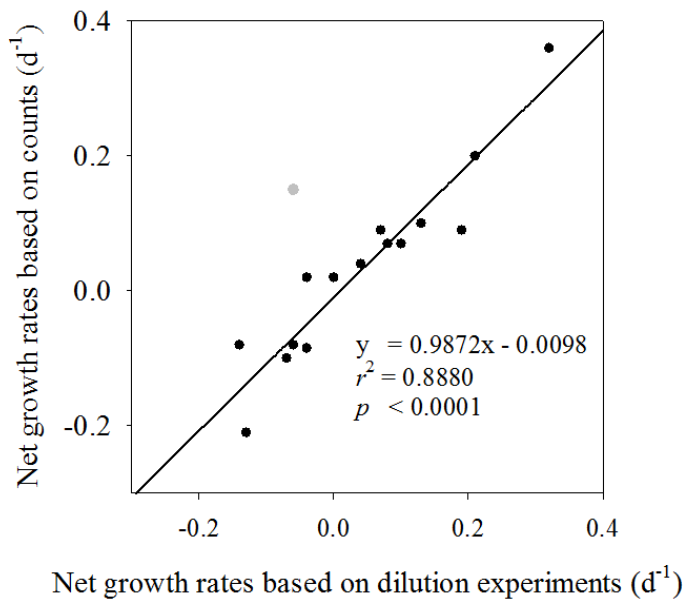
Fig. 3. A comparison of net specific growth rates (μ_{NET}) based on phytoplankton counts and on dilution experiments. Dilution experiment μ_{NET} rates were averaged ($n \geq 3$) over time periods of sustained increase and decrease in population abundance and compared to μ_{NET} rates estimated from *in-situ* abundance counts over the same time period. Note: outlier shown in grey is not included in the linear regression.

and loss processes. Averaged over the entire productive season, specific viral lysis rates were comparable to grazing rates (0.29 ± 0.30 d^{-1} and 0.31 ± 0.27 d^{-1}, respectively, $n = 98$; Fig. 4a). The trend that viral lysis rates were of similar magnitude as grazing rates held for all major phytoplankton populations and taxonomic groups, i.e. picoeukaryotes, *Phaeocystis*, cryptophytes and diatoms (Fig. 4b). Furthermore, total mortality (sum of viral lysis and grazing) matched gross growth when averaged over the entire season (Fig. S4).

The ecological importance of viral lysis is highlighted by a close-to-zero mass balance of seasonal phytoplankton carbon production and losses (Fig. 5). Our data demonstrate that viral lysis is not only an important cause of mortality for Antarctic phytoplankton (of equal magnitude as microzooplankton grazing) but also an essential process to be included for a better understanding of phytoplankton population dynamics. Relatively high growth rates and comparably high total loss rates (grazing plus lysis) of the dominant Antarctic phytoplankton (≤ 20 µm fraction, typically ruling total Chlorophyll *a*; Fig. S2)
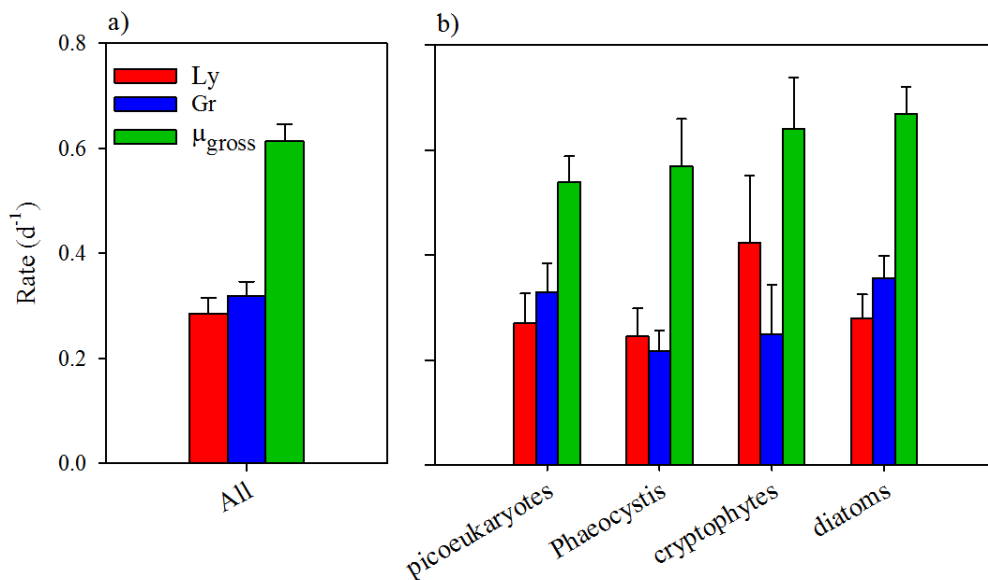
Fig. 4. Seasonal mean specific rates (d^{-1}) of viral lysis (Ly), grazing (Gr) and gross growth (μ_{gross}). (a) All phytoplankton (All), and (b) per phytoplankton group: picoeukaryotes (Phyto I and II), *Phaeocystis* (Phyto III), cryptophytes (Phyto IV) and diatoms (Phyto V, VI, VIII and IX). Error bars represent ± 1 standard error.

suggests that loss processes are coupled to growth and indicate a rapid turnover of photosynthetically fixed carbon that helps to explain the relatively low concentration and slow build-up of biomass in comparison to available resources.
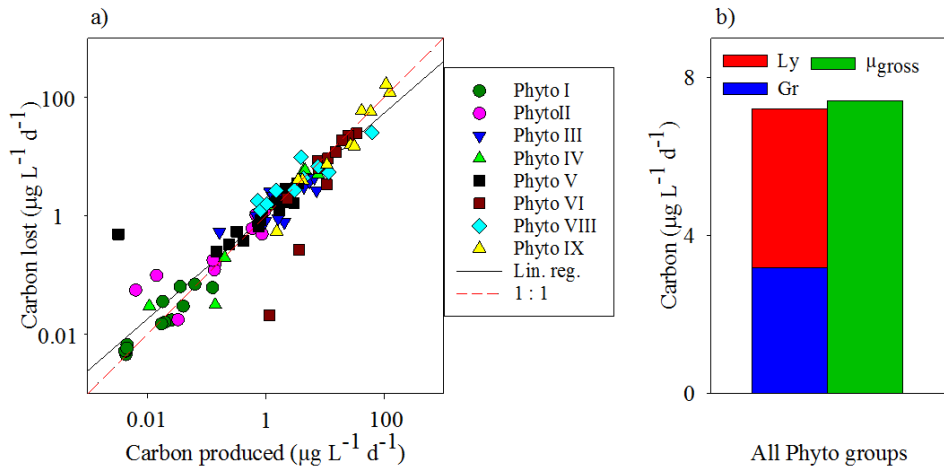
Fig. 5. (a) Phytoplankton carbon lost by viral lysis and grazing plotted against carbon produced by gross growth, obtained after conversion of the different phytoplankton group abundances to carbon (calculated from the specific viral lysis, grazing , total mortality and gross growth rates (d^{-1})). Different data points are from rate measurements at different timepoints during the season. (b) Seasonal mean of total phytoplankton carbon lost by viral lysis (Ly) and grazing (Gr) and total carbon produced by gross growth, over all phytoplankton groups. The regression line (solid black line) of phytoplankton carbon has a slope of 0.87 (r^2 = 0.87; $p < 0.0001$, $n = 95$). Note: zeros ($n = 1$) and negative ($n = 2$) values were excluded from log transformed carbon data in subplot (a).

Carbon flux and potential future implications

Overall, the nano-sized diatoms accounted for the majority of the total seasonal cellular carbon grazed, lysed and produced (91, 91 and 91%, respectively), whereby Phyto IX (average cell diameter 11.5 µm) contributed most (55, 71 and 56%, respectively; data not shown). While these nano-sized diatoms are considered preferred prey for larger zooplankton such as copepods (Gonçalves et al. 2014; Helenius and Saiz 2017; Djeghri et al. 2018), viral lysis of Phyto IX during the December spring bloom period was considerable (Table S3) as it diverted 30% of total diatom carbon produced (91 µg C L^{-1}) away from higher trophic levels. Additionally, during the late summer bloom (dominated by Phyto IX, Fig. 1h) viral

lysis can at least occasionally direct the vast majority of daily carbon produced (up to 120% on 5 March) towards the dissolved pool. This singular lysis 'event' alone represented 18% of the total seasonal carbon produced (727 µg C L^{-1}) over the period December - mid March. Such a considerable flux of organic matter from the particulate to dissolved fraction (viral shunt) stimulates bacterial production (Brussaard et al. 2005b; Zhao et al. 2019) and hence explains the strong increase in bacterial abundance at the end of the season (0.1 to 2.4 x10^6 cells mL^{-1} from mid-February to mid-March, Fig. S5). The substantial viral lysis of Phyto IX could have reduced phytoplankton food availability for key feeding stages of herbivorous copepods and may have impacted lipid accumulation (and annual reproductive success) at a crucial time prior to overwintering (Biggs et al. 2020).

Climate change scenarios predict enhanced sea-ice loss in Antarctic waters (Collins et al. 2013) that is likely to increase the length of the productive period (Montes-Hugo et al. 2009; Arrigo and van Dijken 2015). However, earlier and strengthened stratification (due to higher temperatures and ice melt) (Vernet et al. 2008; Deppeler and Davidson 2017; Van de Poll et al. 2018) will reduce the flux of dissolved inorganic nutrients to surface waters (Ardyna et al. 2014) and is predicted to promote a more flagellate-dominated community (cryptophytes Phyto IV, *Phaeocystis* Phyto III) with less larger-sized diatoms during the summer months (Venables et al. 2013; Mendes et al. 2017; Rozema et al. 2017; Biggs et al. 2019). Our study shows that viral lysis was a major loss factor for cryptophytes and *Phaeocystis* (Fig. 4b). The share of viral lysis as compared to grazing is therefore expected to increase, even if these flagellates become more dominant. Moreover, ocean acidification has been shown to diminish diatom silicification (Petrou et al. 2019) and if this results in silicate stress for the (smaller-sized) diatom cells, viral infection and mortality of diatoms could be enhanced (Kranzler et al. 2019). Under these future scenarios, our study implies that viral lysis will play a more prominent role, reducing trophic level transfer efficiency and ecosystem productivity.

Our study demonstrates that viral lysis not only implements decisive control over the seasonal dynamics of the different ecologically important Antarctic phytoplankton

groups (picoeukaryotes, the prymnesiophyte *Phaeocystis* spp., cryptophytes and diatoms), but also reveals how imperative it is to include viral lysis in mass-balance calculations. Mathematical models that involve Antarctic phytoplankton dynamics and seasonal mass balance, but do not account for viral lysis derived losses, are likely to overestimate the impact of grazing. Our findings highlight that viral lysis currently redirects about half of total seasonal phytoplankton carbon production towards the microbial loop, indicating that carbon sequestration by these Antarctic ecosystems is less effective than previously believed. This necessitates a reconsideration of the efficiency of the biological pump in Antarctic waters.

3

Acknowledgements

Competing Interests

The authors declare no competing interests.

References

Ardyna M, Babin M, Gosselin M, et al (2014) Recent Arctic Ocean sea ice loss triggers novel fall phytoplankton blooms. Geophys Res Lett 41:6207–6212. doi: 10.1002/2014GL061047

Arrigo KR, van Dijken GL (2015) Continued increases in Arctic Ocean primary production. Prog Oceanogr 136:60–70. doi: 10.1016/j.pocean.2015.05.002

Bakker DCE, De Baar HJW, Bathmann UV (1997) Changes of carbon dioxide in surface waters during spring in the Southern Ocean. Deep Sea Res Part II Top Stud Oceanogr 44:91–127. doi: 10.1016/S0967-0645(96)00075-6

Barrera-Oro E (2002) The role of fish in the Antarctic marine food web: Differences between inshore and offshore waters in the southern Scotia Arc and west Antarctic Peninsula. Antarct Sci 14:293–309. doi: 10.1017/S0954102002000111

Baudoux A-C, Noordeloos AAM, Veldhuis MJW, Brussaard CPD (2006) Virally induced mortality of *Phaeocystis globosa* during two spring blooms in temperate coastal waters. Aquat Microb Ecol 44:207–217. doi: 10.3354/ame044207

Baudoux A-C, Veldhuis MJW, Noordeloos AAM, et al (2008) Estimates of virus- vs. grazing induced mortality of picophytoplankton in the North Sea during summer. Aquat Microb Ecol 52:69–82. doi: 10.3354/ame01207

Baudoux A-C, Veldhuis MJW, Witte HJ, Brussaard CPD (2007) Viruses as mortality agents of picophytoplankton in the deep chlorophyll maximum layer during IRONAGES III. Limnol Oceanogr 52:2519–2529. doi: 10.4319/lo.2007.52.6.2519

Behrenfeld MJ, Boss ES (2018) Student's tutorial on bloom hypotheses in the context of phytoplankton annual cycles. Glob Chang Biol 24:55–77. doi: 10.1111/gcb.13858

Belton B, Thilsted SH (2014) Fisheries in transition: Food and nutrition security implications for the global South. Glob Food Sec 3:59–66. doi: 10.1016/j.gfs.2013.10.001

Biggs TEG, Alvarez-Fernandez S, Evans C, et al (2019) Antarctic phytoplankton community composition and size structure: Importance of ice type and temperature as regulatory factors. Polar Biol 42:1997–2015. doi: 10.1007/s00300-019-02576-3

Biggs TEG, Brussaard CPD, Evans C, et al (2020) Plasticity in dormancy behaviour of *Calanoides acutus* in Antarctic coastal waters. ICES J Mar Sci. doi: 10.1093/icesjms/fsaa042

Bratbak G, Egge JK, Heldal M (1993) Viral mortality of the marine alga *Emiliania huxleyi* (Haptophyceae) and termination of algal blooms. Mar Ecol Prog Ser 93:39–48. doi: 10.3354/meps093039

Brussaard CPD (2004) Viral control of phytoplankton populations-A review. J Eukaryot Microbiol 51:125–138. doi: 10.1111/j.1550-7408.2004.tb00537.x

Brussaard CPD, Kuipers B, Veldhuis MJW (2005a) A mesocosm study of *Phaeocystis globosa* population dynamics I. Regulatory role of viruses in bloom control. Harmful Algae 4:859–874. doi: 10.1016/j.hal.2004.12.015

Brussaard CPD, Mari X, Bleijswijk JDL Van, Veldhuis MJW (2005b) A mesocosm study of *Phaeocystis globosa* (Prymnesiophyceae) population dynamics II. Significance for the microbial community. Harmful Algae 4:875–893. doi: 10.1016/j.hal.2004.12.012

Brussaard CPD, Martínez J (2008) Algal bloom viruses. Plant Viruses 2:1–13

Brussaard CPD, Noordeloos AAM, Witte H, et al (2013) Arctic microbial community dynamics influenced by elevated CO_2 levels. Biogeosciences 10:719–731. doi: 10.5194/bg-10-719-2013

Brussaard CPD, Timmermans KR, Uitz J, Veldhuis MJW (2008) Virioplankton dynamics and virally induced phytoplankton lysis versus microzooplankton grazing southeast of the Kerguelen (Southern Ocean). Deep Sea Res Part II Top Stud Oceanogr 55:752–765. doi: 10.1016/j.dsr2.2007.12.034

Calbet A, Landry MR (2004) Phytoplankton growth, microzooplankton grazing, and carbon cycling in marine systems. Limnol Oceanogr 49:51–57. doi: 10.4319/lo.2004.49.1.0051

Clarke A, Meredith MP, Wallace MI, et al (2008) Seasonal and interannual variability in temperature, chlorophyll and macronutrients in northern Marguerite Bay, Antarctica. Deep Res Part II Top Stud Oceanogr 55:1988–2006. doi: 10.1016/j.dsr2.2008.04.035

Collins M, Knutti R, Arblaster J, et al (2013) Long-term climate change: Projections, commitments, and irreversibility. Cambridge University Press, United Kingdom and New York, NY, USA,

Coy SR, Gann ER, Pound HL, et al (2018) Viruses of eukaryotic algae: Diversity, methods for detection, and future directions. Viruses 10:487. doi: 10.3390/v10090487

Deppeler SL, Davidson AT (2017) Southern Ocean phytoplankton in a changing climate. Front Mar Sci 4:doi: 10.3389/fmars.2017.00040. doi: 10.3389/fmars.2017.00040

Djeghri N, Atkinson A, Fileman ES, et al (2018) High prey-predator size ratios and unselective feeding in copepods: A seasonal comparison of five species with contrasting feeding modes. Prog Oceanogr 165:63–74. doi: 10.1016/j.pocean.2018.04.013

Ducklow H, Clarke A, Dickhut R, et al (2012) The marine system of the Western Antarctic Peninsula. In: Rogers AD, Johnston NM, Murphy EJ, Clarke A (eds) Antarctic Ecosystems: An Extreme Environment in a Changing World. Blackwell Publishing Ltd., pp 121–159

Evans C, Brussaard CPD (2012) Viral lysis and microzooplankton grazing of phytoplankton throughout the Southern Ocean. Limnol Oceanogr 57:1826–1837. doi: 10.4319/lo.2012.57.6.1826

Evans C, Wilson WH (2008) Preferential grazing of *Oxyrrhis marina* on virus infected *Emiliania huxleyi*. Limnol Oceanogr 53:2035–2040. doi: 10.4319/lo.2008.53.5.2035

Frölicher TL, Sarmiento JL, Paynter DJ, et al (2015) Dominance of the Southern Ocean in anthropogenic carbon and heat uptake in CMIP5 models. J Clim 28:862–886. doi: 10.1175/JCLI-D-14-00117.1

Garrison DL, Gowing MM, Hughes MP, et al (2000) Microbial food web structure in the Arabian Sea: A US JGOFS study. Deep Sea Res Part II Top Stud Oceanogr 47:1387–1422. doi:

10.1016/S0967-0645(99)00148-4

Gonçalves RJ, Gréve H van S, Couespel D, Kiørboe T (2014) Mechanisms of prey size selection in a suspension-feeding copepod, *Temora longicornis*. Mar Ecol Prog Ser 517:61–74. doi: 10.3354/meps11039

González JM, Suttle CA (1993) Grazing by marine nanoflagellates on viruses and virus-sized particles: Ingestion and digestion. Mar Ecol Prog Ser 94:1–10. doi: 10.3354/meps094001

Gordon AL (2001) Bottom water formation. In: Steele JH, Turekian KK, Thorpe SA (eds) Encyclopedia of Ocean Sciences, 3rd edn. Elsevier, pp 334–340

Haaber J, Middelboe M (2009) Viral lysis of *Phaeocystis pouchetii*: Implications for algal population dynamics and heterotrophic C, N and P cycling. ISME J 3:430–441. doi: 10.1038/ismej.2008.125

Helenius LK, Saiz E (2017) Feeding behaviour of the nauplii of the marine calanoid copepod *Paracartia grani* Sars: Functional response, prey size spectrum, and effects of the presence of alternative prey. PLoS One 12:e0172902. doi: 10.1371/journal.pone.0172902

Jacobs SS (2004) Bottom water production and its links with the thermohaline circulation. Antarct Sci 16:427–437. doi: 10.1017/S095410200400224X

Kattner G, Hagen W (2009) Lipids in marine copepods: Latitudinal characteristics and perspective to global warming. In: Kainz M, Brett M, Arts M (eds) Lipids in Aquatic Ecosystems. Springer New York, pp 257–280

Khatiwala S, Tanhua T, Mikaloff Fletcher S, et al (2013) Global ocean storage of anthropogenic carbon. Biogeosciences 10:2169–2191. doi: 10.5194/bg-10-2169-2013

Kranzler CF, Krause JW, Brzezinski MA, et al (2019) Silicon limitation facilitates virus infection and mortality of marine diatoms. Nat Microbiol 4:1790–1797. doi: 10.1038/s41564-019-0502-x

Li WKW, Dickie PM (2001) Monitoring phytoplankton, bacterioplankton, and virioplankton in a coastal inlet (Bedford Basin) by flow cytometry. Cytometry 44:236–246. doi: 10.1002/1097-0320(20010701)44:3<236::AID-CYTO1116>3.0.CO;2-5

Lønborg C, Middelboe M, Brussaard CPD (2013) Viral lysis of *Micromonas pusilla*: Impacts on dissolved organic matter production and composition. Biogeochemistry 116:231–240. doi: 10.1007/s10533-013-9853-1

Maat DS, Brussaard CPD (2016) Both phosphorus- and nitrogen limitation constrain viral proliferation in marine phytoplankton. Aquat Microb Ecol 77:87–97. doi: 10.3354/ame01791

Maat DS, Crawfurd KJ, Timmermans KR, Brussaard CPD (2014) Elevated CO_2 and phosphate limitation favor *Micromonas pusilla* through stimulated growth and reduced viral impact. Appl Environ Microbiol 80:3119–3127. doi: 10.1128/AEM.03639-13

Marie D, Brussaard CPD, Thyrhaug R, et al (1999) Enumeration of marine viruses in culture and natural samples by flow cytometry. Appl Environ Microbiol 65:45–52

Mendes CRB, Tavano VM, Dotto TS, et al (2017) New insights on the dominance of cryptophytes in Antarctic coastal waters: A case study in Gerlache Strait. Deep Sea Res Part II Top Stud Oceanogr 149:161–170. doi: 10.1016/j.dsr2.2017.02.010

Mojica KDA, Huisman J, Wilhelm SW, Brussaard CPD (2016) Latitudinal variation in virus-induced mortality of phytoplankton across the North Atlantic Ocean. ISME J 10:500–513. doi: 10.1038/ismej.2015.130

Moline MA, Claustre H, Frazer TK, et al (2004) Alteration of the food web along the Antarctic Peninsula in response to a regional warming trend. Glob Chang Biol 10:1973–1980. doi: 10.1111/j.1365-2486.2004.00825.x

Montes-Hugo M, Doney SC, Ducklow HW, et al (2009) Recent changes in phytoplankton communities associated with rapid regional climate change along the western Antarctic Peninsula. Science (80-) 323:1470–1473. doi: 10.1126/science.1164533

Moreau S, Schloss IR, Mostajir B, et al (2012) Influence of microbial community composition and metabolism on air−sea ΔpCO_2 variation off the western Antarctic Peninsula. Mar Ecol Prog Ser 446:45–59. doi: 10.3354/meps09466

Muhling M, Fuller NJ, Millard A, et al (2005) Genetic diversity of marine Synechococcus and co-occurring cyanophage communities: Evidence for viral control of phytoplankton. Environ Microbiol 7:499–508. doi: 10.1111/j.1462-2920.2005.00713.x

Nagasaki K (2008) Dinoflagellates, diatoms, and their viruses. J Microbiol 46:235–243. doi: 10.1007/s12275-008-0098-y

Petrou K, Baker KG, Nielsen DA, et al (2019) Acidification diminishes diatom silica production in the

Southern Ocean. Nat Clim Chang 9:781–786. doi: 10.1038/s41558-019-0557-y

Ploug H, Iversen MH, Fischer G (2008) Ballast, sinking velocity, and apparent diffusivity within marine snow and zooplankton fecal pellets: Implications for substrate turnover by attached bacteria. Limnol Oceanogr 53:1878–1886. doi: 10.4319/lo.2008.53.5.1878

Rozema PD, Venables HJ, van de Poll WH, et al (2017) Interannual variability in phytoplankton biomass and species composition in northern Marguerite Bay (West Antarctic Peninsula) is governed by both winter sea ice cover and summer stratification. Limnol Oceanogr 62:235–252. doi: 10.1002/lno.10391

Safi KA, Brian Griffiths F, Hall JA (2007) Microzooplankton composition, biomass and grazing rates along the WOCE SR3 line between Tasmania and Antarctica. Deep Sea Res Part I Oceanogr Res Pap 54:1025–1041. doi: 10.1016/j.dsr.2007.05.003

Shreeve RS, Ward P, Whitehouse MJ (2002) Copepod growth and development around South Georgia: Relationships with temperature, food and krill. Mar Ecol Prog Ser 233:169–183. doi: 10.3354/meps233169

Sommer U, Lengfellner K (2008) Climate change and the timing, magnitude, and composition of the phytoplankton spring bloom. Glob Chang Biol 14:1199–1208. doi: 10.1111/j.1365-2486.2008.01571.x

Suttle CA (2007) Marine viruses — major players in the global ecosystem. Nat Rev Microbiol 5:801–812. doi: 10.1038/nrmicro1750

Tomaru Y, Takao Y, Suzuki H, et al (2009) Isolation and characterization of a single-stranded RNA virus infecting the bloom-forming diatom *Chaetoceros socialis*. Appl Environ Microbiol 75:2375–2381. doi: 10.1128/AEM.02580-08

Turner JT (2015) Zooplankton fecal pellets, marine snow, phytodetritus and the ocean's biological pump. Prog Oceanogr 130:205–248. doi: 10.1016/j.pocean.2014.08.005

Van de Poll WH, Kulk G, Rozema PD, et al (2018) Contrasting glacial meltwater effects on post-bloom phytoplankton on temporal and spatial scales in Kongsfjorden, Spitsbergen. Elem Sci Anth 6:50. doi: 10.1525/elementa.307

Vardi A, Haramaty L, Van Mooy BAS, et al (2012) Host-virus dynamics and subcellular controls of cell fate in a natural coccolithophore population. Proc Natl Acad Sci 109:19327–19332. doi: 10.1073/pnas.1208895109

Vaulot D (1989) CYTOPC: Processing software for flow cytometric data. Signal and Noise 2:8

Venables HJ, Clarke A, Meredith MP (2013) Wintertime controls on summer stratification and productivity at the western Antarctic Peninsula. Limnol Oceanogr 58:1035–1047. doi: 10.4319/lo.2013.58.3.1035

Vermont AI, Martínez Martínez J, Waller JD, et al (2016) Virus infection of *Emiliania huxleyi* deters grazing by the copepod *Acartia tonsa*. J Plankton Res 38:1194–1205. doi: 10.1093/plankt/fbw064

Vernet M, Martinson D, Iannuzzi R, et al (2008) Primary production within the sea-ice zone west of the Antarctic Peninsula: I—Sea ice, summer mixed layer, and irradiance. Deep Sea Res Part II Top Stud Oceanogr 55:2068–2085. doi: 10.1016/j.dsr2.2008.05.021

Voss M (1991) Content of copepod faecal pellets in relation to food supply in Kiel Bight and its effect on sedimentation rate. Mar Ecol Prog Ser 75:217–225. doi: 10.3354/meps075217

Weitz JS, Wilhelm SW (2012) Ocean viruses and their effects on microbial communities and biogeochemical cycles. F1000 Biol Rep 4:2–9. doi: 10.3410/B4-17

Wilhelm SW, Suttle CA (1999) Viruses and nutrient cycles in the sea. Bioscience 49:781–788. doi: 10.2307/1313569

Worden AZ, Nolan JK, Palenik B (2004) Assessing the dynamics and ecology of marine picophytoplankton: The importance of the eukaryotic component. Limnol Oceanogr 49:168–179. doi: 10.4319/lo.2004.49.1.0168

Yamada Y, Tomaru Y, Fukuda H, Nagata T (2018) Aggregate formation during the viral lysis of a marine diatom. Front Mar Sci 5:. doi: 10.3389/fmars.2018.00167

Zhao Z, Gonsior M, Schmitt-Kopplin P, et al (2019) Microbial transformation of virus-induced dissolved organic matter from picocyanobacteria: Coupling of bacterial diversity and DOM chemodiversity. ISME J 13:2551–2565. doi: 10.1038/s41396-019-0449-1

Supplementary Figures
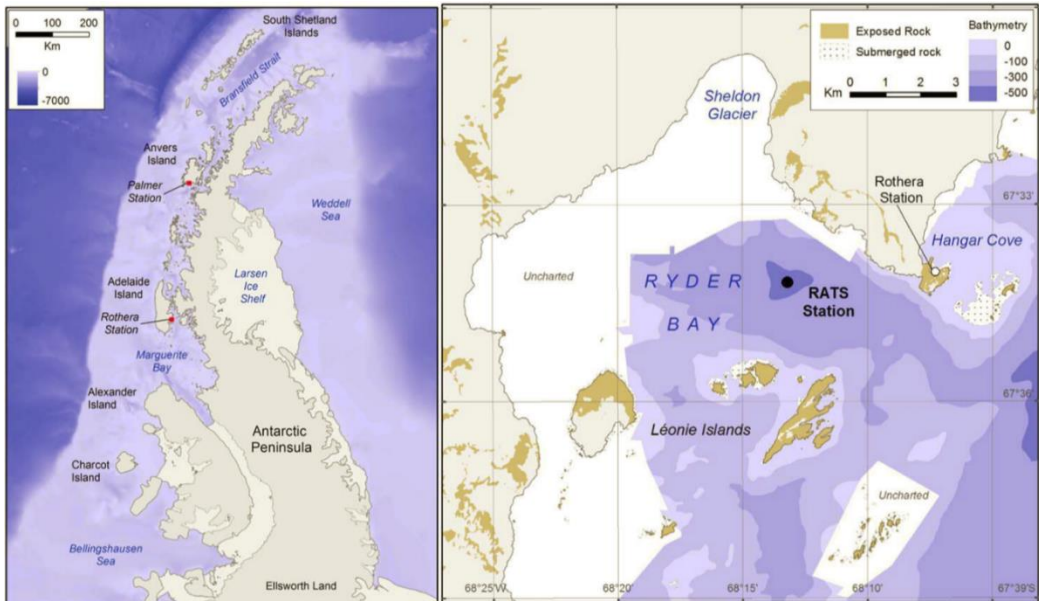
Fig. S1. Map of the study site: (a) the location of Rothera research station in northern Marguerite Bay. Note: Ryder Bay is to the east of Adelaide Island and to the west of the Antarctic Peninsula. (b) large scale map of the Rothera Time Series (RATS) sample site within Ryder Bay. Map adapted from Annett et al. (2015).

Reference

Annett AL, Skiba M, Henley SF, et al (2015) Comparative roles of upwelling and glacial iron sources in Ryder Bay, coastal western Antarctic Peninsula. Mar Chem 176:21–33. doi: 10.1016/j.marchem.2015.06.017
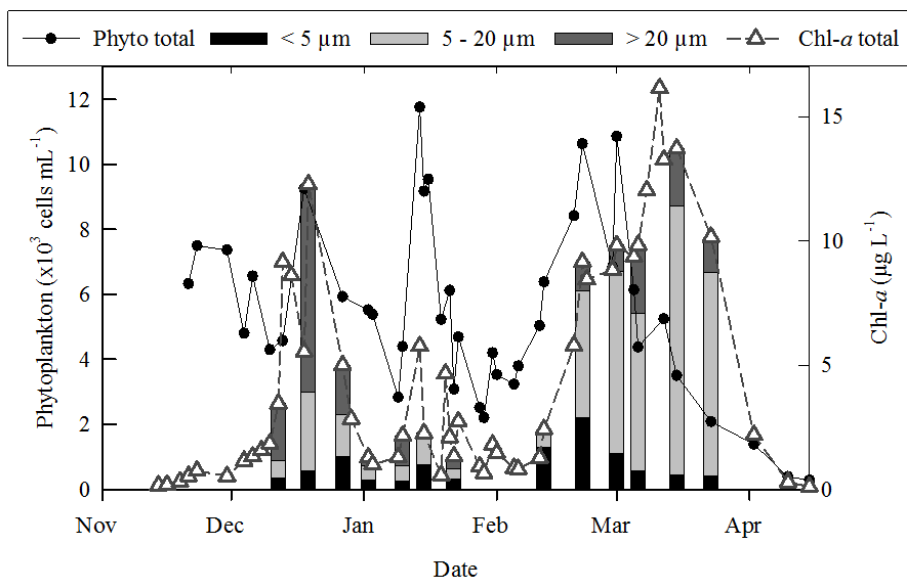
Fig. S2. Time series of total phytoplankton abundance as determined by flow cytometry (Phyto total; black circles and solid line) and total Chlorophyll-*a* (Chl-*a*) concentrations as determined by high performance liquid chromatography (Chl-*a* total; open triangles and dashed line) at the RATS sample site (15 m depth) in Ryder Bay. Bar chart indicates the fraction of Chl-*a* total contained within three size classes, < 5, 5 – 20 and > 20 µm.
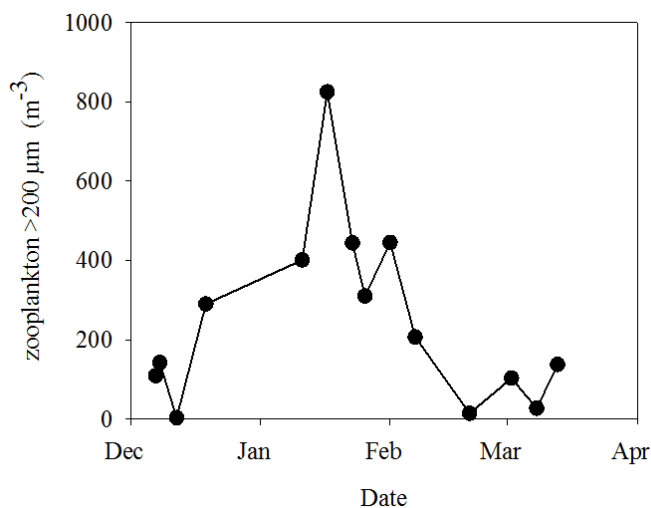
Fig. S3. Time series of zooplankton abundance ≥ 200 µm at the sample site from surface water (200 – 0 m) net hauls.
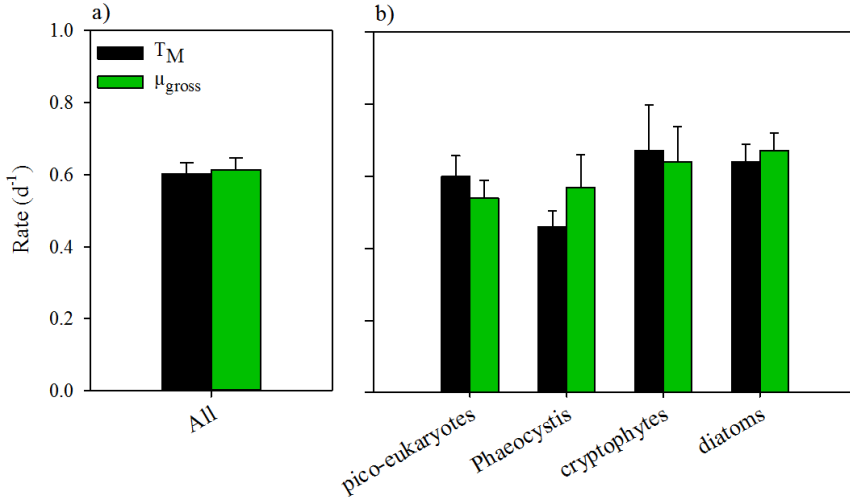
Fig. S4. Seasonal mean specific rates (d^{-1}) of gross growth (μ_{gross}) and total mortality (T_M, i.e. lysis plus grazing) are shown in (a) for all phytoplankton groups (All) and (b) per group: *pico-eukaryotes* Phyto I and II; *Phaeocystis* Phyto III, *cryptophytes* Phyto IV and *diatoms* Phyto V, VI, VIII and IX. Error bars represent ± 1 standard error.
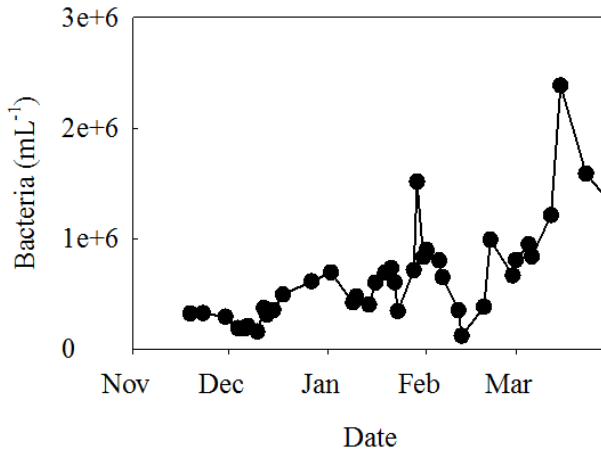
Fig. S5. The temporal dynamics of bacterial abundance (cells mL^{-1}), from flow cytometry counts of samples stained with green fluorescent dye SYBR Green^{TM}.

Supplementary Tables

Table S1. Temporal variation in specific viral lysis (Ly), grazing (Gr), total Mortality (T_M = Ly+Gr) and gross growth (μ_{gross}) rates (d^{-1}) for Phyto groups I-VI and VIII-IX. * indicates a significant difference ($p < 0.05$) of the linear regression from either: zero (μ_{gross} and Gr) or from the grazing regression (Ly); a white background indicates missing data due to either low abundance or high variation.

Date	Phyto I (d^{-1})				Phyto II (d^{-1})				Phyto III (d^{-1})				Phyto IV (d^{-1})				Phyto V (d^{-1})			
	Ly	Gr	T_M	μ_{gross}	Ly	Gr	T_M	μ_{gross}	Ly	Gr	T_M	μ_{gross}	Ly	Gr	T_M	μ_{gross}	Ly	Gr	T_M	μ_{gross}
06/12/12	0.21	0.00	0.21	0.43	0.27	0.10	0.36	0.35*	0.23	0.07	0.30	0.80	0.68*	0.00	0.68*	0.7*	1.11*	0.04	1.15*	1.31*
10/12/12	0.05	0.37*	0.42	0.57*	0.41*	0.32*	0.73*	0.48*	0.65*	0.00	0.65*	0.92*					0.00	0.77*	0.77	0.46*
13/12/12	0.10	0.55*	0.65	0.33*	0.06	0.56*	0.62	0.64*	0.06	0.41*	0.48	0.36*					0.36	0.22	0.58	0.56
18/12/12	0.64*	0.15	0.79*	0.45*	0.42*	0.36*	0.78*	0.59*	0.5*	0.05	0.55*	0.43*					1.01*	0.00	1.01*	0.88*
03/01/13	0.10	0.29*	0.39	0.58*	0.22*	0.12	0.35*	0.61*	0.48*	0.15	0.63*	0.9*					0.00	0.49*	0.49*	0.54*
09/01/13	0.00	0.38*	0.38*	0.47*	0.00	0.43*	0.43*	0.39*	0.02	0.26*	0.27	0.28*					0.44	0.06	0.51	0.64*
14/01/13	0.18	0.39*	0.58	0.52*	0.30	0.26*	0.56	0.59*	0.21	0.21*	0.42	1.12*	0.76*	0.00	0.77*	0.71*	0.25	0.23	0.49	0.88
21/01/13	0.00	0.66*	0.66	0.77*	0.19	0.55*	0.74	0.59*	0.00	0.32*	0.32	0.56*	0.00	0.63	0.63	0.97*	0.03	0.91*	0.94	0.69*
28/01/13	0.10	1.25*	1.35	1.31*	0.41*	0.29*	0.7*	0.78*	0.00	0.44*	0.44	0.54	0.79*	0.27*	1.06*	0.78*	0.08	0.34	0.42	0.57*
05/02/13	0.94*	0.16	1.1*	0.94*	0.00	0.53*	0.53	0.25*	0.19	0.00	0.19	0.06*	0.83*	0.05	0.88*	0.74*	0.37	0.86*	1.23	0.94*
11/02/13	0.03	0.81	0.84	0.68*	0.55*	0.06	0.61*	0.45*	0.35	0.47*	0.82	1.22*	0.67*	0.55*	1.22*	0.96*	0.01	0.91*	0.92	0.9*
19/02/13	1.03*	0.01	1.04*	0.71*	0.01	0.11	0.12	0.23	0.21*	0.26*	0.47*	0.5*	0.01	0.65*	0.66	0.47*	0.12	0.00	0.12	0.07
28/02/13	0.00	0.00	0.00	0.34	0.38*	0.03	0.4*	0.05*	0.36*	0.14	0.5*	0.23*	0.00	0.10	0.10	0.43	0.09	0.21	0.30	0.23
05/03/13	0.72*	0.16	0.88*	0.69*					0.42*	0.17	0.59*	0.37*	0.07	0.00	0.07	0.03	0.13	0.47	0.60	0.00
12/03/13	0.03	0.13	0.16	-0.05					0.00	0.31*	0.31	0.22								

Date	Phyto VI (d^{-1})				Phyto VIII (d^{-1})				Phyto IX (d^{-1})			
	Ly	Gr	T_M	μ_{gross}	Ly	Gr	T_M	μ_{gross}	Ly	Gr	T_M	μ_{gross}
06/12/12	1.34*	0.09*	1.43*	1.29*	0.58	0.35	0.92	0.37	0.19	0.32	0.51	0.86
10/12/12	0.01	0.00	0.01	0.67					0.25	0.27	0.52	1.08
13/12/12	0.11	0.74	0.85	1.03	0.00	0.66*	0.66	0.74	0.35	0.59*	0.94	0.96*
18/12/12		0.93*			0.40*	0.04	0.44*	1.05*	0.14	0.11	0.26	0.18
03/01/13	0.31	0.34*	0.65	0.78*	0.42	0.58*	1.00	1.12*				
09/01/13	0.00	0.04	0.04	0.47								
14/01/13	0.24	0.32*	0.56	0.78*	0.00	0.4*	0.40	0.85*	0.38	0.24	0.62	0.91*
21/01/13	0.08	0.68*	0.76	0.98*	0.00	0.92	0.92	0.38	0.00	0.12	0.12	0.33
28/01/13	0.59*	0.36*	0.96*	1.18*	0.69	0.00	0.69	0.46				
05/02/13	0.00	0.20	0.20	0.64					0.60	0.01	0.61	0.64*
11/02/13	0.27	0.72	1.00	1.08					0.26	0.57*	0.82	0.72*
19/02/13	0.00	0.43*	0.43	0.44*	0.00	0.78*	0.78	0.78*	0.44*	0.07	0.5*	0.52*
28/02/13	0.00	0.00	0.00	0.26	0.69*	0.31	1.01*	0.66*	0.00	0.06	0.06	0.09
05/03/13	0.00	0.26*	0.26	-0.04*	0.66*	0.00	0.66*	0.37*	0.38*	0.11	0.49*	0.31*
12/03/13	0.03	0.13	0.16	-0.05						0.28*		

Table S2. Pearson correlation coefficients (r) between viral lysis (Ly) and grazing (Gr) rates, as well as significance (*p*) and number of datapoints (*n*), for all phytoplankton groups (Phyto ALL) and specifically for groups Phyto I, III and V.

[a] Coefficients are also shown for Phyto I with one datapoint excluded, i.e. Ly and Gr are both 0.00 d^{-1} (see Fig. 2b).

Variables	**r**	***p***	***n***
Phyto All	-0.427	<0.0001	98
Phyto I	-0.479	0.0831	14
Phyto I [a]	-0.590	0.0338	13
Phyto III	-0.609	0.0160	15
Phyto V	-0.560	0.0372	14

3

Table S3. Carbon lost by viral lysis (Ly), grazing (Gr), total mortality (T_M=Ly+Gr) and carbon produced by gross growth (μ_{gross}) rates (µg C L⁻¹ d⁻¹) for Phyto groups I-VI and VIII-IX. St.st. is the standing stock in µg C L⁻¹. Note: No values indicate missing data due to either very low abundance and/or too high variation to obtain reliable estimates. For statistical analysis only sets with both lysis and grazing data were used.

Date	Phyto I (µg C L⁻¹ d⁻¹)					Phyto II (µg C L⁻¹ d⁻¹)					Phyto III (µg C L⁻¹ d⁻¹)					Phyto IV (µg C L⁻¹ d⁻¹)					Phyto V (µg C L⁻¹ d⁻¹)				
	Ly	Gr	T_M	μ_{gross}	St.st.	Ly	Gr	T_M	μ_{gross}	St.st.	Ly	Gr	T_M	μ_{gross}	St.st.	Ly	Gr	T_M	μ_{gross}	St.st.	Ly	Gr	T_M	μ_{gross}	St.st.
06/12/12	0.06	0.00	0.06	0.13	0.26	0.45	0.16	0.61	0.59	1.69	0.59	0.19	0.78	2.06	1.98	0.20	0.00	0.20	0.20	0.28	0.64	0.03	0.66	0.76	0.53
10/12/12	0.00	0.03	0.03	0.04	0.07	0.59	0.45	1.04	0.69	1.60	3.08	0.00	3.08	4.39	4.13						0.00	0.54	0.54	0.32	0.82
13/12/12	0.01	0.03	0.04	0.02	0.06	0.07	0.66	0.73	0.75	1.16	0.26	1.73	1.99	1.51	4.43						0.53	0.32	0.85	0.82	1.47
18/12/12	0.05	0.01	0.06	0.04	0.10	0.69	0.58	1.27	0.96	1.79	2.37	0.25	2.62	2.04	5.04						1.74	0.00	1.74	1.52	1.83
03/01/13	0.00	0.01	0.02	0.03	0.04	0.32	0.17	0.49	0.87	1.23	2.94	0.88	3.82	5.46	5.29						0.00	0.38	0.38	0.42	0.76
09/01/13	0.00	0.02	0.02	0.02	0.04	0.00	0.16	0.16	0.14	0.37	0.05	0.78	0.83	0.84	3.02						1.48	0.21	1.69	2.15	3.12
14/01/13	0.02	0.05	0.07	0.06	0.12	0.93	0.83	1.76	1.85	3.10	1.37	1.33	2.70	7.18	4.43	3.15	0.02	3.17	2.92	4.25	0.87	0.79	1.66	3.00	2.79
21/01/13	0.00	0.01	0.01	0.02	0.02	0.30	0.89	1.19	0.95	1.73	0.00	0.90	0.90	1.61	2.52	0.00	4.97	4.97	7.62	6.63	0.04	1.16	1.20	0.88	1.44
28/01/13	0.00	0.00	0.00	0.00	0.00	0.07	0.05	0.12	0.14	0.17	0.00	0.80	0.80	0.97	1.73	4.41	1.53	5.93	4.38	6.41	0.22	1.01	1.23	1.69	2.72
05/02/13	0.00	0.00	0.01	0.00	0.01						0.52	0.01	0.53	0.17	2.95	1.51	0.09	1.60	1.34	1.95	0.86	2.00	2.85	2.17	2.67
11/02/13	0.00	0.01	0.01	0.00	0.01	0.00	0.10	0.10	0.01	0.23	1.88	2.54	4.42	6.58	4.39	3.22	2.64	5.86	4.61	5.47	0.05	3.50	3.55	3.46	3.88
19/02/13	0.01	0.00	0.01	0.00	0.01	0.16	0.02	0.18	0.13	0.31	1.28	1.64	2.93	3.13	6.15	0.03	1.46	1.49	1.05	2.48	0.25	0.00	0.25	0.15	2.11
28/02/13	0.00	0.00	0.00	0.00	0.00	0.00	0.02	0.02	0.03	0.14	1.83	0.70	2.53	1.18	5.81	0.00	0.03	0.03	0.14	0.28	0.10	0.22	0.33	0.24	1.12
05/03/13	0.00	0.00	0.01	0.00	0.01	0.05	0.00	0.06	0.01	0.16	1.54	0.62	2.16	1.34	4.09	0.03	0.00	0.03	0.01	0.44	0.11	0.38	0.49	0.00	1.08
12/03/13											0.00	1.00	1.00	0.69	3.36										

Date	Phyto VI (µg C L⁻¹ d⁻¹)					Phyto VIII (µg C L⁻¹ d⁻¹)					Phyto IX (µg C L⁻¹ d⁻¹)				
	Ly	Gr	T_M	μ_{gross}	St.st.	Ly	Gr	T_M	μ_{gross}	St.st.	Ly	Gr	T_M	μ_{gross}	St.st.
06/12/12	7.84	0.51	8.35	7.55	6.25	6.08	3.66	9.75	3.94	13.74	5.80	9.88	15.68	26.76	25.84
10/12/12	0.02	0.00	0.02	1.15	1.21						7.17	7.87	15.04	31.08	21.48
13/12/12	0.26	1.67	1.93	2.35	2.08						45.11	75.92	121.03	123.72	127.64
18/12/12						0.00	2.73	2.73	3.04	3.96	33.15	26.18	59.33	41.47	240.34
03/01/13	4.48	4.84	9.32	11.22	13.50	23.21	2.43	25.64	61.42	42.42					
09/01/13	0.00	0.27	0.27	3.64	6.12	2.86	3.95	6.81	7.65	6.41					
14/01/13	10.56	13.90	24.47	33.82	39.13						4.43	2.86	7.28	10.74	10.12
21/01/13	1.25	10.55	11.79	15.09	13.84	0.00	5.46	5.46	11.55	10.70	0.00	0.55	0.55	1.53	4.20
28/01/13	3.93	2.40	6.32	7.79	5.91	0.00	1.78	1.78	0.73	2.50					
05/02/13	0.00	3.36	3.36	10.57	13.16	1.24	0.00	1.24	0.81	2.01	3.89	0.07	3.96	4.16	6.38
11/02/13	6.23	16.44	22.67	24.65	21.78	0.00	4.29	4.29	4.28	5.49	1.25	2.76	4.01	3.50	5.14
19/02/13	0.00	18.64	18.64	19.09	43.45	1.08	0.49	1.57	1.04	1.85	49.91	7.59	57.50	58.69	113.32
28/02/13						2.67	0.00	2.67	1.49	4.67					
05/03/13	0.00	4.28	4.28	-0.75	19.44						131.08	36.86	167.94	107.04	372.35
12/03/13	0.18	0.70	0.87	-0.27	5.99										

100

Chapter 4

Inter-annual comparison of viral lysis and microzooplankton grazing rates of Antarctic phytoplankton

Inter-annual comparison of viral lysis and microzooplankton grazing rates of Antarctic phytoplankton

Tristan E.G. Biggs[1,2]; Claire Evans[3] and Corina P.D. Brussaard[1,2]

[1] Department of Marine Microbiology and Biogeochemistry, NIOZ Royal Netherlands Institute for Sea Research, and University of Utrecht, Texel, The Netherlands.
[2] Department of Freshwater and Marine Ecology, Institute for Biodiversity and Ecosystem Dynamics (IBED), University of Amsterdam, Amsterdam, The Netherlands.
[3] Ocean Biogeochemistry & Ecosystems Research Group, National Oceanography Centre, Southampton, UK.

This chapter will be submitted for publication

Abstract

Antarctic phytoplankton display strong variability in production and loss rates over seasonal and inter-annual timescales, consequently influencing standing stock and community composition. Only recently have viral lysis rates been reported for key phytoplankton taxonomic groups in Antarctic coastal waters, found equal to rates of grazing. Viral lysis and grazing affect the flow of energy and matter very differently through marine pelagic ecosystems, warranting further investigation of their temporal dynamics and inter-annual differences. In this study, viral lysis and microzooplankton grazing rates of Antarctic phytoplankton were examined over a full productive season (S2) and compared to published rates from the previous year (S1; Chapter 3). The results presented here establish that viral lysis is a common loss factor for Antarctic phytoplankton, during both cold (S2) and warm (S1) productive seasons. Lower rates of grazing in S2 were linked to temperatures below 0°C, compared to the warmer year before (S1) when average temperature was above 0°C. In contrast to grazing, viral lysis rates were similar between the two years and responsible for about 60% of total carbon lost (lysis plus grazing), thereby reducing trophic level transfer efficiency. Viral lysis was essential to explain the coupling of growth and mortality as it bridged-the-gap between phytoplankton production and grazing losses to close the seasonal mass balance in both seasons. A closer relationship between viral lysis and phytoplankton rates of growth was linked to a greater share of viral lysis during bloom accumulation, when gross growth rates were largest. Our results show a far greater proportion of phytoplankton biomass is diverted towards the microbial loop than previously considered. The inter-annual differences relate mostly to variation in the quantitative importance of grazing, and consequently the relative importance of viral lysis.

Introduction

Grazing is traditionally considered the major pathway controlling the fate of polar phytoplankton cells (Calbet and Landry 2004; Smetacek et al. 2004; Smith and Lancelot 2004), however, the importance of phytoplankton losses due to viral infection is understudied for Antarctic waters. In temperate and (sub)tropical waters, viral lysis of phytoplankton is increasingly acknowledged as an important loss factor (Bratbak et al. 1993; Baudoux et al. 2006, 2007; Mojica et al. 2016). Whilst grazing functions to channel organic carbon and nutrient flow to higher trophic levels, viral lysis fuels the microbial loop (Brussaard et al. 2005b; Suttle 2007) diverting primary production away from zooplankton and reducing the efficiency of the carbon pump (Suttle 2007). The so called 'viral shunt' (Wilhelm and Suttle 1999) enhances heterotrophic recycling of released organic carbon and nutrients, directly influencing biogeochemical cycling and food web structure (Brussaard et al. 2008; Weitz and Wilhelm 2012). Furthermore, lytic viruses influence phytoplankton community composition and species succession because of their high specificity for hosts (Brussaard and Martínez 2008; Nagasaki 2008; Weitz and Wilhelm 2012). To model variability in planktonic community structure (and carbon cycling) accurately, a better understanding of viral lysis dynamics and how phytoplankton growth is linked to mortality is imperative.

Only recently a quantitative study of viral lysis of Antarctic phytoplankton was performed, showing that all taxonomic groups displayed significant losses due to lytic viral infection (Chapter 3). Since it is ultimately the sum of production and losses over a seasonal cycle that determines the ecosystem carrying capacity (Sarker and Wiltshire 2017), it is essential to know if viral lysis is consistently important or if there are large differences between years. Antarctic primary production is after all subjected to extreme seasonality (Ma et al. 2014) and largely regulated by light and temperature (Venables et al. 2013). More seasonal studies of growth, viral lysis and grazing rates for the different phytoplankton populations are therefore needed.

The coastal waters along the Antarctic Peninsula are highly productive (Vernet et al. 2008) and serve as a model study area to better understand the impact of

environmental change on polar food web functioning (Schofield et al. 2018). Annual variations in chlorophyll concentrations and the phytoplankton community (Venables et al. 2013; Rozema et al. 2017b) allude that viral lysis rates will also likely vary. Moreover, global warming has been linked to a greater importance of nano-sized phytoplankton with less micro-sized diatoms (Rozema et al. 2017b). The size class of phytoplankton determines not only the size class of zooplankton grazing on phytoplankton, but also the amount of organic carbon shunted to the microbial food web. A greater importance of viral lysis results in more recycling of photosynthetically fixed carbon and nutrients through the microbial loop, whereas more grazing results in transfer to larger consumers and top level predators such as fish, penguins and whales.

Here we examine inter-annual variations of the specific loss factors in the coastal waters of Antarctica. We present rates of growth and losses, i.e. viral lysis and grazing, of ecologically important Antarctic phytoplankton populations (of varied taxonomy and cell size) over a seasonal cycle, and compare these to rates collected the previous year at the same sampling site (Chapter 3).

Materials and methods

Sampling site and procedure

Seawater samples for this study were collected at the Rothera time series site (RaTS, latitude 67.572°S; longitude 68.231°W; Clarke et al. 2008) located in Ryder Bay on the Western Antarctic Peninsula (Fig. S1). Sampling was performed during the Austral summer from November 2013 to February 2014. Discrete seawater samples were collected from 15 m depth by a 12 L Niskin bottle deployed from a small boat. Full water column profiles were obtained using a SeaBird 19+ conductivity temperature depth (CTD) instrument supplemented with a LiCor photosynthetically available radiation (PAR) and an in-line fluorescence sensor (WetLabs). Temporal differences in environmental variables are published in Biggs et al. (2019), but also shown for each experiment in Table S1. Seawater samples were shielded from light and processed directly upon return to the research base in a temperature-controlled

lab close to situ temperature (~ 0.5°C). The modified dilution mortality assay was conducted approximately once per week depending on whether boating was possible.

Phytoplankton

For phytoplankton enumeration, fresh 3.5 mL sub-samples were analysed according to Marie et al (1999) using a Becton Dickinson FACSCalibur equipped with an air-cooled Argon laser with an excitation wavelength of 488nm (15mW) and the trigger set on red fluorescence. Phytoplankton populations were distinguished using bivariate scatter plots of red Chlorophyll-*a* (Chl-*a*) autofluorescence versus side scatter. The obtained raw flow cytometry data files were analysed using the freeware CYTOWIN (Vaulot 1989). Over the course of the season 10 phytoplankton populations were distinguished, Phyto I – X, with average cell diameters of 0.9, 1.8, 3.1, 4.0, 4.5, 4.5, 7.4, 8.1, 11.5 and 20.4 µm. Cryptophytes (Phyto IV) were discriminated based on their orange phycoerythrin autofluorescence (Li and Dickie 2001). The Phyto III population was identified as *Phaeocystis* spp and Phyto V-X as diatoms based on microscopic identification and/or taxonomic identification (Biggs et al. 2019). Phytoplankton enumeration during the previous season (December 2012 to March 2013; Chapter 3) was performed on fixed samples. Phytoplankton population counts of live and fixed samples showed no significant difference (Mann-Whitney U Test: $n = 44$ and $p = 0.24$) indicating that phytoplankton data in each season could be compared.

The cellular carbon (C) content of each phytoplankton population was estimated from the average cell diameter and using conversion factors of 237 and 196.5 fg C µm^{-3} for pico- (Phyto I-III) and nano-sized (Phyto IV-IX) phytoplankton populations (Garrison et al. 2000; Worden et al. 2004). For phytoplankton growth and losses, rates were first converted into cells and integrated over time, then to cellular C (Chapter 3).

Growth and mortality rates

The modified dilution assay was used to determine viral lysis and grazing rates of the identified phytoplankton populations (Mojica et al. 2016). Natural seawater was gently passed through 200 µm sized mesh to remove the larger zooplankton and mixed into 1 L polycarbonate bottles with either grazer free (0.45 µm) or grazer + virus free (30kDa) filtrates to create a dilution series (in triplicate) containing 100%, 70%, 40% and 20% of natural seawater. The grazer free diluent was prepared by gravity filtration of natural seawater using a 0.45 µm Sartopore capsule filter with a 0.8 µm pre-filter (Sartopore 2300, Sartorius Stedim Biotech, Göttingen, Germany). The grazer + virus free ultra-filtrate (30-kDa) was created by tangential flow filtration of natural seawater using a polyethersulfone membrane (Vivaflow 200, Sartorius Stedim Biotech, Göttingen, Germany). The 24 experimental bottles were transferred in the dark to an outdoor (natural seawater) flow-through incubator; randomly placed on a slow turning wheel (~0.5 rpm) and incubated for 24 hours at *in-situ* temperature and light conditions (using neutral-density mesh).

Phytoplankton enumeration was performed by flow cytometric analysis of live samples at the beginning (T_0) and end (T_{24}) of each experiment. Actual dilutions (at T_0) were calculated for each incubation bottle as a proportion of the 100% replicates average in each series. Specific growth rates for each phytoplankton population were calculated using the natural logarithm, and when plotted against dilution (*x*-axis), gross growth rates (μ_{gross}) were represented by the *y*-axis intercept of the linear regression. Grazing rates were calculated as the slope of the linear regression in the 0.45 µm dilution series and total mortality (T_M) as the slope in the 30-kDa. Rates of viral lysis were calculated by subtraction (T_M minus grazing). Phytoplankton rates from November 2013 - February 2014 were compared to rates from the previous season (December 2012 and March 2013; Chapter 3), designated season 2 (S2) and season 1 (S1) respectively.

Statistics

A significant difference between the regression coefficent of the 0.45 µm series and zero indicates significant grazing whilst that of the 30-kDa series indicates both significant μ_{gross} and T_M. A significant difference between the regression coefficients of grazing and T_M (as tested by analysis of covariance, $p < 0.05$, using R statistical software; R Development Core Team 2012) represents significant rates of viral lysis. Throughout the text the plus-minus symbol ($\pm$) represents 1 standard deviation. Differences between environmental variables, as well as between μ_{gross}, grazing, viral lysis and T_M rates (also cells and carbon), were tested using either a two-tailed Student's or Welch's *t*-test and a Mann-Whitney U Test if data deviated from normality as assessed by the Shapiro-Wilk test (SigmaPlot v14, from Systat Software, Inc., San Jose California, USA). The strength of relationships between viral lysis, grazing and gross growth were determined using a Pearson's Correlation test (SigmaPlot v14).

Results and Discussion

Phytoplankton dynamics

The temporal dynamics of the different phytoplankton groups (season S2, Fig. 1) displayed largely similar dynamics as during the year before (S1; Chapter 3), with notable exceptions by Phyto VI and IX that did not bloom towards the end of summer as compared to S1. Unlike S1, Phyto IX bloomed only during December of S2 (Fig. 1i). Furthermore, Phyto VII and X were mostly absent in S1. In contrast, cryptophytes Phyto IV and diatoms Phyto VI displayed much lower abundances in S2 than S1 (Biggs et al. 2019). Antarctic cryptophytes have previously been associated with reduced salinities (Buma et al. 1992; Moline et al. 1997, 2004; Mendes et al. 2013), however, more recent research indicates temperature is a primary driver in the WAP region (Mendes et al. 2017; Biggs et al. 2019). Temperature was > 0°C for only 12 days in S2 and their abundance seem mostly related to increased light availability (Biggs et al. 2019). Temperature was on
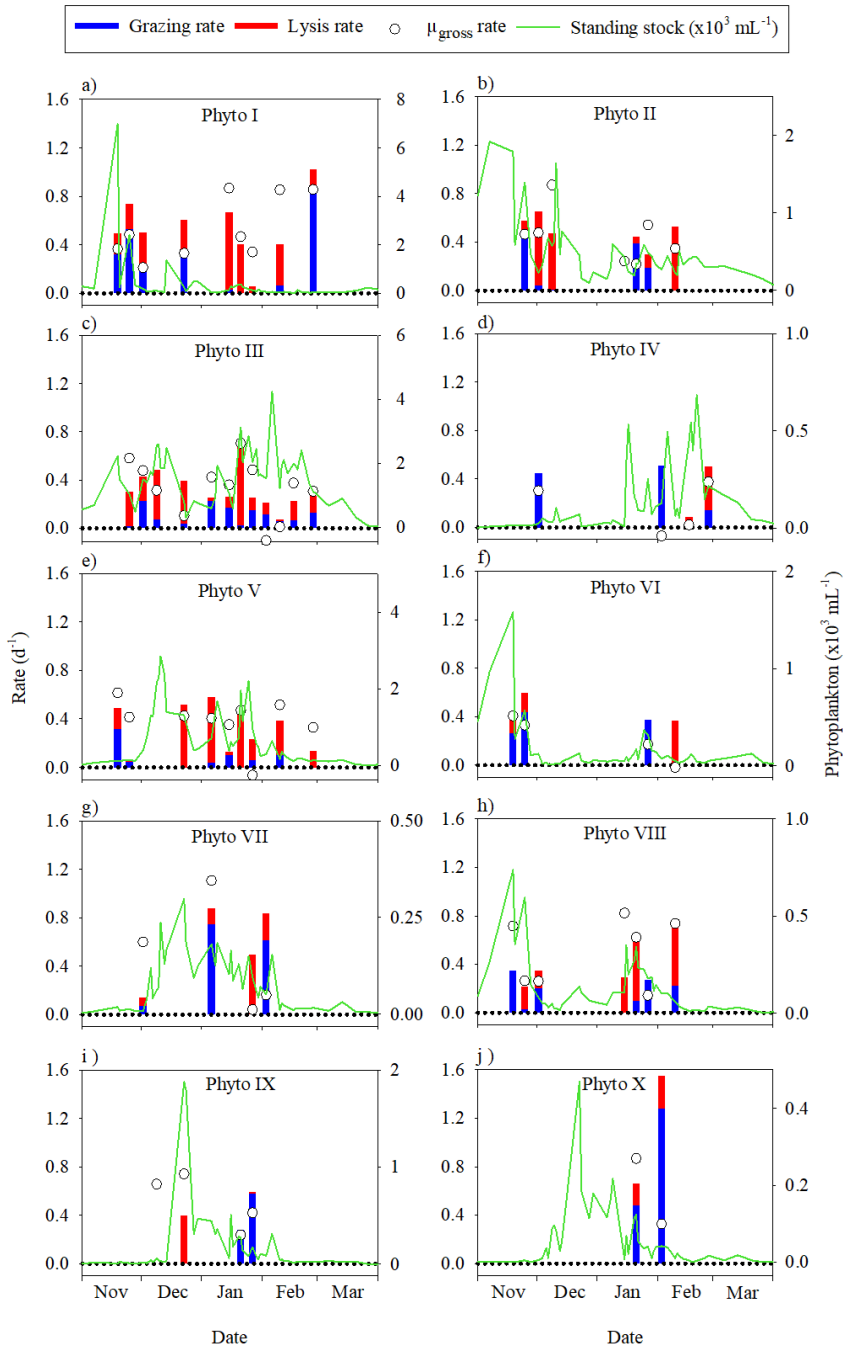
Fig. 1. Seasonal dynamics (November 2013 – March 2014) of phytoplankton abundance (green line), gross growth (μ_{gross}; open circles), viral lysis (Ly; red bars) and grazing (Gr; blue bars) rates for FCM groups Phyto I –X (a – j). NOTE: scale of axis for abundance (vertical axis to the right) differs between subplots and abundance data is composed of 48 data points.

average significantly lower during S2 (-0.37°C) compared to S1 (0.37°C; Student's *t*-test: $t_{87} = 4.669$, $n_1 = 39$ $n_2 = 50$, $p < 0.001$, Table S1). Lower temperatures during S2 were likely the result of a greater frequency of mixing events, especially around mid-summer (late December), that broke through the relatively shallow thermocline and reduced shallow seawater temperatures as cold winter water (< 0°C) was mixed up from below (Biggs et al. 2019). The diatom Phyto IX was associated mainly with low PAR, which explains the peak in abundance during December of S2 (Fig. 1i) and the lack of a late summer bloom as found in S1 (Biggs et al. 2019). Light levels declined to low concentrations during December in S2 (0.2 µmol quanta m^{-2} s^{-1}), however, for the remainder of the season PAR was above potentially limiting levels required for Phyto IX to outcompete (Biggs et al. 2019). Lower total standing stock of Phyto IX in S2 (Mann-Whitney U test: U = 603, $n_1 = 40$ $n_2 = 50$, $p = 0.001$) coincided with much lower peak Chl-*a* concentrations (maximum of 7 µg L^{-1}; Fig. S2) when compared to S1 (16 µg L^{-1}; Biggs et al. 2019). Lower temperatures in S2 also prolonged sea ice melt whereby Phyto VII and X were linked to sea ice during periods of ice-cover. Although numbers of Phyto X were relatively low overall (mean = 52 mL^{-1}), its larger cell size (20 µm diameter) resulted in a 34% contribution to total seasonal carbon standing stock. We speculate that with increasing temperature by global warming, the presence of these two groups will quickly reduce (Phyto X present in the colder S2 and not in the warmer S1), negatively impacting copepod production and thus transfer of matter and energy to higher trophic levels (Irigoien et al. 2014; Dezutter et al. 2019; Biggs et al. 2020). Overall in S2 the $\leq$ 20 µm size fraction constituted 67 ± 27% of total Chl-*a* (except for 31 January to 12 February S2), similar to S1 (Biggs et al. 2019). In line with the literature (Clarke et al. 2008; Rozema et al. 2017b; Biggs et al. 2019), the pico-sized Phyto I and II and *Phaeocystis* Phyto III were numerically dominant earlier in the season (November S2; when mixed layer depth was still 53m; Table S1).

Phytoplankton-specific thermal thresholds and temperature growth curves (Boyd et al. 2013; Coello-Camba and Agustí 2017) are expected to result in a diverse response

to the same change in temperature (i.e. temperatures > and < 0°C). For example, Phyto I abundances were associated with higher light availability, rather than temperature (Biggs et al. 2019), and similar dynamics were observed in both the warmer S1 and colder S2 productive season (Fig. 1a and Biggs et al. 2019). After a mixing event mid-January (peak wind speed 20 m s^{-1}), when also salinity rapidly declined due to sea ice melt (Table S1; Rozema et al. 2017a; Biggs et al. 2019), especially *Phaeocystis* Phyto III and diatoms Phyto V and VIII increased (Fig. 1c, e, h). Diatom Phyto V abundances peaked at the beginning of the 'spring' bloom when the mixed layer shallowed and light intensity and temperature (although still cold < 0°C) increased (Biggs et al. 2019). This matches the reported development of diatom blooms in shallow mixed layers with high light levels (Kropuenske et al. 2009; Arrigo et al. 2010; Alderkamp et al. 2013) where higher temperatures during the stratified period also likely stimulate their growth (Suzuki and Takahashi 1995; Coello-Camba and Agustí 2017). *Phaeocystis* spp. Phyto III was one of the most abundant and persistently present groups in both seasons, as can be expected for the Southern Ocean (Schoemann et al. 2005; Alderkamp et al. 2012b). Light availability can vary considerably during the productive season (Clarke et al. 2008; Biggs et al. 2019) and high contributions by *Phaeocystis* are likely maintained due to relatively high growth rates displayed over a broad range of light intensities (Kropuenske et al. 2009, 2010; Arrigo et al. 2010), as well as under low concentrations of dissolved iron (Alderkamp et al. 2012a).

Viral lysis and grazing rates

Taking only the overlapping time periods of S2 with S1 into account, comparable average viral lysis rates were observed (i.e. 0.23 ± 0.21 d^{-1} for S2 compared to 0.28 ± 0.27 d^{-1} for S1; $n = 44$ and 46, respectively; Fig. S3a). Overall inter-annual variability of the specific viral lysis rates was also low when taking into account all data (on average 0.22 ± 0.19 d^{-1} for S2 compared to 0.29 ± 0.32 d^{-1} for S1, $n = 62$ and 98, respectively; Fig. S3b). Grazing, however, was significantly lower in S2 compared to S1, both during comparable time periods (0.15 ± 0.19 in S2 vs $0.32 \pm$

0.30 d^{-1} in S2, Mann-Whitney U test: U = 657, n_1 = 44 n_2 = 46, p = 0.004, Fig. S3a) and when all rate data were included (0.21 ± 0.25 d^{-1} in S2 and 0.32 ± 0.27 d^{-1} in S1, Mann-Whitney U test: U = 2247, n_1 = 62 n_2 = 98, p = 0.006, Fig. S3b). This implies that grazing was reduced to a greater extent in S2 compared to viral lysis. Even so, viral lysis and grazing rates in S2 (Table S2) showed a negative correlation (Pearson's r = -0.307, n = 62, p = 0.0152), similar to the tradeoff between mortality factors observed in S1 (Chapter 3). This finding hints to a general feature in these Antarctic coastal waters that is only evident when simultaneously assessing rates of viral lysis and grazing. Ecological consequences of such seasonal variation in mortality factors directly feeds through to the efficiency of trophic transfer and the biological carbon pump (Turner 2015; Basu and Mackey 2018; Talmy et al. 2019). The share of grazing was lower in the colder S2 than in the warmer S1 (46 vs 55% respectively), suggesting that temperature may have a greater impact on grazer populations compared to viruses. As temperature declines, rates of herbivorous protist growth have been shown to decrease more than that of phytoplankton (Rose and Caron 2007). This could result in a relative overabundance of (produced) algal cells during times of high phytoplankton growth, especially when temperatures are low. As such, (relatively) higher contact rates may be maintained between virus and host, resulting in viral lysis being the pre-dominant loss factor regulating increases in standing stock. The balance between numbers of phytoplankton (host) and infective viruses, would likely result in a threshold contact rate above which large population declines are observed (Singh et al. 2004) and could explain the trend that high viral lysis was often observed alongside low grazing, and vice versa. Additionally, prey abundance is a key factor controlling microzooplankton growth and so their grazing impact will be relatively low in the early stages of bloom development when phytoplankton food availability, and also microzooplankton growth are low (Sherr and Sherr 2009).
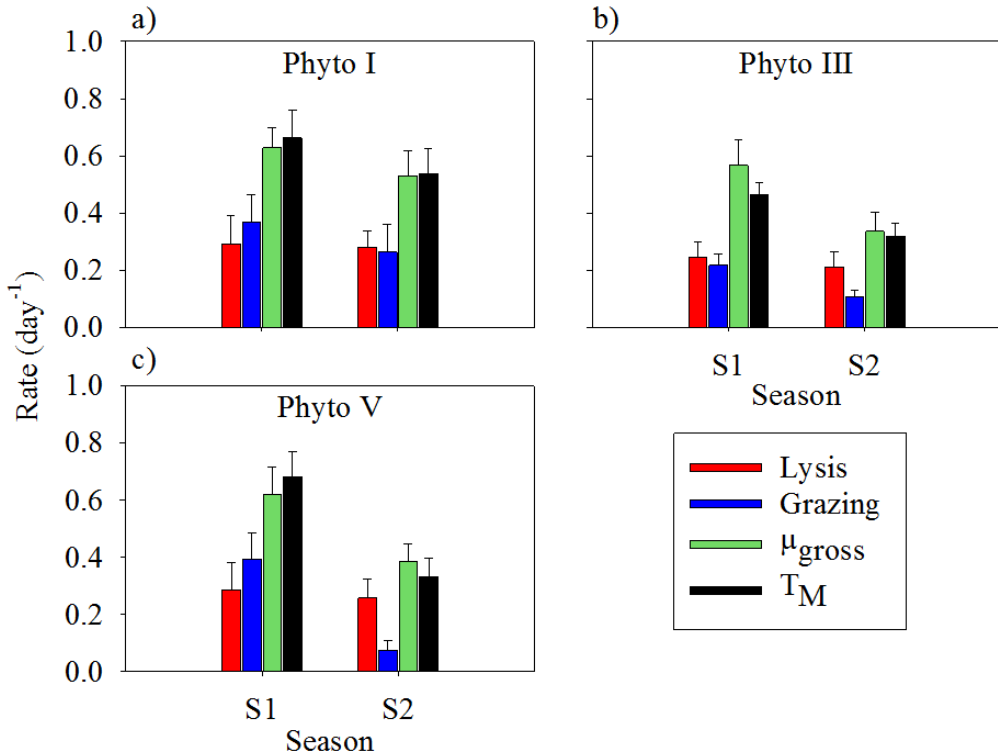
Fig. 2. Seasonal mean specific rates (d^{-1}) of lysis, grazing, gross growth (μ_{gross}) and total mortality (T$_M$ i.e. lysis and grazing) are shown for Phyto I, III and V (subplot a – c, respectively). Error bars represent ± 1 standard error.

The phytoplankton groups with best temporal coverage of mortality rates over the productive season are pico-Phyto I, *Phaeocystis* Phyto III and diatoms Phyto V (Fig. 1a, c, e; each $n \geq 9$, most comparable to S1). Average viral lysis and grazing rates of Phyto I were comparable to each other and to S1 (Fig. 2a). Grazing dominated total mortality of Phyto I during late spring and early summer (November and December S2, 0.36 ± 0.13 d-1, $n = 4$, $p = 0.002$, Fig. 1a) and high abundances may have benefitted the smallest grazers early in the productive season (Rose and Caron 2007). During mid-late summer when abundances were low, grazing rates had declined (0.02 ± 0.03 d^{-1} during January to mid-February S2). Significantly higher rates of viral lysis (than grazing) during the second half of S2 (0.36 ± 0.24 d^{-1}, Student's *t*-test: $t_6 = -2.815$, $n_1 = n_2 = 4$, $p = 0.031$) resulted in a 94% share of total mortality (Fig. 1a). High grazing early season, followed by high viral lysis later on, mimicks

the trend in S1 (69% and 70% of total losses, respectively). Although rates of viral lysis were relatively low in the first half of the season, high host numbers could result in gradually rising stocks of infective viruses. High rates of gross growth displayed in the second half of the season (in S2, 0.63 ± 0.27 d^{-1}, $n = 4$, Fig. 1a and Table S2; in S1, 0.67 ± 0.21 d^{-1}, $n = 5$, Chapter 3) may have increased virus burst sizes and reduced the latent period (Bratbak et al. 1998; Maat et al. 2017) resulting in high contact rates between lytic viruses and their hosts, exerting strong viral control and preventing bloom formation (Brussaard 2004; Brussaard et al. 2005a). Towards the end of February, intense mixing (Table S1) would have diluted stocks of infective viruses which coincided with a rapid increase in the share of grazing once more (Fig. 1a).

For *Phaeocystis* Phyto III (Fig. 1c) and diatom Phyto V (Fig. 1e), grazing rates were significantly lower in S2 than S1 (0.11 ± 0.07 vs 0.22 ± 0.15 d^{-1} for Phyto III, and 0.05 ± 0.1 vs 0.39 ± 0.35 d^{-1} for Phyto V; Welch's *t*-test: $t_{21} = 2.428$, $n_1 = 12$ $n_2 = 15$, $p = 0.0242$; $t_{16} = 3.286$, $n_1 = 9$ $n_2 = 14$, $p = 0.0048$, Fig. 2b, c respectively), regardless of the time period in the productive season. Viral lysis rates were not significantly different, i.e. Phyto III 0.21 ± 0.19 and 0.25 ± 0.21 d^{-1}, and Phyto V 0.26 ± 0.20 and 0.29 ± 0.36 d^{-1}, for S2 and S1 respectively (Fig. 2b, c). In contrast to Phyto I, gross growth rates of Phyto III and Phyto V differed between the years, i.e. lower rates in S2 (0.34 ± 0.23 d-1 and 0.38 ± 0.19 d-1, respectively) compared to S1 (0.57 ± 0.35 d-1 and 0.62 ± 0.36 d-1, Welch's *t*-test: $t_{25} = -2.048$, $n_1 = 12$ $n_2 = 15$, $p = 0.0515$; $t_{20} = -2.052$, $n_1 = 14$ $n_2 = 9$, $p = 0.0532$ respectively). However, the standing stock of Phyto III and V was significantly higher in S2 (1597 and 677 mL^{-1}) compared to S1 (1059 and 188 mL^{-1}, Welch's *t*-test: $t_{17} = 2.376$, $n_1 = 13$ $n_2 = 15$, $p = 0.0298$; Mann-Whitney U Test: U = 49.5 $n_1 = 13$ $n_2 = 15$, $p = 0.029$, respectively). At large, the net growth (resultant of gross growth rate minus total losses) matched the temporal dynamics of the abundances. A similar trend of lower gross growth, a larger share of viral lysis and a significantly higher standing stock was also displayed by diatoms Phyto VIII ($n = 7$) as well as a greater share of viral lysis by picoeukaryote Phyto II ($n = 6$; Fig. S4a, b). This infers a greater importance

of viral lysis in S2. Temperature imposes a fundamental control on metabolic processes (Boscolo-Galazzo et al. 2018) and low temperatures in S2 may have reduced maximum potential growth of both phytoplankton and grazers. Microzooplankton are generally larger than their phytoplankton prey and due to the size scaling of metabolic rates (Finkel et al. 2004), low temperature seasons may result in a larger reduction in grazer growth potential compared to that of phytoplankton (Rose and Caron 2007; Rose et al. 2013).

This study validates that viral lysis is an important loss factor for natural populations of *Phaeocystis*, cryptophytes and diatoms in the cold waters around Antarctica. Considerable viral lysis rates have also been reported for *Phaeocystis* in temperate natural waters (0.4 d^{-1}; Baudoux et al. 2006). To our knowledge, no Antarctic phytoplankton viruses have been brought into culture thus far and there is only one Arctic phytoplankton virus isolated for the picoeukaryote *Micromonas polaris* (Maat et al. 2017). The *Phaeocystis* viruses characterized to date have large double stranded DNA genomes (Jacobsen et al. 1996; Baudoux and Brussaard 2005), whereas the diatom viruses isolated have small RNA and DNA genomes (Nagasaki 2008; Tomaru et al. 2009). At present there is only one cryptophyte virus reported, originating from a subtropical brackish lagoon (Nagasaki et al. 2009). More detailed studies on the types of phytoplankton viruses present in Antarctic waters will improve a much needed understanding of viral control on phytoplankton diversity and production.

Cryptophytes Phyto IV and diatoms Phyto VI were associated with high temperatures in S1, agreeing with significantly lower numbers (Mann-Whitney U = 622.5 and 182.5, $n_1 = 40$ $n_2 = 51$, $p = 0.001$ and < 0.001, respectively) and reduced rates of gross growth in S2 (Student's t-test: $t_{11} = 2.92$, $t_{16} = 2.34$, $p = 0.014$ and 0.032, respectively, Fig. S4c, d). Temperature seems to be a major driver of cryptophyte growth and viral lysis rates, with much lower rates in the colder S2. Whilst grazing of Phyto V was reduced in S2 (Fig. 2c), grazing rates of the similar sized diatom Phyto VI showed little variation between years, as did rates of viral lysis (Fig. S4d). Even though rates of viral lysis were not significantly different between seasons,

average rates were slightly lower in S2 (0.22 d^{-1}) compared to S1 (0.29 d^{-1}) and temperature may have been restrictive (Demory et al. 2017; Maat et al. 2017; Piedade et al. 2018). The optimal temperature for lytic replication (i.e. the temperature that generates fast host lysis and/or high viral yield) generally matches the host optimal growth temperature and the impact of temperature on viral infection could arise from changes in host metabolism (Demory et al. 2017). Positive relationships between host growth rate and viral lysis have been demonstrated for both bacteria and phytoplankton in both the laboratory and field (e.g. Bratbak et al. 1998; Middelboe 2000; Baudoux et al. 2007; Gann et al. 2020). Although virus infectivity and production can be influenced by temperature (Demory et al. 2017; Maat et al. 2017; Piedade et al. 2018), virus replication is directly reliant on host cell physiology potentially resulting in a tighter coupling of viral lysis and phytoplankton growth rates compared to grazers (Menden-Deuer et al. 2018). Net accumulation of phytoplankton could further increase virus-host contact rates resulting in a greater share of viral lysis.
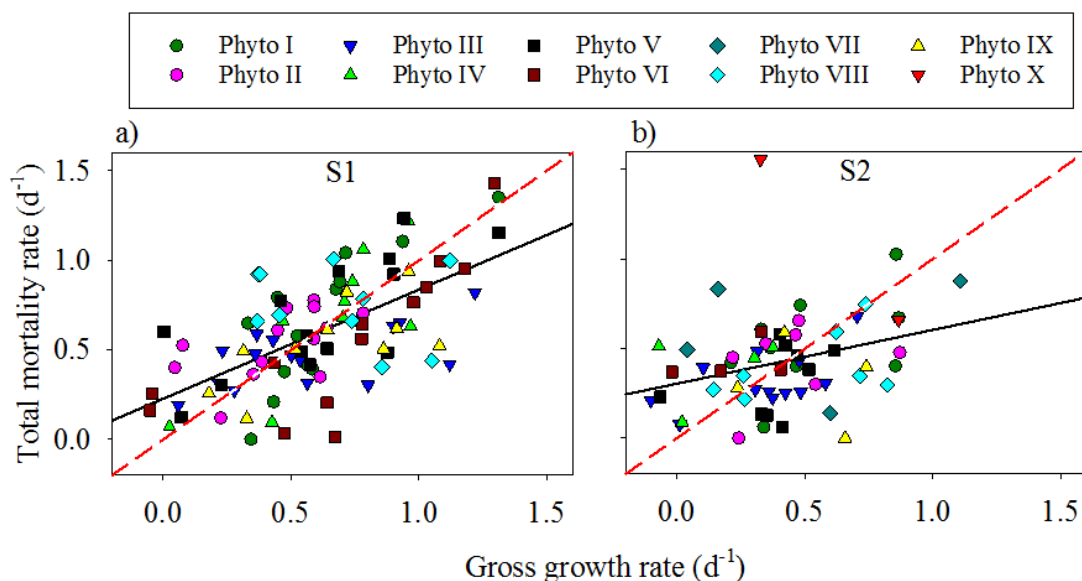
Fig. 3. Gross growth and total mortality rates are plotted for (a) S1 and (b) S2; for Phyto groups I - X. The 1:1 line (red dashed line) and linear regressions (solid black line) are identified in each subplot. The regression line for S1 has a slope of 0.61 ($r^2 = 0.40$; $p < 0.0001$, $n = 98$) and for S2 a slope of 0.30 ($r^2 = 0.10$; $p = 0.0168$, $n = 62$).

Linear regressions of gross growth and losses (Fig. 3) indicate that lower rates of growth were required in S2, compared to S1, to outgrow losses and observe an increase in standing stock. The equilibrium growth rate where net growth is zero (intercept of 1:1 and linear regression, 0.59 d^{-1} in S1 and 0.42 d^{-1} in S2, Fig. 3) is highly similar to the seasonal average of gross growth (0.61 d^{-1} in S1 and 0.41 d^{-1} in S2). During the accumulation phase of phytoplankton, net growth is positive and represented by the linear regression to the right of the intercept (*x*-axis), whereas standing stock decline is represented by the left of the intercept. The total mortality rates are the sum of viral lysis and grazing, and over a seasonal phytoplankton production cycle represented by Fig. 3, the average viral lysis rate during accumulation (growth > equilibrium) was higher than grazing (ratio lysis to grazing: 1.1 in S1 and 1.4 in S2). Overall this implies the efficiency of carbon flow from Antarctic primary producers to zooplankton consumers during accumulation phases is less efficient than previously thought. In contrast, during the decline phase (growth < equilibrium), grazing displayed a greater share than viral lysis (ratio of 0.70 in S1 and 0.84 in S2). This trend occurred over a wide range of growth rates, with the tipping point in the share of loss factors related to the seasonal average growth. More specifically, viral lysis rates were significantly different in both years between accumulation and decline phases, i.e. in S1 0.39 and 0.18 d^{-1}, respectively (Mann-Whitney U test: $U = 762$, $n_1 = n_2 = 49$, $p = 0.002$); and in S2 0.28 d^{-1} and 0.17 d^{-1} (Mann-Whitney U test: $U = 325$, $n_1 = 28$ $n_2 = 34$, $p = 0.033$), but grazing rates were not (0.37 and 0.25 d^{-1} in S1, 0.21 and 0.21 d^{-1} in S2; $p = 0.093$ and 0.826 respectively). This suggests that grazing rates vary less than viral lysis in response to phytoplankton growth and supports the idea that rates of viral lysis are more tightly coupled to phytoplankton growth than grazing. Previous studies have suggested a close coupling of phytoplankton growth and grazing (Pearce et al. 2008; Landry et al. 2009, 2011) and we also recorded a significant relationship (S1+S2 data; Fig. S5a), but largely driven by Phyto I. The significant positive relationship between viral lysis and gross growth rates (Fig. S5b) was more general and in particular *Phaeocystis* Phyto III, cryptophytes Phyto IV and diatoms Phyto V and VI

showed increased viral lysis rates with gross growth. Increasing cell numbers of each particular host during the accumulation phase will lead to a higher probability of encounter between host and virus, leading to more viral lysis. Furthermore, phytoplankton production and growth is controlled by light availability, that in turn affects virus production (Mojica and Brussaard 2014). During dense bloom development, potential shelf-shading may negatively impact virus proliferation caused by reduced light intensities (Baudoux and Brussaard 2008; Maat et al. 2016; Gann et al. 2020) which aids to shifting the balance in favour of grazing (Hoppe et al. 2017).
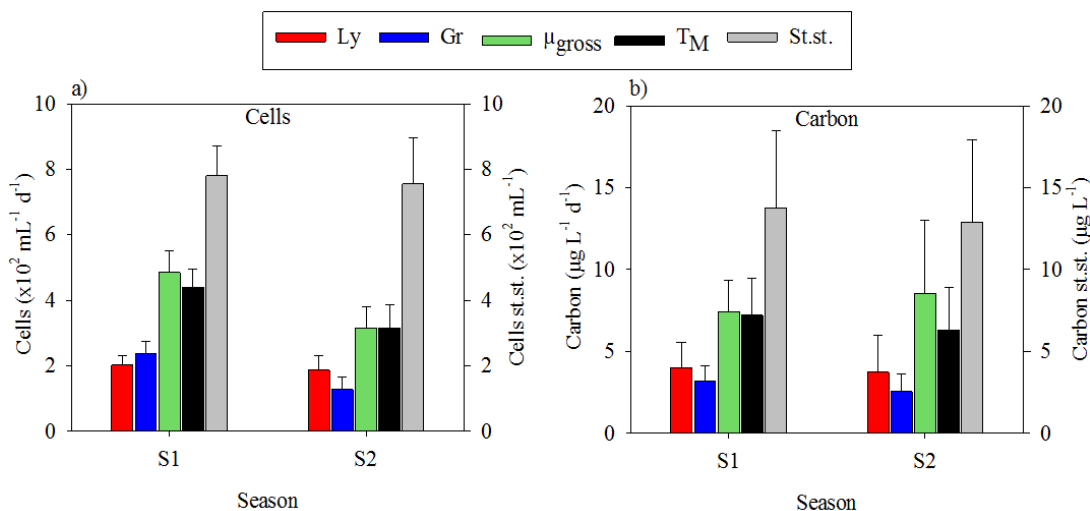
Fig. 4. Seasonal averages of lysis (Ly), grazing (Gr), gross growth (μ_{gross}), total mortality (T_M, i.e. lysis and grazing) and standing stock (st. st.) are shown (a) in cells and (b) in carbon. Error bars represent ± 1 standard error.

Phytoplankton carbon lysed

In contrast to cell abundances (Fig. 4a), cellular carbon produced and lysed were not significantly different between seasons, whilst carbon grazed was significantly lower in S2 (Mann-Whitney U test: $U = 2467$, $n_1 = 62$ $n_2 = 98$, $p = 0.045$, Fig. 4b). For the most dominant Phyto groups (I, III and V), both cells and carbon produced and grazed were similar between seasons unlike cells and carbon lysed that was higher in S2 (Fig. S6). Using average rates from the accumulation and decline phases (and
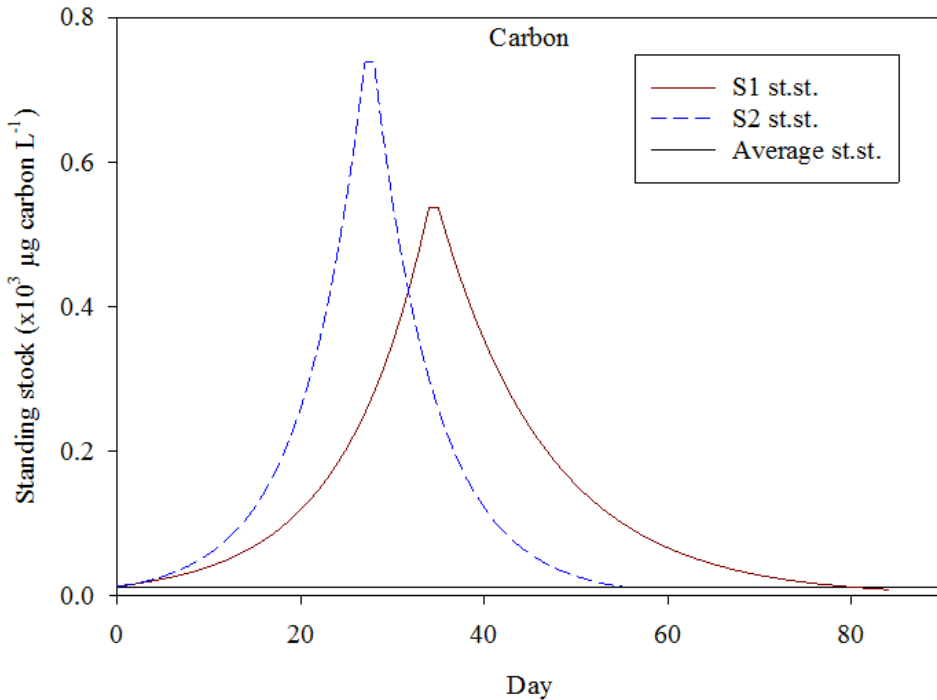
Fig. 5. Modelled phytoplankton biomass (µg carbon L⁻¹) during S1 and S2 using seasonal average rates of gross growth and total mortality from bloom accumulation and decline phases. Average standing stock was used as the starting concentration (*y*-axis reference line) and bloom climax (an arbitrary period of 1 day where net growth equals zero) was determined as peak phytoplankton biomass actually displayed in each season.

integrating over time) to model phytoplankton production in each season (Fig. 5), biomass accumulation was faster in S2 due to relatively lower losses compared to phytoplankton gross growth. A closer coupling of phytoplankton and grazer growth at higher temperatures (Rose and Caron 2007) could explain the relatively higher predation pressure in S1 and subsequently more equal share of viral lysis and slower build-up of biomass when gross growth rates were higher.

Viral lysis bridged-the-gap between production and losses to generate a mass balance of phytoplankton, both for Phyto I, III and V (the most numerous groups, Fig. 6a) as well as all Phyto groups (Fig. 6b). Furthermore, differences in the size class of production between seasons resulted in quantitatively similar carbon flow (Fig. 4b).
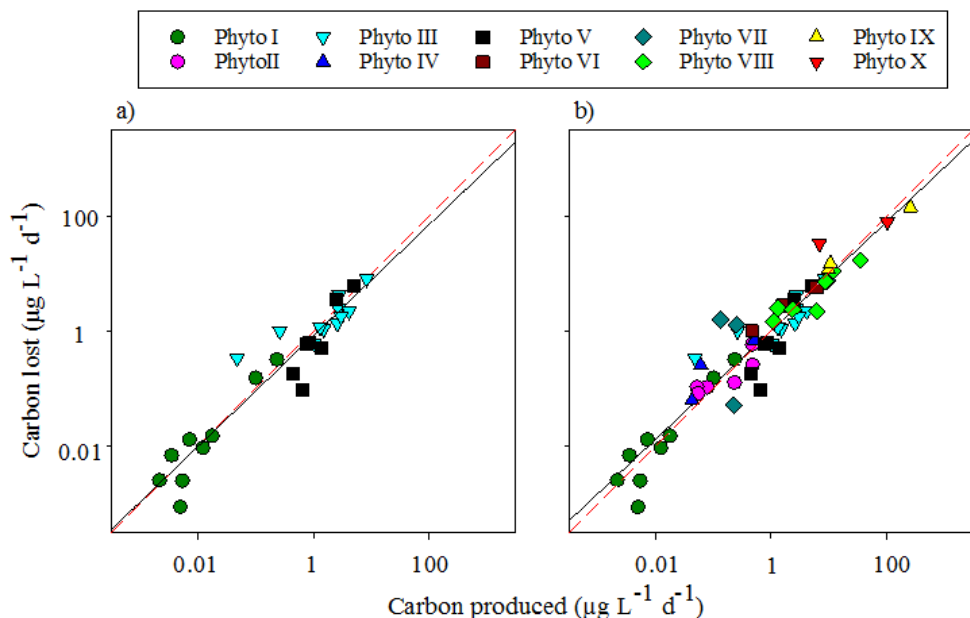
Fig. 6. Phytoplankton carbon lost (i.e. lysis plus grazing,) plotted against carbon produced in season 2 (S2), obtained after conversion of the different phytoplankton group abundances (integrated over time using the specific viral lysis, grazing, total mortality and gross growth rates (d^{-1})). Shown in (a) are the groups with the most data Phyto I, III and V and (b) all phytoplankton data. The 1:1 (red dashed) and linear regression lines (solid black) are included. The linear regression (Lin. reg.) in (a) has a slope of 0.96 ($r^2 = 0.90$; $p < 0.0001$, $n = 28$) and (b) has a slope of 0.90 ($r^2 = 0.90$; $p < 0.0001$, $n = 56$). Note: zeros and negative values were excluded from log transformed carbon data in subplots: (a) $n = 0$ and 2; (b) $n = 2$ and 4, respectively.

This difference was due to greater carbon contributions by the high temperature associated small-sized diatom Phyto VI in S1 (19% of total carbon produced), compared to greater contributions by the large-sized sea ice seeded diatom Phyto X in S2 (21% of carbon produced) when temperatures were colder and sea ice melt was prolonged (Rozema et al. 2017a; Biggs et al. 2019).

Similar to S1, Phyto IX contributed most to total carbon production in S2 (56 and 54% respectively). During peak abundance of Phyto IX in late December of S2, viral lysis was responsible for the majority of carbon lost (146 µg C L^{-1} d^{-1}; Table S3) as also found during large lysis events of Phyto IX throughout S1 (Chapter 3). As such, these medium nano-sized diatoms (11.5 µm) are potentially a key conduit of carbon flow to higher trophic levels in Antarctic ecosystems, allowing larger zooplankton

efficient access to primary production (Atkinson 1994; Sommer and Sommer 2006). Herbivorous grazing by larger zooplankton (such as copepods and krill) not only represents efficient carbon flow to higher trophic levels, but also carbon sequestration to the deep ocean due to the rapid sedimentation of large, biogenic silica ballasted faecal pellets (Voss 1991; Pasternak and Schnack-Schiel 2001; Turner 2015). Therefore, a few such biomass-large lysis events (Phyto IX or Phyto III, V, VIII and X during mid-January in S2) could have a disproportionately larger impact on carbon flow, stimulating microbial utilization (Fig. S7). Besides increased community respiration by the microbial loop, viral lysis of diatoms may still induce aggregate formation and rapid sinking (Yamada et al. 2018), consequentially contributing to carbon sequestration (Brussaard et al. 2008). During phytoplankton accumulation the viral shunt could thus already be an important and alternative (to grazer faecal pellets) driver of sedimentation that establishes a potential teleconnection between surface and deep water that ultimately influences the life cycle of herbivorous copepods, such as the lack of a second spawning event in S2 compared to S1 (Biggs et al. 2020).

4

Competing Interests

The authors declare no competing interests.

References

Alderkamp A, Mills M, van Dijken G, Arrigo K (2013) Photoacclimation and non-photochemical quenching under in situ irradiance in natural phytoplankton assemblages from the Amundsen Sea, Antarctica. Mar Ecol Prog Ser 475:15–34. doi: 10.3354/meps10097

Alderkamp AC, Kulk G, Buma AGJ, et al (2012a) The effect of iron limitation on the photophysiology of *Phaeocystis antarctica* (Prymnesiophyceae) and *Fragilariopsis cylindrus* (Bacillariophyceae) under dynamic irradiance. J Phycol 48:45–59. doi: 10.1111/j.1529-8817.2011.01098.x

Alderkamp AC, Mills MM, van Dijken GL, et al (2012b) Iron from melting glaciers fuels phytoplankton blooms in the Amundsen Sea (Southern Ocean): Phytoplankton characteristics and productivity. Deep Res Part II Top Stud Oceanogr 71–76:32–48. doi: 10.1016/j.dsr2.2012.03.005

Arrigo KR, Mills MM, Kropuenske LR, et al (2010) Photophysiology in two major southern ocean phytoplankton taxa: Photosynthesis and growth of *Phaeocystis antarctica* and *Fragilariopsis cylindrus* under different irradiance levels. Integr Comp Biol 50:950–966. doi: 10.1093/icb/icq021

Atkinson A (1994) Diets and feeding selectivity among the epipelagic copepod community near South Georgia in summer. Polar Biol 14:551–560. doi: 10.1007/BF00238225

Basu S, Mackey KRM (2018) Phytoplankton as key mediators of the biological carbon pump: Their responses to a changing climate. Sustainability 10:869. doi: 10.3390/su10030869

Baudoux A-C, Brussaard CPD (2005) Characterization of different viruses infecting the marine harmful algal bloom species *Phaeocystis globosa*. Virology 341:80–90. doi: 10.1016/j.virol.2005.07.002

Baudoux A-C, Brussaard CPD (2008) Influence of irradiance on virus-algal host interactions. J Phycol 44:902–908. doi: 10.1111/j.1529-8817.2008.00543.x

Baudoux A-C, Noordeloos AAM, Veldhuis MJW, Brussaard CPD (2006) Virally induced mortality of *Phaeocystis globosa* during two spring blooms in temperate coastal waters. Aquat Microb Ecol 44:207–217. doi: 10.3354/ame044207

Baudoux A-C, Veldhuis MJW, Witte HJ, Brussaard CPD (2007) Viruses as mortality agents of picophytoplankton in the deep chlorophyll maximum layer during IRONAGES III. Limnol Oceanogr 52:2519–2529. doi: 10.4319/lo.2007.52.6.2519

Biggs TEG, Alvarez-Fernandez S, Evans C, et al (2019) Antarctic phytoplankton community composition and size structure: Importance of ice type and temperature as regulatory factors. Polar Biol 42:1997–2015. doi: 10.1007/s00300-019-02576-3

Biggs TEG, Brussaard CPD, Evans C, et al (2020) Plasticity in dormancy behaviour of *Calanoides acutus* in Antarctic coastal waters. ICES J Mar Sci. doi: 10.1093/icesjms/fsaa042

Boscolo-Galazzo F, Crichton KA, Barker S, Pearson PN (2018) Temperature dependency of metabolic rates in the upper ocean: A positive feedback to global climate change? Glob Planet Change 170:201–212. doi: 10.1016/j.gloplacha.2018.08.017

Boyd PW, Rynearson TA, Armstrong EA, et al (2013) Marine phytoplankton temperature versus growth responses from polar to tropical waters – Outcome of a scientific community-wide study. PLoS One 8:e63091. doi: 10.1371/journal.pone.0063091

Bratbak G, Egge JK, Heldal M (1993) Viral mortality of the marine alga *Emiliania huxleyi* (Haptophyceae) and termination of algal blooms. Mar Ecol Prog Ser 93:39–48. doi: 10.3354/meps093039

Bratbak G, Jacobsen A, Heldal M, et al (1998) Virus production in *Phaeocystis pouchetii* and its relation to host cell growth and nutrition. Aquat Microb Ecol 16:1–9. doi: 10.3354/ame016001

Brussaard CPD (2004) Viral control of phytoplankton populations-A review. J Eukaryot Microbiol 51:125–138. doi: 10.1111/j.1550-7408.2004.tb00537.x

Brussaard CPD, Kuipers B, Veldhuis MJW (2005a) A mesocosm study of *Phaeocystis globosa* population dynamics I. Regulatory role of viruses in bloom control. Harmful Algae 4:859–874. doi: 10.1016/j.hal.2004.12.015

Brussaard CPD, Mari X, Bleijswijk JDL Van, Veldhuis MJW (2005b) A mesocosm study of *Phaeocystis globosa* (Prymnesiophyceae) population dynamics II. Significance for the microbial community. Harmful Algae 4:875–893. doi: 10.1016/j.hal.2004.12.012

Brussaard CPD, Martínez J (2008) Algal bloom viruses. Plant Viruses 2:1–13

Brussaard CPD, Wilhelm SW, Thingstad F, et al (2008) Global-scale processes with a nanoscale drive:

The role of marine viruses. ISME J 2:575–578. doi: 10.1038/ismej.2008.31

Buma AGJ, Gieskes WWC, Thomsen HA (1992) Abundance of Cryptophyceae and chlorophyll b-containing organisms in the Weddell-Scotia Confluence area in the spring of 1988. Polar Biol 12:43–52. doi: 10.1007/BF00239964

Calbet A, Landry MR (2004) Phytoplankton growth, microzooplankton grazing, and carbon cycling in marine systems. Limnol Oceanogr 49:51–57. doi: 10.4319/lo.2004.49.1.0051

Clarke A, Meredith MP, Wallace MI, et al (2008) Seasonal and interannual variability in temperature, chlorophyll and macronutrients in northern Marguerite Bay, Antarctica. Deep Res Part II Top Stud Oceanogr 55:1988–2006. doi: 10.1016/j.dsr2.2008.04.035

Coello-Camba A, Agustí S (2017) Thermal thresholds of phytoplankton growth in polar waters and their consequences for a warming polar ocean. Front Mar Sci 4:1–12. doi: 10.3389/fmars.2017.00168

Demory D, Arsenieff L, Simon N, et al (2017) Temperature is a key factor in *Micromonas*–virus interactions. ISME J 11:601–612. doi: 10.1038/ismej.2016.160

Dezutter T, Lalande C, Dufresne C, et al (2019) Mismatch between microalgae and herbivorous copepods due to the record sea ice minimum extent of 2012 and the late sea ice break-up of 2013 in the Beaufort Sea. Prog Oceanogr 173:66–77. doi: 10.1016/j.pocean.2019.02.008

Finkel Z, Irwin A, Schofield O (2004) Resource limitation alters the 3/4 size scaling of metabolic rates in phytoplankton. Mar Ecol Prog Ser 273:269–279. doi: 10.3354/meps273269

Gann ER, Gainer PJ, Reynolds TB, Wilhelm SW (2020) Influence of light on the infection of *Aureococcus anophagefferens* CCMP 1984 by a "giant virus." PLoS One 15:e0226758. doi: 10.1371/journal.pone.0226758

Garrison DL, Gowing MM, Hughes MP, et al (2000) Microbial food web structure in the Arabian Sea: A US JGOFS study. Deep Sea Res Part II Top Stud Oceanogr 47:1387–1422. doi: 10.1016/S0967-0645(99)00148-4

Hoppe CJM, Klaas C, Ossebaar S, et al (2017) Controls of primary production in two phytoplankton blooms in the Antarctic Circumpolar Current. Deep Sea Res Part II Top Stud Oceanogr 138:63–73. doi: 10.1016/j.dsr2.2015.10.005

Irigoien X, Klevjer TA, Røstad A, et al (2014) Large mesopelagic fishes biomass and trophic efficiency in the open ocean. Nat Commun 5:3271. doi: 10.1038/ncomms4271

Jacobsen A, Bratbak G, Heldal M (1996) Isolation and characterization of a virus infecting *Phaeocystis pouchetii* (Prymnesiophyceae). J Phycol 32:923–927. doi: 10.1111/j.0022-3646.1996.00923.x

Kropuenske LR, Mills MM, van Dijken GL, et al (2009) Photophysiology in two major Southern Ocean phytoplankton taxa: Photoprotection in *Phaeocystis antarctica* and *Fragilariopsis cylindrus*. Limnol Oceanogr 54:1176–1196. doi: 10.4319/lo.2009.54.4.1176

Kropuenske LR, Mills MM, Van Dijken GL, et al (2010) Strategies and rates of photoacclimation in two major southern ocean phytoplankton taxa: *Phaeocystis antarctica* (haptophyta) and *Fragilariopsis cylindrus* (Bacillariophyceae). J Phycol 46:1138–1151. doi: 10.1111/j.1529-8817.2010.00922.x

Landry MR, Ohman MD, Goericke R, et al (2009) Lagrangian studies of phytoplankton growth and grazing relationships in a coastal upwelling ecosystem off Southern California. Prog Oceanogr 83:208–216. doi: 10.1016/j.pocean.2009.07.026

Landry MR, Selph KE, Taylor AG, et al (2011) Phytoplankton growth, grazing and production balances in the HNLC equatorial Pacific. Deep Sea Res Part II Top Stud Oceanogr 58:524–535. doi: 10.1016/j.dsr2.2010.08.011

Li WKW, Dickie PM (2001) Monitoring phytoplankton, bacterioplankton, and virioplankton in a coastal inlet (Bedford Basin) by flow cytometry. Cytometry 44:236–246. doi: 10.1002/1097-0320(20010701)44:3<236::AID-CYTO1116>3.0.CO;2-5

Ma S, Tao Z, Yang X, et al (2014) Estimation of marine primary productivity from satellite-derived phytoplankton absorption data. IEEE J Sel Top Appl Earth Obs Remote Sens 7:3084–3092. doi: 10.1109/JSTARS.2014.2298863

Maat DS, Biggs TEG, Evans C, et al (2017) Characterization and temperature dependence of arctic *Micromonas polaris* viruses. Viruses 9:6–9. doi: 10.3390/v9060134

Maat DS, de Blok R, Brussaard CPD (2016) Combined phosphorus limitation and light stress prevent viral proliferation in the phytoplankton species *Phaeocystis globosa*, but not in *Micromonas pusilla*. Front Mar Sci. doi: 10.3389/fmars.2016.00160

4

Marie D, Partensky F, Vaulot D, Brussaard CPD (2001) Enumeration of phytoplankton, bacteria, and viruses in marine samples. Curr Protoc Cytom 10:11.11.1-11.11.15. doi: 10.1002/0471142956.cy1111s10

Menden-Deuer S, Lawrence C, Franzè G (2018) Herbivorous protist growth and grazing rates at in situ and artificially elevated temperatures during an Arctic phytoplankton spring bloom. PeerJ 6:e5264. doi: 10.7717/peerj.5264

Mendes CRB, Tavano VM, Dotto TS, et al (2017) New insights on the dominance of cryptophytes in Antarctic coastal waters: A case study in Gerlache Strait. Deep Sea Res Part II Top Stud Oceanogr 149:161–170. doi: 10.1016/j.dsr2.2017.02.010

Mendes CRB, Tavano VM, Leal MC, et al (2013) Shifts in the dominance between diatoms and cryptophytes during three late summers in the Bransfield Strait (Antarctic Peninsula). Polar Biol 36:537–547. doi: 10.1007/s00300-012-1282-4

Middelboe M (2000) Bacterial growth rate and marine virus-host dynamics. Microb Ecol 40:114–124. doi: 10.1007/s002480000050

Mojica KDA, Brussaard CPD (2014) Factors affecting virus dynamics and microbial host - virus interactions in marine environments. FEMS Microbiol Ecol 89:495–515. doi: 10.1111/1574-6941.12343

Mojica KDA, Huisman J, Wilhelm SW, Brussaard CPD (2016) Latitudinal variation in virus-induced mortality of phytoplankton across the North Atlantic Ocean. ISME J 10:500–513. doi: 10.1038/ismej.2015.130

Moline MA, Claustre H, Frazer TK, et al (2004) Alteration of the food web along the Antarctic Peninsula in response to a regional warming trend. Glob Chang Biol 10:1973–1980. doi: 10.1111/j.1365-2486.2004.00825.x

Moline MA, Prezelin BB, Schofield OM, Smith RC (1997) Temporal dynamics of coastal Antarctic phytoplankton: Environmental driving forces and impact of a 1991/92 summer diatom bloom on the nutrient regimes. In: Battaglia B, Valencia H, Walton DWH (eds) Antarctic communities: Species, structure and survival. Cambridge University Press, pp 67–72

Nagasaki K (2008) Dinoflagellates, diatoms, and their viruses. J Microbiol 46:235–243. doi: 10.1007/s12275-008-0098-y

Nagasaki K, Kim J-J, Tomaru Y, et al (2009) Isolation and characterization of a novel virus infecting *Teleaulax amphioxeia* (Cryptophyceae). Plankt Benthos Res 4:122–124. doi: 10.3800/pbr.4.122

Pasternak AF, Schnack-Schiel SB (2001) Feeding patterns of dominant Antarctic copepods: An interplay of diapause, selectivity, and availability of food. Hydrobiologia 453–454:25–36. doi: 10.1023/A:1013147413136

Pearce I, Davidson AT, Wright S, Van Den Enden R (2008) Seasonal changes in phytoplankton growth and microzooplankton grazing at an Antarctic coastal site. Aquat Microb Ecol 50:157–167. doi: 10.3354/ame01149

Piedade GJ, Wesdorp EM, Borbolla EM, Maat DS (2018) Influence of irradiance and temperature on the virus MpoV-45T infecting the Arctic picophytoplankter *Micromonas polaris*. Viruses 1–17. doi: 10.3390/v10120676

R Development Core Team (2012) R: A language and environment for statistical computing

Rose JM, Caron DA (2007) Does low temperature constrain the growth rates of heterotrophic protists? Evidence and implications for algal blooms in cold waters. Limnol Oceanogr 52:886–895. doi: 10.4319/lo.2007.52.2.0886

Rose JM, Fitzpatrick E, Wang A, et al (2013) Low temperature constrains growth rates but not short-term ingestion rates of Antarctic ciliates. Polar Biol 36:645–659. doi: 10.1007/s00300-013-1291-y

Rozema PD, Kulk G, Veldhuis MP, et al (2017a) Assessing drivers of coastal primary production in northern Marguerite Bay, Antarctica. Front Mar Sci 4:1–20. doi: 10.3389/fmars.2017.00184

Rozema PD, Venables HJ, van de Poll WH, et al (2017b) Interannual variability in phytoplankton biomass and species composition in northern Marguerite Bay (West Antarctic Peninsula) is governed by both winter sea ice cover and summer stratification. Limnol Oceanogr 62:235–252. doi: 10.1002/lno.10391

Sarker S, Wiltshire KH (2017) Phytoplankton carrying capacity: Is this a viable concept for coastal seas? Ocean Coast Manag 148:1–8. doi: 10.1016/j.ocecoaman.2017.07.015

Schoemann V, Becquevort S, Stefels J, et al (2005) *Phaeocystis* blooms in the global ocean and their

controlling mechanisms: A review. J Sea Res 53:43–66. doi: 10.1016/j.seares.2004.01.008

Schofield O, Brown M, Kohut J, et al (2018) Changes in the upper ocean mixed layer and phytoplankton productivity along the West Antarctic Peninsula. Philos Trans R Soc A Math Phys Eng Sci 376:20170173. doi: 10.1098/rsta.2017.0173

Sherr E, Sherr B (2009) Capacity of herbivorous protists to control initiation and development of mass phytoplankton blooms. Aquat Microb Ecol 57:253–262. doi: 10.3354/ame01358

Singh BK, Chattopadhyay J, Sinha S (2004) The role of virus infection in a simple phytoplankton zooplankton system. J Theor Biol 231:153–166. doi: 10.1016/j.jtbi.2004.06.010

Smetacek V, Assmy P, Henjes J (2004) The role of grazing in structuring Southern Ocean pelagic ecosystems and biogeochemical cycles. Antarct Sci 16:541–558. doi: 10.1017/S0954102004002317

Smith WO, Lancelot C (2004) Bottom-up versus top-down control in phytoplankton of the Southern Ocean. Antarct Sci 16:531–539. doi: 10.1017/S0954102004002305

Sommer U, Sommer F (2006) Cladocerans versus copepods: The cause of contrasting top–down controls on freshwater and marine phytoplankton. Oecologia 147:183–194. doi: 10.1007/s00442-005-0320-0

Suttle CA (2007) Marine viruses — major players in the global ecosystem. Nat Rev Microbiol 5:801–812. doi: 10.1038/nrmicro1750

Suzuki Y, Takahashi M (1995) Growth responses of several diatom species isolated from various environments to temperature. J Phycol 31:880–888. doi: 10.1111/j.0022-3646.1995.00880.x

Talmy D, Beckett SJ, Taniguchi DAA, et al (2019) An empirical model of carbon flow through marine viruses and microzooplankton grazers. Environ Microbiol 21:2171–2181. doi: 10.1111/1462-2920.14626

Tomaru Y, Takao Y, Suzuki H, et al (2009) Isolation and characterization of a single-stranded RNA virus infecting the bloom-forming diatom *Chaetoceros socialis*. Appl Environ Microbiol 75:2375–2381. doi: 10.1128/AEM.02580-08

Turner JT (2015) Zooplankton fecal pellets, marine snow, phytodetritus and the ocean's biological pump. Prog Oceanogr 130:205–248. doi: 10.1016/j.pocean.2014.08.005

Vaulot D (1989) CYTOPC: Processing software for flow cytometric data. Signal and Noise 2:8

Venables HJ, Clarke A, Meredith MP (2013) Wintertime controls on summer stratification and productivity at the western Antarctic Peninsula. Limnol Oceanogr 58:1035–1047. doi: 10.4319/lo.2013.58.3.1035

Vernet M, Martinson D, Iannuzzi R, et al (2008) Primary production within the sea-ice zone west of the Antarctic Peninsula: I—Sea ice, summer mixed layer, and irradiance. Deep Sea Res Part II Top Stud Oceanogr 55:2068–2085. doi: 10.1016/j.dsr2.2008.05.021

Voss M (1991) Content of copepod faecal pellets in relation to food supply in Kiel Bight and its effect on sedimentation rate. Mar Ecol Prog Ser 75:217–225. doi: 10.3354/meps075217

Weitz JS, Wilhelm SW (2012) Ocean viruses and their effects on microbial communities and biogeochemical cycles. F1000 Biol Rep 4:2–9. doi: 10.3410/B4-17

Wilhelm SW, Suttle CA (1999) Viruses and nutrient cycles in the sea. Bioscience 49:781–788. doi: 10.2307/1313569

Worden AZ, Nolan JK, Palenik B (2004) Assessing the dynamics and ecology of marine picophytoplankton: The importance of the eukaryotic component. Limnol Oceanogr 49:168–179. doi: 10.4319/lo.2004.49.1.0168

Yamada Y, Tomaru Y, Fukuda H, Nagata T (2018) Aggregate formation during the viral lysis of a marine diatom. Front Mar Sci 5:. doi: 10.3389/fmars.2018.00167

4

Supplementary Figures

Fig. S1. Map of the study site: (a) the location of Ryder Bay in northern Marguerite Bay to the east of Adelaide Island and to the west of the Antarctic Peninsula. (b) large scale map of Antarctica showing the location of the Antarctic Peninsula and surrounding seas.
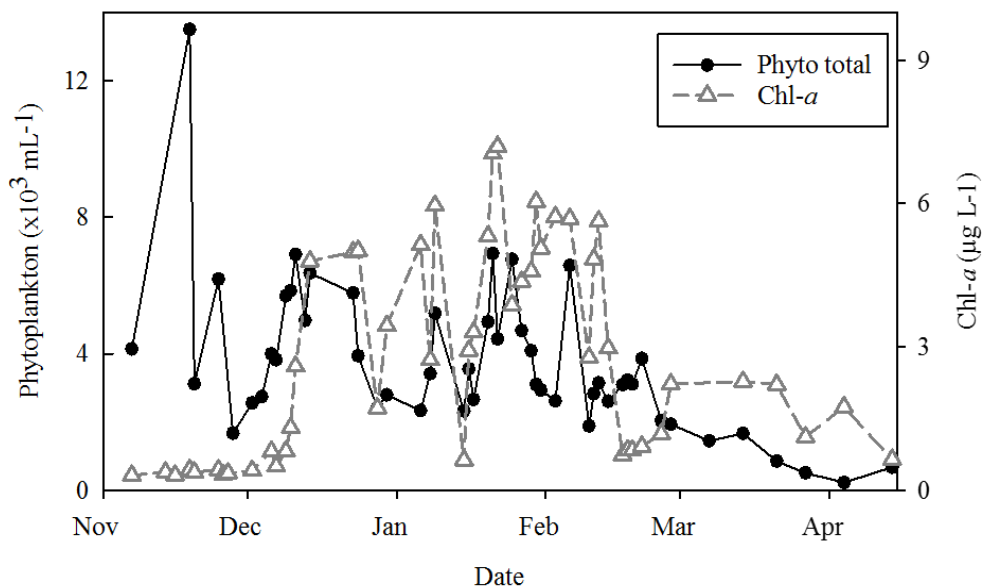
Fig. S2. Time series of total phytoplankton abundance (Phyto total; black circles and solid line) and total Chlorophyll-*a* (Chl-*a*) concentrations (Chl-*a* total; open triangles and dashed line) at the RaTS sample site (15 m depth) in Ryder Bay between November 2013 and April 2014 in season 2.
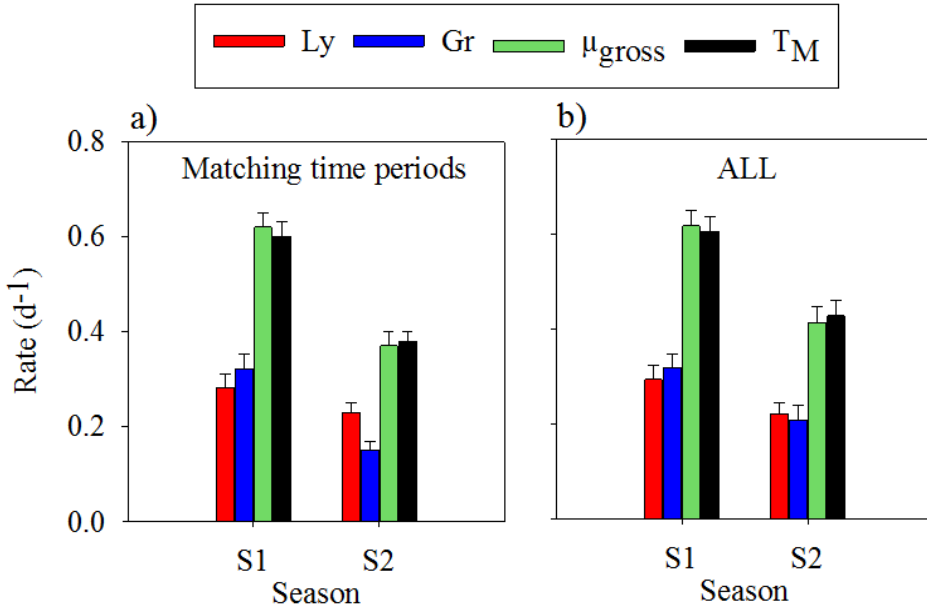
Fig. S3. Comparison between season 1 (S1) and season 2 (S2) of mean specific rates (d^{-1}) of lysis (Ly), grazing (Gr), gross growth (μ_{gross}) and total mortality (T$_M$, i.e. lysis and grazing), both over a) matching time periods and b) all phytoplankton data (All). Error bars represent $\pm$ 1 standard error.
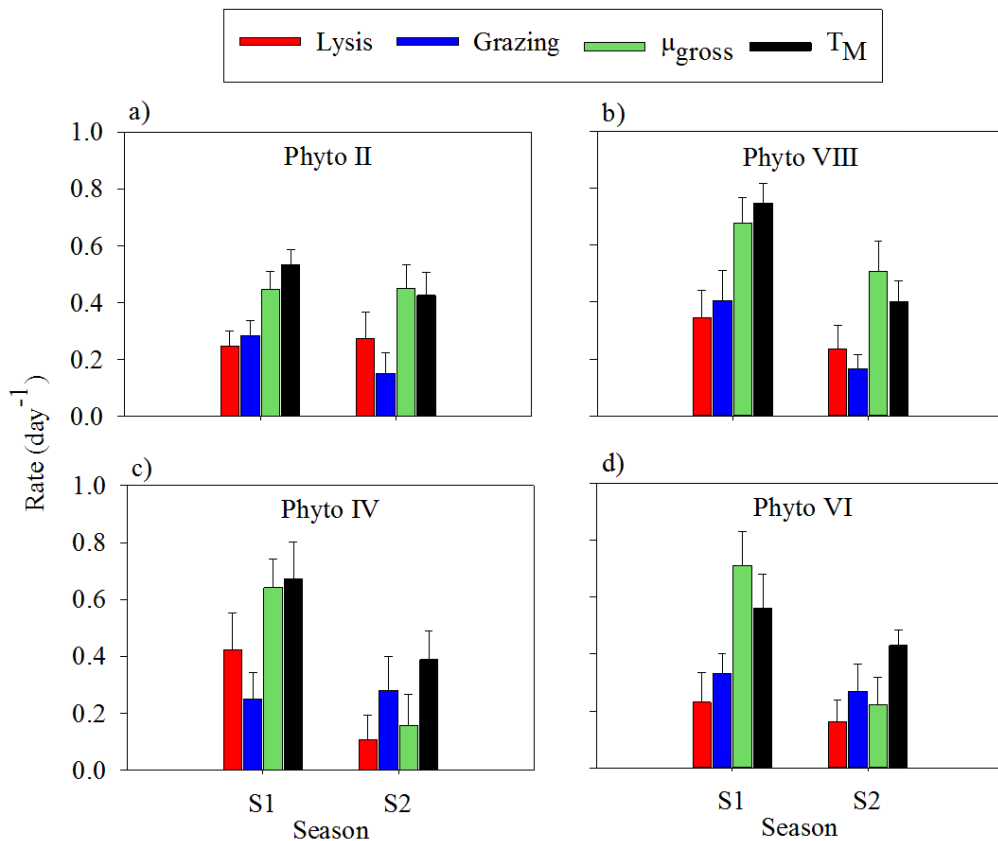
Fig. S4. Mean specific rates (d^{-1}) of lysis, grazing, gross growth (μ_{gross}) and total mortality (T_M, i.e. lysis and grazing) are shown in (a) for Phyto II and (b) for VIII. Error bars represent $\pm$ 1 standard error.
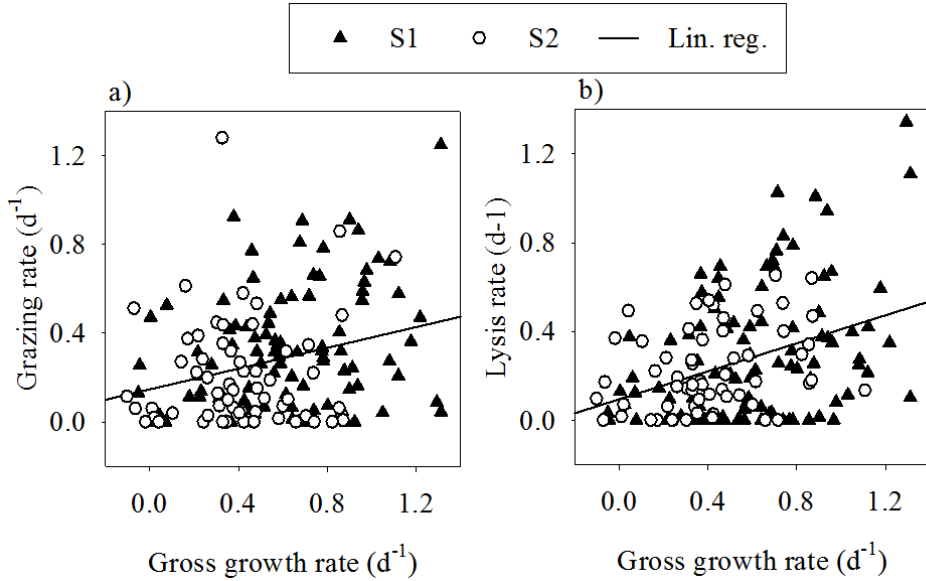
Fig. S5. Phytoplankton rates (d^{-1}) of gross growth in S1 (black triangle) and S2 (open circles) plotted against (a) grazing and (b) viral lysis. The linear regression lines (solid black) are for all data (i.e. S1 and S2 combined). The linear regression slope is (a) 0.23 ($r^2 = 0.08$; $p = 0.0005$, $n = 160$) and (b) 0.32 ($r^2 = 0.14$; $p < 0.0001$, $n = 160$).
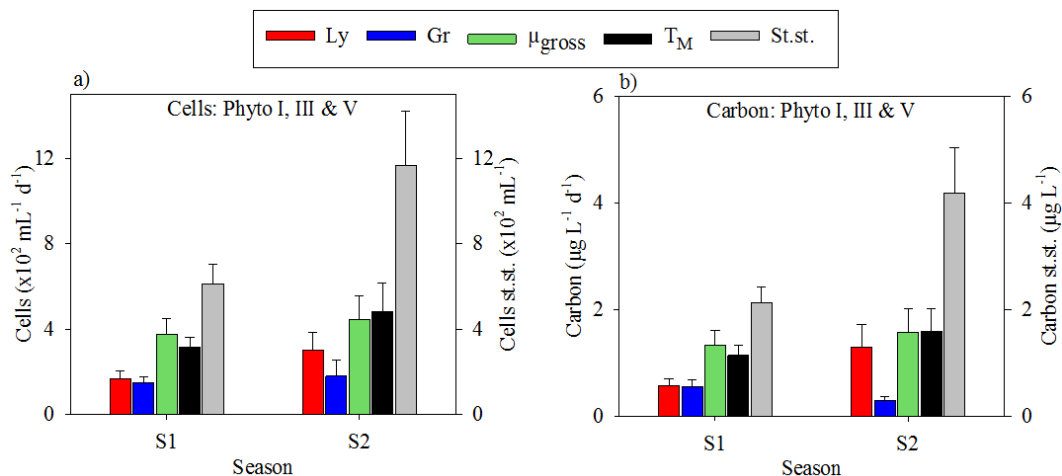
Fig. S6. Seasonal averages of lysis (Ly), grazing (Gr), gross growth (μ_{gross}), total mortality (T_M, i.e. lysis and grazing) and standing stock (st. st.) are shown for Phyto I, III and V (a) in cells and (b) in carbon. Error bars represent ± 1 standard error.
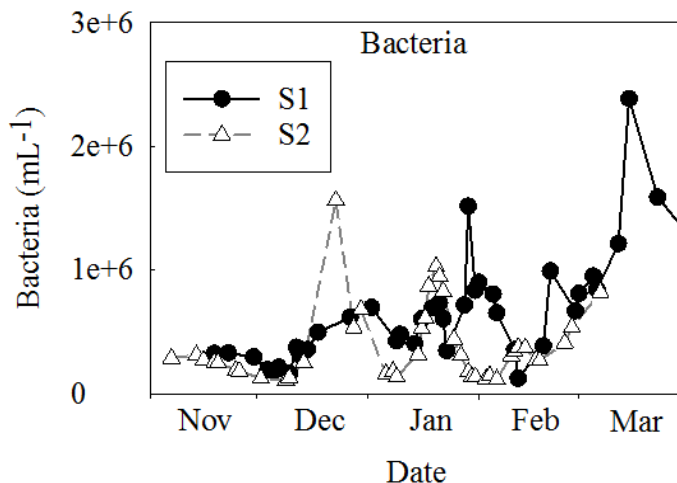
Fig. S7. Time series of bacterial abundance (mL^{-1}) from flow cytometry counts of samples stained with SYBR Green.

Supplementary Tables

Table S1. Physical and chemical environmental variables at the Rothera time series site (RaTS) at the start of dilution experiments. Note: Zeu depth was determined as 1% of surface PAR (1 m).

Date	Temp.	Salinity	PAR	MLD	Zeu	Strat.	Phos-phate	Nitrate	N:P ratio	Si	Wind speed	Air-PAR	Ice cover
	°C	psu	μM quanta $m^{-2} s^{-1}$	m	m	$J\,m^{-2}$	μM	μM		μM	$m\,s^{-1}$	μM quanta $m^{-2} s^{-1}$	%
19/11/13	-1.5	33.8	96	23	79	138	1.5	29	19	NA	8	33	1
25/11/13	-1.2	33.9	83	53	56	51	2.1	30	14	85	9	36	1
02/12/13	-0.8	33.7	112	11	48	248	1.9	28	15	81	4	66	4
09/12/13	-0.3	33.6	60	8	38	681	1.7	27	16	75	3	52	6
23/12/13	-0.3	33.4	0.3	3	9	NA	0.9	13	14	38	12	27	3
06/01/14	-0.4	33.5	9	1	23	877	0.9	17	18	43	5	47	4
15/01/14	-0.8	33.7	89	5	39	316	1.8	25	14	70	11	51	3
21/01/14	-0.3	32.9	6	3	14	947	0.5	8	15	31	4	61	2
27/01/14	0.6	32.8	9	3	17	728	0.1	1	17	20	9	57	1
03/02/14	0.9	32.8	9	8	19	NA	0.1	2	22	20	4	27	5
10/02/14	-0.2	33.1	12	1	22	1537	0.9	12	14	50	7	34	6
17/02/14	-0.2	32.9	62	13	41	298	1.0	12	12	39	7	35	1
27/02/14	-0.2	33.0	59	39	35	37	1.1	15	14	46	10	22	2

4

Table S2. Temporal variation in specific viral lysis (Ly), grazing (Gr), total Mortality (T_M = Ly+Gr) and gross growth (μ_{gross}) rates (d^{-1}) for Phyto groups I- X. * indicates a significant difference ($p < 0.05$) of the linear regression from either: zero (μ_{gross}, Gr and T_M) or from the grazing regression (Ly); a white background indicates missing data due to either low abundance or high variation.

Date	Phyto I				Phyto II				Phyto III				Phyto IV				Phyto V			
	Ly	Gr	T_M	μ_{gross}	Ly	Gr	T_M	μ_{gross}	Ly	Gr	T_M	μ_{gross}	Ly	Gr	T_M	μ_{gross}	Ly	Gr	T_M	μ_{gross}
19/11/13	0.17*	0.32*	0.49*	0.37*	FG	F	0.17*	0.27*		0.32*		0.41*					0.17*	0.32	0.49*	0.62*
25/11/13	0.21	0.53*	0.74	0.48*	0.14	0.44*	0.58	0.46*	0.29*	0.01	0.31*	0.58*					0.01	0.05	0.06	0.41
02/12/13	0.20	0.22	0.42	0.19*	0.61*	0.04	0.65*	0.48*	0.20	0.23*	0.43	0.48*	0.00	0.45	0.45	0.30			0.33*	0.53*
09/12/13					0.47*	0.01	0.48*	0.87*	0.41*	0.07	0.48*	0.31*							0.31*	0.47*
23/12/13	0.25	0.35	0.61	0.33					0.35*	0.04	0.39*	0.1*					0.52*	0.00	0.52*	0.42*
06/01/14									0.03	0.23	0.25	0.42					0.54	0.04	0.58	0.40
15/01/14	0.64*	0.03	0.67*	0.87*	0.00	0.00	0.00	0.24	0.09	0.17*	0.26	0.36*					0.03	0.10	0.13	0.35
21/01/14	0.4*	0.00	0.4*	0.47*	0.06	0.39	0.45	0.22	0.65*	0.03	0.68*	0.7*					0.46*	0.00	0.46*	0.47*
27/01/14	0.06	0.00	0.06	0.34	0.11	0.19	0.30	0.54	0.11	0.15	0.26	0.48					0.17*	0.06	0.23*	-0.06*
03/02/14									0.10	0.11	0.21	-0.1*	0.00	0.51	0.51	-0.07				
10/02/14	0.34	0.06	0.40	0.85	0.53*	0.00	0.53*	0.35*	0.02	0.06	0.08	0.01	0.07	0.02	0.09	0.02	0.28	0.11	0.38	0.52
17/02/14									0.16	0.07	0.23	0.37								
27/02/14	0.17	0.86*	1.03	0.86*					0.14	0.13*	0.27	0.31*	0.36	0.14	0.51	0.38	0.13	0.00	0.13	0.33

Date	Phyto VI				Phyto VII				Phyto VIII				Phyto IX				Phyto X			
	Ly	Gr	T_M	μ_{gross}	Ly	Gr	T_M	μ_{gross}	Ly	Gr	T_M	μ_{gross}	Ly	Gr	T_M	μ_{gross}	Ly	Gr	T_M	μ_{gross}
19/11/13	0.12	0.27*	0.38	0.41*					0.00	0.35	0.35	0.72*								
25/11/13	0.16	0.44*	0.60	0.33*					0.19	0.03	0.22	0.26*								
02/12/13					0.07	0.07	0.14	0.60	0.15	0.20	0.35	0.26								
09/12/13													0.00	0.00	0.00	0.66				
23/12/13													0.40	0.00	0.40	0.74				
06/01/14					0.13	0.74	0.88	1.11												
15/01/14									0.30	0.00	0.30	0.82								
21/01/14									0.49*	0.10	0.59*	0.62*	0.00	0.28	0.28	0.24	0.18	0.48	0.66	0.87
27/01/14	0.00	0.38*	0.38	0.17*	0.49	0.00	0.49	0.04	0.00	0.27	0.27	0.14	0.01	0.58*	0.59*	0.42*				
03/02/14					0.22	0.61*	0.83	0.16*												
10/02/14	0.37	0.00	0.37	-0.02					0.53	0.22	0.75	0.74					0.27	1.28	1.55	0.33
17/02/14																				
27/02/14																				

Table S3. Temporal variation in rates of carbon flow and standing stock (st.st.), converted from viral lysis (Ly), grazing (Gr), total Mortality (T_M = Ly+Gr) and gross growth (μ_{gross}) rates (d⁻¹) for Phyto groups I-X. Note: a white background indicates missing data due to either low abundance or high variation.

Date	Phyto I (μg C L⁻¹ (d⁻¹))					Phyto II (μg C L⁻¹ (d⁻¹))					Phyto III (μg C L⁻¹ (d⁻¹))					Phyto IV (μg C L⁻¹ (d⁻¹))					Phyto V (μg C L⁻¹ (d⁻¹))				
	Ly	Gr	T_M	μ_{gross}	st.st.	Ly	Gr	T_M	μ_{gross}	st.st.	Ly	Gr	T_M	μ_{gross}	st.st.	Ly	Gr	T_M	μ_{gross}	st.st.	Ly	Gr	T_M	μ_{gross}	st.st.
19/11/13	0.11	0.20	0.32	0.23	0.68	0.14	0.45	0.59	0.47	1.08	1.29	0.07	1.36	2.58	3.86						0.21	0.39	0.61	0.76	1.16
25/11/13	0.04	0.11	0.15	0.10	0.24	0.10	0.01	0.11	0.08	0.18	1.17	1.30	2.47	2.73	5.58						0.02	0.08	0.10	0.65	1.31
02/12/13	0.00	0.00	0.01	0.00	0.02	0.26	0.00	0.26	0.47	0.44	3.60	0.64	4.24	2.76	9.54	0.00	0.06	0.06	0.04	0.15					
09/12/13											0.90	0.10	1.00	0.26	2.93										
23/12/13	0.01	0.01	0.01	0.01	0.02						0.06	0.55	0.61	1.01	2.19						6.14	0.00	6.14	5.03	12.41
06/01/14											0.38	0.71	1.09	1.50	3.97						3.30	0.25	3.55	2.47	6.67
15/01/14	0.01	0.00	0.01	0.01	0.01	0.00	0.00	0.00	0.09	0.33	7.70	0.30	8.00	8.31	11.64						0.12	0.39	0.51	1.39	3.52
21/01/14	0.02	0.00	0.02	0.02	0.04	0.01	0.09	0.11	0.05	0.26	0.91	1.29	2.20	4.15	7.62						8.58	0.00	8.58	8.78	18.56
27/01/14	0.00	0.00	0.00	0.00	0.01	0.05	0.08	0.13	0.23	0.38	0.47	0.56	1.02	-0.50	5.67						1.34	0.47	1.81	-0.50	9.09
03/02/14											0.07	0.26	0.34	0.05	4.55	0.00	0.34	0.34	-0.05	0.87					
10/02/14	0.00	0.00	0.00	0.01	0.00	0.08	0.00	0.08	0.05	0.17	1.28	0.53	1.81	3.00	7.42	0.20	0.05	0.26	0.06	3.01	0.46	0.17	0.64	0.86	1.56
17/02/14											0.61	0.54	1.16	1.31	4.19	0.50	0.20	0.69	0.51	1.46					
27/02/14	0.00	0.00	0.00	0.00	0.00																0.18	0.00	0.18	0.45	1.22

Date	Phyto VI (μg C L⁻¹ (d⁻¹))					Phyto VII (μg C L⁻¹ (d⁻¹))					Phyto VIII (μg C L⁻¹ (d⁻¹))					Phyto IX (μg C L⁻¹ (d⁻¹))					Phyto X (μg C L⁻¹ (d⁻¹))				
	Ly	Gr	T_M	μ_{gross}	st.st.	Ly	Gr	T_M	μ_{gross}	st.st.	Ly	Gr	T_M	μ_{gross}	st.st.	Ly	Gr	T_M	μ_{gross}	st.st.	Ly	Gr	T_M	μ_{gross}	st.st.
19/11/13	1.72	3.99	5.71	6.07	14.73						0.00	16.84	16.84	34.73	40.14										
25/11/13	0.74	2.03	2.77	1.54	5.30						6.32	0.90	7.22	8.71	32.37										
02/12/13						0.03	0.03	0.05	0.22	0.29	0.63	0.84	1.47	1.09	4.40										
09/12/13																									
23/12/13																0.00	0.00	0.00	8.69	9.34					
06/01/14						1.14	6.32	7.46	9.43	7.57	2.22	0.00	2.22	6.17	5.70	139.3	0.00	139.3	258.3	292.5					
15/01/14																									
21/01/14											9.22	1.90	11.12	11.66	18.47	0.00	11.71	11.71	9.85	42.34	21.32	56.89	78.21	102.6	106.7
27/01/14	0.00	1.00	1.00	0.46	2.96	1.59	0.00	1.59	0.13	4.01	0.00	2.47	2.47	1.30	9.72	0.26	14.61	14.87	10.60	27.40					
03/02/14						0.34	0.95	1.29	0.25	2.13											5.74	26.86	32.60	6.86	36.42
10/02/14	0.14	0.00	0.14	-0.01	0.46						1.68	0.70	2.38	2.35	3.20										
17/02/14																									
27/02/14																									

4

Chapter 4

Chapter 5

Control of Antarctic phytoplankton community composition and growth rates by light availability

Control of Antarctic phytoplankton community composition and growth rates by light availability

Tristan E.G. Biggs[1,2,]; Patrick D. Rozema[3]; Claire Evans[4]; Klaas R. Timmermans[1,3,]; Hugh J. Venables[5]; David W. Pond[6] and Corina P.D. Brussaard[1,2,]

[1] NIOZ Royal Netherlands Institute for Sea Research, and University of Utrecht, Texel and Yerseke, The Netherlands.
[2] Department of Freshwater and Marine Ecology, Institute for Biodiversity and Ecosystem Dynamics (IBED), University of Amsterdam, Amsterdam, The Netherlands.
[3] Department of Ocean Ecosystems, University of Groningen, Groningen, The Netherlands
[4] Ocean Biogeochemistry & Ecosystems Research Group, National Oceanography Centre, Southampton, UK.
[5] British Antarctic Survey, Natural Environmental Research Council, Cambridge, UK.
[6] Institute of Aquaculture, University of Stirling, Stirling, Scotland UK.

Abstract

Polar phytoplankton are subject to pronounced annual and seasonal changes in light availability owing to changes in photoperiod as well as fluctuations in ice cover, mixed layer depth, cloud cover and the degree of self-shading. Despite the likely importance for phytoplankton community dynamics, composition, and growth rates, as well as levels of primary production, the role of light in these environments is not well understood. To investigate the polar phytoplankton community response to light availability, incubation experiments were performed throughout the productive season with seawater collected from Ryder Bay off the Western Antarctic Peninsula. The growth rates of individual phytoplankton populations determined by flow cytometry were found to respond distinctly to a gradient of ecologically relevant light intensities (low 4-7, medium 30-50, and high 150-200 µmol quanta m^{-2} s^{-1}). *Phaeocystis* (phytoplankton population Phyto III) displayed relatively fast growth rates under all light levels tested, whereas growth of both the smaller- and larger-sized diatoms Phyto VI and Phyto X (average diameter 4.5 and 20 µm, respectively) consistently exhibited faster growth in high and medium light. In contrast, diatom Phyto IX (11.5 µm) displayed fastest growth under low light, where they dominated the phytoplankton community. Low light was the primary factor limiting net growth and peak phytoplankton biomass. One of the incubations displayed relatively high phytoplankton net growth rates under low light which were most likely forced by a prolonged low light period prior to the experiment, allowing adaptation to low light (switching from high to low growth mode) to maximize growth potential. Acclimation from mid to high light intensities took typically around 3 days but to low light more than 2 weeks. Especially the ability of the different natural Antarctic phytoplankton populations to 'switch' between modes of growth over short time periods (e.g. low light due to ice, clouds or high biomass bloom-induced self-shading) determines whether they sustain, thrive or decline.

5

Introduction

Variability in ice cover, cloudiness, the strength of water column stratification, and the frequency, duration and intensity of wind driven mixing (not accounting for advection) largely determines the light climate over the productive season (Clarke et al. 2008; Venables and Moore 2010; Ducklow et al. 2012; Venables et al. 2013). Overall, the response of the phytoplankton community to light may involve changes within genotypes, specific dominating species, taxonomic groups, cell size or pigment concentrations (Timmermans et al. 2001; Moore et al. 2006; Arrigo et al. 2010; Alderkamp et al. 2012). The mechanisms behind seasonal phytoplankton dynamics and the community response to light, especially after periods of low photosynthetic active radiation (PAR), are not fully understood and require further investigation.

At high latitudes, phytoplankton accumulation begins as the light returns after mid-winter when phytoplankton cells are still subjected to deep mixing and low average light levels (~1 µmol quanta m^{-2} d^{-1}; Venables et al. 2013). Seasonality in the initial growth response of polar phytoplankton has been observed (Sloughter et al. 2019), where reduced growth in overwintered phytoplankton (after long periods of low PAR) is related to physiological changes that balance maintenance respiration against photosynthetic efficiency and energy expenditure. When average light exposure rises above the compensation level where respiration and gross growth balance, and net growth is zero, the balance can shift from a slow to a fast growth response at higher light. The growth capability of the community in response to light may have significant impacts on the timing, magnitude and composition of phytoplankton blooms. Adaptive variability can be long term, such as over the winter period, or shorter term as a result of low light levels during the productive season (Clarke et al. 2008; Venables and Moore 2010; Venables et al. 2013). The high biomass phytoplankton blooms that typically develop in polar regions (Thomalla et al. 2011; Llort et al. 2015) limit the penetration of light into the water column (Vernet et al. 2008; Park et al. 2017) and can span considerable time periods during the growth season (Arrigo et al. 2015). Acclimation to low light levels is likely of critical

importance in relation to potential growth. The response of natural communities to light availability is argued to have important implications for marine productivity models, especially for predications in rapidly changing environments (Sloughter et al. 2019). Yet, the role of light in controlling peak biomass and seasonal dynamics in Antarctic waters is less clear (Arrigo et al. 2015).

Understanding the ecological and physiological mechanisms driving phytoplankton community structure are vital to assess the response of marine systems to global climate change. Shifts in size class distribution have the potential to drastically alter the Southern Ocean food web (Atkinson et al. 2004). Global warming is expected to increase sea surface temperature (Collins et al. 2013) and prolong and intensify vertical stratification that will in turn impact nutrient flux to surface waters, reduce light variability and increase light intensity. Such changes could cause shifts in phytoplankton community composition, from larger diatoms to smaller flagellated cells (e.g. cryptophytes; Garibotti et al. 2005; Mendes et al. 2018; Biggs et al. 2019) which alter trophic transfer efficiency and elemental cycling (Petrou et al. 2016; Rembauville et al. 2016). Temperature driven reductions in sea ice duration and extent will also lengthen the productive season, primarily due to increased light availability in the water column in spring and autumn (Montes-Hugo et al. 2009; Arrigo and van Dijken 2015).

5

To investigate how phytoplankton communities respond to light availability, 6 incubation experiments (growth bioassays) were conducted on seawater collected from a coastal site off the Western Antarctic Peninsula (WAP) throughout the productive season. Growth rates of the individual phytoplankton populations identified were determined under a gradient of ecologically relevant light levels representative of the mid-summer photoperiod.

Methods

Physicochemical measurements

Data for this study were obtained from the Rothera time series site (RaTS, latitude 67.572°S; longitude 68.231°W; Clarke et al. 2008) located in Ryder Bay on the

WAP. Environmental conditions were recorded over two Austral productive periods, season 1 (S1) from Dec 2012 to April 2013 and season 2 (S2) between Nov 2013 and April 2014 (Biggs et al. 2019). Water column profiles were obtained using a SeaBird 19+ conductivity temperature depth instrument (CTD) supplemented with a flat LiCor sensor to measure photosynthetically available radiation (PAR) and an in-line fluorescence sensor (WetLabs). *In-situ* density, temperature, salinity and PAR were obtained from the CTD. Detailed time series data of environmental conditions at the sample site, such as MLD, euphotic zone depth (Z_{eu}), light limitation index ($Z_{eu}/15m$), stratification level, dissolved inorganic phosphate, nitrate and silicate and sea ice coverage, as well as methodological details, are published in Biggs et al. (2019). Daily wind speed and air-PAR (24h average) were recorded at a weather station on Rothera Station (British Antarctic Survey).

Light experiments

Seawater for the incubation experiments was collected from 15 m depth by a 12 L Niskin bottle deployed from a small boat. Taking care to prevent light exposure, the 24L polycarbonate Nalgene carboys (used for the incubations) were filled to the brim. Seawater was transported to a temperature-controlled lab maintained at c.a. 0.5°C, immediately sub-sampled (20 L final volume) and then transferred (while kept dark) to an indoor flow-through (seawater) incubator to replicate *in-situ* temperature dynamics. Three PAR intensities were used for each experiment of 150 – 200 (high light, HL), 30 – 50 (medium light, ML) and 4 - 7 µmol quanta m^{-2} s^{-1} (low light, LL). For each light treatment triplicate bottles were incubated, hence nine bottles in total. Light was supplied by 18W/965 OSRAM daylight spectrum fluorescent tubes (München, Germany) and the light intensity was adjusted using neutral density screens. Incubation bottles were turned three times a day to simulate water column mixing. Six incubation experiments (INC) were performed in total: INC 1 and 2 lasted 10 days and were conducted during the second half of S1 on 6 Feb and 11 Mar (2013). INC 3 – 6 were performed over 9 days and conducted over S2 on 4 and 28 Dec 2013, and 29 Jan and 25 Feb 2014. At the beginning (T_0) and

end (T_{END}) of each incubation, 6 mL subsamples were collected for nutrients (phosphate, nitrate and silicate) and 1 L subsamples for phytoplankton pigment analysis. On day 0 (T_0), 3 (T_3), 7 (T_7) and T_{END}, 55 mL subsamples were collected for phytoplankton enumeration and photosynthetic efficiency analysis.

Phytoplankton variables

Photosynthetic efficiency (F_v/F_m) was determined using pulse amplitude modulated (PAM) fluorometry (Water-PAM). Samples were dark acclimated for 15 min on ice after which the minimum (F_0) and maximum (F_m) chlorophyll fluorescence were measured. The variable fluorescence (Fv) is calculated as $F_m - F_0$ (Maxwell and Johnson 2000).

For flow cytometric phytoplankton enumeration, 3.5 mL subsamples were fixed with 100 µl formaldehyde-hexamine (18 % v/v:10 % w/v) at 4 °C, after which they were snap-frozen in liquid nitrogen and stored at -80 °C until analysis. Samples were analysed according to Marie et al (1999) using a Becton Dickinson FACSCalibur flow cytometer (BD Biosciences) equipped with an air-cooled Argon laser with an excitation wavelength of 488 nm (15 mW). The trigger was set on red fluorescence channel and phytoplankton populations were distinguished using bivariate scatter plots of red Chlorophyll-*a* autofluorescence versus side scatter. Cryptophytes were further discriminated based on their orange phycoerythrin autofluorescence. Ten phytoplankton groups were identified, coded Phyto I to X, with average cell diameters of 0.9, 1.8, 3.1, 4.0, 4.5, 4.5, 7.4, 8.1, 11.5 and 20.4 µm respectively (Biggs et al. 2019). Flow cytometry and Chlorophyll-*a* fractionation data were combined with chemical taxonomy to identify the larger algal groups (Phyto V-X) as diatoms, Phyto IV as cryptophytes (based on orange autofluoscence and microscopy) and Phyto III as *Phaeocystis* spp. (based on microscopy and resembling temporal dynamics with Prymnesiophyceae, Biggs et al. 2019).

Cellular carbon content for the phytoplankton populations identified by FCM (FCM-C) were derived using their average cell diameter (assuming cells to be spherical)

and conversion factors of 196.5 and 237 fg C μm^{-3} for nano- and pico-sized phytoplankton populations respectively (Garrison et al. 2000; Worden et al. 2004). Specific net growth rates (d^{-1}) were calculated from the abundance dynamics (Table S1, S2, S3 and S4) for the different phytoplankton groups as well as for total phytoplankton (the latter both based on cell count and cellular carbon) over the entire incubation period, i.e., T_0 to T_{END} (10 days for INC 1 and 2 and 9 days for INC 3-6). Additionally, we calculated the net growth rates specifically for the start (T_{0-3} days), mid (T_{3-7} days) and end (T_{0-END}) of the incubations.

Samples for Chlorophyll-*a* (Chl-*a*) concentration and phytoplankton taxonomic composition (based on pigment ratios) were obtained by filtering 1 L through GF/F glass fiber filters (47 mm, Whatman, The Netherlands). Filters were wrapped in aluminum-foil, snap-frozen in liquid nitrogen and stored at -80°C until analysis. Phytoplankton pigments were analysed by high performance liquid chromatography (HPLC) according to Brussaard et al (2016) and pigment quantification was performed using reference standards (DHI, Hørsholm, Denmark). Peaks identified were manually checked for quality assessment. Phytoplankton class abundances were calculated using pigment data from HPLC by CHEMTAX v1.95 (Mackey et al. 1996). This program uses a factor analysis and steepest decent algorithm to find the best fit based on a pigment ratio matrix. Six taxonomic classes were chosen to classify the WAP phytoplankton, in line with those used previously for RaTS site data (Biggs et al. 2019) and confirmed by microscopy observations (unpublished data): Prasinophyceae, Chlorophyceae, Dinophyceae, Cryptophyceae, Prymnesiophyceae and Bacillariophyceae (diatoms). CHEMTAX was run 60 times using all pigment concentration data with randomized (±35%) pigment ratios to minimize the root mean square error (RMSE) using settings recommended in Kozlowski et al. (2011). The run with the lowest RMSE was deemed final with initial and final ratios shown in Table S5. Chl-*a* concentrations were converted to cellular carbon (Chl-C) using taxon-specific conversion factors according to Garibotti et al. (2003), with the exception of Dinophyceae for which we used an average of ratios by Llewellyn et al. (2005) and Agirbas et al. (2015). Specific net growth rates (d^{-1})

were determined for the different phytoplankton taxonomic groups, as well as for total Chl-*a* and Chl-C (Tables S6 and S7) over the entire incubation period, i.e., T_0 to T_{END}.

Statistics

Significant differences between light treatments were tested using a one-way analysis of variance (ANOVA, SigmaPlot v14, from Systat Software, Inc., San Jose California, USA), whilst differences between experiments were tested using a two-tailed Student's t-test (SigmaPlot v14).

Table 1. Environmental conditions at the sample site, average of 3 weeks prior to the start of the incubations (21 day mean) and on the day of sampling for incubation T_0 (6 Feb and 11 Mar 2013, 4 and 28 Dec 2013 and 29 Jan and 25 Feb 2014, respectively). Abbreviations: photosynthetically active radiation (PAR); mixed layer depth (MLD, defined as a 0.05 kg m^{-3} difference in density relative to the surface); euphotic zone depth (Zeu, depth of the euphotic zone to 1% of surface PAR); level of stratification over the top 40m of the water column (Strat); silicate concentration (Si).

5

At T_0	Temp.	Salinity	PAR	MLD	Zeu	Strat.	Phosphate	Nitrate	N:P ratio	Si	Wind speed	Air PAR day^{-1}	Ice cover
	°C	psu	µM quanta m^{-2} s^{-1}	m	m	J m^{-2}	µM	µM		µM	m s^{-1}	µM quanta m^{-2} s^{-1}	%
1	1.2	33.2	40	12	44	433	1.1	14	13	58	12.7	30	20
2	0.7	33.2	0.3	10	13	231	0.3	7.9	28	58	5.4	6	40
3	-0.8	33.7	310	1.0	50	365	1.9	27	14	79	7.6	69	40
4	-1.0	33.6	3	2.0	15	911	1.8	25	14	74	2.7	44	30
5	0.5	32.8	7	3.7	25	997	0.2	3.9	18	25	5.4	49	10
6	-0.5	33.3	32	8.0	45	684	1.4	18	13	55	21.3	16	10
21 day mean													
1	1.3	33.3	24	6.7	30	573	0.9	13	14	57	11.2	33	24
2	1.0	33.2	2	9.0	15	424	0.4	11	27	57	11.1	21	31
3	-1.2	33.8	139	15	59	193	1.8	28	16	81	12.0	43	25
4	-0.5	33.6	26	2.4	23	887	1.5	22	15	68	7.3	47	63
5	-0.2	33.0	23	3.2	20	955	0.5	9.2	18	34	7.6	42	23
6	0.0	33.0	39	9.6	35	617	0.9	12	13	40	14.0	26	16

Results

Phytoplankton communities and physiochemical conditioning of experimental inoculates

Although experiments INC 1 and 5, and INC 2 and 6 commenced at approximately the same point in the austral summer during S1 and S2 respectively (6 Feb and 29 Jan, 11 March and 25 Feb), the phytoplankton community and the characteristics of the water column, and thus conditioning of the phytoplankton, differed in the seawater used between the two years (Table 1). Temperature at the start of the experiments was above 0˚C for INC 1, 2 and 5, while for INC 6 it was -0.5˚C (Table 1). INC 3 and 4 were performed earlier in S2 (4 and 28 Dec) when the water column exhibited the lowest temperatures (-0.8 and -1˚C, respectively). The water column had the deepest MLD (>8m) when sampled for INC 1, 2 and 6 than when sampled for the setup of the other experiments. The very shallow MLD at setup of INC 3, 4 and 5 (<4m) was reflected by pronounced stratification (Table 1). There was lower ice cover in the latter half of productive season S2 (<10% for INC 5 and 6) when compared with the same period in S1 (INC 1 and 2; Table 1), with ice melt most visible in the relatively low salinity (32.8 psu) seawater used to setup INC 5. Dissolved inorganic phosphate and nitrate concentrations (Table 1) were lowest at the start of INC 2 and 5 (<0.4 and <8 µM, respectively), while silicate concentrations were >25 µM for all experiments.

Mean (24h) air-PAR is largely determined by day length and was consequently lowest at the end of the productive season, both for S1 and S2 (6 and 16 µmol quanta m^{-2} s^{-1} for INC 2 and 6, respectively; Table 1). Similar to air-PAR, the PAR intensities at the 15m sampling depth were low for INC 2 (0.3 µmol quanta m^{-2} s^{-1}) and highest at the time of INC 3 setup (310 µmol quanta m^{-2} s^{-1}). While PAR levels were low in the water column at the time of sampling for INC 4 and 5, they had been considerably higher in the preceding period (i.e., average PAR 26 and 23 µmol quanta m^{-2} s^{-1}; Table 1).
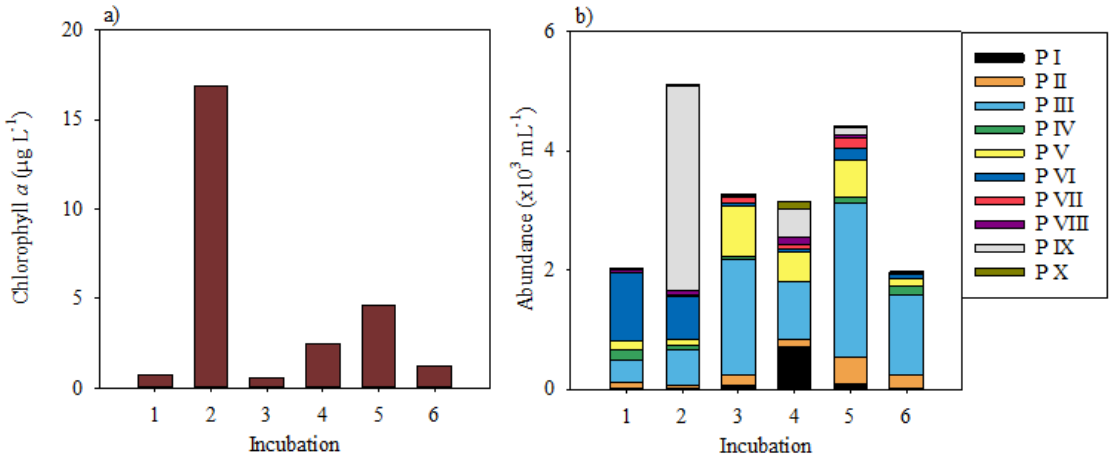
Fig. 1. The phytoplankton community at the start of the six incubation experiments in terms of (a) total Chlorophyll-*a* and (b) community composition as determined by flow cytometric identification of the ten distinct groups designated Phyto I – X.

The phytoplankton community in seawater used for INC 1 (0.7 ± 0.1 µg Chl-*a* L^{-1}, *n* = 2, Fig. 1a) seeded a high biomass bloom under natural conditions (Biggs et al. 2019), comprised of equal shares of diatoms, cryptophytes and prymnesiophytes (32, 33 and 31%; Table S8). Specifically, diatom Phyto VI and *Phaeocystis* Phyto III dominated total phytoplankton abundance (56 and 18%, respectively; Fig. 1b and Table S9). Cellular carbon derived from counts (and cell volume) was largely comprised of Phyto VI (45%) but also the larger-sized Phyto IX (26% of total). INC 2 had the highest Chl-*a* starting concentration (16.9 ug L-1, Fig. 1a) and phytoplankton abundances (5.1 x 10^3 mL^{-1}; Fig. 1b), representing a diatom dominated bloom climax (Chl-*a* 99%, Chl-C 100%). Phyto IX made up 67% of total counts (Table S9) and 94% of cellular carbon (565 µg L^{-1}). During S2, INC 3 was setup with seawater containing the start community of the initial phytoplankton bloom (0.6 ± 0.1 µg Chl-*a* L^{-1}, *n* = 9), consisting mostly of diatoms (89%) and to a lesser extent prymnesiophytes (10%, Table S8). *Phaeocystis* Phyto III represented the majority 59% (Table S9) of the 3.3 x 10^3 mL^{-1} initial total phytoplankton cell concentration, with diatom Phyto V the second most abundant (26%; Fig. 1b and Table S9). Cellular carbon was dominated by the larger-sized Phyto X (52%) and to a lesser extent by Phyto III (15%) and V (16%). At the time of INC 4, Chl-*a*

concentrations were still relatively high (2.5 ± 0.5 µg L^{-1} n = 9, Fig. 1a) primarily due to the abundance of diatoms (97%), in particular Phyto IX and X (484 and 106 mL^{-1}) which made up 40 and 49% of cellular carbon, respectively. Chl-a concentrations were still high at the start of INC 5 (4.6 ± 0.3 µg L^{-1}, Fig. 1a), again primarily due to diatoms (87%) but with an increased contribution of Prymnesiophyceae (10%; Table S8). The share of *Phaeocystis* Phyto III was similar to the start community for INC 3 but its abundance was 1.3-fold higher (2.6 x 10^3 mL^{-1}; Fig. 1b). Diatoms Phyto IX and X remained the primary contributors to the phytoplankton cellular carbon pool (21 and 42% respectively). Seawater for INC 6 was collected after the decline of the initial S2 phytoplankton bloom when Chl-a was reduced (1.2 ± 0.1 µg L^{-1}, n = 9, Fig. 1a). Total phytoplankton abundance was 2 x 10^3 mL^{-1} (Fig. 1b) and largely represented by *Phaeocystis* Phyto III (69%) and picoeukaryote Phyto II (11%; Table S9). The contributions of cryptophytes and prymnesiophytes had increased (18 and 22%) but diatoms still dominated the phytoplankton community (56% of total Chl-a; Table S8). Despite their low abundance (< 11 mL^{-1}, Table S3), specifically the larger-sized Phyto IX and X comprised 42% of total cellular carbon.

Light experiments

The photosynthetic efficiency (Fv/Fm) at the start of all the experiments indicated that the phytoplankton were not photosynthetically stressed, i.e. values between 0.54 and 0.71 (Fig. 2). For the LL and ML treatments the Fv/Fm ratios stayed high during the nine day incubations. Fv/Fm initially dropped slightly in all the HL experiments, with some recovery by the phytoplankton in INC 3 and 5 (Day 3 to 7). Unlike for the other experiments, ambient light levels preceding the start of INC 2 were very low (Table 1), which may explain the steady drop in Fv/Fm under HL over the ten days of INC 2 (minimum 0.26; Fig. 2).

At the end of INC 1, under ML (the light level most alike the ambient light availability) the composition of the phytoplankton community (Phyto III 19%, VI 58% and IX 11%) were highly comparable to that of the natural community sampled

around that time (20, 55 and 9%, respectively; Biggs et al. 2019). This suggests that the incubations successfully replicated natural conditions, where the phytoplankton community was exposed to a consistent light intensity close to ML (~ 30 – 50 µmol quanta m^{-2} s^{-1}).
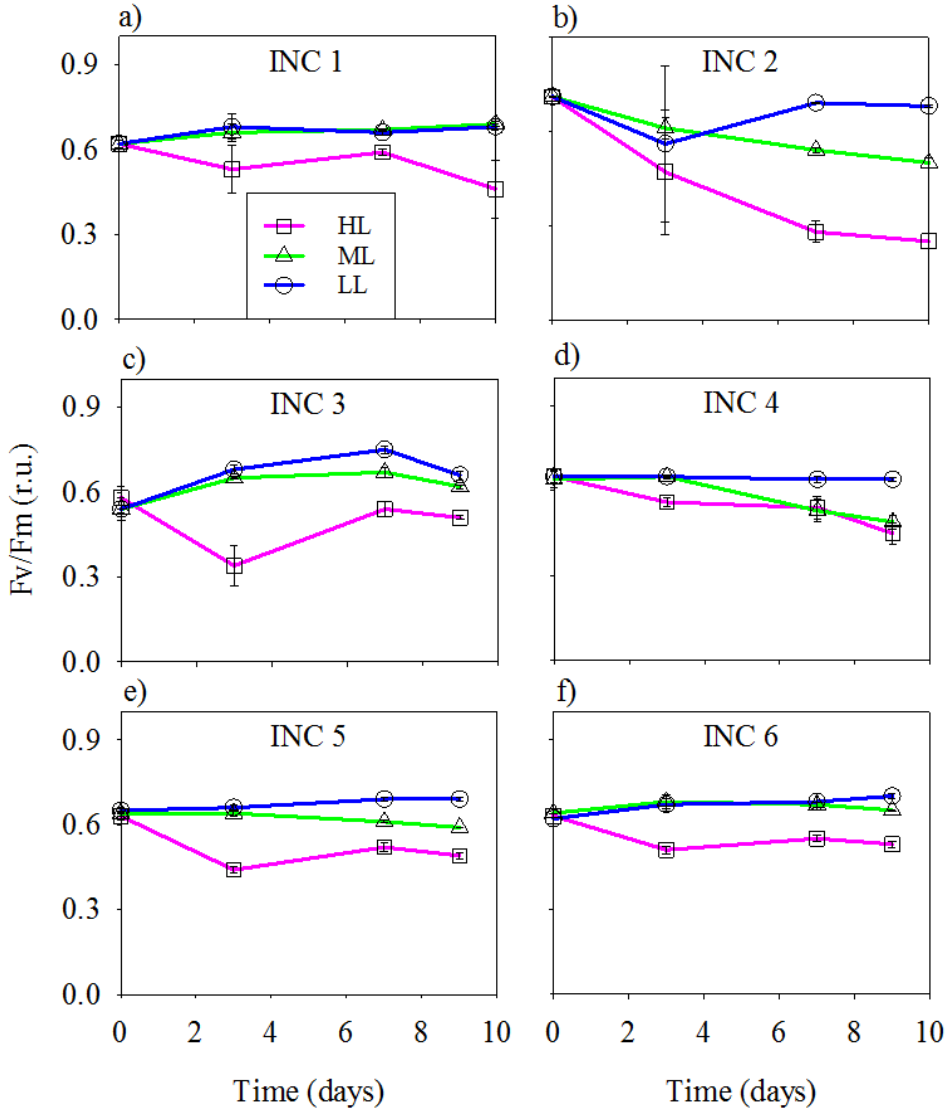
Fig. 2. The influence of light on the photosynthetic efficiency (F$_v$/F$_m$) of the phytoplankton community under the light regimes 150 – 200 (high light, HL), 30 – 50 (medium light, ML) and 4 - 7 µmol quanta m^{-2} s^{-1} (low light, LL) during incubation experiments (INC) 1 - 6 (a to f respectively).
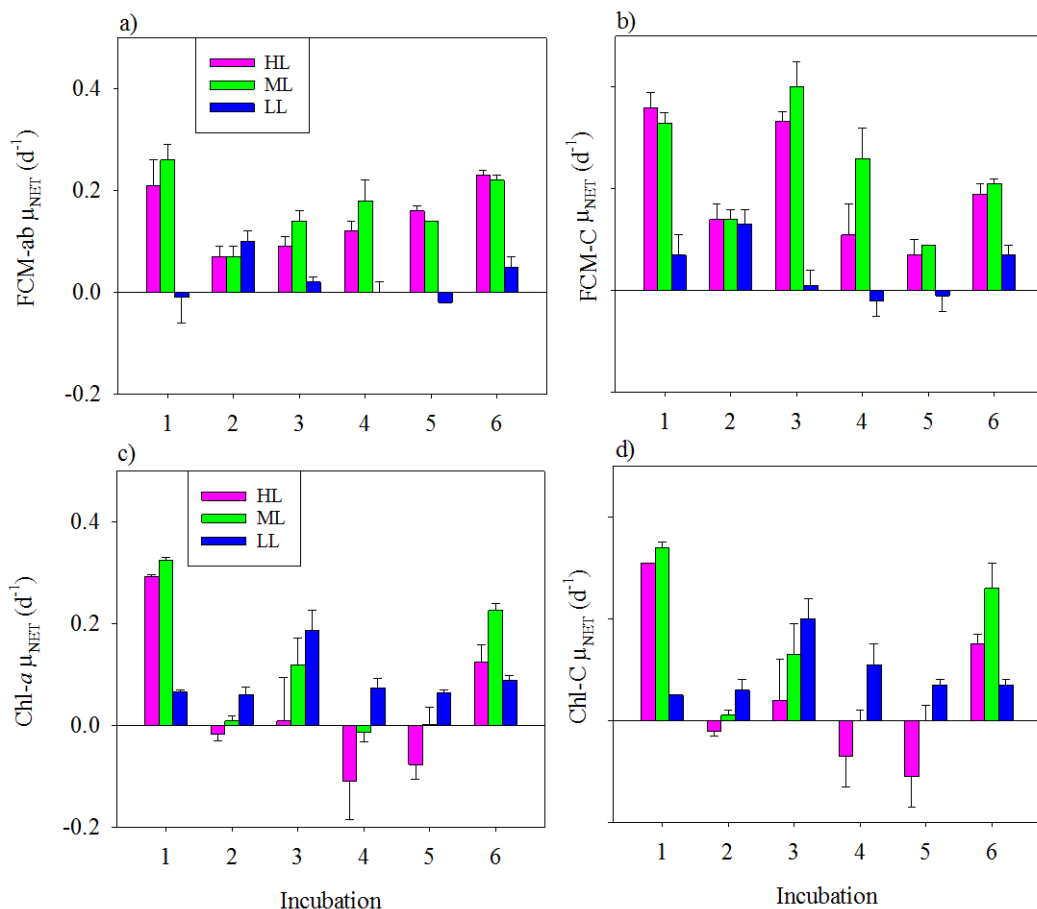
Fig. 3. Phytoplankton net growth rates (μ_{NET}) calculated over the full duration of the incubations according to (a) total phytoplankton abundance (FCM-ab), (b) estimated phytoplankton carbon (FCM-C), (c) Chlorophyll-*a* (Chl-*a*) and (d) estimated Chlorophyll carbon (Chl-C). Error bars are calculated from triplicates and represent +1 standard deviation.

INC 1

The highest abundance-based phytoplankton net growth rates during the first days of INC 1 (T_{0-3}; Table S10) were observed in the ML treatment, which was most comparable to the natural light intensity at the start of the experiment (Table 1). In comparison, growth rates declined under HL and LL (0.31 vs -0.06 and -0.01 d^{-1}, respectively). Thereafter, phytoplankton in the HL treatment (particularly Phyto III, VI and IX, Table S10) recovered with net growth rates ($p = 0.351$, Fig. 3a and b) and yield (Fig. 4a) comparable to ML. Diatom Phyto VI was the most abundant phytoplankton group (initial concentrations of 1.1 x 10^3 mL^{-1}, Fig. 1b) and grew well

throughout the experiment (0.27 d^{-1}, Table S10), subsequently contributing the dominant portion of total abundance-based net growth rates in the ML incubations (Fig. 3a). The higher total phytoplankton abundances in the ML treatment at the end of the experiment (Fig. 4a) may have contributed to greater nitrate and phosphate drawdown compared to HL (Fig. 5). The diatoms Phyto VI and Phyto IX dominated the FCM-C under both ML and HL (628 and 848 µg C L^{-1}, respectively at the end of the experiment; Fig. 4b), and were responsible for the relatively high carbon-based net growth rates (Fig. 3b). The dynamics of diatom Chl-C under HL and ML (net growth rates of 0.41 and 0.43 d^{-1}) were indeed similar to that of the larger-sized (11.5 µm diameter) diatom Phyto IX (0.48 and 0.42 d^{-1}). Under LL, the abundance-based net growth rates sped up slightly towards the end of the incubation (T$_{7-10}$: 0.09 d^{-1}, Table S4 and S10). Taxonomic analysis showed that diatoms dominated also at LL, but that prymnesiophytes and cryptophytes still contributed 21% of total Chl-*a* and 30% of total Chl-C, respectively (Table S6 and S7). The Chl-C net growth rates of these taxonomic groups under LL resembled those of *Phaeocystis* Phyto III and the cryptophyte Phyto IV (Table S10).

INC 2

The initial (T$_{0-3}$) net growth rates in INC 2 were comparable under all three light regimes (abundance-based 0.22 – 0.26 d^{-1} and FCM-C based 0.31 – 0.36 d^{-1}, $p = 0.79$ and 0.77 respectively, Table S10). Still, growth rates for Phyto II, III, V, VII, VIII and IX were significantly higher under LL, compared with under HL and ML ($p < 0.001$ and $p = 0.014$, respectively), whereas for Phyto VI and X growth was significantly lower ($p = 0.002$ and 0.011; $p = 0.004$ and 0.005, respectively). The generally low net growth rates under all light levels thereafter, were most likely caused by the low nitrate and phosphate concentrations (Fig. 5b, c). Diatoms dominated total Chl-*a* (99-100%, Table S6 and S7) and diatom Phyto IX was most abundant throughout the experiment (Table S1). The large diatom Phyto X (20 µm Ø) thrived under ML and HL (Table S1 and S10) and drove overall net growth rates
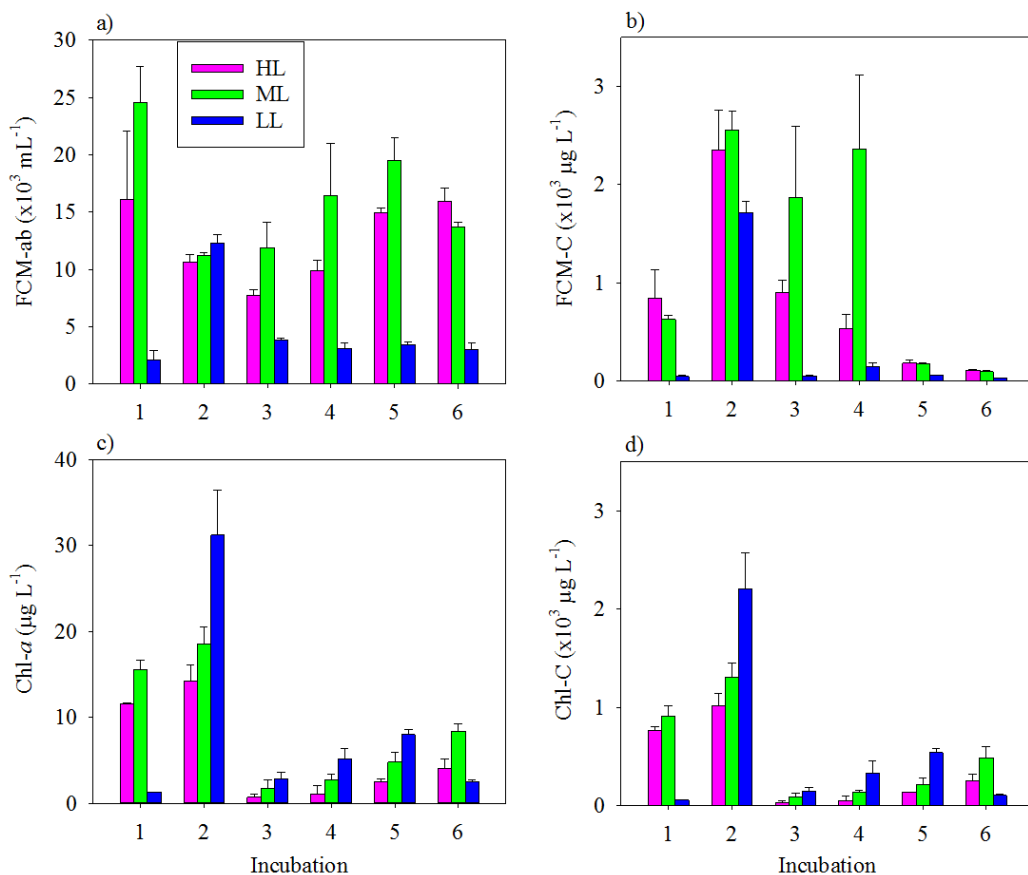
Fig. 4. Phytoplankton (a) abundances, (b) abundance-based carbon (FCM-C), (c) chlorophyll-*a* (Chl-*a*) concentrations, and (d) Chlorophyll-based carbon (Chl-C) at the termination of incubation experiments (INC) 1 to 6. Error bars are calculated from triplicates and represent +1 standard deviation.

based on FCM-C (Fig. 3a, b and Table S10). However, Chl-*a* concentrations declined under HL (Table S6) and net growth rates were lowest overall under HL, and even negative when based on chlorophyll (Fig. 3c, d). Abundances and carbon biomass of the dominant diatoms Phyto IX and X (roughly equal share) were similar at ML and HL, therefore it is likely that the drop in Chl-*a* was due to decreased Chl-*a* concentrations cell^{-1}. Similarly, the lower abundances (Phyto X hardly present) but higher Chl-*a* under LL, compared to ML, also implies photoacclimation (Table S1, S6 and S7).
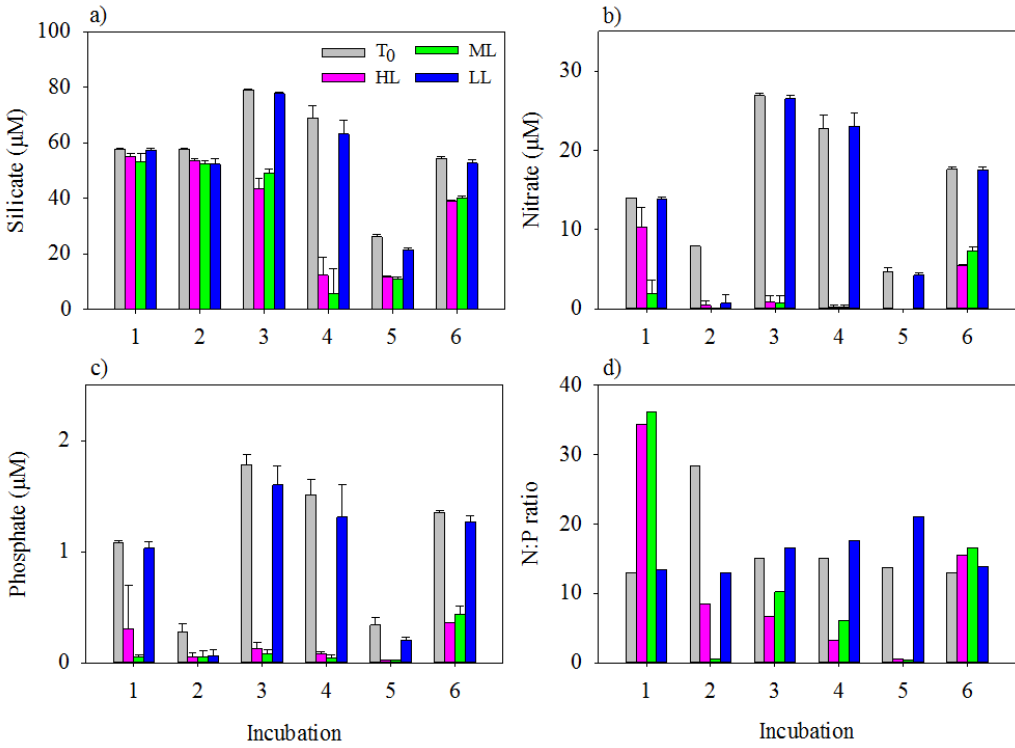
Fig. 5. Average dissolved inorganic nutrient concentrations in water used for the experimental setup (grey bar; T_0) and at termination of the experiment, for light treatments high light (HL, magenta bars), medium light (ML, green bars) and low light (LL, blue bars) for a) phosphate, b) nitrate, c) silicate and (d) the average nitrate to phosphate ratios. Error bars represent ± 1 standard deviation whereby all time zero replicates are combined (INC 1 and 2 $n = 2$, INC 3 – 6 $n = 9$) and shown at the beginning of each INC and at the end under HL, ML and LL treatments.

INC 3

The abundance-based net growth rates for all phytoplankton groups at the end of INC 3 (except Phyto I) were similar under both HL and ML, but significantly higher compared to LL treatment ($p < 0.025$), (Fig. 3a, b and Table S11). Most phytoplankton groups did not grow well under LL, with Phyto V most successful (46% of total abundance, compared to 31 and 36% at ML and HL respectively; Table S3). This was reflected in the nutrient concentrations under LL that remained essentially unchanged (Fig. 5). Whilst Phyto III and V were most abundant under ML and HL (Table S3), biomass was dominated by the largest diatom Phyto X (Table S4). High growth rates of the larger diatoms (Phyto VIII, IX and X) until Day

7 under HL and ML resulted in strong nutrient draw-down. Consequently nutrient availability may have limited growth in these treatments towards the end of the experiment (T_{7-9}) as growth rates declined and were often negative (Table S11). The larger diatoms illustrate the dominance of diatoms found from the taxonomic analysis (Table S6 and S7), driving both Chl-*a* and Chl-C dynamics under all light treatments. Similar to INC 2, 4 and 5, Chl-C based net growth rates reduced as the light level increased (Fig. 3c, d) as a result of decreasing Chl-*a* concentrations (Fig. 4, Table S6). These results are thus unlike FCM-C net growth, which was minimal under LL (Fig. 3b).

INC 4

Over the three weeks preceding the setup of INC 4 PAR declined from 223 to 3 µmol quanta m^{-2} s^{-1}. Initial (T_{0-3}) abundance-based net growth rates were identical under the three light treatments ($p = 0.25$; Table S11). However, the average FCM-C net growth rate under HL was lower than under the other light regimes (0.01 vs 0.11 and 0.10 for HL, ML and LL, respectively) because Phyto X net growth did not yet increase (Table S11). Unlike INC 2 (which was also subject to low light intensities prior to the experimental setup), overall net growth rates were significantly higher under HL and ML ($p < 0.03$) than under LL, where abundances were maintained. This response was more similar to that observed in experiments INC 1 and 3 (Fig. 3a, b, and Table S3). Phyto III, V, IX and X contributed most to abundance and carbon related net growth rates (Table S4 and S11), with a larger share of FCM-C for Phyto IX (45 and 32% under HL and ML respectively) when compared to INC 3 (14 and 4% respectively). Even more so than during INC 3, low nitrate and phosphate concentrations (Fig. 5) may have limited growth under HL and ML towards the end (T_{7-9}; Table S11).

INC 5

Nutrient concentrations at the beginning of INC 5 were similarly low to INC 2, but the phytoplankton community was different (Table S1 and S3). The phytoplankton

abundance and FCM-C based net growth rates under HL and ML remained relatively high throughout the experiment (unlike in INC 2 where growth was close to zero; Table S10 and S11). The high abundance of *Phaeocystis* Phyto III at the start of INC 5 (2.6×10^3 mL^{-1}) developed further under ML and HL (Table S3) resulting in a 54% share of total abundance under both light regimes at termination of the experiment and an 8 and 11% share respectively of the total Chl-*a* (Table S6). The share of the pico-sized Phyto II also increased (around 20% at HL and ML; Table S3) with similar net growth rates as for Phyto III (Table S11). The LL treatment typically resulted, as previously observed, in minimal and often negative net growth rates (similar to INC 1, 3 and 4; Table S11). Although Phyto IX still contributed most to FCM-C at the end of INC 5 (HL and ML, 30 and 38% respectively), large numbers of Phyto III (10.6 and 8.0×10^3 mL^{-1} respectively) made it the second largest cellular carbon contributor (22 and 17% respectively). Numbers of Phyto X generally remained low at all times under all light treatments (< 50 mL^{-1}) and correspondingly low FCM-C (Fig. 4b), may have been the result of the low nitrate concentrations (0.01 µM in HL and ML; Fig. 5b). In contrast to the diatom dominated Chl-C based net growth rates (Fig. 3 and Table S12), cryptophyte carbon indicated significantly higher growth rates of this group under HL and ML (0.23 and 0.23 d^{-1}), compared to LL (0.10 d^{-}1; $p < 0.025$; Table S12).

5

INC 6

As with INC 5, Phyto II and III dominated phytoplankton abundance in INC 6 under all light treatments, both at the beginning (combined 78, 79 and 80%, respectively) and end (72, 78 and 80%, respectively) of the incubation period. Phyto III, V and X made up the majority of FCM-detected phytoplankton biomass (71, 74 and 72% in HL, ML and LL respectively, Table S4). Despite enhanced nutrient concentrations at the setup of this incubation when compared to INC 5 (Table 1), the share of larger diatoms at the end of the experiment was relatively small (Table S3 and S4). Abundance-based net growth rates were generally positive for all phytoplankton, but greater under HL and ML compared with LL (as for INC 1 and 3-5), both at the start

(T_{0-3}) and overall ($p < 0.001$; Table S11). The taxonomic analysis indicated that in addition to diatoms, prasinophytes had overall positive net growth rates (0.1-0.2 d^{-1}, Table S12) with a significant difference between treatments ($p = 0.008$). In contrast to the results of INC 2-5 (but similar to INC 1), Chl-C net growth rates increased the most under ML (0.25 d^{-1}) and HL (0.15 d^{-1}) compared to LL (0.08 d^{-1}, Fig. 3d), with a significant difference between all light treatments ($p < 0.02$ $n = 9$). Chlorophyll carbon concentrations at the end of INC 6 were considerably higher than FCM-C under all light levels (Fig. 4d, b), potentially indicating a greater contribution of larger (> 20 µm) phytoplankton cells.

Discussion

Phytoplankton community response to light intensity

The Chl-*a* net growth rates recorded in this study (up to 0.32 d^{-1}) are in line with those previously reported for Antarctic waters (0.35 d^{-1}; Hutchins et al. 2001), as are the FCM-C net growth rates (average 0.73 d^{-1}) when compared to ^{14}C uptake methods (1.0 d^{-1}; Smith, 1999). The combined use of flow cytometry, size fractionation and chemical taxonomy allows for improved interpretation of light-regulated phytoplankton growth from incubation experiments. Not only does it aid in the identification and differentiation of phytoplankton groups (Biggs et al. 2019), their average cell size and taxonomic composition, but it also clarifies which groups were contributing most to the offset in Chl-*a* concentrations in relation to light level observed in INC 2-5. Acclimation to the different light levels typically caused the Chl-*a* concentration to decline under HL and strongly increase under LL (Fig. 3c). This resulted in net growth rates that were not representative of the phytoplankton community response (e.g. decrease in Chl-*a* while increase in FCM-C). Corrected for cell volume (carbon dominating diatoms Phyto V to X ranged from 50 to 4000 µm^3), the concentrations of Chl-*a* (as well Chl-c2 and fucoxanthin; expressed in fg µm^{-3}) were for all experiments lowest under HL and highest under LL (Table S13), indeed indicative of a standard light response of pigment concentrations (i.e. photosynthetic pigment concentrations decrease in response to increasing irradiance;

Eppley and Sloan 1966; MacIntyre et al. 2002; Álvarez et al. 2017). Large contributions by Phyto X in INC 2-4 coincided with extremely low concentrations of Chl-*a* (cell volume^{-1}) at HL, suggesting this diatom population is able to rapidly adjust Chl-*a* concentrations in relation to light level (Finkel 2001; Álvarez et al. 2017) to optimise growth. Whilst Chl-*a* per cell volume increased under LL in INC 3-5, concentrations remained relatively unchanged in INC 1 and 6 (Table S13), coinciding with peak prasinophyte contributions and positive net growth rates for prasinophytes at all light levels (only in INC 1 and 6; Table S12). Large-sized (> 20 µm Ø, Bird and Karl, 1991) and mixotrophic prasinophytes such as *Pyramimonas* spp. (Bell and Laybourn-Parry 2003), could help explain the lack of a pigment response to light level as they would not need to adjust their photosynthetic pigment content under low light intensity.

Overall (except for INC 2), exposure to low light (LL) did not result in noteworthy net growth, suggesting that the low light intensity used was close to a boundary where (reduced) phytoplankton growth is equal to naturally occurring losses (Behrenfeld and Boss 2018). The slight decrease in nutrient concentrations in these incubations indicates that phytoplankton gross growth rates were likely to be positive (Fig. 5) (Chapter 3, 4; Biggs et al. 2020). An interesting exception to this trend was observed in INC 2 where biomass accumulation (FCM-C; t-test, $p < 0.05$), was observed under low light. Equivalent phytoplankton abundance and FCM-C based net growth was recorded for all three light treatments (especially T_{0-3}), implying the growth potential of the phytoplankton community used to setup INC 2 was different compared to the other experiments. For the three weeks prior to INC 2, natural PAR was very low (average 1.7 µmol quanta m^{-2} s^{-1}) which could have instigated physiological changes that allowed higher growth rates under LL but with reduced growth potential under ML and HL conditions (Dubinsky and Stambler 2009). Sloughter and colleagues (2019) estimated a range of compensation intensities from the literature at 5-25 µE m^{-2} s^{-1} (Langdon 1988; Boyd et al. 1995; Quigg and Beardall 2003) with the lower end of this range similar to the low light intensity employed in this study. Biomass accumulation in Antarctic waters begins when average PAR

rises above a threshold of 1 µmol quanta m^{-2} s^{-1} (Venables et al. 2013) and levels between 1 and 4-7 µmol quanta m^{-2} s^{-1} could represent an important range within which phytoplankton start to switch to a low growth mode. Seasonality in light response curves has been suggested by Sloughter et al. (2019) who proposed a trade-off between the initial slope (α) of the photosynthesis-irradiance (PE) curve and respiration such that below a compensation light intensity it becomes advantageous to decrease α to offset the costs of respiration. During prolonged periods of low light, such as after but also before (INC 2, 11 March) the winter dark period, a switch to a 'low growth' mode would allow higher growth rates under low light compared to during summer when increased light availability should allow a 'high growth' mode to achieve maximum rates of potential growth (other incubations). These results suggest it becomes advantageous to 'switch' between modes of growth over relatively short time periods to best utilize available light during the austral summer. Prolonged periods of low light may also occur during phytoplankton blooms in this coastal environment (where Chl-*a* concentrations regularly exceed 15 µg L^{-1}; Clarke et al. 2008; Venables and Moore 2010; Venables et al. 2013; Brown eta al. 2017; Park et al. 2017). The extremely low light level coinciding with the setup of INC 2 (0.3 µM quanta m^{-2} s^{-1}) likely resulted from light attenuation owing to peak density of a phytoplankton bloom.. The low light levels used in this study could thus, in addition, represent a tipping point around which growth potential is maximized, and the length of time spent above or below this threshold determines if blooms either develop or decline. The length of the photoperiod follows a seasonal pattern and shorter day length would also affect the phytoplankton community sampled for INC 6 in late February (S2). Indeed, net growth rates were positive (0.05 and 0.07 d^{-1} for phytoplankton abundance and FCM-C), however, light intensity was still relatively high (average 39 µmol quanta m^{-2} s^{-1}). The community may have been acclimating to lower daily PAR (Dubinsky and Stambler 2009) but still in a high growth 'state' (Sloughter et al. 2019) due to exposure to high intensity PAR at mid-day, especially if coinciding with deeper vertical mixing (Alderkamp et al. 2010). Ambient light levels were also low for at least six days prior to INC 4 (average of 1.2 µmol quanta

m^{-2} s^{-1}) and this period probably extended to 14 days due to 90 – 100% ice cover (and high biomass), however, the net growth of FCM-C and Chl-C under LL was zero. Therefore, the switch to a low growth mode (Sloughter et al. 2019) seems to be forced by low light exposure over a period as little as three weeks. The need for prolonged low light for optimal photoacclimation would also explain why the community responses to light during INC 3 (high light prior to experiment) and INC 4 were similar. Temperature could also be an influential factor as relatively higher respiration costs compared to photosynthesis at higher temperatures (Boscolo-Galazzo et al. 2018) could increase the compensation light level that triggers this 'switch' between states. This study supports the general observation that light exerts a major control on the seasonal development of net primary productivity in highly productive Antarctic marine ecosystems (Vernet et al. 2008; Petrou and Ralph 2011; Park et al. 2017).

Losses

The phytoplankton dynamics observed in the experiments are the net result of growth and loss processes, such as zooplankton grazing and viral lysis (Chapter 3; Brussaard 2004; Mojica et al. 2016; Biggs et al. 2019, 2020;). Meso- and macrozooplankton graze selectively on diatoms (rather than cryptophytes and prymnesiophytes, even when diatoms are rare; Nejstgaard et al. 1994; Haberman et al. 2003; Mitra et al. 2014) and larger-sized diatoms are preferred prey (Sommer and Stibor 2002; Gonçalves et al. 2014; Djeghri et al. 2018). In contrast to observations from INC 2-4, low abundances of the large diatom Phyto X were observed in INC 1, 5 and 6. Selective grazing by the meso- and macrozooplankton, which were predicted to number 5 – 11 ind. bottle^{-1} (Biggs et al. 2020), in combination with losses due to viral lysis and microzooplankton grazing (Chapter 3 and 4), may have restricted the accumulation of the large diatom Phyto X in INC 1, 5 and 6. In contrast, INC 2-4 were likely subjected to far less meso- and macroplankton induced mortality owing to their lower predicted abundance at 2 - 4 ind. bottle^{-1}.

Cell mortality due to virus infection has been shown as a substantial loss factor for phytoplankton in general (Brussaard and Martínez 2008; Mojica et al. 2016). More specifically, viruses were important mortality agents for all ecologically relevant Antarctic phytoplankton groups (Chapter 3 and 4). The appearance of an algal virus-like group in INC 6 (Fig. S1) also hints to the potential influence of viruses in our incubations. Known diatom viruses are predominantly small genome-sized, single stranded RNA and DNA viruses (Nagasaki 2008; Kimura and Tomaru 2015). The staining characteristics of the virus we observed implies it comprised a larger genome virus akin to non-silicified phytoplankton viruses such as those that infect *Phaeocystis* (Brussaard et al. 1999; Baudoux and Brussaard 2005). *Phaeocystis* Phyto III was very abundant in INC 6 and found to be subjected to considerable lysis at the start (Chapter 4). The abundance of this virus cluster increased under the medium and high light treatments, but not under the low light intensity, in accordance Phyto III growth was on average 0.2 d^{-1} at ML and HL and zero at LL. These virus and phytoplankton dynamics could imply coupling of lytic infection rates and host growth rates. Such a strategy is ecologically sound as it supports persistence of the virus population throughout the growth season without decimating the host population, and allowing the persistence of cells over the winter period. Hypothesizing it is a *Phaeocystis* virus, that there is no loss of viruses and the viral burst size to be 300 viruses per lysed host cell (Brussaard et al. 2007), about 570 cells were lysed over the incubation period (at ML and HL) which equals ~10% of the standing stock of the host and relates well to the specific viral lysis rates around the starting date of INC6 (0.16 and 0.14 d^{-1} on 17 and 27 February, Chapter 4). Delayed and reduced virus production under low light conditions has been reported for several phytoplankton species (Baudoux and Brussaard 2008; Maat et al. 2016; Piedade et al. 2018; Gann et al. 2020) including temperate *P. globosa* as a result of photolimitation, which could explain the lack of virus production under the low light intensities employed in our study.

Phytoplankton group-specific differences

The response of each phytoplankton group to the different light levels provides insight in their temporal dynamics under natural conditions and the ability of phytoplankton growth to escape predation pressure (grazing and viral lysis; Chapter 3 and 4; Atkinson et al. 2012; Mojica et al. 2016; Biggs et al. 2020). *Phaeocystis* Phyto III typically grew best under medium and high light but the relatively high net growth rates under low light in INC 2 and INC 6 suggest this phytoplankton group can compete under all ecologically relevant light conditions. Light intensities during *Phaeocystis antarctica* dominated blooms can be low (Schofield et al. 2015; Park et al. 2017; Oliver et al. 2019) and *P. antarctica* seems better suited, compared to diatoms, to a more dynamic light regime associated with deeper mixed layers (Arrigo et al. 2010; Mills et al. 2010). Photoacclimation has been shown to effectively minimize photoinhibition in natural populations of *Phaeocystis antarctica* (Alderkamp et al. 2013). A modeling study of *P. antarctica* blooms (Amundsen Sea Polygna; Oliver et al. 2019) supports our study and suggests a high degree of photophysiological control (relative to nutrient processes) and the importance of shifts in α for bloom progression under low light. Increasing photosynthetic pigment concentrations under low light could potentially pass a threshold triggering the switch to a low growth mode (and *vice versa*, Alderkamp et al. 2010). The capability to switch modes of growth over relatively short time scales may contribute to its ecological success.

The relative few studies into photoacclimation of Antarctic phytoplankton indicate that diatoms show a variable response to changes in light intensity, resulting in a high degree of specialized niche differentiation (Petrou et al. 2016). In our study, diatom Phyto IX acclimated best to low light with the highest net growth rates of all phytoplankton groups, matching the strong association of Phyto IX with low and limiting PAR under natural conditions (Biggs et al. 2019). Phyto X needed longer to acclimate, potentially due to its larger cell size (Marañón 2015) and related higher maintenance respiration costs (Langdon 1988; Quigg and Beardall 2003). The low Chl-*a* concentrations of Phyto X (cell volume^{-1}) could be a mechanism to reduce the

5

package effect (Finkel 2001) and allow Phyto IX and X to co-dominate the phytoplankton community. The smaller-sized diatoms Phyto V and VI have both been associated with high light and temperature; Phyto VI more with temperature and Phyto V with light (Biggs et al. 2019). This would explain the good growth of Phyto V when exposed to HL in the relatively warmer INC 1 and of Phyto VI at HL in the colder INC 3, 4 and 6. Nano-sized diatoms are poorly characterized yet play an important role in 'spring' blooms and carbon export (Leblanc et al. 2018). Our study indicates that in the current times of global climate change, it is highly relevant to study combined effects of growth controlling variables (such as light, temperature and biotic controls) on Antarctic phytoplankton (Petrou et al. 2016; Lacour et al. 2017, 2018).

In summary, the low light levels in this study ($4 - 7$ µmol quanta m^{-2} s^{-1}) could represent an important boundary where phytoplankton 'make the switch' to a low growth mode. The acclimation of phytoplankton growth response curves over time periods as short as three weeks may allow phytoplankton to reduce their light compensation intensity, increase growth rates under low light and extend periods of phytoplankton accumulation i.e. positive net growth. Low light levels during seasonal phytoplankton bloom development is not uncommon (Vernet et al. 2008; Park et al. 2017) and being able to efficiently adapt to such conditions represents a distinct advantage, allowing specific phytoplankton groups to become a key feature of Antarctic phytoplankton blooms.

Competing Interests

The authors declare no competing interests.

References

Agirbas E, Feyzioglu AM, Kopuz U, Llewellyn CA (2015) Phytoplankton community composition in the south-eastern Black Sea determined with pigments measured by HPLC-CHEMTAX analyses and microscopy cell counts. J Mar Biol Assoc United Kingdom 95:35–52. doi: 10.1017/S0025315414001040

Alderkamp A, Mills M, van Dijken G, Arrigo K (2013) Photoacclimation and non-photochemical quenching under in situ irradiance in natural phytoplankton assemblages from the Amundsen Sea, Antarctica. Mar Ecol Prog Ser 475:15–34. doi: 10.3354/meps10097

Alderkamp AC, De Baar HJW, Visser RJW, Arrigo KR (2010) Can photoinhibition control phytoplankton abundance in deeply mixed water columns of the Southern Ocean? Limnol Oceanogr 55:1248–1264. doi: 10.4319/lo.2010.55.3.1248

Alderkamp AC, Kulk G, Buma AGJ, et al (2012) The effect of iron limitation on the photophysiology of *Phaeocystis antarctica* (Prymnesiophyceae) and *Fragilariopsis cylindrus* (Bacillariophyceae) under dynamic irradiance. J Phycol 48:45–59. doi: 10.1111/j.1529-8817.2011.01098.x

Álvarez E, Nogueira E, López-Urrutia Á (2017) In vivo single-cell fluorescence and size scaling of phytoplankton chlorophyll content. Appl Environ Microbiol 83:1–16. doi: 10.1128/aem.03317-16

Annett AL, Carson DS, Crosta X, et al (2010) Seasonal progression of diatom assemblages in surface waters of Ryder Bay, Antarctica. Polar Biol 33:13–29. doi: 10.1007/s00300-009-0681-7

Arrigo KR, Mills MM, Kropuenske LR, et al (2010) Photophysiology in two major southern ocean phytoplankton taxa: Photosynthesis and growth of *Phaeocystis antarctica* and *Fragilariopsis cylindrus* under different irradiance levels. Integr Comp Biol 50:950–966. doi: 10.1093/icb/icq021

Arrigo KR, van Dijken GL (2015) Continued increases in Arctic Ocean primary production. Prog Oceanogr 136:60–70. doi: 10.1016/j.pocean.2015.05.002

Arrigo KR, van Dijken GL, Strong AL (2015) Environmental controls of marine productivity hot spots around Antarctica. J Geophys Res Ocean 120:5545–5565. doi: 10.1002/2015JC010888

Atkinson A, Siegel V, Pakhomov EA, Rothery P (2004) Long-term decline in krill stock and increase in salps within the Southern Ocean. Nature 432:100–103. doi: 10.1038/nature02950.1.

Atkinson A, Ward P, Hunt BP V., et al (2012) An overview of Southern Ocean zooplankton data: Abundance, biomass, feeding and functional relationships. CCAMLR Sci 19:171–218

Baudoux A-C, Brussaard CPD (2005) Characterization of different viruses infecting the marine harmful algal bloom species *Phaeocystis globosa*. Virology 341:80–90. doi: 10.1016/j.virol.2005.07.002

Baudoux A-C, Brussaard CPD (2008) Influence of irradiance on virus-algal host interactions. J Phycol 44:902–908. doi: 10.1111/j.1529-8817.2008.00543.x

Behrenfeld MJ, Boss ES (2018) Student's tutorial on bloom hypotheses in the context of phytoplankton annual cycles. Glob Chang Biol 24:55–77. doi: 10.1111/gcb.13858

Bell EM, Laybourn-Parry J (2003) Mixotrophy in the Antarctic phytoflagellate, *Pyramimonas gelidicola* (Chlorophyta: Prasinophyceae). J Phycol 39:644–649. doi: 10.1046/j.1529-8817.2003.02152.x

Biggs TEG, Alvarez-Fernandez S, Evans C, et al (2019) Antarctic phytoplankton community composition and size structure: Importance of ice type and temperature as regulatory factors. Polar Biol 42:1997–2015. doi: 10.1007/s00300-019-02576-3

Biggs TEG, Brussaard CPD, Evans C, et al (2020) Plasticity in dormancy behaviour of *Calanoides acutus* in Antarctic coastal waters. ICES J Mar Sci. doi: 10.1093/icesjms/fsaa042

Bird DF, Karl DM (1991) Massive prasinophyte bloom in northern Gerlache Strait. Antarct J United States 26:152–154

Boscolo-Galazzo F, Crichton KA, Barker S, Pearson PN (2018) Temperature dependency of metabolic

5

rates in the upper ocean: A positive feedback to global climate change? Glob Planet Change 170:201–212. doi: 10.1016/j.gloplacha.2018.08.017

Boyd PW, Robinson C, Savidge G, Williams PJ leB. (1995) Water column and sea-ice primary production during Austral spring in the Bellingshausen Sea. Deep Sea Res Part II Top Stud Oceanogr 42:1177–1200. doi: 10.1016/0967-0645(95)00070-7

Brussaard CPD (2004) Viral control of phytoplankton populations-A review. J Eukaryot Microbiol 51:125–138. doi: 10.1111/j.1550-7408.2004.tb00537.x

Brussaard CPD, Bratbak G, Baudoux A-C, Ruardij P (2007) *Phaeocystis* and its interaction with viruses. Biogeochemistry 83:201–215. doi: 10.1007/s10533-007-9096-0

Brussaard CPD, Martínez J (2008) Algal bloom viruses. Plant Viruses 2:1–13

Brussaard CPD, Peperzak L, Beggah S, et al (2016) Immediate ecotoxicological effects of short-lived oil spills on marine biota. Nat Commun 7:1–11. doi: 10.1038/ncomms11206

Brussaard CPD, Thyrhaug R, Marie D, Bratbak G (1999) Flow cytometric analyses of viral infection in two marine phytoplankton species, *Micromonas pusilla* (Prasinophyceae) and *Phaeocystis pouchetii* (Prymnesiophyceae). J Phycol 35:941–948. doi: 10.1046/j.1529-8817.1999.3550941.x

Clarke A, Meredith MP, Wallace MI, et al (2008) Seasonal and interannual variability in temperature, chlorophyll and macronutrients in northern Marguerite Bay, Antarctica. Deep Res Part II Top Stud Oceanogr 55:1988–2006. doi: 10.1016/j.dsr2.2008.04.035

Collins M, Knutti R, Arblaster J, et al (2013) Long-term climate change: Projections, commitments, and irreversibility. Cambridge University Press, United Kingdom and New York, NY, USA,

DiTullio GR, Garcia N, Riseman SF, Sedwick PN (2007) Effects of iron concentration on pigment composition in *Phaeocystis antarctica* grown at low irradiance. Biogeochemistry 83:71–81. doi: 10.1007/s10533-007-9080-8

Djeghri N, Atkinson A, Fileman ES, et al (2018) High prey-predator size ratios and unselective feeding in copepods: A seasonal comparison of five species with contrasting feeding modes. Prog Oceanogr 165:63–74. doi: 10.1016/j.pocean.2018.04.013

Dubinsky Z, Stambler N (2009) Photoacclimation processes in phytoplankton: Mechanisms, consequences, and applications. Aquat Microb Ecol 56:163–176. doi: 10.3354/ame01345

Ducklow H, Clarke A, Dickhut R, et al (2012) The marine system of the Western Antarctic Peninsula. In: Rogers AD, Johnston NM, Murphy EJ, Clarke A (eds) Antarctic Ecosystems: An Extreme Environment in a Changing World. Blackwell Publishing Ltd., pp 121–159

Eppley RW, Sloan PR (1966) Growth rates of marine phytoplankton: Correlation with light absorption by cell Chlorophyll *a*. Physiol Plant 19:47–59. doi: 10.1111/j.1399-3054.1966.tb09073.x

Finkel Z V. (2001) Light absorption and size scaling of light-limited metabolism in marine diatoms. Limnol Oceanogr 46:86–94. doi: 10.4319/lo.2001.46.1.0086

Gann ER, Gainer PJ, Reynolds TB, Wilhelm SW (2020) Influence of light on the infection of *Aureococcus anophagefferens* CCMP 1984 by a "giant virus." PLoS One 15:e0226758. doi: 10.1371/journal.pone.0226758

Garibotti IA, Vernet M, Kozlowski WA, Ferrario ME (2003) Composition and biomass of phytoplankton assemblages in coastal Antarctic waters: A comparison of chemotaxonomic and microscopic analyses. Mar Ecol Prog Ser 247:27–42. doi: 10.3354/meps247027

Garibotti IA, Vernet MM, Ferrario ME, et al (2005) Annually recurrent phytoplanktonic assemblages during summer in the seasonal ice zone west of the Antarctic Peninsula (Southern Ocean). Deep Res Part I Oceanogr Res Pap 52:1823–1841. doi: 10.1016/j.dsr.2005.05.003

Garrison DL, Gowing MM, Hughes MP, et al (2000) Microbial food web structure in the Arabian Sea: A US JGOFS study. Deep Sea Res Part II Top Stud Oceanogr 47:1387–1422. doi: 10.1016/S0967-0645(99)00148-4

Gonçalves RJ, Gréve H van S, Couespel D, Kiørboe T (2014) Mechanisms of prey size selection in a suspension-feeding copepod, *Temora longicornis*. Mar Ecol Prog Ser 517:61–74. doi: 10.3354/meps11039

Haberman KL, Quetin LB, Ross RM (2003) Diet of the Antarctic krill (*Euphausia superba* Dana). J Exp Mar Bio Ecol 283:79–95. doi: 10.1016/S0022-0981(02)00466-5

Hutchins DA, Sedwick PN, DiTullio GR, et al (2001) Control of phytoplankton growth by iron and silicic acid availability in the subantarctic Southern Ocean: Experimental results from the SAZ Project. J Geophys Res Ocean 106:31559–31572. doi: 10.1029/2000JC000333

Kim H, Ducklow HW, Abele D, et al (2018) Correction to 'Inter-decadal variability of phytoplankton

biomass along the coastal West Antarctic Peninsula.' Philos Trans R Soc A Math Phys Eng Sci 376:20180170. doi: 10.1098/rsta.2018.0170

Kimura K, Tomaru Y (2015) Discovery of two novel viruses expands the diversity of single-stranded DNA and single-stranded RNA viruses infecting a cosmopolitan marine diatom. Appl Environ Microbiol 81:1120–1131. doi: 10.1128/AEM.02380-14

Kozlowski WA, Deutschman D, Garibotti I, et al (2011) An evaluation of the application of CHEMTAX to Antarctic coastal pigment data. Deep Res Part I Oceanogr Res Pap 58:350–364. doi: 10.1016/j.dsr.2011.01.008

Lacour T, Larivière J, Babin M (2017) Growth, Chl *a* content, photosynthesis, and elemental composition in polar and temperate microalgae. Limnol Oceanogr 62:43–58. doi: 10.1002/lno.10369

Lacour T, Larivière J, Ferland J, et al (2018) The role of sustained photoprotective non-photochemical quenching in low temperature and high light acclimation in the bloom-forming Arctic diatom *Thalassiosira gravida*. Front Mar Sci 5:. doi: 10.3389/fmars.2018.00354

Langdon C (1988) On the causes of interspecific differences in the growth-irradiance relationship for phytoplankton. II. A general review. J Plankton Res 10:1291–1312. doi: 10.1093/plankt/10.6.1291

Leblanc K, Quéguiner B, Diaz F, et al (2018) Nanoplanktonic diatoms are globally overlooked but play a role in spring blooms and carbon export. Nat Commun 9:1–12. doi: 10.1038/s41467-018-03376-9

Llewellyn CA, Fishwick JR, Blackford JC (2005) Phytoplankton community assemblage in the English Channel: A comparison using chlorophyll *a* derived from HPLC-CHEMTAX and carbon derived from microscopy cell counts. J Plankton Res 27:103–119. doi: 10.1093/plankt/fbh158

Llort J, Lévy M, Sallée J-B, Tagliabue A (2015) Onset, intensification, and decline of phytoplankton blooms in the Southern Ocean. ICES J Mar Sci J du Cons 72:1971–1984. doi: 10.1093/icesjms/fsv053

Maat DS, de Blok R, Brussaard CPD (2016) Combined phosphorus limitation and light stress prevent viral proliferation in the phytoplankton species *Phaeocystis globosa*, but not in *Micromonas pusilla*. Front Mar Sci. doi: 10.3389/fmars.2016.00160

MacIntyre HL, Kana TM, Anning T, Geider RJ (2002) Photoacclimation of photosynthesis irradiance response curves and photosynthetic pigments in microalgae and cyanobacteria. J Phycol 38:17–38. doi: 10.1046/j.1529-8817.2002.00094.x

Mackey MD, Mackey DJ, Higgins HW, Wright SW (1996) CHEMTAX - A program for estimating class abundances from chemical markers: Application to HPLC measurements of phytoplankton. Mar Ecol Prog Ser 144:265–283. doi: 10.3354/meps144265

Marañón E (2015) Cell size as a key determinant of phytoplankton metabolism and community structure. Ann Rev Mar Sci 7:241–64. doi: 10.1146/annurev-marine-010814-015955

Marie D, Partensky F, Vaulot D, Brussaard CPD (2001) Enumeration of phytoplankton, bacteria, and viruses in marine samples. Curr Protoc Cytom 10:11.11.1-11.11.15. doi: 10.1002/0471142956.cy1111s10

Maxwell K, Johnson GN (2000) Chlorophyll fluorescence—a practical guide. J Exp Bot 51:659–668. doi: 10.1093/jexbot/51.345.659

Mendes CRB, Tavano VM, Dotto TS, et al (2017) New insights on the dominance of cryptophytes in Antarctic coastal waters: A case study in Gerlache Strait. Deep Sea Res Part II Top Stud Oceanogr 149:161–170. doi: 10.1016/j.dsr2.2017.02.010

Mills MM, Kropuenske LR, Van Dijken GL, et al (2010) Photophysiology in two Southern Ocean phytoplankton taxa: Photosynthesis of *Phaeocystis antarctica* (Prymnesiophyceae) and *Fragilariopsis cylindrus* (Bacillariophyceae) under simulated mixed-layer irradiance. J Phycol 46:1114–1127. doi: 10.1111/j.1529-8817.2010.00923.x

Mitra A, Castellani C, Gentleman WC, et al (2014) Bridging the gap between marine biogeochemical and fisheries sciences; configuring the zooplankton link. Prog Oceanogr 129:176–199. doi: 10.1016/j.pocean.2014.04.025

Mojica KDA, Huisman J, Wilhelm SW, Brussaard CPD (2016) Latitudinal variation in virus-induced mortality of phytoplankton across the North Atlantic Ocean. ISME J 10:500–513. doi: 10.1038/ismej.2015.130

Montes-Hugo M, Doney SC, Ducklow HW, et al (2009) Recent changes in phytoplankton communities

5

associated with rapid regional climate change along the western Antarctic Peninsula. Science (80-) 323:1470–1473. doi: 10.1126/science.1164533

Moore CM, Suggett DJ, Hickman AE, et al (2006) Phytoplankton photoacclimation and photoadaptation in response to environmental gradients in a shelf sea. Limnol Oceanogr 51:936–949. doi: 10.4319/lo.2006.51.2.0936

Nagasaki K (2008) Dinoflagellates, diatoms, and their viruses. J Microbiol 46:235–243. doi: 10.1007/s12275-008-0098-y

Nejstgaard JC, Witte HJ, van der Wal P, Jacobsen A (1994) Copepod grazing during a mesocosm study of an *Emiliania huxleyi* (Prymnesiophyceae) bloom. Sarsia 79:369–377. doi: 10.1080/00364827.1994.10413568

Oliver H, St-Laurent P, Sherrell RM, Yager PL (2019) Modeling iron and light controls on the summer *Phaeocystis antarctica* bloom in the Amundsen Sea Polynya. Global Biogeochem Cycles 2018GB006168. doi: 10.1029/2018GB006168

Park J, Kuzminov FI, Bailleul B, et al (2017) Light availability rather than Fe controls the magnitude of massive phytoplankton bloom in the Amundsen Sea polynyas, Antarctica. Limnol Oceanogr 62:2260–2276. doi: 10.1002/lno.10565

Petrou K, Kranz SA, Trimborn S, et al (2016) Southern Ocean phytoplankton physiology in a changing climate. J Plant Physiol 203:135–150. doi: 10.1016/j.jplph.2016.05.004

Petrou K, Ralph PJ (2011) Photosynthesis and net primary productivity in three Antarctic diatoms: Possible significance for their distribution in the Antarctic marine ecosystem. Mar Ecol Prog Ser 437:27–40. doi: 10.3354/meps09291

Piedade GJ, Wesdorp EM, Borbolla EM, Maat DS (2018) Influence of irradiance and temperature on the virus MpoV-45T infecting the Arctic picophytoplankter *Micromonas polaris*. Viruses 1–17. doi: 10.3390/v10120676

Quigg A, Beardall J (2003) Protein turnover in relation to maintenance metabolism at low photon flux in two marine microalgae. Plant, Cell Environ 26:693–703. doi: 10.1046/j.1365-3040.2003.01004.x

Rembauville M, Blain S, Caparros J, Salter I (2016) Particulate matter stoichiometry driven by microplankton community structure in summer in the Indian sector of the Southern Ocean. Limnol Oceanogr 61:1301–1321. doi: 10.1002/lno.10291

Schofield O, Miles T, Alderkamp A-C, et al (2015) In situ phytoplankton distributions in the Amundsen Sea Polynya measured by autonomous gliders. Elem Sci Anthr 3:000073. doi: 10.12952/journal.elementa.000073

Sloughter TM, Banas NS, Sambrotto RN (2019) Seasonal variation in light response of polar phytoplankton. J Mar Syst 191:64–75. doi: 10.1016/j.jmarsys.2018.12.003

Smith W (1999) Phytoplankton growth rates in the Ross Sea, Antarctica, determined by independent methods: Temporal variations. J Plankton Res 21:1519–1536. doi: 10.1093/plankt/21.8.1519

Sommer U, Stibor H (2002) Copepoda - Cladocera - Tunicata: The role of three major mesozooplankton groups in pelagic food webs. Ecol Res 17:161–174. doi: 10.1046/j.1440-1703.2002.00476.x

Stammerjohn SE, Martinson DG, Smith RC, et al (2008) Trends in Antarctic annual sea ice retreat and advance and their relation to El Niño–Southern Oscillation and Southern Annular Mode variability. J Geophys Res 113:C03S90. doi: 10.1029/2007JC004269

Thomalla SJ, Fauchereau N, Swart S, Monteiro PMS (2011) Regional scale characteristics of the seasonal cycle of chlorophyll in the Southern Ocean. Biogeosciences 8:2849–2866. doi: 10.5194/bg-8-2849-2011

Timmermans KR, Davey MS, Van der Wagt B, et al (2001) Co-limitation by iron and light of *Chaetoceros brevis, C. dichaeta and C. calcitrans* (Bacillariophyceae). Mar Ecol Prog Ser 217:287–297. doi: 10.3354/meps217287

Venables H, Moore CM (2010) Phytoplankton and light limitation in the Southern Ocean: Learning from high-nutrient, high-chlorophyll areas. J Geophys Res 115:C02015. doi: 10.1029/2009JC005361

Venables HJ, Clarke A, Meredith MP (2013) Wintertime controls on summer stratification and productivity at the western Antarctic Peninsula. Limnol Oceanogr 58:1035–1047. doi: 10.4319/lo.2013.58.3.1035

Vernet M, Martinson D, Iannuzzi R, et al (2008) Primary production within the sea-ice zone west of the Antarctic Peninsula: I—Sea ice, summer mixed layer, and irradiance. Deep Sea Res Part II

Top Stud Oceanogr 55:2068–2085. doi: 10.1016/j.dsr2.2008.05.021

Worden AZ, Nolan JK, Palenik B (2004) Assessing the dynamics and ecology of marine picophytoplankton: The importance of the eukaryotic component. Limnol Oceanogr 49:168–179. doi: 10.4319/lo.2004.49.1.0168

Supplementary Figure

a)

b)

Green fluoresence

Bacteria

V 4

V1 - V3

X = log SSC-H Y = log FL1-H

Side scatter

VLPs (x 10^4 mL^{-1})

INC 6

HL
ML
LL

20

10

0

0   3   6   9

Time (d)

5
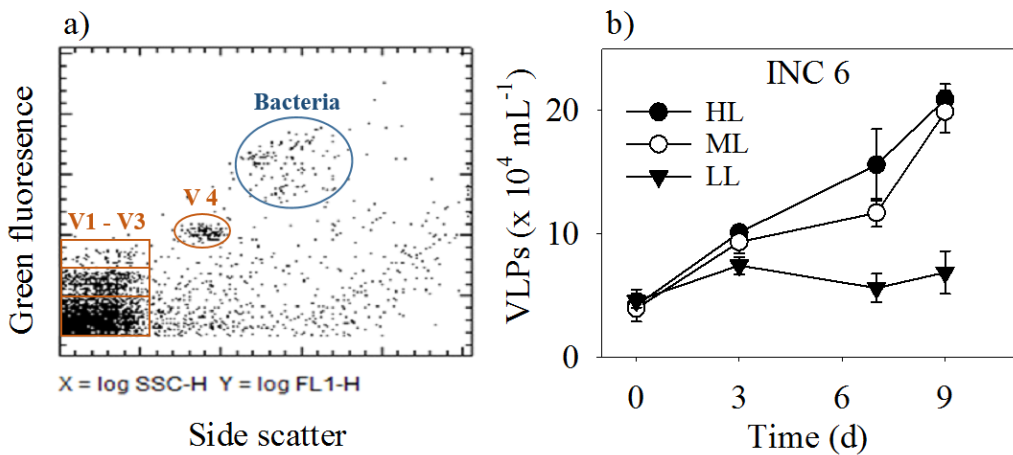
Fig. S1. The V4 algal virus group. a) A cytogram showing the location of the V4 virus group in relation to bacteria and smaller virus groups V1 – V3 and (b) the abundance of V4 in INC 6. Error bars represent ± 1 standard deviation of triplicates.

Supplementary Tables

Table S1. Phytoplankton abundance (mL^{-1}), as determined by flow cytometry for INC 1 and 2 during Season 1. Abundances of the 10 phytoplankton groups (Phyto I-X) represent an average of three replicates.

INC	Time (days)	Light level	Phyto I	Phyto II	Phyto III	Phyto IV	Phyto V	Phyto VI	Phyto VII	Phyto VIII	Phyto IX	Phyto X	TOTAL
			mL^{-1}	mL^{-1}	mL^{-1}	mL^{-1}	mL^{-1}	mL^{-1}	mL^{-1}	mL^{-1}	mL^{-1}	mL^{-1}	mL^{-1}
1	0	HL	4	92	350	173	133	1088	16	45	39	1	1941
1	3	HL	11	222	223	136	201	751	14	42	137	2	1737
1	7	HL	9	264	188	127	585	558	49	57	455	1	2293
1	10	HL	1	840	2466	333	2200	5167	90	148	4843	2	16088
1	0	ML	4	98	405	180	162	1074	19	30	43	0	2015
1	3	ML	1	351	981	171	347	2506	48	69	115	2	4589
1	7	ML	1	675	2439	107	869	5313	48	183	706	6	10348
1	10	ML	13	1124	4684	138	1133	14323	65	248	2822	11	24560
1	0	LL	6	128	376	173	159	1215	12	29	37	0	2135
1	3	LL	0	159	358	156	148	1152	6	34	76	1	2090
1	7	LL	1	85	239	80	140	886	12	61	119	1	1623
1	10	LL	0	70	198	98	260	1161	51	82	156	2	2079
2	0	HL	0	72	661	87	108	668	66	83	3591	33	5381
2	3	HL	1	33	529	60	98	1529	66	109	7176	645	10339
2	7	HL	3	129	525	49	95	1252	64	95	7932	1117	11388
2	10	HL	4	92	414	51	100	696	64	93	7731	1301	10661
2	0	ML	3	69	635	70	104	684	39	72	3859	20	5570
2	3	ML	2	40	883	57	126	1275	49	91	7898	602	11048
2	7	ML	2	77	543	36	86	1266	60	148	8163	425	11002
2	10	ML	1	33	451	5	81	720	64	138	7774	1510	11202
2	0	LL	2	60	501	63	78	770	24	72	2824	11	4417
2	3	LL	1	80	905	52	160	901	70	122	7128	9	9463
2	7	LL	1	60	831	39	146	854	79	149	11037	21	13261
2	10	LL	2	30	481	29	101	603	59	184	10725	35	12293

Table S2. Carbon estimates (FCM-C, µg L^{-1}), converted from phytoplankton abundance, for each Phyto group during INC 1 and 2 in Season 1. Abbreviations represent: P_I (Phyto I), P_II (Phyto II), P_III (Phyto III) etc. Concentrations represent an average of three replicates.

INC	Time (days)	Light level	Phyto I	Phyto II	Phyto III	Phyto IV	Phyto V	Phyto VI	Phyto VII	Phyto VIII	Phyto IX	Phyto X	TOTAL
			C µgL^{-1}	C_ µgL^{-1}	C_ µgL^{-1}	C_ µgL^{-1}	C_ µgL^{-1}	C_ µgL^{-1}	C_ µgL^{-1}	C_ µgL^{-1}	C_ µgL^{-1}	C_ µgL^{-1}	C_ µgL^{-1}
1	0	HL	0	0	1	1	1	10	1	2	6	1	24
1	3	HL	0	0	1	1	2	7	1	2	21	1	36
1	7	HL	0	0	1	1	6	5	2	3	71	0	89
1	10	HL	0	1	9	2	21	48	4	8	754	1	848
1	0	ML	0	0	2	1	2	10	1	2	7	0	23
1	3	ML	0	0	4	1	3	23	2	4	18	2	57
1	7	ML	0	1	9	1	8	49	2	10	110	5	195
1	10	ML	0	1	17	1	11	133	3	13	439	9	628
1	0	LL	0	0	1	1	2	11	1	2	6	0	23
1	3	LL	0	0	1	1	1	11	0	2	12	1	30
1	7	LL	0	0	1	1	1	8	1	3	19	1	34
1	10	LL	0	0	1	1	2	11	2	4	24	2	47
2	0	HL	0	0	2	1	1	6	3	1	559	29	602
2	3	HL	0	0	2	0	1	15	3	5	1117	559	1703
2	7	HL	0	0	2	0	1	12	3	7	1235	968	2229
2	10	HL	0	0	2	0	1	7	3	6	1203	1128	2351
2	0	ML	0	0	2	0	1	6	2	1	601	17	631
2	3	ML	0	0	3	0	1	12	2	1	1229	522	1773
2	7	ML	0	0	2	0	1	12	3	11	1271	369	1669
2	10	ML	0	0	2	0	1	7	3	23	1210	1309	2556
2	0	LL	0	0	2	0	1	7	1	0	440	10	462
2	3	LL	0	0	3	0	1	9	3	2	1110	8	1137
2	7	LL	0	0	3	0	1	8	3	2	1718	18	1756
2	10	LL	0	0	2	0	1	6	2	2	1670	30	1715

5

Table S3. Phytoplankton abundance (mL^{-1}), determined by flow cytometry for INC 3-6 during Season 2. Abundances of the 10 phytoplankton groups (Phyto I-X) represent an average of three replicates.

INC	Time (days)	Light level	Phyto I	Phyto II	Phyto III	Phyto IV	Phyto V	Phyto VI	Phyto VII	Phyto VIII	Phyto IX	Phyto X	TOTAL
			mL^{-1}	mL^{-1}	mL^{-1}	mL^{-1}	mL^{-1}	mL^{-1}	mL^{-1}	mL^{-1}	mL^{-1}	mL^{-1}	mL^{-1}
3	0	HL	67	203	1875	53	881	65	97	4	23	29	3298
3	3	HL	46	128	2532	44	2409	32	60	13	17	79	5360
3	7	HL	257	147	5149	96	5072	171	56	382	331	2102	13905
3	9	HL	264	380	2848	37	2385	161	60	161	523	896	7751
3	0	ML	61	156	2032	47	825	46	99	5	19	29	3318
3	3	ML	29	94	2394	48	2306	18	76	17	34	78	5092
3	7	ML	51	122	4908	61	4516	112	29	312	207	885	11204
3	9	ML	83	283	4010	58	4299	123	42	524	501	1969	11893
3	0	LL	62	152	1915	67	807	44	112	5	15	29	3208
3	3	LL	19	182	1880	54	1158	54	111	1	20	35	3513
3	7	LL	8	140	2119	57	1802	22	67	6	13	24	4258
3	9	LL	10	107	1692	54	1805	49	128	17	12	25	3899
4	0	HL	670	130	992	11	489	34	75	98	406	93	3001
4	3	HL	864	234	1199	15	363	82	304	368	366	100	3896
4	7	HL	1049	439	2505	11	3124	208	1874	923	2362	680	13174
4	9	HL	326	746	2383	14	2173	441	1194	880	1549	184	9890
4	0	ML	740	137	985	18	512	39	98	139	532	131	3330
4	3	ML	1135	270	1461	16	562	41	70	304	396	289	4544
4	7	ML	673	587	3384	15	1686	224	559	1913	3468	1914	14425
4	9	ML	181	354	1836	18	3369	379	135	3846	4803	1564	16486
4	0	LL	692	133	890	18	493	40	75	127	515	94	3076
4	3	LL	764	152	1088	14	481	58	81	101	816	135	3691
4	7	LL	317	104	1089	8	527	46	79	265	616	138	3190
4	9	LL	177	276	881	13	753	40	62	290	570	35	3097
5	0	HL	73	462	2760	82	708	202	171	87	141	47	4733
5	3	HL	122	857	3522	73	540	424	62	145	162	23	5929
5	7	HL	222	2527	7743	156	1177	1285	30	346	228	12	13724
5	9	HL	283	4020	10617	139	1564	1950	91	508	350	25	19547
5	0	ML	93	405	2537	93	610	203	168	58	90	38	4294
5	3	ML	114	945	3533	59	559	384	37	146	159	43	5980
5	7	ML	60	2335	6982	110	1019	745	31	373	354	29	12038
5	9	ML	121	2995	8002	99	1402	1297	102	471	432	23	14945
5	0	LL	105	448	2488	90	551	179	179	61	84	28	4213
5	3	LL	93	306	2033	69	571	198	116	66	48	35	3534
5	7	LL	56	340	2109	39	238	478	26	36	20	22	3365
5	9	LL	69	286	2110	31	280	527	49	55	23	38	3467
6	0	HL	28	214	1420	159	141	76	16	9	10	10	2081
6	3	HL	56	347	2113	212	254	82	12	17	6	6	3102
6	7	HL	186	1608	6211	436	863	232	24	96	13	20	9688
6	9	HL	224	2719	8786	683	2490	756	123	133	36	23	15973
6	0	ML	22	213	1307	149	116	68	14	10	7	4	1910
6	3	ML	44	390	1957	188	206	118	38	16	9	8	2974
6	7	ML	108	1523	4591	346	774	232	35	28	45	20	7703
6	9	ML	130	2629	8081	459	1452	601	58	106	27	30	13747
6	0	LL	13	201	1350	129	122	60	17	10	11	5	1917
6	3	LL	20	168	1667	171	130	62	10	7	13	8	2257
6	7	LL	36	184	1671	152	156	76	11	7	25	7	2325
6	9	LL	82	265	2147	141	212	131	14	7	30	12	3041

Table S4. Carbon estimates (FCM-C, µg L^{-1}), converted from phytoplankton abundance, for each phytoplankton group in season 2 during INC 3 - 6. Carbon estimates for each phytoplankton group (Phyto I-X) represent an average of three replicates.

INC	Time (days)	Light level	Phyto I	Phyto II	Phyto_ III	Phyto IV	Phyto V	Phyto VI	Phyto VII	Phyto VIII	Phyto IX	Phyto X	TOTAL
			C_µgL^{-1}	C_µgL^{-1}	C_µgL^{-1}	C_µgL^{-1}	C_µgL^{-1}	C_µgL^{-1}	C_µgL^{-1}	C_µgL^{-1}	C_µgL^{-1}	C_µgL^{-1}	C_µgL^{-1}
3	0	HL	0	0	7	0	8	1	4	0	4	25	49
3	3	HL	0	0	9	0	23	0	2	1	3	69	107
3	7	HL	0	0	19	1	48	2	2	21	51	1822	1967
3	9	HL	0	0	11	0	23	1	3	9	81	777	905
3	0	ML	0	0	8	0	8	0	4	0	3	25	48
3	3	ML	0	0	9	0	22	0	3	1	5	67	108
3	7	ML	0	0	18	0	43	1	1	17	32	768	880
3	9	ML	0	0	15	0	41	1	2	28	78	1707	1872
3	0	LL	0	0	7	0	8	0	5	0	2	25	48
3	3	LL	0	0	7	0	11	1	5	0	3	30	56
3	7	LL	0	0	8	0	17	0	3	0	2	21	51
3	9	LL	0	0	6	0	17	0	5	1	2	22	54
4	0	HL	0	0	4	0	5	0	3	5	63	80	161
4	3	HL	0	0	4	0	3	1	13	20	57	87	186
4	7	HL	0	0	9	0	30	2	78	50	368	589	1127
4	9	HL	0	1	9	0	21	4	50	48	241	160	533
4	0	ML	0	0	4	0	5	0	4	8	83	113	217
4	3	ML	0	0	5	0	5	0	3	16	62	251	343
4	7	ML	0	0	13	0	16	2	23	104	540	1660	2358
4	9	ML	0	0	7	0	32	4	6	209	748	1357	2361
4	0	LL	0	0	3	0	5	0	3	7	80	82	181
4	3	LL	0	0	4	0	5	1	3	6	127	117	262
4	7	LL	0	0	4	0	5	0	3	14	96	119	242
4	9	LL	0	0	3	0	7	0	3	16	89	30	148
5	0	HL	0	0	10	1	7	2	7	5	22	41	95
5	3	HL	0	1	13	0	5	4	3	8	25	20	79
5	7	HL	0	2	29	1	11	12	1	19	35	10	121
5	9	HL	0	3	40	1	15	18	4	28	54	22	184
5	0	ML	0	0	9	1	6	2	7	3	14	33	75
5	3	ML	0	1	13	0	5	4	2	8	25	37	95
5	7	ML	0	2	26	1	10	7	1	20	55	25	147
5	9	ML	0	2	30	1	13	12	4	26	67	20	175
5	0	LL	0	0	9	1	5	2	7	3	13	24	65
5	3	LL	0	0	8	1	5	2	5	4	8	30	62
5	7	LL	0	0	8	0	2	4	1	2	3	19	40
5	9	LL	0	0	8	0	3	5	2	3	4	33	57
6	0	HL	0	0	5	1	1	1	1	0	1	8	19
6	3	HL	0	0	8	1	2	1	0	1	1	5	20
6	7	HL	0	1	23	3	8	2	1	5	2	17	63
6	9	HL	0	2	33	5	24	7	5	7	6	20	108
6	0	ML	0	0	5	1	1	1	1	1	1	4	14
6	3	ML	0	0	7	1	2	1	2	1	1	7	23
6	7	ML	0	1	17	2	7	2	1	2	7	18	58
6	9	ML	0	2	30	3	14	6	2	6	4	26	94
6	0	LL	0	0	5	1	1	1	1	1	2	4	15
6	3	LL	0	0	6	1	1	1	0	0	2	7	19
6	7	LL	0	0	6	1	1	1	0	0	4	6	20
6	9	LL	0	0	8	1	2	1	1	0	5	10	28

5

Table S5. Initial pigment ratio matrix (top, n = 94) included in the CHEMTAX analysis constructed using ratios taken from literature and a diatom (*Proboscia* sp.) isolate. Two types of Prymnesiophyceae were included to accommodate the high plasticity in pigment composition of *Phaeocystis* sp. under high light/low light and/or high/low iron conditions (DiTullio et al. 2007). Additionally, two types of diatoms were included due to the high abundances of *Pseudonitzschia* sp. and *Proboscia* sp. which both contain *Chlorophyll-c3 (Chl-c3;* unpublished data; Annett et al. 2010). The initial ratio matrix was based on Wright et al. (2009), Wright et al. (2010) and unpublished culture data for Diatoms 2. The bottom section presents the final ratios. Pigment ratios were standardised to 1 unit Chlorophyll-a (Chl-a) and pigments used in the analysis were Chl-c3, peridinin (Per), 19-butanoyloxyfucoxanthin (19-But), fucoxanthin (Fuco), neoxanthin (Neo), 19-hexanoyloxyfucoxanthin (19-Hex), alloxanthin (Allo), lutein (Lut), chlorophyll b (Chl-b) and Chl-*a*.

Initial: Class / Pigment	Chl-c3	Per	19-Buta	Fuco	Neo	19-Hex	Allo	Lut	Chl-b	Chl-*a*
Prasinophyceae	-	-	-	-	0.030	-	-	0.006	0.620	1
Chlorophyceae	-	-	-	-	0.062	-	-	0.220	0.180	1
Dinophyceae	-	1.060	-	-	-	-	-	-	-	1
Cryptophyceae	-	-	-	-	-	-	0.220	-	-	1
Prymnesiophyceae 1	0.130	-	0.120	0.080	-	0.400	-	-	-	1
Prymnesiophyceae 2	0.270	-	0.006	0.010	-	1.100	-	-	-	1
Diatoms 1	-	-	-	0.520	-	-	-	-	-	1
Diatoms 2	0.220	-	-	0.864	-	-	-	-	-	1
Final ratio's										
Prasinophyceae	-	-	-	-	0.035	-	-	0.004	0.520	1
Chlorophyceae	-	-	-	-	0.052	-	-	0.312	0.120	1
Dinophyceae	-	1.126	-	-	-	-	-	-	-	1
Cryptophyceae	-	-	-	-	-	-	0.187	-	-	1
Prymnesiophyceae 1	0.121	-	0.177	0.061	-	0.108	-	-	-	1
Prymnesiophyceae 2	0.242	-	0.004	0.009	-	1.215	-	-	-	1
Diatoms 1	-	-	-	0.671	-	-	-	-	-	1
Diatoms 2	0.712	-	-	2.339	-	-	-	-	-	1

Table S6. Average Chlorophyll-*a* (Chl-*a*) concentrations (µg L^{-1}) as determined by high performance liquid chromatography (HPLC) and chemical taxonomy (CHEMTAX) for incubation experiments (INC) 1 – 6. Abbreviations stand for: diatoms (Dia), cryptophytes (Cryp), chlorophytes (Chlor), prasinophytes (Pras), prymnesiophytes (Prym), dinoflagellates (Dino) and total chl-*a* (Total) as well as high light (HL), medium light (ML) and low light (LL) treatments at the beginning (T$_0$) and end (T$_{END}$) of each INC. Chl-*a* concentrations represent an average of triplicates apart from T$_0$ of INC 1 and 2 where the average is based on a duplicate set, collected at the beginning and end of seawater collection and used for all light levels.

INC 1	Light level	Chl-*a* total	Dia	Cryp	Chlor	Pras	Prym	Dino
T$_0$	HL	0.7	0.2	0.2	0.0	0.0	0.2	0.0
T$_{END}$	HL	11.6	10.5	0.3	0.0	0.5	0.2	0.1
T$_0$	ML	0.7	0.2	0.2	0.0	0.0	0.2	0.0
T$_{END}$	ML	15.6	12.6	0.2	0.0	0.4	2.4	0.0
T$_0$	LL	0.7	0.2	0.2	0.0	0.0	0.2	0.0
T$_{END}$	LL	1.3	0.8	0.2	0.0	0.1	0.3	0.0

INC 2	Light level	Chl-*a* total	Dia	Cryp	Chlor	Pras	Prym	Dino
T$_0$	HL	16.9	16.7	0.0	0.0	0.0	0.2	0.0
T$_{END}$	HL	14.3	14.2	0.0	0.0	0.0	0.0	0.0
T$_0$	ML	16.9	16.7	0.0	0.0	0.0	0.2	0.0
T$_{END}$	ML	18.5	18.4	0.0	0.0	0.0	0.0	0.0
T$_0$	LL	16.9	16.7	0.0	0.0	0.0	0.2	0.0
T$_{END}$	LL	31.2	31.1	0.0	0.0	0.0	0.0	0.0

INC 3	Light level	Chl-*a* total	Dia	Cryp	Chlor	Pras	Prym	Dino
T$_0$	HL	0.6	0.5	0.0	0.0	0.0	0.1	0.0
T$_{END}$	HL	0.7	0.7	0.0	0.0	0.0	0.0	0.0
T$_0$	ML	0.6	0.5	0.0	0.0	0.0	0.1	0.0
T$_{END}$	ML	1.8	1.7	0.0	0.0	0.0	0.1	0.0
T$_0$	LL	0.5	0.5	0.0	0.0	0.0	0.1	0.0
T$_{END}$	LL	2.9	2.9	0.0	0.0	0.0	0.1	0.0

INC 4	Light level	Chl-*a* total	Dia	Cryp	Chlor	Pras	Prym	Dino
T$_0$	HL	2.3	2.2	0.0	0.0	0.1	0.0	0.0
T$_{END}$	HL	1.1	1.0	0.0	0.1	0.0	0.0	0.0
T$_0$	ML	2.6	2.5	0.0	0.0	0.0	0.0	0.0
T$_{END}$	ML	2.7	2.6	0.0	0.0	0.0	0.0	0.0
T$_0$	LL	2.6	2.5	0.0	0.0	0.0	0.0	0.0
T$_{END}$	LL	5.2	4.8	0.0	0.0	0.1	0.1	0.2

INC 5	Light level	Chl-*a* total	Dia	Cryp	Chlor	Pras	Prym	Dino
T$_0$	HL	4.7	4.2	0.0	0.0	0.1	0.4	0.0
T$_{END}$	HL	2.5	2.0	0.3	0.0	0.0	0.2	0.0
T$_0$	ML	4.7	4.1	0.0	0.0	0.0	0.5	0.0
T$_{END}$	ML	4.8	4.3	0.1	0.0	0.0	0.5	0.0
T$_0$	LL	4.5	3.8	0.0	0.0	0.1	0.5	0.0
T$_{END}$	LL	8.0	7.5	0.1	0.0	0.1	0.2	0.0

INC 6	Light level	Chl-*a* total	Dia	Cryp	Chlor	Pras	Prym	Dino
T$_0$	HL	1.3	0.8	0.2	0.0	0.1	0.2	0.0
T$_{END}$	HL	4.1	3.2	0.9	0.0	0.2	0.1	0.0
T$_0$	ML	1.2	0.6	0.2	0.0	0.1	0.3	0.0
T$_{END}$	ML	8.4	7.0	0.6	0.0	0.4	0.4	0.0
T$_0$	LL	1.2	0.7	0.2	0.0	0.1	0.3	0.0
T$_{END}$	LL	2.5	1.9	0.1	0.0	0.1	0.3	0.0

5

Table S7. Carbon estimates (µg L^{-1}) converted from CHEMTAX Chl-*a* concentrations for each taxonomic group during INC 1 - 6. Abbreviations represent: Diatom (Bacillareophyceae), Cryp (Cryptophyceae), Chlor (Chlorophyceae), Pras (Prasinophyceae), Prym (Prymnesiophyceae) and Dino (dinoflagellates). Chl-C concentrations represent an average of triplicates apart from Timepoint 0 of INC 1 and 2 where the average is based on a duplicate set, collected at the beginning and end of seawater collection and used for all light levels.

INC	Light level	Timepoint	Diatom	Cryp	Chlor	Pras	Prym	Dino	Total
			C µg L^{-1}	C µg L^{-1}	C µg L^{-1}	C µg L^{-1}	C µg L^{-1}	C µg L^{-1}	C µg L^{-1}
1	HL	0	12	23.7	0.00	0.27	0.76	0.36	38
1	ML	0	12	23.7	0.00	0.27	0.76	0.36	38
1	LL	0	12	23.7	0.00	0.27	0.76	0.36	38
1	HL	10	744	12.2	0.36	5.41	0.66	4.23	767
1	ML	10	895	6.83	0.01	4.28	7.87	0.01	914
1	LL	10	36	16.9	0.00	0.69	0.88	0.96	56
2	HL	0	1182	0.75	0.05	0.01	0.72	0.03	1183
2	ML	0	1182	0.75	0.05	0.01	0.72	0.03	1183
2	LL	0	1182	0.75	0.05	0.01	0.72	0.03	1183
2	HL	10	1011	0.99	0.14	0.02	0.09	0.05	1012
2	ML	10	1305	0.98	0.38	0.03	0.09	0.05	1306
2	LL	10	2206	0.66	0.14	0.02	0.10	0.05	2210
3	HL	0	28	0.23	0.01	0.00	0.19	0.00	28
3	ML	0	28	0.28	0.01	0.00	0.19	0.01	29
3	LL	0	25	0.24	0.01	0.00	0.21	0.00	26
3	HL	9	33	0.00	0.04	0.00	0.06	0.00	33
3	ML	9	83	0.00	0.00	0.00	0.33	0.00	84
3	LL	9	146	0.37	0.01	0.00	0.25	0.01	147
4	HL	0	105	0.23	0.00	0.52	0.11	0.00	106
4	ML	0	120	0.02	0.00	0.48	0.11	0.00	121
4	LL	0	119	0.12	0.00	0.37	0.12	0.00	120
4	HL	9	48	0.00	1.41	0.00	0.19	0.00	50
4	ML	9	130	0.00	0.21	0.00	0.06	1.61	132
4	LL	9	316	0.00	0.00	0.71	0.21	12.57	329
5	HL	0	295	1.64	0.09	0.85	1.44	0.08	299
5	ML	0	292	1.28	0.07	0.48	1.58	0.06	295
5	LL	0	267	1.36	0.06	1.26	1.82	0.06	271
5	HL	9	123	14.1	0.12	0.01	0.65	0.01	138
5	ML	9	205	10.7	0.15	0.02	1.81	0.04	217
5	LL	9	533	3.2	0.19	1.10	0.75	0.15	539
6	HL	0	37	23.9	0.00	0.55	0.83	0.01	62
6	ML	0	29	21.4	0.00	0.50	1.00	0.00	52
6	LL	0	32	19.8	0.00	0.54	0.86	0.01	53
6	HL	9	226	35.3	0.04	1.66	0.31	0.00	254
6	ML	9	448	32.3	0.00	3.61	1.39	0.00	485
6	LL	9	91	10.9	0.04	1.42	0.98	0.04	105

Table S8. Table of relative contributions to total chlorophyll-*a* of each taxonomic group (separated by CHEMTAX) at the start (Exp. T_0) of each experimental incubation (INC 1-6). Taxonomic groups are identified as Bacillariophyceae (diatom), Cryptophyceae (Cryp), Chlorophyceae (Chlor), Prasinophyceae (Pras), Prymnesiophyceae (Prym) and dinoflagellates (Dino).

Exp. T_0	Diatom	Cryp	Chlor	Pras	Prym	Dino
INC 1	32	33	0	4	31	1
INC 2	99	0	0	0	1	0
INC 3	89	0	0	0	10	0
INC 4	97	0	0	2	1	0
INC 5	87	1	0	2	10	0
INC 6	56	18	0	4	22	0

Table S9. Table of relative phytoplankton abundance (% of total) at the start (Exp. T_0) of each experimental incubation (INC 1-6) for phytoplankton groups Phyto I-X.

5

Exp. T_0	Phyto I	Phyto II	Phyto III	Phyto IV	Phyto V	Phyto VI	Phyto VII	Phyto VIII	Phyto IX	Phyto X
INC 1	0	5	18	9	7	56	1	2	2	0
INC 2	0	1	12	1	2	14	1	1	67	0
INC 3	2	5	59	2	26	2	3	0	1	1
INC 4	22	4	30	0	16	1	3	4	15	3
INC 5	2	10	59	2	14	4	4	2	2	1
INC 6	1	11	69	7	6	3	1	0	0	0

Table S10. Net growth rates (μ_{NET}, d^{-1}) of Phyto I to X and total phytoplankton abundance (FCM-ab), and of carbon (FCM-C) during Season 1 in INC 1 and 2. Note: N/A represents missing data due to one or more zero counts in each set of triplicates.

INC	Light level	Time period	Phyto I	Phyto II	Phyto III	Phyto IV	Phyto V	Phyto VI	Phyto VII	Phyto VIII	Phyto IX	Phyto X	FCM -ab	FCM -C
			d^{-1}	d^{-1}	d^{-1}	d^{-1}	d^{-1}	d^{-1}	d^{-1}	d^{-1}	d^{-1}	d^{-1}	d^{-1}	d^{-1}
1	HL	T_{0-3}	0.25	0.29	-0.18	-0.07	0.13	-0.27	-0.05	0.00	0.39	0.00	-0.06	0.11
1	HL	T_{3-7}	0.01	0.01	0.02	-0.06	0.23	0.00	0.39	0.13	0.36	-0.14	0.10	0.33
1	HL	T_{7-10}	-0.60	0.27	0.40	0.06	0.32	0.44	0.05	0.27	0.59	0.23	0.40	0.49
1	HL	T_{0-END}	NA	0.22	0.18	0.08	0.27	0.14	0.20	0.12	0.48	-0.09	0.21	0.36
1	ML	T_{0-3}	-0.44	0.43	0.36	0.04	0.28	0.30	0.31	0.28	0.36	N/A	0.31	0.33
1	ML	T_{3-7}	0.10	0.16	0.23	-0.12	0.23	0.19	0.00	0.24	0.45	0.24	0.20	0.31
1	ML	T_{7-10}	0.46	0.17	0.21	0.09	0.03	0.33	0.10	0.10	0.46	0.11	0.29	0.39
1	ML	T_{0-END}	0.13	0.23	0.25	-0.03	0.14	0.27	0.12	0.22	0.42	N/A	0.26	0.33
1	LL	T_{0-3}	-0.21	0.08	-0.01	-0.03	-0.02	-0.03	-0.23	0.06	0.24	N/A	-0.01	0.08
1	LL	T_{3-7}	N/A	-0.16	-0.14	-0.17	-0.01	-0.10	0.18	0.13	0.12	-0.14	-0.08	0.03
1	LL	T_{7-10}	N/A	-0.05	-0.08	0.07	0.20	0.09	0.52	0.10	0.09	0.18	0.09	0.11
1	LL	T_{0-END}	-0.05	-0.06	-0.08	-0.05	0.05	-0.02	0.16	0.10	0.14	N/A	-0.01	0.07
2	HL	T_{0-3}	N/A	-0.27	-0.08	-0.11	-0.03	0.28	0.05	0.09	0.24	1.02	0.22	0.36
2	HL	T_{3-7}	N/A	0.34	0.00	-0.06	-0.01	-0.05	0.00	-0.03	0.03	0.14	0.02	0.07
2	HL	T_{7-10}	0.12	-0.12	-0.08	0.01	0.02	-0.20	-0.01	-0.02	-0.01	0.03	-0.02	0.02
2	HL	T_{0-END}	N/A	0.02	-0.05	-0.05	-0.01	0.01	0.01	0.01	0.08	0.37	0.07	0.14
2	ML	T_{0-3}	-0.07	-0.18	0.11	-0.07	0.07	0.21	0.07	0.08	0.24	1.14	0.23	0.35
2	ML	T_{3-7}	0.00	0.17	-0.12	-0.12	-0.10	0.00	0.06	0.12	0.01	-0.07	0.00	-0.01
2	ML	T_{7-10}	N/A	-0.29	-0.06	-0.69	-0.02	-0.19	0.02	-0.02	-0.01	0.43	0.01	0.14
2	ML	T_{0-END}	N/A	-0.07	-0.03	-0.28	-0.02	0.01	0.05	0.07	0.07	0.44	0.07	0.14
2	LL	T_{0-3}	-0.27	0.09	0.20	-0.07	0.24	0.05	0.33	0.17	0.32	-0.03	0.26	0.31
2	LL	T_{3-7}	N/A	-0.07	-0.02	-0.08	-0.02	-0.01	0.05	0.05	0.11	0.19	0.08	0.11
2	LL	T_{7-10}	N/A	-0.24	-0.19	-0.10	-0.13	-0.12	-0.10	0.07	-0.01	0.18	-0.03	-0.01
2	LL	T_{0-END}	N/A	-0.07	-0.01	-0.08	0.03	-0.02	0.09	0.09	0.14	0.12	0.10	0.13

Table S11. Net growth rates (μ_{NET}, d^{-1}) of Phyto I to X as well as total phytoplankton abundance (FCM-ab), and of carbon (FCM-C) during Season 2 in INC 3 - 6. Net growth rates represent an average of triplicates.

INC	Light level	Time period	Phyto I	Phyto II	Phyto III	Phyto IV	Phyto V	Phyto VI	Phyto VII	Phyto VIII	Phyto IX	Phyto X	FCM -ab	FCM -C
			d^{-1}	d^{-1}	d^{-1}	d^{-1}	d^{-1}	d^{-1}	d^{-1}	d^{-1}	d^{-1}	d^{-1}	d^{-1}	d^{-1}
3	HL	T_{0-3}	-0.14	-0.17	0.10	-0.08	0.34	-0.33	-0.16	0.14	-0.09	0.35	0.16	0.27
3	HL	T_{3-7}	0.42	0.05	0.17	0.19	0.18	0.50	-0.02	1.04	0.74	0.82	0.24	0.73
3	HL	T_{7-9}	-0.10	0.45	-0.24	-0.31	-0.28	-0.08	0.15	-0.44	0.17	-0.42	-0.24	-0.38
3	HL	T_{0-END}	0.16	0.07	0.05	-0.04	0.10	0.11	-0.05	0.44	0.31	0.40	0.09	0.33
3	ML	T_{0-3}	-0.24	-0.17	0.05	0.00	0.34	-0.33	-0.08	0.39	0.21	0.31	0.14	0.26
3	ML	T_{3-7}	0.14	0.06	0.18	0.05	0.17	0.48	-0.24	0.74	0.45	0.62	0.20	0.53
3	ML	T_{7-9}	0.23	0.41	-0.10	-0.01	-0.04	0.02	0.17	0.25	0.43	0.37	0.02	0.35
3	ML	T_{0-END}	0.03	0.06	0.08	0.02	0.18	0.11	-0.10	0.51	0.37	0.46	0.14	0.40
3	LL	T_{0-3}	-0.39	0.06	-0.01	-0.06	0.12	0.07	0.00	-0.37	0.09	0.07	0.03	0.06
3	LL	T_{3-7}	-0.22	-0.07	0.03	0.01	0.11	-0.22	-0.13	0.25	-0.13	-0.12	0.05	-0.03
3	LL	T_{7-9}	0.07	-0.15	-0.11	-0.03	0.00	0.37	0.32	0.49	0.02	0.06	-0.04	0.03
3	LL	T_{0-END}	-0.21	-0.04	-0.01	-0.02	0.09	0.01	0.01	0.13	-0.02	-0.02	0.02	0.01
4	HL	T_{0-3}	0.08	0.19	0.06	0.03	-0.10	0.29	0.42	0.46	-0.08	-0.03	0.08	0.01
4	HL	T_{3-7}	0.03	0.14	0.19	-0.03	0.54	0.21	0.49	0.23	0.51	0.54	0.31	0.49
4	HL	T_{7-9}	-0.42	0.15	-0.03	0.15	-0.20	0.26	-0.34	-0.10	-0.34	-0.67	-0.18	-0.44
4	HL	T_{0-END}	-0.09	0.19	0.09	0.01	0.16	0.30	0.33	0.27	0.12	0.05	0.12	0.11
4	ML	T_{0-3}	0.13	0.23	0.13	-0.05	0.04	0.00	-0.11	0.27	-0.10	0.19	0.10	0.11
4	ML	T_{3-7}	-0.21	0.18	0.19	-0.08	0.27	0.43	0.53	0.46	0.51	0.54	0.29	0.51
4	ML	T_{7-9}	-0.50	-0.23	-0.31	0.06	0.31	0.27	-0.73	0.31	0.19	-0.11	0.05	0.00
4	ML	T_{0-END}	-0.16	0.10	0.06	-0.05	0.20	0.25	0.03	0.37	0.24	0.28	0.18	0.26
4	LL	T_{0-3}	0.02	0.04	0.07	-0.07	-0.02	0.11	0.00	-0.10	0.15	0.06	0.06	0.10
4	LL	T_{3-7}	-0.22	-0.10	0.00	-0.14	0.03	-0.05	0.00	0.26	-0.07	0.04	-0.04	-0.01
4	LL	T_{7-9}	-0.28	0.50	-0.11	0.30	0.18	-0.09	-0.10	0.03	-0.04	-0.66	-0.02	-0.24
4	LL	T_{0-END}	-0.15	0.08	0.00	-0.02	0.05	0.00	-0.02	0.09	0.01	-0.11	0.00	-0.02
5	HL	T_{0-3}	0.17	0.21	0.08	-0.04	-0.09	0.25	-0.34	0.17	0.05	-0.28	0.08	-0.06
5	HL	T_{3-7}	0.15	0.27	0.20	0.19	0.20	0.28	-0.18	0.22	0.08	-0.15	0.21	0.11
5	HL	T_{7-9}	0.12	0.23	0.16	-0.07	0.14	0.21	0.56	0.19	0.20	0.39	0.18	0.21
5	HL	T_{0-END}	0.15	0.24	0.15	0.05	0.09	0.25	-0.07	0.20	0.10	-0.07	0.16	0.07
5	ML	T_{0-3}	0.07	0.28	0.11	-0.15	-0.04	0.21	-0.51	0.31	0.19	0.03	0.11	0.07
5	ML	T_{3-7}	-0.17	0.23	0.17	0.15	0.15	0.17	-0.05	0.24	0.20	-0.09	0.18	0.11
5	ML	T_{7-9}	0.36	0.12	0.07	-0.05	0.15	0.28	0.60	0.12	0.10	-0.12	0.11	0.09
5	ML	T_{0-END}	0.03	0.22	0.13	0.01	0.09	0.21	-0.06	0.24	0.18	-0.06	0.14	0.09
5	LL	T_{0-3}	-0.04	-0.13	-0.07	-0.07	0.01	0.04	-0.17	0.01	-0.19	0.17	-0.06	0.00
5	LL	T_{3-7}	-0.12	0.03	0.02	-0.11	-0.20	0.22	-0.38	-0.16	-0.23	-0.14	-0.01	-0.11
5	LL	T_{7-9}	0.11	-0.09	0.00	-0.10	0.08	0.05	0.30	0.21	0.08	0.27	0.01	0.17
5	LL	T_{0-END}	-0.05	-0.05	-0.02	-0.12	-0.08	0.12	-0.15	-0.01	-0.15	0.05	-0.02	-0.01
6	HL	T_{0-3}	0.25	0.16	0.13	0.10	0.20	0.03	-0.13	0.22	-0.16	-0.18	0.13	0.01
6	HL	T_{3-7}	0.30	0.39	0.27	0.18	0.31	0.26	0.19	0.45	0.21	0.31	0.28	0.29
6	HL	T_{7-9}	0.11	0.26	0.17	0.22	0.53	0.59	0.81	0.16	0.48	0.13	0.25	0.27
6	HL	T_{0-END}	0.24	0.28	0.20	0.16	0.32	0.26	0.22	0.31	0.15	0.11	0.23	0.19
6	ML	T_{0-3}	0.23	0.20	0.13	0.08	0.19	0.18	0.35	0.16	0.07	0.22	0.15	0.17
6	ML	T_{3-7}	0.23	0.34	0.21	0.15	0.33	0.17	-0.01	0.15	0.41	0.24	0.24	0.23
6	ML	T_{7-9}	0.09	0.27	0.28	0.14	0.32	0.48	0.25	0.68	-0.26	0.16	0.29	0.25
6	ML	T_{0-END}	0.20	0.28	0.20	0.13	0.28	0.24	0.17	0.27	0.15	0.22	0.22	0.21
6	LL	T_{0-3}	0.15	-0.06	0.07	0.09	0.02	0.01	-0.19	-0.10	0.11	0.13	0.05	0.08
6	LL	T_{3-7}	0.15	0.02	0.00	-0.03	0.05	0.05	0.04	0.04	0.16	-0.02	0.01	0.01
6	LL	T_{7-9}	0.25	0.15	0.12	-0.04	0.15	0.26	0.07	-0.08	0.08	0.31	0.13	0.17
6	LL	T_{0-END}	0.17	0.02	0.05	0.01	0.06	0.08	-0.03	-0.04	0.12	0.10	0.05	0.07

5

Table S12. Carbon net growth rates (C-μ_{NET} d^{-1}), from T$_0$ – T$_{END}$, converted from CHEMTAX Chl-a concentrations for each taxonomic group during INC 1 - 6. Abbreviations represent: Diatom (Bacillareophyceae), Cryp (Cryptophyceae), Chlor (Chlorophyceae), Pras (Prasinophyceae), Prym (Prymnesiophyceae) and Dino (dinoflagellates). Note: where NA is stated, one or more zeros prevented the estimation of net growth rates.

INC	Light level	Diatom	Cryp	Chlor	Pras	Prym	Dino	Total
		C μ_{NET} (d^{-1})						C μ_{NET} (d^{-1})
1	HL	0.41	-0.17	NA	0.30	-0.04	0.04	0.30
1	ML	0.43	-0.09	NA	0.28	0.23	-0.26	0.32
1	LL	0.11	-0.04	NA	0.09	0.01	0.09	0.04
2	HL	-0.02	0.03	0.08	0.05	-0.21	0.03	-0.02
2	ML	0.01	0.02	0.20	0.09	-0.21	0.03	0.01
2	LL	0.06	0.08	0.09	0.04	-0.22	0.02	0.06
3	HL	0.01	NA	0.13	NA	-0.15	NA	0.00
3	ML	0.11	NA	NA	NA	0.06	NA	0.11
3	LL	0.20	0.10	0.10	0.10	0.02	0.10	0.19
4	HL	-0.12	NA	NA	NA	-0.03	NA	-0.11
4	ML	-0.01	NA	NA	NA	-0.08	NA	-0.01
4	LL	0.10	NA	NA	0.07	0.07	0.99	0.11
5	HL	-0.10	0.23	0.04	-0.49	-0.09	-0.21	-0.09
5	ML	-0.04	0.23	0.09	-0.18	-0.03	-0.05	-0.04
5	LL	0.08	0.10	0.13	-0.02	-0.10	0.10	0.08
6	HL	0.20	-0.00	NA	0.12	-0.11	0.03	0.15
6	ML	0.30	0.04	NA	0.22	0.04	NA	0.25
6	LL	0.12	-0.07	0.75	0.11	0.02	0.19	0.08

Table S13. Pigment concentrations corrected for cell volume (fg µm^{-3}) for INC 1 – 6. All time zero replicates were combined (ALL; INC 1 and 2 $n = 2$, INC 3 – 6 $n = 9$) as well as replicates for each light level at the end ($n = 3$). Abbreviations stand for chlorophyll-c2 (Chl-c2), fucoxanthin (Fuco), diadinoxanthin + diatoxanthin (Dd+Dt), chlorophyll-*a* (Chl-*a*) and all pigments quantified (Total) i.e. including additional pigments chlorophyll-c3, peridinine, butanoyloxyfucoxanthin, neoxanthin, prasinoxanthin, violaxanthin, hexa fucoxanthin, alloxanthin, zeaxanthin, lutein, chlorophyll-b, divinyl chlorophyll-*a*, α-caroteen and ß-caroteen.

INC	Light level	Time (days)	Chl-c2 fg µm^{-3}	Fuco fg µm^{-3}	Dd+Dt fg µm^{-3}	Chl-*a* fg µm^{-3}	Total fg µm^{-3}
1	ALL	0	0.74	2.09	0.49	6.16	11.36
1	HL	10	0.30	1.61	0.44	3.10	5.71
1	ML	10	0.52	2.76	0.30	4.91	8.94
1	LL	10	0.80	3.38	0.33	5.66	11.50
2	ALL	0	0.51	4.00	0.25	6.06	11.14
2	H1	10	0.06	0.77	0.72	1.23	2.83
2	C1	10	0.10	0.90	0.32	1.43	2.80
2	L1	10	0.32	2.31	0.23	3.58	6.57
3	ALL	0	0.34	1.01	1.04	2.40	5.22
3	HL	9	0.89	0.78	2.81	0.11	4.74
3	ML	9	1.36	0.76	1.14	0.20	3.65
3	LL	9	2.98	7.35	1.15	10.70	23.36
4	ALL	0	1.03	2.43	0.76	2.77	7.47
4	HL	9	1.27	1.45	5.76	0.41	9.12
4	ML	9	1.01	1.57	1.32	0.60	4.65
4	LL	9	2.69	6.73	1.13	6.89	18.79
5	ALL	0	2.93	8.71	0.76	12.27	28.22
5	HL	9	0.71	1.96	2.54	2.77	8.58
5	ML	9	2.01	4.45	1.31	5.65	14.70
5	LL	9	6.43	20.12	1.75	28.13	63.67
6	ALL	0	2.68	10.13	1.89	16.24	36.60
6	HL	9	2.73	5.68	6.53	8.03	24.44
6	ML	9	8.45	22.17	5.89	19.01	61.91
6	LL	9	3.76	11.11	1.16	18.15	39.62

5

Chapter 6

Characterization and temperature dependence of Arctic *Micromonas polaris* viruses

Characterization and temperature dependence of Arctic *Micromonas polaris* viruses.

Douwe S. Maat[1,a], Tristan E.G. Biggs[1,a], Claire Evans[1,2], Judith D.L. van Bleijswijk[1], Nicole N. van der Wel[3], Corina P.D. Brussaard[1,]

[a] **These authors contributed equally to this work**

[1]Department of Marine Microbiology and Biogeochemistry, NIOZ Royal Netherlands Institute for Sea Research, and University of Utrecht, PO Box 59, 1790 AB Den Burg, Texel, The Netherlands;
[2]Present address: Ocean Biogeochemistry & Ecosystems Research Group, National Oceanography Centre, Southampton, European Way, Southampton SO14 3ZH, United Kingdom;
[3]Electron Microscopy Center Amsterdam, Department of Cell Biology and Histology, Academic Medical Center, University of Amsterdam, Meibergdreef 15, 1105 AZ Amsterdam, The Netherlands;

Abstract

Global climate change-induced warming of the Artic seas is predicted to shift the phytoplankton community towards dominance of smaller-sized species due to global warming. Yet, little is known about their viral mortality agents despite the ecological importance of viruses regulating phytoplankton host dynamics and diversity. Here we report the isolation and basic characterization of four prasinoviruses infectious to the common Arctic picophytoplankter *Micromonas*. We furthermore assessed how temperature influenced viral infectivity and production. Phylogenetic analysis indicated that the putative double-stranded DNA (dsDNA) *Micromonas polaris* viruses (MpoVs) are prasinoviruses (Phycodnaviridae) of approximately 120 nm in particle size. One MpoV showed intrinsic differences to the other three viruses, i.e., larger genome size (205 $\pm$ 2 vs. 191 $\pm$ 3 Kb), broader host range, and longer latent period (39 vs. 18 h). Temperature increase shortened the latent periods (up to 50%), increased the burst size (up to 40%), and affected viral infectivity. However, the variability in response to temperature was high for the different viruses and host strains assessed, likely affecting the Arctic picoeukaryote community structure both in the short term (seasonal cycles) and long term (global warming).

6

Introduction

Marine phycovirology, i.e., the study of viruses infecting marine eukaryotic algae, started with the lytic viruses infectious to the picophytoplankter *Micromonas pusilla* (Mayer and Taylor 1979; Waters and Chan 1982; Cottrell and Suttle 1991, 1995; Suttle and Cottrell 1995). The genus *Micromonas* (class Mamiellophyceae) is ubiquitous, occurring from tropical to polar regions, and is readily infected by viruses (Cottrell and Suttle 1991; Not et al. 2004; Foulon et al. 2008; Worden et al. 2009; Martínez Martínez et al. 2015). The majority of *Micromonas* virus isolates belong to the double-stranded DNA (dsDNA) prasinoviruses (Cottrell and Suttle 1991, 1995; Suttle and Cottrell 1995; Martínez Martínez et al. 2015), although a dsRNA *Micromonas* virus has also been reported (Brussaard et al. 2004; Attoui et al. 2006). The prasinoviruses are considered the most abundant group of marine phycodnaviruses (Hingamp et al. 2013) and virus abundances show synchrony with their hosts' temporal dynamics consistent with infection (Zingone et al. 1999; Baudoux et al. 2015).

Micromonas is a globally important prasinophyte, which typically dominates the picophytoplankton fraction in marine Arctic waters (Not et al. 2005; Lovejoy et al. 2007; Balzano et al. 2012b, a; Kilias et al. 2013, 2014; Metfies et al. 2016; Joli et al. 2017). Previous studies have shown that Arctic *Micromonas* forms a separate ecotype from lower latitude strains (Lovejoy et al. 2007; Balzano et al. 2012a) adapted to grow at temperatures between 0 and 12 °C (with an optimum around 6–8 °C; Lovejoy et al. 2007). Considering Arctic sea surface temperature over the year to be in the range of −1 to a maximum 7 °C (Loeng 2005; Richter-Menge and Mathis 2016; Timmermans 2016) and steadily increasing as a result of global warming (0.03–0.05 °C per year over the 21st century; Timmermans 2016), the *Micromonas* polar ecotype species (tentatively named *M. polaris*; Simon et al. 2017) can be expected to belong to the picophytoplankton predicted to benefit from a warming Arctic region (Loeng 2005; Li et al. 2009, 2013; Coello-Camba et al. 2015). Despite this predicted increase in abundance and relative share of picophytoplankton in the changing Arctic Ocean, it is still unclear how the viruses infecting the picophytoplankton are affected by

changes in temperature. Little is known about Arctic phycoviruses in general, and to our knowledge, no viruses infectious to Arctic *Micromonas* species have yet been brought into culture (Brussaard et al. 2013; Lara et al. 2013; Payet and Suttle 2014).

Changes in an environmental variable, such as temperature, may directly affect virus infectivity and/or more indirectly impact virus proliferation due to alterations in the metabolic activity of   the host (Mojica and Brussaard 2014). Thus far the thermal stability of psychrophilic marine virus-host interactions has only been assessed for several phage-bacterium systems (Olsen 1967; Borriss et al. 2003), despite the potential for special physiological adaptations by cold-adapted hosts and viruses (D'Amico et al. 2006; Wells 2008). It is likely that different viruses infecting the same host strain have distinct responses to shifting environmental factors and therefore environmental change may drive virus selection and host population dynamics. Nagasaki and Yamaguchi (1998) found that the temperature ranges for successful infection were different for two virus strains infecting the raphidophyte *Heterosigma akashiwo* and that the host strain sensitivity to infection varied according to the temperature. Furthermore, temperature regulates growth by controlling cellular metabolic activity (Toseland et al. 2013), which has been proportionally related to latent period length and burst sizes for *Vibrio natriegens* phages (Zachary 1978). Recently, Demeroy and colleagues (2017) demonstrated that temperature-regulated growth rates of *Micromonas* strains that originated from the English Channel were responsible for shortened latent periods and increased viral burst sizes upon infection. Ongoing change in the Arctic necessitates a better understanding of how Arctic phycoviruses are affected by temperature.

Here we report on the isolation of four *Micromonas* viruses from the Arctic. In addition to determining their viral characteristics (capsid morphology and size, genome type and size, latent period, phylogeny, host range, burst size, virion inactivation upon chloroform and freezing treatment), we investigated the impact of temperature change on virus infectivity and production. We hypothesize that (i) viral infectivity will increase with temperature, and (ii) increasing temperatures will stimulate virus production (shorter latent periods and higher burst sizes). For testing

6

the latter hypothesis, we performed one-step virus growth experiments at a range of temperatures representative of the extremes over the polar growth season (0.5–7 °C) (Richter-Menge and Mathis 2016).

Materials and Methods

Isolation and Culturing

The Micromonas host TX-01 was isolated from Kongsfjorden, Spitsbergen, Norway (78°55.073'N, 12°24.646'E) on the 19 April 2014, by making an end-point, 10-fold dilution series of fjord water in F/4 medium (based on Whatman glass microfiber GF/F filtered, autoclaved fjord water; Guillard and Ryther 1962). The other *Micromonas* species and strains used were obtained from the Bigelow National Center for Marine Algae and Microbiota (culture collection of marine phytoplankton (CCMP) coded strains; West Boothbay Harbor, ME, USA), the Culture Collection Marine Research Center of Göteborg University (LAC38; Göteborg, Sweden), and the Roscoff Culture Collection (RCC coded strains; Roscoff, France).

Micromonas TX-01 was classified based on its position in a Maximum-Likelihood dendrogram (Fig. S1) of 18S rRNA sequences (1574 valid columns) of *Micromonas* strains with clade designations A–E after Šlapeta et al. (2006) and Ea after Lovejoy et al. (2007). Analysis was done using Randomized Axelerated Maximum Likelihood (RAxML) (Stamatakis 2014) implemented in the ARB software package (Ludwig et al. 2004). *Micromonas* TX-01 (1051 Bp) was added to the tree using ARB Parsimony. Neighbor-Joining analysis gave a similar tree topology, whereby the tree was rooted using *Mantoniella squamata*. Primers 328F and 329R were used to amplify a part of the small subunit (SSU) ribosomal RNA gene of the *Micromonas* host according to Romari and Vaulot (2004). The same primers plus internal primer 528F were used for sequencing. Isolate TX-01 clustered in clade Ea which is composed of only Arctic clones (Lovejoy et al. 2007). Recently it has become clear that the genus *Micromonas* is not made up by solely *M. pusilla,* but instead consists of distinct genetic lineages and new species are described (Worden et al. 2009; van Baren et al. 2016; Simon et al. 2017). The strains in the Ea cluster are recently described as a new species of

Micromonas, i.e., *M. polaris* (Simon et al. 2017), and with pending approval we consider TX-01 to be a putative *M. polaris* strain.

Micromonas species and strains (Table 1) were cultured in Mix-TX medium, a 1:1 mixture of f/2 medium (Guillard and Ryther 1962) and artificial seawater (Harrison et al. 1980) enriched with Tris-HCl and Na_2SeO_3 (Cottrell and Suttle 1991), under a light:dark cycle of 16:8 h. Light was supplied by 18W/965 OSRAM daylight spectrum fluorescent tubes (München, Germany) at intensities of 70–90 µmol quanta $m^{-2} s^{-1}$. Cultivation temperatures for the different *Micromonas* species and strains used for testing the host range of the virus isolates are listed in Table 1. The standard temperature at which the *M. polaris* strains used for the virus infection experiments were cultured was 3 ℃. For investigating the effect of temperature on the viral growth cycle and virus infectivity, the host strains had been acclimated to various other temperatures (0.5, 2.5, 3.5, and 7 ℃ for TX-01; and 7 ℃ for RCC2257 and RCC2258) for several months prior to experimentation. Although the host strain LAC38 is not, the TX-01 and the RCC strains are obligate low-temperature strains, as they did not grow at 15 ℃. Four virus strains were isolated from the waters around Spitsbergen and were named MpoV as they infect Arctic *M. polaris* (Simon et al. 2017). MpoV-44T was isolated during winter in 2006 using *Micromonas commoda* strain LAC38 (formerly known as *M. pusilla*; van Baren et al. 2016), and MpoV-45T

to 47T during spring and summer in 2014 and 2015, respectively, using *M. polaris* TX-01 (Table 2). The reason that a low-temperature acclimated LAC38 culture was used for the isolation of MpoV-44T was due to the lack of available Arctic *Micromonas* host strains at the time of isolation. The lytic virus isolate MpoV-44T was isolated by adding whole seawater (15% *v/v*) to an exponentially growing culture of *M. commoda* LAC38 (acclimated to grow at 3 °C), and MpoV-45T, 46T, and 47T by adding 25% *v/v* 0.2 µm filtered (polyethersulfone membrane filter; Sartopore Midicap, Sartorius A.G. Goettingen, Germany) seawater to exponentially growing *M. polaris* TX-01 (standard culturing at 3 °C, but isolation was performed at 4 °C).

6

Table 1**.** Lytic activity of the four *Micromonas polaris* viruses (MpoV) against different *Micromonas* species and strains. Columns show from left to right: host strain code, origin of isolation, *Micromonas* species, culturing temperature, and the MpoV strain names. Grey cells mean that the virus from the column is able to infect and lyse the host from the row.
BB stands for Baffin Bay, BzS for Barents Sea, BS for Beaufort Sea, EC for English Channel, GS for Greenland Sea, KF for Kongsfjorden Spitsbergen and OFN for Oslofjord Norway.
[1] formerly known as *M. pusilla*; (van Baren et al. 2016), * original CCMP1545.

Host code	Origin	*Micromonas*	Culture temp.	Lytic activity against *Micromonas*			
				MpoV-44T	MpoV-45T	MpoV-46T	MpoV-47T
TX-01	KF (2014)	*M. polaris*	3 °C	■	■	■	■
LAC 38	OFN (1998)	*M. commoda*[1]	3 °C	■			
LAC 38	OFN (1998)	*M. commoda*[1]	15 °C	■			
CCMP 1545	EC (1950)	*M. pusilla*	15 °C	■			
CCMP 2099	BB (1998)	*Micromonas sp.*	3 °C	■		■	■
RCC 461	EC (2001)	*M. pusilla*	15 °C	■			
RCC 834*	EC (1950)	*M. pusilla*	20 °C	■			
RCC 2242	BzS (2009)	*M. polaris*	3 °C		■		
RCC 2246	BS (2009)	*M. polaris*	3 °C	■	■		
RCC 2257	BS (2009)	*M. polaris*	3 °C	■	■		
RCC 2258	BS (2009)	*M. polaris*	3 °C	■	■		
RCC 2306	BS (2009)	*M. polaris*	3 °C	■	■		
RCC 4298	GS (2014)	*M. polaris*	3 °C	■	■		
RCC 4778	GS (2014)	*M. polaris*	3 °C	■		■	
RCC 4779	GS (2014)	*M. polaris*	3 °C	■		■	

MpoV-46T was the only one isolated from Storfjorden; the others came from Kongsfjorden (Table 2). Clearing of the infected algal cultures as compared to the non-infected control cultures was indicative of lysis. The lytic agents were confirmed as biological as the obtained lysates could be successfully propagated when 0.2 µm filtered, but not when autoclaved. The lysates were made clonal by end-point dilution (10-fold dilutions) and were maintained by regularly infecting exponentially growing host cultures with 10% *v/v* earlier produced lysates.

Table 2. Overview of the origin and basic characterization of the Arctic double-stranded DNA (dsDNA) virus isolates (MpoV-44T, 45T, 46T, and 47T) infecting *Micromonas*. Isolation coordinates Spitsbergen: Kongsfjorden 78°56'28.55" N, 12°0'2.50" E, Storfjorden: 77°37'35.26" N, 20°46'3.74" E. *Tested on *M. polaris* TX-01 at 3 °C.

MpoV strain	Geographical origin Spitsbergen	Date of Isolation	Host strain of isolation	Isolation temperature (°C)	Genome size (Kbp)	Lipid membrane	Latent period (h)*	Burst size (viruses cell^{-1})*
44T	Kongsfjorden	Dec 2006	LAC38	3	205 ±2	+	30 - 51	267 ±67
45T	Kongsfjorden	April 2014	TX-01	4	191 ±2	+	16 - 24	296 ±26
46T	Storfjorden	Aug 2015	TX-01	4	192 ±3	+	16 - 24	233 ±7
47T	Kongsfjorden	June 2014	TX-01	4	190 ±6	+	16 - 24	256 ±13

Virus Growth Characteristics

To obtain (comparative) information about the latent period and viral burst size of the four MpoVs isolated, viral growth experiments were performed in triplicate at 3 °C in 100 mL Erlenmeyer flasks with an exponentially growing algal host culture of TX-01 and freshly made 0.2 µm filtered (polyethersulfone membrane filter; Sartopore Midicap, Sartorius A.G. Goettingen, Germany) viral lysates. Culture conditions were as described above for host culturing. The virus to host ratio was 10–60:1 (on average 25 ± 12), at all times sufficient to allow one-step viral growth curves. The host strain TX-01 was chosen as a model host system because it was indigenous to this Arctic region and isolated together with three of the four new MpoVs. Growth medium equal to the volume of the lysate was added to non-infected control cultures (in triplicate). Host cell and viral abundances were sampled every 6–24 h post infection (p.i.) at in situ temperatures. Flow cytometry was used to enumerate algae in unpreserved samples, which were kept chilled until analysis whereas samples for virus enumeration were fixed immediately after sampling.

Algal samples were counted using a Becton Dickinson (Becton Dickinson, Franklin lakes, NJ, USA) FACSCalibur benchtop flow cytometer (equipped with a 488 nm argon laser), with the trigger set on red chlorophyll autofluorescence (Marie et al. 1999). Viral abundances were determined on fixed samples (final concentration 0.5% glutaraldehyde, EM-grade; Sigma-Aldrich, St. Louis, MO, USA) that were

6

snap-frozen in liquid nitrogen and stored at −80 °C until analysis. Thawed virus samples were diluted in TE buffer (10 mM Tris-Base, 1 mM EDTA, pH 8.0), stained with the nucleic acid-specific green fluorescent dye SYBR Green-I (Invitrogen, Thermo Fisher, Waltham, MA, USA) and analyzed according to Brussaard (2004). *Micromonas* virus clusters were discriminated by a higher green fluorescence (similar to Brussaard 2004, and Martínez Martínez et al. 2015).

Host Range

A range of *Micromonas* species and *M. polaris* strains were tested for susceptibility to infection by the four MpoVs (Table 1). Five hundred microliters of viral lysate was added to 4.5 mL of exponentially growing host, after which the lysis of the culture was monitored by visual inspection (clearing of the culture compared to non-infected control cultures). Cultures which had not lysed after 3 weeks were considered resistant to the lytic Arctic MpoVs. Lysed cultures were screened for virus production using flow cytometry.

Ultrastructure Analysis by Transmission Electron Microscopy (TEM)

For ultrastructural analysis by TEM, thin sectioned samples were prepared. Briefly, exponentially growing algal cells of *M. polaris* RCC2258 were infected with the respective virus, after which samples (3–6 tubes of 15 mL per sampling point) were taken at several time points within the latent period. Samples were prefixed with glutaraldehyde (EM-grade; 0.5% final concentration) for 30 min on ice. Algal cells were concentrated by low-speed centrifugation ($3200\times g$, 10 min, 4 °C), after which the supernatant was decanted and the pellets were transferred to 1.5 mL Eppendorf tubes (three per tube) using a Pasteur pipet. These samples were further concentrated by centrifugation ($3200\times g$, 10 min), followed by the transfer of two of the pellets into one Eppendorf tube and another round of centrifugation ($3200\times g$, 10 min). Finally, these samples were fixed with glutaraldehyde (EM-grade; 2% final concentration) in 1 mL citrate-phosphate buffer (0.1 M $Na_2HPO_4\cdot12\ H_2O$, 9.7 mM citric acid, pH 7.2) containing 2.5 mM $CaCl_2$ on ice.

After fixation, the algae were washed in distilled water, osmicated for 60 min in 1% OsO_4 in water, and washed again in distilled water with centrifugation steps in between to spin down the algae. After the last spin down, the supernatant was removed and the algae were re-suspended in the remaining volume. An equal volume of 12% gelatin was added to the algal sample and centrifuged again to a non-compact pellet. The gelatin was solidified on ice and after 20 min a fixative (2% glutaraldehyde) was added to let the gelatin fixate overnight. The gelatin containing the algae was cut into small blocks of 1–2 mm^2 and dehydrated through a series of ethanols (70%, 80%, 90%, 96%). As a last dehydration step, propylene oxide was used before the samples were embedded in LX-112 resin. After polymerization at 60 °C, ultrathin sections of 90 nm were cut on a Reichert EM UC6 with a diamond knife, collected on Formvar coated grids and stained with uranyl acetate and lead citrate. Sections were examined with a FEI Tecnai-12 G2 Spirit Biotwin electron microscope (Fei, Eindhoven, The Netherlands), and images were taken with a Veleta camera using Radius software (EMSIS, Münster, Germany). The data analysis program within Radius was used to perform measurements of the virus particle size. The capsid diameter was measured for 100–400 virus particles per infection, discriminating intracellular and extracellular particles.

Sensitivity to Chloroform

Recently, a new group of *Micromonas* viruses has been reported to possess a lipid membrane (Martínez Martínez et al. 2015). To test for the presence of a viral lipid membrane in these Arctic strains, fresh viral lysates were exposed to chloroform. This organic solvent is an effective indicator of inner- and outer-viral lipid membranes (Feldman and Wang 1961; Olsen et al. 1974). Aliquots of 1 mL were incubated in 10% and 50% (*v/v*) chloroform for 10 min, after which the chloroform was separated by centrifugation (4000× *g*, 5 min) and the aqueous phase containing the viruses was recovered (in new 1.5 mL Eppendorf tubes). Tubes were left overnight at 3 °C to allow any remaining chloroform to evaporate. Treated lysates were added to exponentially growing cultures in 5 mL borosilicate tubes (10% *v/v*

6

final concentration; total volume 5 mL) and incubated at standard light conditions and 3 °C. Non-infected negative controls received the same volume of media. Tubes were screened for lysis twice a week for three weeks.

Genome Size

MpoV lysates (~25 mL) were partially purified from cell debris and bacteria by centrifugation at 10,000× *g* for 30 min at 4 °C using a fixed angle rotor (type F 34-6-38) with conical adapters to fit the 30 mL Nalgene Oak Ridge centrifuge tubes in a Eppendorf 5810R centrifuge (Hamburg, Germany). Viral genome sizes were determined by Pulse Field Gel Electrophoresis (PFGE) according to Baudoux and Brussaard (2005). In short, the clarified supernatant was decanted and viral particles were concentrated by ultracentrifugation (184,000× *g* for 2 h at 8 °C, using a fixed-angle rotor Beckman Coulter type 50.2Ti, in a Beckman Coulter Optima XPN-80 ultracentrifuge) (Pasadena, CA, USA). Pellets were resuspended in 150 µL SM buffer (0.1 M NaCl, 8 mM MgSO$_4$·7 H$_2$O, 50 mM Tris-HCl, 0.0005% (*w/v*) glycerin), after which agarose plugs were prepared by mixing equal volumes of molten 1.5% (*w/v*) agarose (InCert; Lonza Group Ltd., Basel, Switzerland) with the virus concentrate in plastic molds. Plugs were incubated overnight at 30 °C in lysis buffer with proteinase K, followed by washing in TE buffer (10:1, pH 8.0) and storage in TE buffer (20:50, pH 8.0) at 4 °C until analysis. Plugged samples were loaded onto 1% SeaKem GTG agarose gels (InCert; Lonza Group Ltd., Basel, Switzerland) prepared in 1 × TBE gel buffer (90 mM Tris-Borate and 1 mM EDTA, pH 8.0) and run in a PFGE Bio-Rad CHEF DR-II cell unit (Bio-Rad, Hercules, CA, USA), and corresponding CHEF DR-II chiller system, filled with 2 L 0.5 × TBE buffer (45 mM Tris-Borate and 0.5 mM EDTA, pH 8.0), pre-cooled at 15 °C. Plugs were loaded with 0.5 × TBE buffer (45 mM Tris-Borate and 0.5 mM EDTA, pH 8.0), at 6 V cm^{-1} with pulse ramps of 20 to 45 s at 14 °C for 22 h. Molecular size markers were included: DNA Lambda ladder plugs (Bio-Rad) and *Saccharomyces cerevisiae* DNA ladder plugs (Bio-Rad). Gels were visualized in a FluorS imager (Bio-Rad Instrument) after staining with SYBR Green I (1 × 10^4 of commercial solution,

Invitrogen). Viral genome sizes were estimated in comparison to a molecular size marker ($n \geq 2$). Mean ±standard deviation were determined and the differences were tested by ANOVA (significance level p = 0.05) and Holm-Šidák multiple comparisons.

Virus Phylogeny

To determine the phylogenetic relationship between our new Arctic virus isolates and other *Micromonas* viruses, we amplified a part of the DNA polymerase B gene (*polB*) using the primer pair AVS1/AVS2 (Chen and Suttle 1996). The viral lysate was diluted 1:5 in ultrapure water and sonicated (MSE Soniprep 150, London, UK) at an amplitude of 8 µm for 3×10 s with intervals of 30 s cooling on ice. Ten microliters of sonicated viral lysate was used as a template in a 50 µL PCR reaction containing 4.0 U of BiothermPlus DNA Polymerase (GeneCraft, Lüdinghausen, Germany), $1 \times$ buffer (including 1.5 mM $MgCl_2$), 0.25 mM of each dNTP, 0.8 µM of each primer, and 0.4 mg/mL BSA. Negative controls contained all reagents except the template. PCR cycling included an initial denaturation at 94 °C (4 min) followed by 37 cycles of denaturation at 94 °C (30 s), annealing at 45 °C (30 s), and extension at 72 °C (1 min), followed by a final extension at 72 °C (7 min). Sequencing was performed by BaseClear Ltd. (Leiden, The Netherlands). Based on 178 amino acid positions, a Maximum-Likelihood dendrogram was constructed with RAxML (Stamatakis 2014) implemented in ARB software (Ludwig et al. 2004). The tree was rooted using *polB* sequences of *Bathycoccus* viruses (HM004432, FJ267515, FJ267518, KF501013, MEHZ011588827). These, and the *polB* sequences of *Ostreococcus* viruses (FJ267496, FJ267500, FJ267508, JN225873) were grouped to obtain a more compact tree. For comparison we added published *polB* sequences of the *Micromonas* virus isolates and contigs of an Arctic metagenome (Joli et al. 2017) that showed exact overlap with the *polB* fragment that we analyzed. Contig-95-10186 and contig-79-31207 were shorter (127 and 96 amino acid positions, respectively) and were later added to the dendrogram via ARB Parsimony.

6

Thermal Stability

We studied the effect of different temperatures on virus growth characteristics as well as on virus stability (loss of infectivity). To determine how the virus-host interaction might be affected over a range of different ecologically relevant temperatures, we used our model system of TX-01 with MpoV-45T, as both the host and virus were isolated in the same location and same period. Temperature sensitivity of the viral latent period and burst size were examined by one-step viral growth experiments at a range of growth temperatures, i.e., 0.5, 2.5, 3.5, and 7 °C. This range of temperatures represents natural water temperatures during the Arctic growth season (Loeng 2005; Richter-Menge and Mathis 2016; Timmermans 2016). Additionally, to test whether there are any species- and/or strain-specific responses to temperature, we furthermore tested both MpoV-44T and 45T on RCC 2257 and RCC2258 at 3 and 7 °C, whereby 3 °C represents the spring sea surface temperature around Spitsbergen (origin of TX-01) and southern Beaufort Sea (origin of RCC2257 and RCC2258; Mustapha et al. 2016) and 7 °C represents the maximum Arctic summer temperatures (e.g., Hop et al. 2006; Richter-Menge and Mathis 2016). MpoV-44T and 45T were chosen as representative virus model systems because of their different viral growth characteristics with both being isolated from Kongsfjorden. Algal host and virus samples were taken regularly (every 6–8 h in the first 24 h and every 12–24 h for the rest of the experiment) and analyzed by flow cytometry as described above (Marie et al. 1999; Brussaard 2004). Other culture conditions were the same as for the virus growth experiments described above.

Viral infectivity was determined after exposure at -196, -80, -20, 0, 3, 7, and 15 °C and determined using the Most Probable Number (MPN) assay on the host strain RCC2258. This host strain was used instead of TX-01, because the latter did not grow well in the 5 mL tubes that we used for the assays (the large amount of dilutions and replicates did not allow the use of larger tubes or flasks). Aliquots of virus lysates (3 mL) were exposed to the different temperatures for 24 h when the exposure temperature was below zero and for 1 h when exposure temperature was above zero. Following exposure, viral lysates were added to the algal host ($n = 5$; 12

× 10-fold dilutions). In each MPN rack one additional row of tubes containing non-infected culture (also 5 mL per tube) served as a negative control. The MPN cultures were incubated at 3 °C under standard light conditions and were inspected at least once a week for 3 weeks for lysis. The titers were determined with the MPN Assay Analyzer (Passmore et al. 2000) and data were normalized to the highest value, i.e., 9.8×10^8, 4.6×10^9, 2.1×10^1, and 4.6×10^9 mL^{-1} for MpoV-44T, 45T, 46T, and 47T, respectively. Statistics were carried out in SigmaPlot 13.0 (Systat Software Inc., Chicago, Il, USA). Differences between the viruses and temperature treatments were tested by ANOVA ($n = 3$, significance level $p = 0.05$) and Holm-Šidák multiple comparisons, either directly or after log transformation.

Diversity and Abundance in Metagenomes

To assess the diversity of MpoV in diverse marine environments, we searched the contigs generated by the Tara Oceans consortium (Sunagawa et al. 2015), as well as KEGG Environmental sequences for MpoV homologs using blastn (Altschul et al. 1990). All hits had an E-value < 10-30. Hit regions were excised from the contigs, aligned with the four MpoV sequences using Clustal Omega 1.2.0 (Sievers et al. 2011), and converted into a phylogenetic tree using PhyML 3.0.1 (Guindon et al. 2010) with the HKY85 model of substitution; four discrete gamma categories; shape parameter: 1.074; invariant proportion: 0.455; and transition/transversion ratio: 4.540. Finally, we assessed the ubiquity and abundance of all the MpoV-related sequences in the Tara Oceans samples (Sunagawa et al. 2015). Abundance was determined by mapping 2.5 billion metagenomic sequencing reads from 26 Tara Oceans metagenomes to the contig fragments using Burrows-Wheeler Aligner (BWA-MEM algorithm) with default parameters (Li and Durbin 2009), with the number of mapped reads reflecting the relative abundance in the original samples. The IDs of the 26 screened metagenomes were: ERR594313.1, ERR598949.1, ERR598972.1, ERR598982.1, ERR599023.1, ERR599039.1, ERR599095.1, ERR594320.1, ERR598950.1, ERR598976.1, ERR598994.1, ERR599025.1, ERR599053.1, ERR599122.1, ERR594324.1, ERR598962.1, ERR598977.1,

6

ERR599001.1, ERR599027.1, ERR599068.1, ERR594325.1, ERR598966.1, ERR598979.1, ERR599007.1, ERR599035.1, and ERR599078.1.

Results

Basic Virus Characteristics

The transmission electron microscope analysis of the four Arctic *Micromonas* viruses revealed virus-like particles in the cytoplasm of the host with a hexagonal shape (icosahedral symmetry) and a thick outer layer surrounding an electron-dense inner core (Fig. 1). We detected no significant difference between the diameter of the different isolates nor for the intra- versus extracellular virus particles. The diameters of the virus particles were 119 ± 8, 121 ± 14, 120 ± 12, and 119 ± 9 nm respectively for MpoV-44T, 45T, 46T, and 47T. Furthermore, chloroform treatment revealed that all viruses lost their infectivity upon treatment with chloroform, indicative for the presence of a lipid membrane. Cytograms of the viruses stained with the nucleic acid-specific dye SYBR Green I showed high green fluorescence signatures, similar to other known dsDNA *Micromonas* viruses (Fig. S2; Brussaard 2004; Martínez Martínez et al. 2015). The dsDNA nature of the MpoV genomes was confirmed by the positive results from the PCR amplification of the partial DNA polymerase
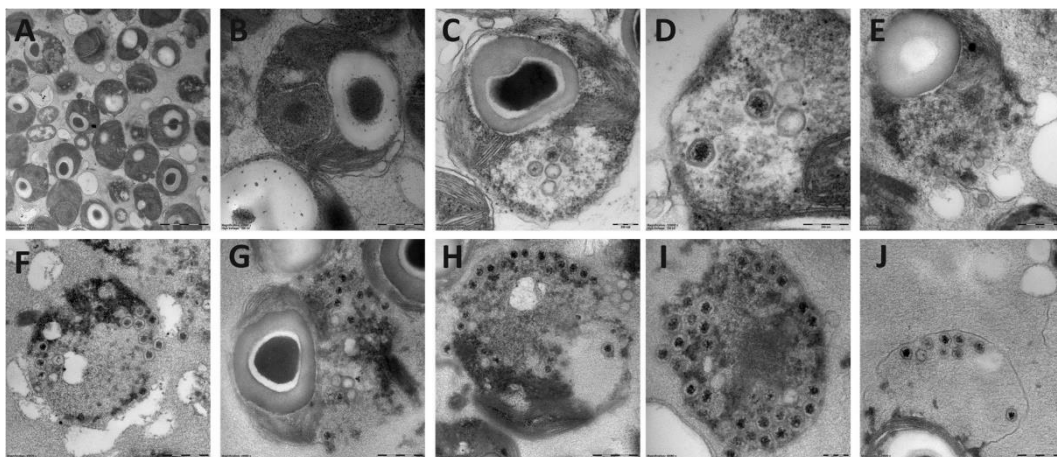
Fig. 1. Transmission electron micrographs of thin sections of the uninfected *Micromonas* strain TX-01 (**A,B**), and infected with virus MpoV-44T (**C,D**), 45T (**E**), 46T (**F**–**H**), and 47T (**I,J**). Scale bar represents 200 nm (**A,C,D,I**) or 500 nm (**B,E**–**H,J**).
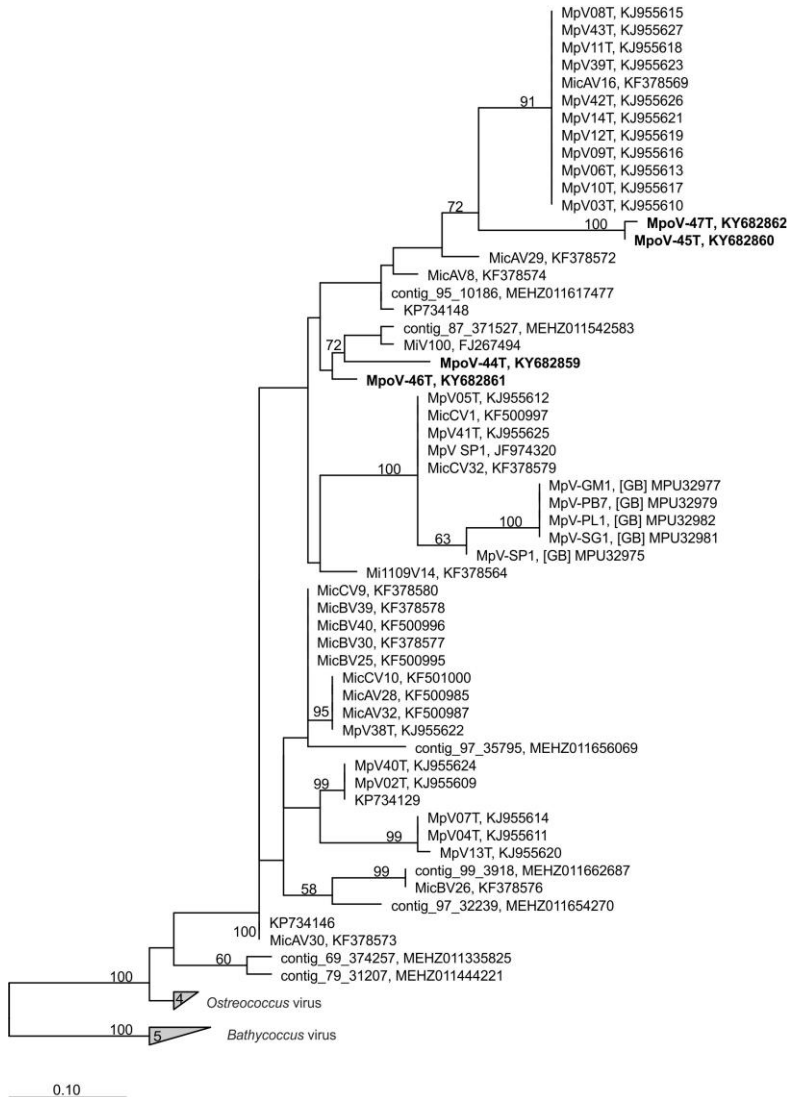
Fig. 2. Position of the four *Micromonas polaris* viruses (MpoVs) (in bold) in a maximum likelihood dendrogram (100 bootstrap replicates), based on a multiple alignment of 178 amino acid positions of DNA polymerase B (*polB*). Only nodes with bootstrap values >50% are displayed. Virus strains and accession numbers are indicated. "Contigs" are *polB* sequences extracted from an Arctic marine metagenome (Joli et al. 2017). The tree was rooted using *polB* sequences of *Bathycoccus* viruses.

B gene (*polB*) using AVS1/AVS2 primers that were originally designed for dsDNA prasinoviruses (Chen and Suttle 1996). The *polB* phylogeny based on inferred amino acid sequences indeed grouped the newly isolated MpoVs with other *Micromonas* viruses, but did not show a close match (i.e., >13 amino acid substitutions) to any of

the other Arctic sequences (Fig. 2). MpoV-45T and MpoV-47T were highly similar to each other (1 amino acid difference), but clearly distinct from MpoV-46T and 44T (>31 amino acids difference). MpoV-44T differed from MpoV-46T in 17 amino acid positions. The viral genome sizes of MpoV-45T, 46T, and 47T, (191 ±3 Kb estimated by PFGE) were not significantly different from each other (one-way ANOVA $p >$ 0.818, $n = 4$, 2, and 2, respectively) but were significantly smaller ($p < 0.008$) than the genome of MpoV-44T which displayed a genome size of 205 ±2 Kb ($n = 3$; Table 2, Fig. S3).
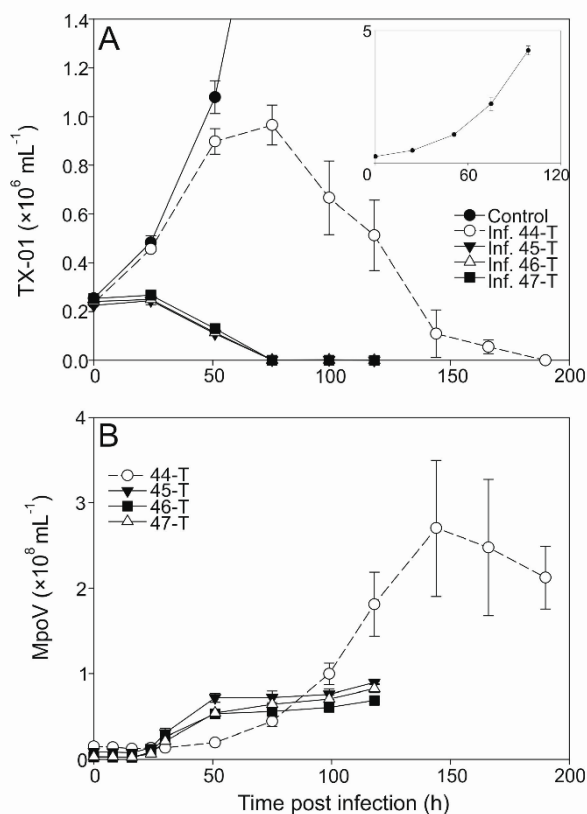
Fig. 3. Abundances of *Micromonas* cells (×10^6 mL^{-1}) and viruses MpoV-44T, 45T, 46T, and 47T (×10^8 mL^{-1}) infecting host strain TX-01. Panel (A) shows the algal abundances (mean ± standard deviation (S.D.) over time, with the filled circles depicting the non-infected control cultures, open circles depicting the cultures infected with MpoV-44T, filled triangles depicting the ones infected with MpoV-45T, closed triangles depicting the ones infected with MpoV-46T, and the filled squares depicting the ones infected with MpoV-47T. The inlay panel shows the growth of the non-infected controls in detail. Panel (B) shows the viral abundances (mean ± S.D.) over time, with the symbols corresponding to panel (A), i.e., each virus is depicted by the same symbol as the culture it infected.

The virus isolates were specific for the genus *Micromonas* (Table S1), but were not species-specific. For example, MpoV-44T was isolated on *M. commoda* LAC38, but also infected TX-01, *M. pusilla*, and *M. polaris* strains (Roscoff Culture Collection; Table 1). Besides the host strain TX-01, RCC2257 and 2258 were also sensitive to infection by all four MpoVs. MpoV-44T displayed the broadest host range and was the only virus that could infect *Micromonas* strains LAC38, CCMP1545, RCC461, and 834 that grow at higher temperatures (8, 15, or 20 °C). No relationship could be established between virus infectivity or host susceptibility to infection based on the time of isolation, geographical origin, or host culture temperature.

One-step infection was observed for all the MpoV lytic virus growth cycles except for MpoV-44T when propagated on TX-01 (Fig. 3A). TX-01 kept growing for the two days following virus addition to a higher extent than commonly observed (Baudoux and Brussaard 2008; Maat et al. 2016). However, this was not observed for other host strains, e.g., RCC2257, RCC2258, and LAC38 (Fig. S4). MpoV45T, 46T, and 47T showed similar infection dynamics and latent periods, i.e., 16–24 h with a median of 18 h (Fig. 3B; Table 2). The median latent period for MpoV-44T on host strain TX-01 was, at 39 h, twice as long. Viral burst sizes did not differ significantly for the four MpoVs on TX-01 (one-way ANOVA; $p = 0.317$) and the averages varied between 233 and 296 viruses produced per lysed host cell (Table 2).

Testing the sensitivity of the four Arctic MpoVs to temperature showed that all viruses lost most of their infectivity after 24 h exposure to temperatures < -20 °C (Fig. 4). After a -20 °C treatment, only 1% of MpoV-44T remained infective while the other viruses retained over 25% of their infectivity when compared to the treatment at 3 °C. Moreover, the variability between the viruses in response to non-freezing temperatures was high. MpoV-45T and 46T displayed relatively narrow tolerance ranges, with maximal infectivity after the 0 °C and 3 °C treatments, respectively. MpoV-44T and 47T retained infectivity at the highest temperature tested (7 °C), with MpoV-47T being the least sensitive to temperature (consistent infectivity at 0–7 °C).

6
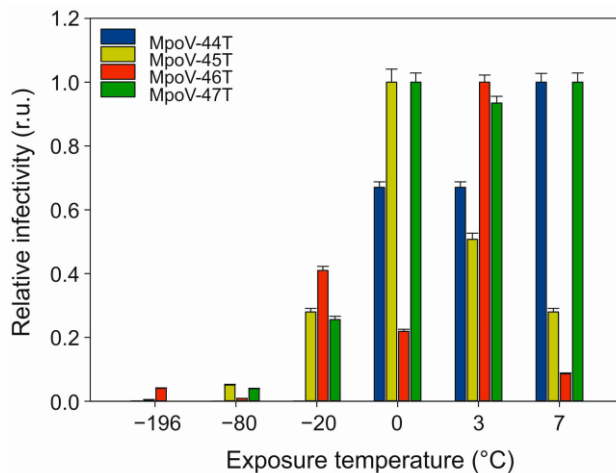
Fig. 4. Effects of temperature exposure on the infectivity of MpoV-44T, 45T, 46T, and 47T (actual infection assay performed at 3 °C). The *x*-axis depicts the exposure temperature and the *y*-axis depicts the relative infectivity (normalized to highest infectivity) of the virus as determined by the most probable number (MPN) dilution assay. r.u. stands for relative units. Error bars show standard error (*n* = 5).

Temperature Dependent Virus Production

The lysis dynamics of the MpoV-45T infecting host TX-01 was similar for all four temperatures tested (0.5, 2.5, 3.5, 7 °C; Fig. 5A) despite increasing exponential growth rates of the host (0.40 $\pm$ 0.05, 0.49 $\pm$ 0.06, 0.66 $\pm$ 0.01, 0.85 $\pm$ 0.02 d^{-1}, respectively). The latent period of MpoV-45T did not change with temperature (16–24 h; Fig. 5B), but the viral burst sizes did show significant differences between 0.5, 2.5, and 3.5 °C (one-way ANOVA; 0.001 $< p <$ 0.019) and declined with lower temperatures by 15% and 28% for 2.5 and 0.5 °C, respectively, compared to 3.5 °C (Fig. 5C).

Assessing the other virus-host combinations for temperature sensitivity (7 °C compared to 3 °C), the virus growth characteristics revealed host-specific effects. MpoV-45T showed a shorter latent period at higher temperature when RCC2257 was the host (from 12–18 h to 6–12 h), whereas no such effects were observed on hosts TX-01 and RCC2258; Fig. 6A). Moreover, while TX-01 (infected with MpoV45T) did not show an increase in burst size from 3.5 to 7.0 °C (but did from 2.5 to 7.0 °C; see above), RCC2257 and RCC2258 showed increased burst sizes at 7 °C by respectively 150% and 140% (one-way ANOVAs; *p* < 0.045; Fig. 6B, Table S2).

Fig. 5. Abundances of *Micromonas* strain TX-01 ($\times 10^5$ mL^{-1}) and virus MpoV-45T ($\times 10^6$ mL^{-1}) tested at 0.5, 2.5, 3.5, and 7.0 °C. Panel (**A**) shows the algal abundances (mean ± S.D.) over time, with filled circles representing 0.5 °C, filled triangles representing 2.5 °C, open circles representing 3.5 °C, and open triangles representing 7.0 °C. The inlay panel shows the growth of the non-infected controls. Panel (**B**) shows the viral abundances (mean ± S.D.) over time, with the symbols corresponding to panel A, i.e., each virus is depicted by the same symbol as the culture it infected. Panel (**C**) depicts the median viral latent periods (black bars; determined with an 8 h sampling resolution) and viral burst sizes (grey bars; mean ± S.D.).
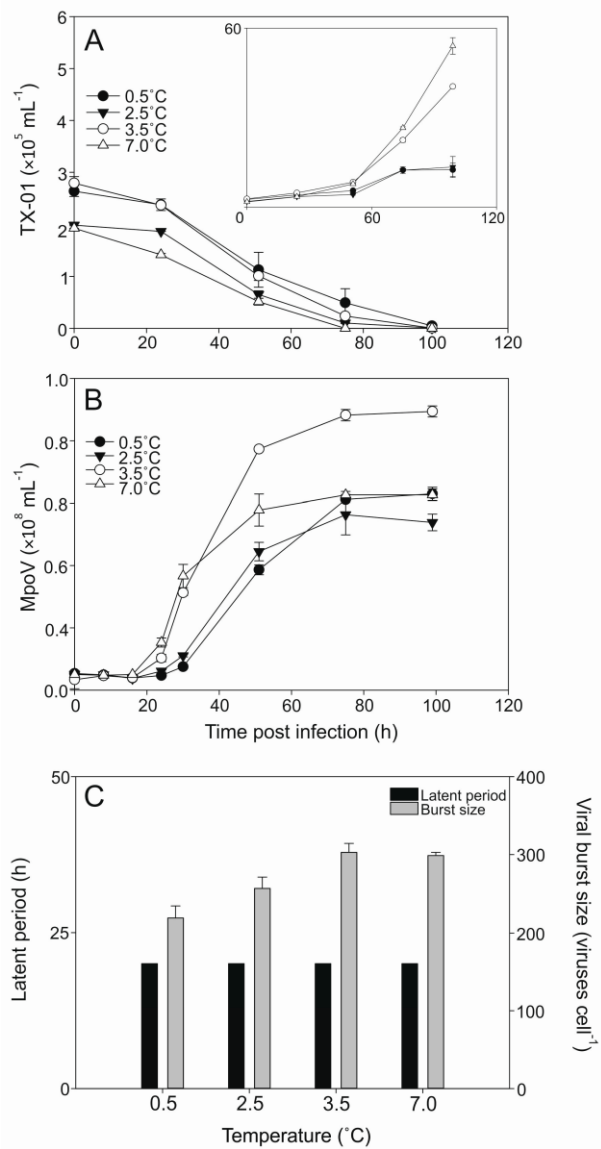
There were also virus-specific responses to temperature, as an increase from 3 °C to 7 °C showed a stronger effect on the latent periods of MpoV-44T rather than that of MpoV-45T, reducing it by roughly 50% from >30 h to 12–18 h on both hosts. Moreover, the viral burst sizes of MpoV-44T showed only a significant increase at 7 °C on host RCC2257 (one-way ANOVA; $p = 0.044$), which was also smaller than that for MpoV-45T (115% compared to 150%). Irrespective of temperature, on host RCC2258 the viral burst sizes of MpoV-45T were higher than those of MpoV-44T,
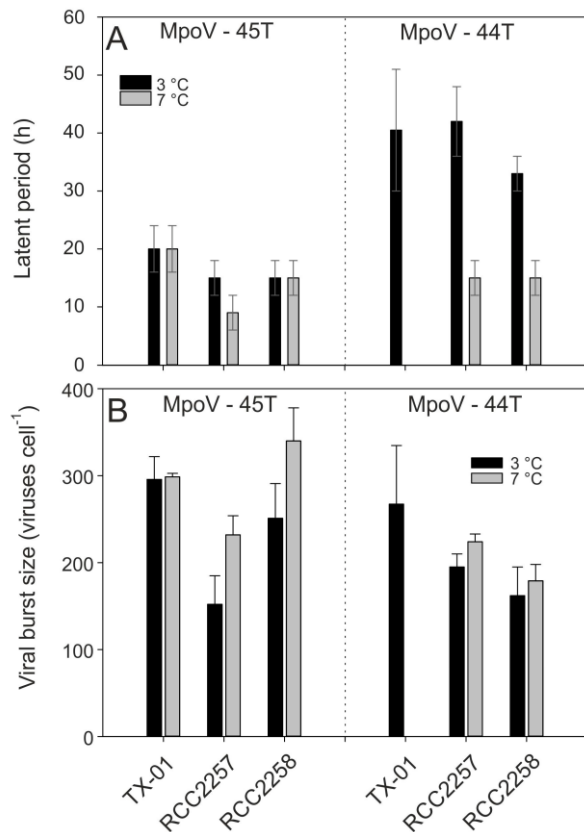
Fig. 6. Median latent periods (**A**) and mean burst sizes (**B**) of MpoV-45T (left panels) and MpoV-44T (right panels) infecting host TX-01, RCC2257, and RCC2258 at 3 °C (black bars) and 7 °C (grey bars). Note that the TX-01 data are from the same as in Fig. 5. The range bars in panel A depict the actual time interval on which the latent period is based. The error bars in panel B depict the standard deviation (S.D.). Statistical analysis of inter- and intra-strain differences are depicted in Table S2.

but for host RCC2257 no such difference was observed (two-way ANOVA; two- p < 0.001 and $p < 0.916$, respectively).

Diversity and Abundance in Metagenomes

Finally, we assessed the diversity and abundance in the metagenomes by screening sequence databases for homologs of the amplified nucleotide region. The phylogenetic tree in Fig. 7 shows that MpoVs are part of a family of viruses whose sequences were previously detected in marine samples from around the world from various studies including Tara Oceans (Sunagawa et al. 2015) and the Ocean Sampling Day.

Fig. 7. Unrooted maximum likelihood phylogeny of MpoV-related sequences from various studies, and their abundance in environmental metagenomes. Abundance is expressed as the total number of aligned reads out of 2.5 billion reads in 26 Tara Oceans datasets.

Discussion

To our knowledge this is the first report of the isolation and characterization of phycoviruses from polar marine waters. Similar to other reports of *Micromonas* virus isolates, and consistent with the *Phycodnaviridae*, the virus-like particles accumulated in the cytoplasm of the host cells (Martínez Martínez et al. 2015). The particles of the four MpoV were morphologically similar (no significant variance in virus particle size, i.e., on average 120 nm), and all contained a lipid membrane (sensitive to chloroform). Lipid-containing MpoVs were first reported by Martínez Martínez and colleagues (2015). These authors were able to clearly and convincingly divide nineteen newly isolated *Micromonas* viruses, across an area spanning the North Sea to the Mediterranean Sea, into two groups based on (i) their sensitivity to infection of LAC38 or CCMP1545, (ii) genome size (206 ±6 Kb ($n = 12$) vs. 191 ±4

Kb (*n* = 8)), and (iii) presence of a lipid membrane. Strikingly, all LAC38-infecting viruses with larger genomes contained a lipid membrane, whereas the smaller genome sized CCMP1545-infecting ones did not. Our data show a similar larger genome size for MpoV-44T which infects LAC38 (205 ±2 Kb, in contrast to the 191 ±3 Kb genomes of the other MpoVs), but in our case all MpoVs contained a lipid membrane.

Molecular phylogeny inferred from the amino acid sequences of the DNA polymerase gene B fragments established that the four Arctic MpoV isolates grouped distinctly with the other dsDNA *Micromonas* viruses belonging to the genus Prasinovirus. The genus Prasinovirus infects *Ostreococccus* and *Micromonas* species and is one of the six virus genera belonging to the *Phycodnaviridae* family; eukaryotic algal viruses with large dsDNA genomes (100–560 Kbp) (Wilson et al. 2009; Clerissi et al. 2014). A recent metagenomic survey (Tara Ocean Expedition) revealed that prasinoviruses are the most abundant group of phycodnaviruses in the oceans (Hingamp et al. 2013). The newly isolated MpoVs did not group together; instead MpoV-44T and 46T were phylogenetically distinct, both from each other and from MpoV-45T and 47T. Furthermore, it is clear from the phylogenic analysis based on *polB* that the Arctic *Micromonas* viruses do not form a separate cluster. Screening the Tara Oceans' contigs and the KEGG Environmental database for homologs of the amplified nucleotide region of our MpoV isolates revealed a worldwide distribution and high diversity on thermal stability (i.e., from the Greenland Sea to the temperate regions to Antarctica and in waters from −1.6 to 17.3 °C, Table S3). These results confirm that the *Micromonas* viruses and their relatives are globally dispersed, show a high degree of genotypic diversity, and are ecologically relevant.

There was no general relationship between the phylogenies of the virus and host strains as revealed by Martínez Martínez et al. (2015) for viruses infecting temperate *Micromonas* strains, but MpoV-44T could be distinguished from the other Arctic MpoV isolates based on its capability to virally infect *M. commoda* LAC38. Although LAC38 was being cultured at low temperature (3 °C) at the time of virus isolation, it is originally a temperate *Micromonoas* strain (Baltic Sea) (Sahlsten 1998). We

cannot exclude that the isolation of MpoV-44T on a different host is underlying its intrinsic differences to the other MpoVs isolated 8–9 years later using a local Arctic *Micromonas* host strain. These differences may also be due to MpoV-44T having been isolated during midwinter and years before the other MpoVs (isolated in summertime during two consecutive years). Successional patterns for marine virus communities with associations to temperature and host dynamics have been demonstrated (e.g., Pagarete et al. 2013). Even though Arctic *Micromonas* still grows well at low temperatures (0.4 d^{-1} at 0.5 °C, this study) and low light (0.2 d^{-1}; Lovejoy et al. 2007), photosynthesis may not be possible during part of the Arctic winter. Several *Micromonas* species however exhibit phagotrophy (e.g., *M. polaris* CCMP2099; McKie-Krisberg and Sanders 2014) that could serve as an alternative energy source to maintain growth and/or virus production during the winter (see also Joli et al. 2017). Yet, our study shows that MpoV-44T is well adapted to relatively fast and high production of infective progeny at relatively higher temperatures, which makes it more likely that advection of relatively warm Atlantic water from the West Spitsbergen Current (WSC) (Hop et al. 2002) was responsible for being able to isolate MpoV-44T in winter. Water temperature in autumn of the year of isolation was in fact higher than the average of the preceding years (Tverberg et al. 2008). Additionally, the ability of MpoV-44T to successfully infect *Micromonas* strains growing at higher temperatures up to 20 °C seems indicative that this specific virus has a high temperature tolerance. Still, a relatively high temperature optimum for a virus occurring in a cold environment could theoretically be an adaptation to be less virulent in order to avoid extinction of the host (Suttle 2007; Baudoux et al. 2015). The relatively long latent periods and reduced infectivity of MpoV-44T at low temperatures would effectuate such low virulence for the slow growing hosts during the winter months. Then in the following more productive season, when the host growth rates increase, the latent period of MpoV-44T shortens and burst sizes increase to be able to keep in sync with host growth. Intriguingly, MpoV-47T also displayed thermostability, with an infectivity optimum at 7 °C. MpoV-47T was isolated only 2 months later than the temperature sensitive MpoV-45T (infectivity optimum at 0 °C),

6

indicative of a high degree of diversity of virus thermostability in Arctic waters.

At temperatures above zero, the infectivity data do not confirm our first hypothesis that MpoV infectivity increases with temperature. The viral response to higher temperatures (0–7 °C) was highly variable and strain-specific. Two of the four virus isolates (MpoV-45 and 46T) even showed a loss of infectivity above 0 °C. All of the virus isolates, except for MpoV-44T, were able to maintain over 25% of their infectivity after being frozen at –20 °C. This suggests that these viruses are well able to withstand the freezing process during ice formation, a property which would maintain high titers during winter. Similar findings have been reported for Arctic marine bacteriophages (Wells and Deming 2006a) and dsDNA algal viruses during winter in a seasonally frozen pond (Long and Short 2016). Cottrell and Suttle (1995) reported relatively high decay rates for MpV-SP1, however, this virus strain originated from subtropical waters and the decay rates were largely determined by sunlight (UV intensity). There is limited knowledge of dsDNA algal virus thermal stability and the mechanisms underlying the loss of infectivity have not been elucidated (Tomaru et al. 2004, 2005; Baudoux and Brussaard 2005; Nagasaki et al. 2005; Martínez Martínez et al. 2015; Demory et al. 2017). Only a few cold-active viruses (i.e., viruses that successfully infect hosts at 4 °C or below) have been brought into culture and all are bacteriophages (Borriss et al. 2003; Wells and Deming 2006b; Luhtanen et al. 2014). Variability in MpoVs' temperature sensitivity demonstrates a specificity of infection efficiency related to temperature. Hypothesizing that our data are generally applicable, seasonal temperature shifts could regulate *Micromonas* host and virus succession. The infectivity loss at higher temperature (7 °C) for MpoV-45T and MpoV-46T shortens their window of optimal activity during the warmer summer months. Considering that the range of temperatures we tested are ecologically relevant for the Artic seas (water temperatures between –1 and 7 °C; Richter-Menge and Mathis 2016), our results indicate the need to determine the causal processes such as the means of virus entry and conformational changes in the virus particle (e.g., viral capsid proteins and lipid membrane properties).

When propagated on the putative *M. polaris* strain TX-01, MpoV-44T displayed a much longer median latent period than the other Arctic MpoVs (39 vs. 18 h, respectively). A comparably long latent period had, until recently, only been described for the dsRNA virus MpRV infecting *M. commoda* LAC38 (36 h; Brussaard et al. 2004). However, Baudoux and colleagues (2015) reported a latent period of 27–31 h for a dsDNA virus infecting *Micromonas* isolates from the English Channel growing at 20 ℃. The latent period of MpoV-44T displayed a strong temperature-dependence, i.e., with a temperature increase of 4 ℃, the time of viral release decreased by >15 h (latent period 12–18 h; approximately 50% of the latent period at 3 ℃). Although Baudoux et al. (2015) did not find a correlation between differences in latent period (or burst size) with the host growth rates for the isolated MicVs, Demory et al. (2017) reported for the virus-host model system Mic-B/MicV-B (virus infecting largely Clade B strains) an inverse relationship of the viral latent period with the host growth rate (whereby the growth rates were affected by the host culture temperature). We did not find such a relationship with growth rate for the latent periods of MpoV-44T growing on TX-01, but did find a similar significant linear relationship when infecting host RCC2258 ($r^2 = 0.952$, $p = 0.018$). Virus MpoV-45T did not show a dependency on host growth rate (TX-01, RCC2258, and RCC2257), but instead showed a shortened latent period on host RCC2257 at the highest temperature (7 ℃ compared to 3 ℃). Furthermore, the latent period of MpoV-44T was strongly affected by temperature whereas increasing temperature only shortened the MpoV-45T latent period on RCC2257. On host TX-01, the latent period was unaffected over the whole range of 0.5 to 7 ℃, however, we found a steeper increase of viruses with increasing temperature, i.e., virus production rates of 0.18, 0.37, 1.4, and 1.6×10^5 viruses h^{-1} between 16 and 30 h for 0.5, 2.5, 3.5, and 7.0 ℃, respectively. While the data confirm our second hypothesis that the temperature increase stimulates MpoV production (through shortened latent periods, enhanced production rate and/or higher burst sizes), there is nonetheless a virus-specific response for the range of temperatures tested. Instead we found a high variability in response for the different virus isolates and host strains. When looking

6

at a temperature increase from 3 to 7 °C, most virus-host combinations in our study showed enhanced viral burst sizes with a temperature-regulated increase in the host growth rates (0.53–0.59 d^{-1} at 3 °C and approximately 1.2-fold higher at 7 °C). However, MpoV-45T infecting TX-01 did not show this increase from 3 to 7 °C, but did exhibit an increasing burst size with temperatures from 0.5 up to 3.5 °C (growth rate TX-01 increased from 0.40 to 0.66 d^{-1}, respectively). Hence, the optimum temperature for virus production was not the same as the optimum host growth temperature. Wells and Deming (2006b) showed a similar situation in which phage 9A, infecting the psychrophile *Colwellia psychrerythraea* strain 34H, had a burst size optimum at −1 °C while the host's growth rate optimum was at 8 °C. These authors suggested that specific virally encoded enzymes have their own optimum temperatures.

Temperature strongly regulates Arctic *Micromonas* growth rates with increasing growth rates up to 7 °C (this study; Lovejoy et al. 2007; Coello-Camba et al. 2015). These temperatures are at or above the present summer sea surface temperatures in the lower latitude regions of the Arctic (Richter-Menge and Mathis 2016; Timmermans 2016). At the time that TX-01 was isolated (half April), in situ picophotoeukaryotic gross growth rates were 0.58 d^{-1} at temperatures between 1 and 2 °C (Maat and Brussaard, unpublished data). By the end of May, the temperatures and consequently the growth rates had increased to 2–3 °C and 1.1 d^{-1}, respectively. This 20–50% growth rate increase is similar to TX-01 in the present study over the same temperature range. Our results indicate that over an Arctic growing season with increasing temperatures and host growth rates, viral activity can be expected to increase as a result of the decreasing latent periods and increasing burst sizes. Our data imply that temperature could affect host and virus diversity (strain dynamics), as for MpoV-45T with host TX-01 the latent period and viral burst size did not further change above 3 °C, but with other hosts (RCC2257 and 2258) and other viruses (MpoV-44T) the latent periods shortened and/or burst sizes increased to several extents. The different susceptibilities of viral infectivity to temperature, with a tolerance for the highest temperatures for MpoV-44T, strengthened this idea even

more. Tarutani et al. (2000) showed how within the observed abundances of *Heterosigma akashiwo* and the lytic virus HaV, a successional shift in clonal composition occurred due to differences in susceptibility/resistance of the host to the viruses. Based on our data a similar shift in strain and clonal composition of *Micromonas* and MpoV may occur, not only due to differences in susceptibility to the viruses but also because of differences in virus proliferation success at different temperatures (Mojica and Brussaard 2014).

In summary, the present study describes the first isolation and characterization of viruses infecting a cold-adapted polar phytoplankter. The relevance seems high, as it concerns the ubiquitous genus *Micromonas* which belongs to the picophytoplankton fraction and is expected to be favored under future Arctic conditions (due to warming and freshening induced vertical stratification; Loeng 2005; Li et al. 2009, 2013; Coello-Camba et al. 2015). The Arctic region is warming to a greater extent than lower latitudinal marine waters (Loeng 2005; Richter-Menge and Mathis 2016) and current summer sea surface temperatures (August 2016) as high as 5 °C above the 1982–2010 mean (Timmermans 2016) have been observed. *Micromonas* growth rates will enhance faster and earlier in the season and our study indicates that viral production will likely do the same. We show variable infection dynamics in response to temperature for the different virus-host strain systems examined, which complicates the assessment of the environmental relevance of each isolate. However, we do like to advocate that virus (and host) isolation, characterization of virus-host dynamics, and responses to changing ecologically relevant environmental factors are fundamentally essential to understanding the role of algal viruses in (Arctic) marine waters. The newly isolated viruses make it possible to comprehensively investigate the interactions of these unique virus-host combinations under climate change relevant environmental variables. Joli et al. (2017) showed the importance of Arctic *Micromonas* viruses by metagenome sequencing. It would be interesting to investigate the ecological relevance of the strains tested in our study using molecular approaches. In the natural environment, selective effects of temperature may drive (intra)species diversity, potentially affecting the ability of *Micromonas* to respond to

6

the changing conditions of the vulnerable Arctic. Modeling studies could help to comprehend (and predict) the extent to which the Arctic phytoplankton community would be influenced by changes in infection dynamics associated with temperature changes.

Conflicts of Interest

The authors declare no conflict of interest.

References

Altschul SF, Gish W, Miller W, et al (1990) Basic local alignment search tool. J Mol Biol 215:403–410. doi: 10.1016/S0022-2836(05)80360-2

Attoui H, Jaafar FM, Belhouchet M, et al (2006) *Micromonas pusilla* reovirus: A new member of the family Reoviridae assigned to a novel proposed genus (Mimoreovirus). J Gen Virol 87:1375–1383. doi: 10.1099/vir.0.81584-0

Balzano S, Gourvil P, Siano R, et al (2012a) Diversity of cultured photosynthetic flagellates in the northeast Pacific and Arctic Oceans in summer. Biogeosciences 9:4553–4571. doi: 10.5194/bg-9-4553-2012

Balzano S, Marie D, Gourvil P, Vaulot D (2012b) Composition of the summer photosynthetic pico and nanoplankton communities in the Beaufort Sea assessed by T-RFLP and sequences of the 18S rRNA gene from flow cytometry sorted samples. ISME J 6:1480–1498. doi: 10.1038/ismej.2011.213

Baudoux A-C, Brussaard CPD (2005) Characterization of different viruses infecting the marine harmful algal bloom species *Phaeocystis globosa*. Virology 341:80–90. doi: 10.1016/j.virol.2005.07.002

Baudoux A-C, Brussaard CPD (2008) Influence of irradiance on virus-algal host interactions. J Phycol

44:902–908. doi: 10.1111/j.1529-8817.2008.00543.x

Baudoux AC, Lebredonchel H, Dehmer H, et al (2015) Interplay between the genetic clades of *Micromonas* and their viruses in the Western English Channel. Environ Microbiol Rep 7:765–773. doi: 10.1111/1758-2229.12309

Borriss M, Helmke E, Hanschke R, Schweder T (2003) Isolation and characterization of marine psychrophilic phage-host systems from Arctic sea ice. Extremophiles 7:377–384. doi: 10.1007/s00792-003-0334-7

Brussaard CPD (2004) Optimization of procedures for counting viruses by flow cytometry. Appl Environ Microbiol 70:1506–1513. doi: 10.1128/AEM.70.3.1506-1513.2004

Brussaard CPD, Noordeloos AAM, Sandaa RA, et al (2004) Discovery of a dsRNA virus infecting the marine photosynthetic protist *Micromonas pusilla*. Virology 319:280–291. doi: 10.1016/j.virol.2003.10.033

Brussaard CPD, Noordeloos AAM, Witte H, et al (2013) Arctic microbial community dynamics influenced by elevated CO_2 levels. Biogeosciences 10:719–731. doi: 10.5194/bg-10-719-2013

Chen F, Suttle CA (1996) Evolutionary relationships among large double-stranded DNA viruses that infect microalgae and other organisms as inferred from DNA polymerase genes. Virology 219:170–178. doi: 10.1006/viro.1996.0234

Clerissi C, Grimsley N, Ogata H, et al (2014) Unveiling of the diversity of prasinoviruses (Phycodnaviridae) in marine samples by using high-throughput sequencing analyses of PCR-amplified DNA polymerase and major capsid protein genes. Appl Environ Microbiol 80:3150–3160. doi: 10.1128/AEM.00123-14

Coello-Camba A, Agustí S, Vaqué D, et al (2015) Experimental assessment of temperature thresholds for Arctic phytoplankton communities. Estuaries and Coasts 38:873–885. doi: 10.1007/s12237-014-9849-7

Cottrell MT, Suttle CA (1991) Wide-spread occurrence and clonal variation in viruses which cause lysis of a cosmopolitan, eukaryotic marine phytoplankter, *Micromonas pusilla*. Mar Ecol Prog Ser 78:1–9. doi: 10.3354/meps078001

Cottrell MT, Suttle CA (1995) Genetic diversity of algal viruses which lyse the photosynthetic picoflagellate *Micromonas pusilla* (prasinophyceae). Appl Environ Microbiol 61:3088–3091. doi: 10.1128/aem.61.8.3088-3091.1995

D'Amico S, Collins T, Marx JC, et al (2006) Psychrophilic microorganisms: Challenges for life. EMBO Rep 7:385–389. doi: 10.1038/sj.embor.7400662

Demory D, Arsenieff L, Simon N, et al (2017) Temperature is a key factor in *Micromonas*–virus interactions. ISME J 11:601–612. doi: 10.1038/ismej.2016.160

Feldman HA, Wang SS (1961) Sensitivity of various viruses to chloroform. Proc Soc Exp Biol Med 106:736–738. doi: 10.3181/00379727-106-26459

Foulon E, Not F, Jalabert F, et al (2008) Ecological niche partitioning in the picoplanktonic green alga *Micromonas pusilla*: Evidence from environmental surveys using phylogenetic probes. Environ Microbiol 10:2433–2443. doi: 10.1111/j.1462-2920.2008.01673.x

Guillard RRL, Ryther JH (1962) Studies of marine planktonic diatoms: I. *Cyclotella nana* Hustedt, and *Detonula confervacea* (CLEVE) Gran. Can J Microbiol 8:229–239. doi: 10.1139/m62-029

Guindon S, Dufayard JF, Lefort V, et al (2010) New algorithms and methods to estimate maximum-likelihood phylogenies: Assessing the performance of PhyML 3.0. Syst Biol 59:307–321. doi: 10.1093/sysbio/syq010

Harrison PJ, Waters RE, Taylor FJR (1980) A broad-spectrum artificial seawater medium for coastal and open ocean phytoplankton. J Phycol 16:28–35. doi: 10.1111/j.0022-3646.1980.00028.x

Hingamp P, Grimsley N, Acinas SG, et al (2013) Exploring nucleo-cytoplasmic large DNA viruses in Tara Oceans microbial metagenomes. ISME J 7:1678–1695. doi: 10.1038/ismej.2013.59

Hop H, Falk-Petersen S, Svendsen H, et al (2006) Physical and biological characteristics of the pelagic system across Fram Strait to Kongsfjorden. Prog Oceanogr 71:182–231. doi: 10.1016/j.pocean.2006.09.007

Hop H, Pearson T, Hegseth EN, et al (2002) The marine ecosystem of Kongsfjorden, Svalbard. Polar Res 21:167–208. doi: 10.1111/j.1751-8369.2002.tb00073.x

Joli N, Monier A, Logares R, Lovejoy C (2017) Seasonal patterns in Arctic prasinophytes and inferred ecology of *Bathycoccus* unveiled in an Arctic winter metagenome. ISME J 11:1372–1385. doi: 10.1038/ismej.2017.7

6

Kilias E, Wolf C, Nöthig EM, et al (2013) Protist distribution in the Western Fram Strait in summer 2010 based on 454-pyrosequencing of 18S rDNA. J Phycol 49:996–1010. doi: 10.1111/jpy.12109

Kilias ES, Nöthig EM, Wolf C, Metfies K (2014) Picoeukaryote plankton composition off West Spitsbergen at the entrance to the Arctic Ocean. J Eukaryot Microbiol 61:569–579. doi: 10.1111/jeu.12134

Lara E, Arrieta JM, Garcia-Zarandona I, et al (2013) Experimental evaluation of the warming effect on viral, bacterial and protistan communities in two contrasting Arctic systems. Aquat Microb Ecol 70:17–32. doi: 10.3354/ame01636

Li H, Durbin R (2009) Fast and accurate short read alignment with Burrows-Wheeler transform. Bioinformatics 25:1754–1760. doi: 10.1093/bioinformatics/btp324

Li WKW, Carmack EC, McLaughlin FA, et al (2013) Space-for-time substitution in predicting the state of picoplankton and nanoplankton in a changing Arctic Ocean. J Geophys Res Ocean 118:5750–5759. doi: 10.1002/jgrc.20417

Li WKW, McLaughlin FA, Lovejoy C, Carmack EC (2009) Smallest algae thrive as the arctic ocean freshens. Science (80-) 326:539. doi: 10.1126/science.1179798

Loeng H (2005) Chapter 9: Marine Systems. In: Arctic Climate Impact Assessment. Cambridge University Press, Cambridge, UK, pp 453–538

Long AM, Short SM (2016) Seasonal determinations of algal virus decay rates reveal overwintering in a temperate freshwater pond. ISME J 10:1602–1612. doi: 10.1038/ismej.2015.240

Lovejoy C, Vincent WF, Bonilla S, et al (2007) Distribution, phylogeny, and growth of cold-adapted picoprasinophytes in Arctic seas. J Phycol 43:78–89. doi: 10.1111/j.1529-8817.2006.00310.x

Ludwig W, Strunk O, Westram R, et al (2004) ARB: A software environment for sequence data. Nucleic Acids Res 32:1363–1371. doi: 10.1093/nar/gkh293

Luhtanen AM, Eronen-Rasimus E, Kaartokallio H, et al (2014) Isolation and characterization of phage-host systems from the Baltic Sea ice. Extremophiles 18:121–130. doi: 10.1007/s00792-013-0604-y

Maat DS, de Blok R, Brussaard CPD (2016) Combined phosphorus limitation and light stress prevent viral proliferation in the phytoplankton species *Phaeocystis globosa*, but not in *Micromonas pusilla*. Front Mar Sci. doi: 10.3389/fmars.2016.00160

Marie D, Brussaard CPD, Thyrhaug R, et al (1999) Enumeration of marine viruses in culture and natural samples by flow cytometry. Appl Environ Microbiol 65:45–52

Martínez Martínez J, Boere A, Gilg I, et al (2015) New lipid envelope-containing dsDNA virus isolates infecting *Micromonas pusilla* reveal a separate phylogenetic group. Aquat Microb Ecol 74:17–28. doi: 10.3354/ame01723

Mayer JA, Taylor FJR (1979) A virus which lyses the marine nanoflagellate *Micromonas pusilla*. Nature 281:299–301. doi: 10.1038/281299a0

McKie-Krisberg ZM, Sanders RW (2014) Phagotrophy by the picoeukaryotic green alga *Micromonas*: Implications for Arctic Oceans. ISME J 8:1953–1961. doi: 10.1038/ismej.2014.16

Metfies K, Von Appen WJ, Kilias E, et al (2016) Biogeography and photosynthetic biomass of arctic marine pico-eukaroytes during summer of the record sea ice minimum 2012. PLoS One 11:1–20. doi: 10.1371/journal.pone.0148512

Mojica KDA, Brussaard CPD (2014) Factors affecting virus dynamics and microbial host - virus interactions in marine environments. FEMS Microbiol Ecol 89:495–515. doi: 10.1111/1574-6941.12343

Mustapha S Ben, Larouche P, Dubois JM (2016) Spatial and temporal variability of sea-surface temperature fronts in the coastal Beaufort Sea. Cont Shelf Res 124:134–141. doi: 10.1016/j.csr.2016.06.001

Nagasaki K, Shirai Y, Tomaru Y, et al (2005) Algal viruses with distinct intraspecies host specificities include identical intein elements. Appl Environ Microbiol 71:3599–3607. doi: 10.1128/AEM.71.7.3599-3607.2005

Nagasaki K, Yamaguchi M (1998) Effect of temperature on the algicidal activity and the stability of HaV (*Heterosigma akashiwo* virus). Aquat Microb Ecol 15:211–216. doi: 10.3354/ame015211

Not F, Latasa M, Marie D, et al (2004) A single species, *Micromonas pusilla* (Prasinophyceae), dominates the eukaryotic picoplankton in the Western English Channel. Appl Environ Microbiol 70:4064–4072. doi: 10.1128/AEM.70.7.4064

Not F, Massana R, Latasa M, et al (2005) Late summer community composition and abundance of

photosynthetic picoeukaryotes in Norwegian and Barents Seas. Limnol Oceanogr 50:1677–1686. doi: 10.4319/lo.2005.50.5.1677

Olsen RH (1967) Isolation and growth of psychrophilic bacteriophage. Appl Microbiol 15:198. doi: 10.1128/aem.15.1.198-.1967

Olsen RH, Siak J-S, Gray RH (1974) Characteristics of PRD1, a plasmid-dependent broad host range DNA bacteriophage. J Virol 14:689–699. doi: 10.1128/jvi.14.3.689-699.1974

Pagarete A, Chow CET, Johannessen T, et al (2013) Strong seasonality and interannual recurrence in marine myovirus communities. Appl Environ Microbiol 79:6253–6259. doi: 10.1128/AEM.01075-13

Passmore R., Hsu J., Liu RX., et al (2000) MPN Assay Analyzer. Available online: http://www.webcitation.org/6ogxAqLbE (accessed on 3 March 2017)

Payet JP, Suttle CA (2014) Viral infection of bacteria and phytoplankton in the Arctic Ocean as viewed through the lens of fingerprint analysis. Aquat Microb Ecol 72:47–61. doi: 10.3354/ame01684

Richter-Menge J, Mathis J (2016) The Arctic. In: State of the climate in 2015. Bull Am Meteorol Soc 97:S131–S153

Romari K, Vaulot D (2004) Composition and temporal variability of picoeukaryote communities at a coastal site of the English Channel from 18S rDNA sequences. Limnol Oceanogr 49:784–798. doi: 10.4319/lo.2004.49.3.0784

Sahlsten E (1998) Seasonal abundance in Skagerrak-Kattegat coastal waters and host specificity of viruses infecting the marine photosynthetic flagellate *Micromonas pusilla*. Aquat Microb Ecol 16:103–108. doi: 10.3354/ame016103

Sievers F, Wilm A, Dineen D, et al (2011) Fast, scalable generation of high-quality protein multiple sequence alignments using Clustal Omega. Mol Syst Biol 7:. doi: 10.1038/msb.2011.75

Simon N, Foulon E, Grulois D, et al (2017) Revision of the genus *Micromonas* Manton et Parke (Chlorophyta, Mamiellophyceae), of the type species *M. pusilla* (Butcher) Manton & Parke and of the species *M. commoda* van Baren, Bachy and Worden and description of two new species base. Protist 168:612–635. doi: 10.1016/j.protis.2017.09.002

Šlapeta J, López-García P, Moreira D (2006) Global dispersal and ancient cryptic species in the smallest marine eukaryotes. Mol Biol Evol 23:23–29. doi: 10.1093/molbev/msj001

Stamatakis A (2014) RAxML version 8: A tool for phylogenetic analysis and post-analysis of large phylogenies. Bioinformatics 30:1312–1313. doi: 10.1093/bioinformatics/btu033

Sunagawa S, Coelho LP, Chaffron S, et al (2015) Structure and function of the global ocean microbiome. Science (80-) 348:1–10. doi: 10.1126/science.1261359

Suttle CA (2007) Marine viruses — major players in the global ecosystem. Nat Rev Microbiol 5:801–812. doi: 10.1038/nrmicro1750

Suttle CA, Cottrell MT (1995) Dynamics of a lytic virus infecting the photosynthetic marine picoflagellate *Micromonas pusilla*. Limnol Oceanogr 40:730–739

Tarutani K, Nagasaki K, Yamaguchi M (2000) Viral impacts on total abundance and clonal composition of the harmful bloom-forming phytoplankton *Heterosigma akashiwo*. Appl Environ Microbiol 66:4916–4920. doi: 10.1128/AEM.66.11.4916-4920.2000

Timmermans M-L (2016) Sea surface temperature. In Arctic Report Card. Available online: http://www. webcitation.org/6ogrhzGOI (accessed on 3 March 2017)

Tomaru Y, Katanozaka N, Nishida K, et al (2004) Isolation and characterization of two distinct types of HcRNAV, a single-stranded RNA virus infecting the bivalve-killing microalga *Heterocapsa circularisquama*. Aquat Microb Ecol 34:207–218. doi: 10.3354/ame034207

Tomaru Y, Tanabe H, Yamanaka S, Nagasaki K (2005) Effects of temperature and light on stability of microalgal viruses, HaV, HcV and HcRNAV. Plankt Biol Ecol 52:1–6

Toseland A, Daines SJ, Clark JR, et al (2013) The impact of temperature on marine phytoplankton resource allocation and metabolism. Nat Clim Chang 3:979–984. doi: 10.1038/nclimate1989

Tverberg V, Nilsen F, Goszczko I, et al (2008) The warm winter temperatures of 2006 and 2007 in the Kongsfjorden water masses compared to historical data. 8th Ny-Ålesund Sci Manag Comm 40–43

van Baren MJ, Bachy C, Reistetter EN, et al (2016) Evidence-based green algal genomics reveals marine diversity and ancestral characteristics of land plants. BMC Genomics 17:1–22. doi: 10.1186/s12864-016-2585-6

Waters RE, Chan AT (1982) *Micromonas pusilla* virus: the virus growth cycle and associated

6

physiological events within the host cells; host range mutation. J Gen Virol 63:199–206. doi: 10.1099/0022-1317-63-1-199

Wells LE (2008) Cold-active viruses. In: Margesin R, Schinner F, Marx J-C, Gerday C (eds) Psychrophiles: From biodiversity to biotechnology. Springer Berlin Heidelberg, pp 157–173

Wells LE, Deming JW (2006a) Modelled and measured dynamics of viruses in Arctic winter sea-ice brines. Environ Microbiol 8:1115–1121. doi: 10.1111/j.1462-2920.2006.00984.x

Wells LE, Deming JW (2006b) Characterization of a cold-active bacteriophage on two psychrophilic marine hosts. Aquat Microb Ecol 45:15–29. doi: 10.3354/ame045015

Wilson WH, Van Etten JL, Allen MJ (2009) The Phycodnaviridae: The story of how tiny giants rule the world. Curr Top Microbiol Immunol 328:1–42. doi: 10.1007/978-3-540-68618-7-1

Worden AZ, Lee J-H, Mock T, et al (2009) Green evolution and dynamic adaptations revealed by genomes of the marine picoeukaryotes *Micromonas*. Science (80-) 324:268–272. doi: 10.1126/science.1167222

Zachary A (1978) An ecological study of bacteriophages of *Vibrio natriegens*. Can J Microbiol 24:321–324. doi: 10.1139/m78-053

Zingone A, Sarno D, Forlani G (1999) Seasonal dynamics in the abundance of *Micromonas pusilla* (Prasinophyceae) and its viruses in the Gulf of Naples (Mediterranean Sea). J Plankton Res 21:2143–2159. doi: 10.1093/plankt/21.11.2143
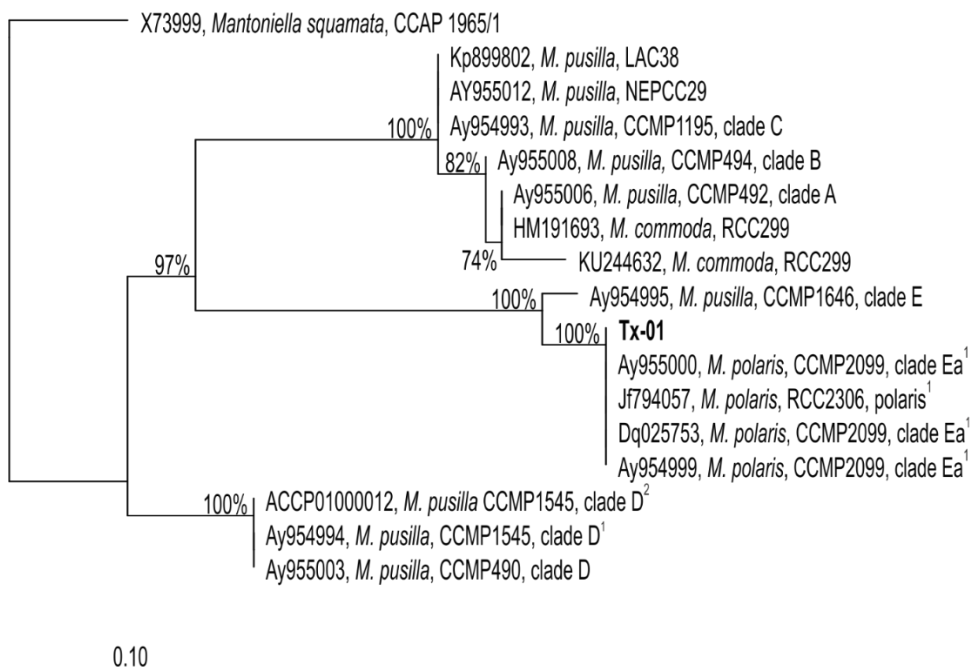
Supplementary Figures

Fig. S1. Position of strain TX-01 in a Maximum-Likelyhood dendrogram of 18S rRNA sequences (1574 valid columns) of *Micromonas* strains with clade designations A-E from Šlapeta et al. (2006) and Ea from Lovejoy et al. (2007). The letter M. stands for the genus *Micromonas*. [1]Simon et al. (2017), [2]van Baren et al. (2016).
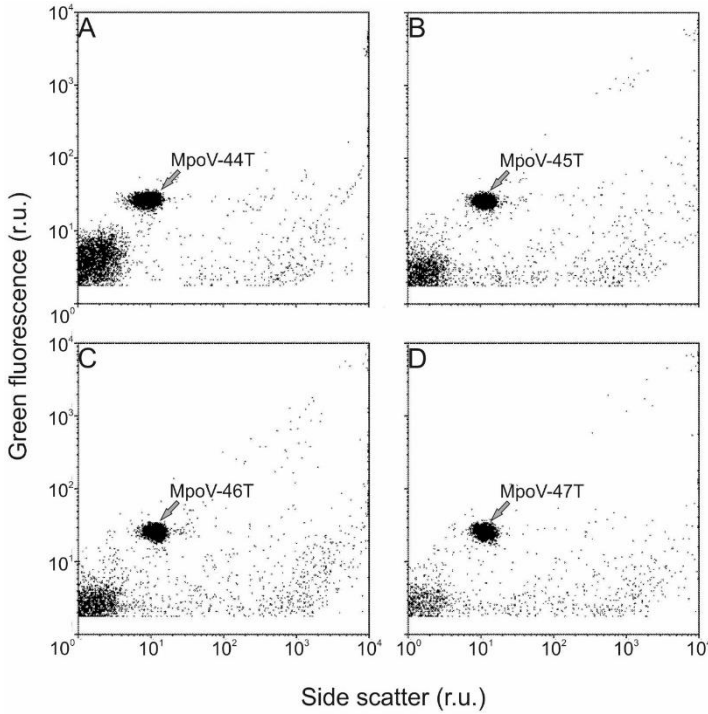
Fig. S2. Flow cytograms of the four *Micromonas* virus strains MpoV-44T, 45T, 46T and 47T (A, B, C, D) with green fluorescence on the Y-axis and side scatter on the X-axis. The grey arrow, which is on the same location in each plot, indicates the MpV cluster.
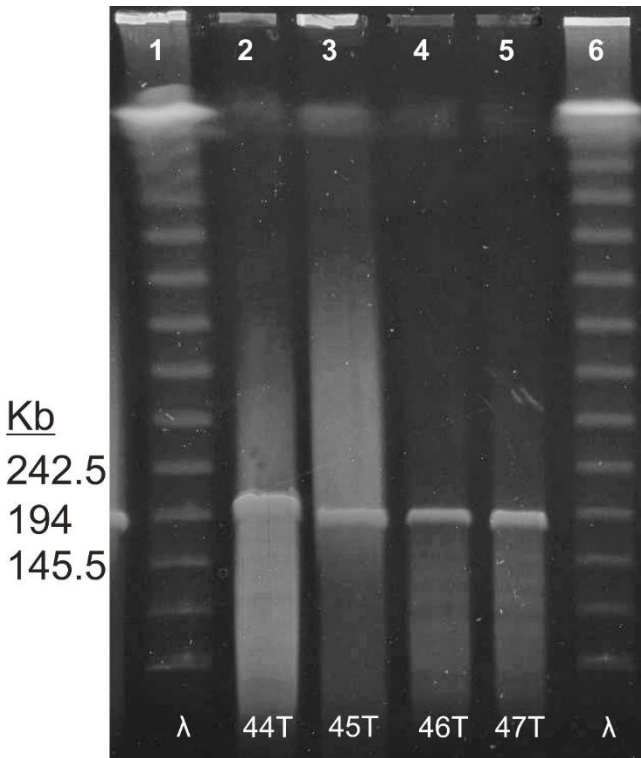

Fig. S3. Photograph of a Pulse Field Gel Electrophoresis (PFGE) gel for viral genome size estimation. The virus isolates MpoV-44T to 47T are depicted below lanes 2 to 5. The DNA Lambda ladder is shown in lane 1 and 6 (indicated λ symbol), with the relevant band sizes in Kb on the left.
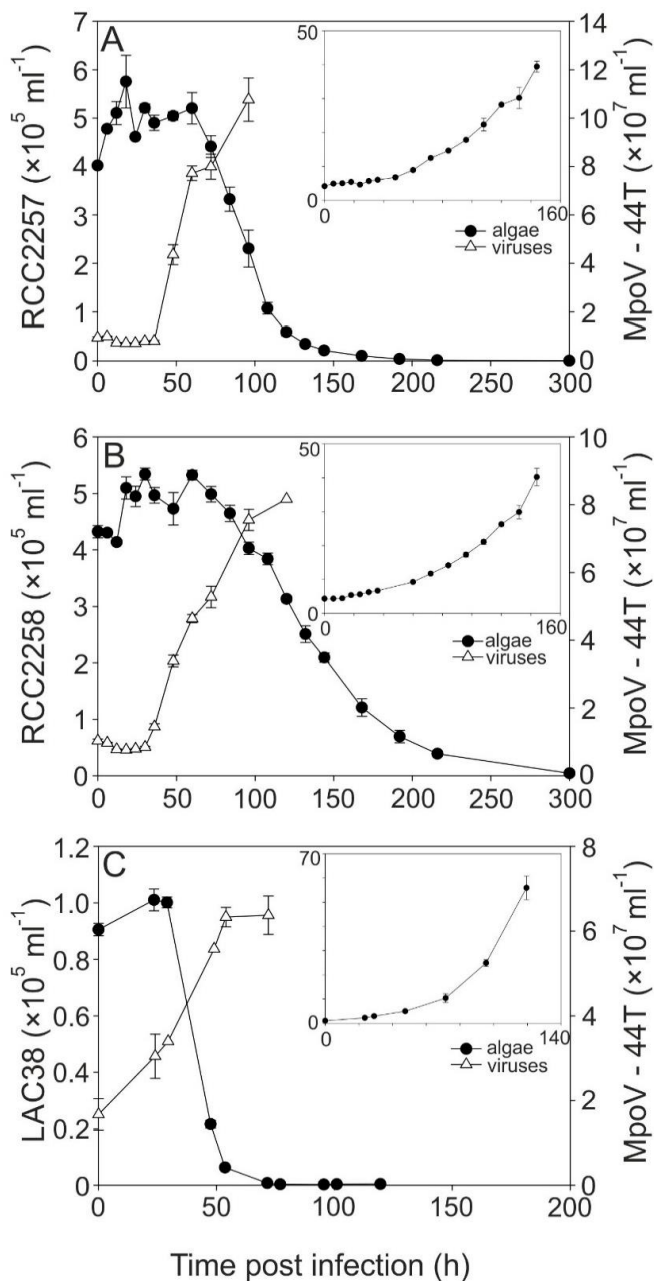
6

Fig. S4. Growth curves of the infection cycle of MpoV-44T infecting *M. polaris* RCC2257 (A), *M. polaris* RCC2258 (B) and *M. commoda* LAC38 (C) as illustration of MpoV-44T - host combinations that do not show the growth extent of the infected TX-01 infected with this virus. Algal cell abundances (mean ± s.d.; $n=3$) are depicted as filled circles, of which the temporal dynamics of the infected cultures are shown in the main panel and those of the of the non-infected controls in the inlay panel. Viral abundances (mean ± s.d.; $n=3$) over time are depicted as open triangles. Invisible error bars fall within the symbol.

Supplementary Tables

Table S1. Phytoplankton genera and species from different phyla that were tested for infection by the Arctic *Micromonas* virus isolates MpoV-44T, 45T, 46T and 47T. In none of the cultures occurred lysis. Cultures were maintained at 3 °C (except for *Ostreococcus* which was cultured at 15 °C) in MIX-TX medium at 16:8h light:dark and 70–90 µmol quanta m^{-2} s^{-1} (see for details Materials & Methods).
Species depicted with TX* are from the Netherlands Institute for Sea Research (NIOZ) TX culture collection and were isolated from Kongsfjorden at the same time as *Micromonas* TX-01. RUG** is from the culture collection of the University of Groningen (RuG), The Netherlands.

Phytoplankton species	Location of isolation
Phaeocystis sp. CCMP1374	Southern Ocean
Phaeocystis antarctica CCMP1871	Southern Ocean
Imantonia sp. TX*	Kongsfjorden
Chrysochromulina sp. CCMP1215	Bellingshausen Sea
Chlamydomonas sp. CCMP681	Bellingshausen Sea
Pyramimonas sp. RuG**	Southern Ocean
Rhodomonas sp. TX*	Kongsfjorden
Proboscia alata TX22	Southern Ocean
Chaetoceros debilis TX20	Southern Ocean
Chaetoceros brevis TX21	Kongsfjorden
Thallassiosira hispida TX*	Kongsfjorden
Porosira glacialis CCMP650	Narragansett Bay
Ostreococcus tauri RCC745	Mediterranean Sea

6

Table S2: *P*-values of the burst size differences between groups, as tested by 1-way ANOVAs, to demonstrate inter- and intra-strain differences (e.g. for RCC2257 increasing temperature leads to significantly increased burst sizes of both viruses, but for RCC2258 this is only found for MpoV-45T). For each host strain, the effect of the used virus (44T x 45T) or temperature (3 °C x 8 °C) on burst size was tested within each separate treatment. Significant differences are depicted in bold.

	3 °C 44T x 45T	8 °C 44T x 45T	44T 3°C x 8°C	45T 3°C x 8°C
TX-01	0.493	-	-	-
RCC2257	0.130	0.855	**0.044**	**0.045**
RCC2258	**0.008**	**<0.001**	0.227	**0.003**

Table S3. Top 3 BLASTN hits of the isolates against KEGG environmental metagenomes with relevant information on sampling location and temperature. OSD: Ocean Sampling Day; TARA: TARA Oceans.

Isolate	Campaign	Region	Year	Temp (°C)	Identity	Sample
MpV46T	OSD	Greenland Sea	2014	−1.6	85%	OSD146_2014-06-21_5m_NPL022
	TARA	Southern Ocean	2001	−0.8	84%	85_DCM_0d2-3
	TARA	North Atlantic	2003	17.3	83%	151_SUR_0d2-3
MpV45T	OSD	Greenland Sea	2014	10.1	83%	OSD130_2014-06-21_1m_NPL022
	OSD	North Atlantic	2014	12.8	88%	OSD152_2014-06-20_1m_NPL022
	TARA	Southern Ocean	2012	7.3	81%	82_SRF_0d2-3
MpV47T	OSD	North Atlantic	2014	12.8	87%	OSD152_2014-06-20_1m_NPL022
	OSD	Greenland Sea	2014	10.1	82%	OSD130_2014-06-21_1m_NPL022
	TARA	South Atlantic	2012	7.3	80%	82_SRF_0d2-3
MpV44	TARA	Southern Ocean	2001	−0.8	80%	85_DCM_0d2-3
	TARA	South Atlantic	2009	12.8	80%	67_SUR_0d2-0d45
	TARA	North Pacific	2010	13.2	79%	133_DCM_0d2-3

Chapter 7

Plasticity in dormancy behaviour of *Calanoides acutus* in Antarctic coastal waters

Plasticity in dormancy behaviour of *Calanoides acutus* in Antarctic coastal waters

Tristan E.G. Biggs[1,2]; Corina P.D. Brussaard[1,2]; Claire Evans[3]; Hugh J. Venables[4] and David W. Pond[5]

[1] Department of Marine Microbiology and Biogeochemistry, NIOZ Royal Netherlands Institute for Sea Research, and University of Utrecht, Texel, The Netherlands.
[2] Department of Freshwater and Marine Ecology, Institute for Biodiversity and Ecosystem Dynamics (IBED), University of Amsterdam, Amsterdam, The Netherlands.
[3] Ocean Biogeochemistry & Ecosystems Research Group, National Oceanography Centre, Southampton, UK.
[4] British Antarctic Survey, Natural Environmental Research Council, Cambridge, UK.
[5] Institute of Aquaculture, University of Stirling, Stirling, Scotland, UK.

Abstract

Copepods that enter dormancy, such as *Calanoides acutus*, are key primary consumers in Southern Ocean food webs where they convert a portion of the seasonal phytoplankton biomass into a longer term energetic and physiological resource as wax ester (WE) reserves. We studied the seasonal abundance and lipid profiles of pre-adult and adult *C. acutus* in relation to phytoplankton dynamics on the Western Antarctic Peninsula. Initiation of dormancy occurred when WE unsaturation was relatively high and Chl-*a* concentrations, predominantly attributable to diatoms, were reducing. Declines in WE unsaturation during the winter may act as a dormancy timing mechanism with increased Chl-*a* concentrations likely to promote sedimentation which results in a teleconnection between surface and deep water that induces ascent. A late summer diatom bloom was linked to early dormancy termination of females and a second spawning event. The frequency and duration of high biomass phytoplankton blooms may have consequences for the lifespan of the iteroparous *C. acutus* females (either 1 or 2 years) if limited by a total of two main spawning events. Late summer recruits, generated by a second spawning event, likely benefited from lower predation and high phytoplankton food availability. The flexibility of copepods to modulate their life-cycle strategy in response to bottom up and top down conditions enables individuals to optimize their probability of reproductive success in the very variable environment prevalent in the Southern Ocean.

7

Introduction

Lipid rich copepods are important conduits of carbon flow from the base of the marine food web to higher trophic levels and support fish, mammal and seabird communities (Pervushin 1968; Hopkins and Torres 1989; Voronina 1998). At high latitudes, primary production is strongly influenced by the availability of light resulting in distinct phytoplankton bloom cycles and a relatively short productive season (Ma et al. 2014). As the photoperiod increases after the winter minimum, the annual onset of stratification initiates the highly productive phytoplankton 'Spring' bloom (Sverdrup 1953; Huisman et al. 1999). The life cycles of copepods are strongly affected by this distinct seasonality and they have developed specific adaptations to take advantage of short-term food availability in order to survive long periods of food scarcity. Calanoid copepods are an ecologically important order of marine copepods and several species, particularly those in the Calanidae and Eucalanidae families (Baumgartner and Tarrant 2017), undergo ontogenetic vertical migration from relatively shallow to deep water where they spend a large proportion of their life cycle in dormancy (Hagen et al. 1993; Sartoris et al. 2010), a resting stage with reduced metabolism and swimming activity (Maps et al. 2014). To outlast the winter months, these copepods accumulate large lipid stores within a membrane bound oil sac that can occupy a large part of the body cavity (Lee et al. 2006). Not only does this lipid store have to provide fuel for metabolic processes during dormancy, but also it must provide the energy needed to re-ascend to the surface, continue development to adulthood, and fuel early egg production (Pond et al. 2012). As in other oceans, copepods dominate the mesozooplankton across most of the Southern Ocean, in terms of biomass, abundance, grazing activity and secondary production (Atkinson et al. 2012b). *Calanoides acutus* is a major contributor to zooplankton biomass (Shreeve et al. 2005; Marrari et al. 2011) and an abundant species of herbivorous copepod that spends a large proportion of their life cycle (up to 7 – 9 months) in dormancy (Hagen et al. 1993; Drits et al. 1994; Tarling et al. 2004; Atkinson et al. 2012b). Mating occurs in deep water during late winter and the males perish shortly after while the females migrate to surface waters to feed on the

phytoplankton bloom and begin spawning at the start of spring/summer. Nauplii and early copepodites develop in the euphotic zone until vertical migration to deeper water of pre-adult (CIV and CV) and adult (CVI) stages at the end of summer when feeding in surface waters is terminated (Atkinson et al. 1997; Tarling et al. 2004). Little is known about the life span of overwintered late stage copepodites with some studies suggesting a 1 year life cycle (Marin 1988; Atkinson et al. 1997) whilst others suggest that individuals may re-enter dormancy and survive an extra year (Drits et al. 1994; Hagen and Schnack-Schiel 1996).

Prior to dormancy, overwintering stages concentrate phytoplankton lipids and accumulate large stores of total lipid (TL), mainly as wax esters (WE). High concentrations of TL can be accumulated per individual (>500 µg) representing an energy-rich food source for higher trophic levels (such as fish) and a large reservoir of essential fatty acids such as 20:5(n-3) (eicosapentaenoic acid, EPA) and 22:6(n-3) (docosahexaenoic acid, DHA). This accumulation of lipids represents the long-term storage of short term phytoplankton production. The presence or absence of copepod species that enter dormancy plays a fundamental role on a global scale in determining whether or not a region supports a lipid-rich food web (Record et al. 2018). The timing and duration of dormancy has implications for carbon flow as ontogenetic vertical migration events (VMEs) dictate time periods when stored lipids (carbon) are either available in surface waters or sequestered to the deep ocean due to respiration during dormancy (Jónasdóttir et al. 2015). Potential triggers influencing vertical distribution patterns have been identified, such as lipid accumulation above a threshold level (Rey-Rassat et al. 2002; Maps et al. 2012) and utilization during dormancy (Johnson et al. 2008), however, cues remain poorly understood and seasonal datasets are scarce. Following the development of a population over an entire lifecycle could provide a better understanding how these mechanisms influence behaviour. Pond et al. (2012) showed that a critical minimum threshold of ~ 50 % WE unsaturation within the copepod is important for dormancy initiation. The composition of these lipids, and not the bulk amount, then provides the ability of the WE store to shift from a liquid to a solid phase allowing dormant

7

copepods to become neutrally buoyant in cold deep water and conserve energy (Visser and Jónasdóttir 1999; Lee et al. 2006; Pond and Tarling 2011). Although copepod species that enter a period of dormancy have evolved in the open ocean, where such a strategy could provide a key evolutive advantage, genetic programming of individuals that inhabit relatively shallow coastal and shelf sea environments is likely to result in accumulation of large WE reserves with high levels of unsaturation (Falk-Petersen et al. 2009; Clark et al. 2012). As the FA component of WE is mainly derived from the diet, a suitable food source is critical. High proportions of FA 16:1(n-7), 20:5(n-3), 18:4(n-3) and 22:6(n-3) in storage lipids indicate the importance of diatoms and dinoflagellates in the zooplankton diet (Graeve et al. 1994; Falk-Petersen et al. 2000; Budge et al. 2006). Diatoms often dominate the biomass of phytoplankton blooms in the Southern Ocean (Ducklow et al. 2012) and are an important source of primary nutrition as they produce long chain polyunsaturated fatty acids (such as 20:5(n-3)) in abundance (Kattner and Hagen 2009). The timing and duration of blooms varies spatially and temporally, as a result of physicochemical factors, and could help explain why the timing of descent in dormancy inducing copepods can be so variable between regions and years (Heath et al. 2004; Johnson et al. 2008; Pepin and Head 2009). More research is required to better understand the trophic transfer of lipids, particularly in a time of global climate change shown to affect the composition, timing and magnitude of phytoplankton blooms (Smetacek and Nicol 2005; Sommer and Lengfellner 2008; Rozema et al. 2017). These changes are expected to have major implications for the capacity of copepods to undertake their seasonal life cycles successfully (Pond et al. 2014). Understanding population dynamics is fundamental to predict how copepods might respond to future climate change and how Antarctic ecosystems may be influenced by bottom-up forcing.

In this study, in Ryder Bay on the Western Antarctic Peninsula, the lipid content and composition of *C. acutus* individuals (the pre-adult CV, and adult CVI) were analysed over a 'summer (S1) - winter - summer (S2)' time series and the FA composition was determined to investigate links between the accumulation and

composition of WE and diet. Research in the Southern Ocean often focuses on copepods inhabiting the deep-water open ocean (> 500 - 1000 m depth), however, many populations successfully overwinter in relatively shallow coastal and shelf-sea environments (< 500 m depth; Clark et al. 2012). Ryder Bay is a marginal habitat that is relatively advection free due to localized gyre like circulation features (Beardsley et al. 2004; Moffat et al. 2008; personal observation) which promotes the retention of phytoplankton and zooplankton populations. This study, that repeatedly sampled the same population in the same local area, is one of very few that presents complete seasonal sampling, including winter and the transition periods between winter and the productive summer, and provides valuable information to better understand the behaviour of copepods in a coastal environment.
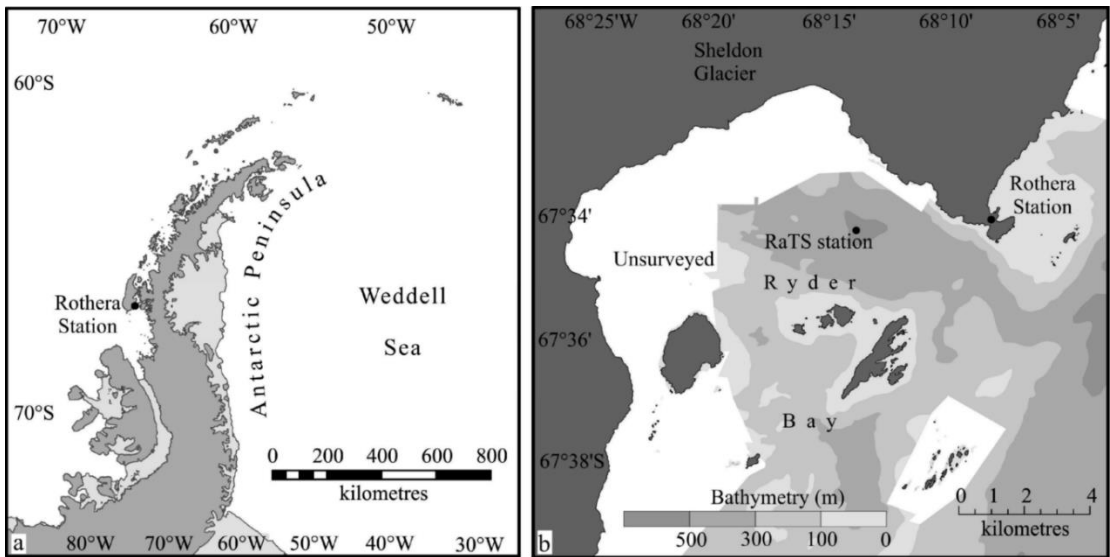

Fig. 1. Map of the sampling area: (a) location of Rothera station on the northern tip of Marguerite Bay along the Western Antarctic Peninsula (b) large scale map of the sampling site (RaTS) within Ryder Bay and close to Rothera station.

Methods

Sample collection

This study was conducted at the Rothera time series site (RaTS, latitude 67.572°S; longitude 68.231°W, bottom depth 520 m) in Ryder Bay on the Western Antarctic Peninsula (Fig. 1). Seawater samples for Chlorophyll-*a* (Chl-*a*) concentration and taxonomic composition analysis were collected from the standard monitoring depth of 15 m by using a 12 L Niskin bottle deployed from a small boat. One to eight liters were filtered over GF/F glass fiber filters (47mm, Whatman, Eindhoven, The Netherlands), after which the filters were carefully folded and wrapped in aluminium foil, snap-frozen in liquid nitrogen and stored at -80°C until analysis in the home laboratory using high performance liquid chromatography (HPLC) and chemical taxonomy analysis (CHEMTAX, see Biggs et al. 2019 for methodological details).

Calanoides acutus samples were collected from 2 depth profiles, i.e. 500-200 m (deep) and 200-0 m (shallow), to separate the overwintering 'winter' population from the active 'summer' population (Huntley and Escritor 1991; Schnack-Schiel et al. 1991). A 200 µm mesh ring net (0.26 m^2 opening) was used to obtain population abundance counts (copepodite stages CI – CVI) in shallow water and a 500 µm mesh ring net (0.26 m^2 opening equipped with a double release mechanism) was used to obtain CV (pre-adult) and CVI (adult males and females) individuals from both shallow and deep water. Sampling of copepods occurred weekly (weather dependent) during summer 1 (S1, November 23rd 2012 to 18th April 2013) and summer 2 (S2, 14th November 2013 to 21st February 2014). In order to include community dynamics year round, sampling was performed on three occasions during 'winter'. Zooplankton were kept in a plastic portable cooler and transported back to the laboratory within 2 h of capture. *Calanoides acutus* in good condition were quickly sorted for lipid analysis using a binocular microscope and the remainder (of the net haul) preserved in 200 mL formaldehyde (5 % final concentration) and stored at 4 °C. Formaldehyde preserved zooplankton samples were split (1/3) using a plankton splitter and abundances determined using a binocular microscope.

Lipid analysis

A total of 331 samples of *C. acutus* were collected for lipid analysis consisting of 1635 individuals. Lipids were extracted from stage CV and CVI (male and female) following Pond and Tarling (2011). Individuals and bulk samples were initially transferred to 1.1 mL tapered vials (Chromacol) containing 500 µL of chloroform : methanol (2:1 v:v) and stored at -80 °C. After transport to the home laboratory, the solvent containing each *C. acutus* sample was pipetted into 8 mL glass vials using glass pipettes. The 1.1 mL vials (containing the exoskeleton) were briefly re-extracted and vortexed a further three times with 1 mL chloroform : methanol (2:1 v:v) and the final volume adjusted to 4 mL. After the addition of 1 mL of potassium chloride (0.88 % w:v), samples were vortexed and centrifuged for 2 min at 400 x g to promote phase separation. The lower chloroform phase, containing the total lipid (TL) extract, was removed using Hamilton glass syringes containing a Teflon tipped plunger, into pre-weighed 4 mL glass vials before being evaporated under nitrogen and stored in a vacuum desiccator overnight prior to reweighing.

Lipid class analysis

Aliquots of total lipid (10 µg) were subjected to high-performance thin-layer chromatography (HPTLC) using a hexane : 4 diethyl ether : acetic acid (90 : 10 : 1) solvent system (Pond and Tarling 2011). The plates were sprayed with 8 % (v : v) phosphoric acid containing 3 % (w : v) copper acetate solution, followed by heating at 160 °C for 13 min to char the lipid classes and create dark areas on the HPTLC plate. Lipid classes were then quantified by scanning densitometry (Shimadzu Dual-wavelength TLC Scanner, CS-930), the different lipid classes being identified by comparison with known standards (Pond et al. 1995). The degree of wax ester (WE) unsaturation was used to calculate an unsaturation index as described in Pond and Tarling (2011). In short, HPTLC separated the wax esters into two bands: the upper band was rich in saturated fatty and monounsaturated fatty acids, whereas the lower band was dominated by polyunsaturated fatty acids (PUFAs). The unsaturation index was calculated by dividing the amount of PUFA wax ester by the total wax ester,

7

providing an index of the degree of unsaturation ranging between 0 and 1.0 (Stevens et al. 2004) and presented as a percentage between 0 – 100 %.

Fatty acid analysis of total lipid

Dried aliquots of 150 µg of TL were used for fatty acid (FA) analysis. Samples were derivatised with 1 mL of 2 % sulfuric acid – methanol (after the addition of standards: 5 µg 19:0 and 1 µg 12:0) and incubated for 4 hours at 80 °C. After cooling in water, 2 mL Milli-Q water and 2 mL hexane was added, vortexed and the upper layer transferred to a 10 mL glass vial. Two milliliters of hexane were added once more, vortexed, and the upper layer transferred to a 10 mL glass vial. The sample containing the fatty acid methyl esters (FAMEs) was transferred in 200 µL hexane to a 2 mL vial and stored at -20 °C until analysis on a ULTRA Trace gas chromatograph (GC). The GC was equipped with a BPX-70 column with hydrogen as the carrier gas.

Statistics

Comparisons of fatty acid and wax ester unsaturation data were performed by linear regression in SigmaPlot V14.0 (Systat Software Inc., San Jose California, USA).

Results

Two main periods of phytoplankton accumulation occurred in S1 (2012 – 2013), 30th November – 2nd January and 11th February – 15th April (Fig. 2), as indicated by chlorophyll-*a* (Chl-*a*) dynamics, which were both dominated by diatoms (86 ± 14 % $n = 13$ and 88 ± 19 % $n = 17$, of total Chl-*a* respectively; Biggs et al. 2019). Female *C. acutus* are important for population growth (due to spawning) and contributed most across all time points to populations in both shallow (37 ± 40 %, $n = 32$) and deep (61 ± 33 %, $n = 28$) water. At the start of S1, females were the most abundant stage and only found in deep water (Fig. 3a, b) until the abundance of females inhabiting shallow waters (shallow female) increased between 30 Nov and 12 Dec (Fig. 3b), from 4 to 108 ind 100 m^{-3}, indicating the first ontogenetic vertical
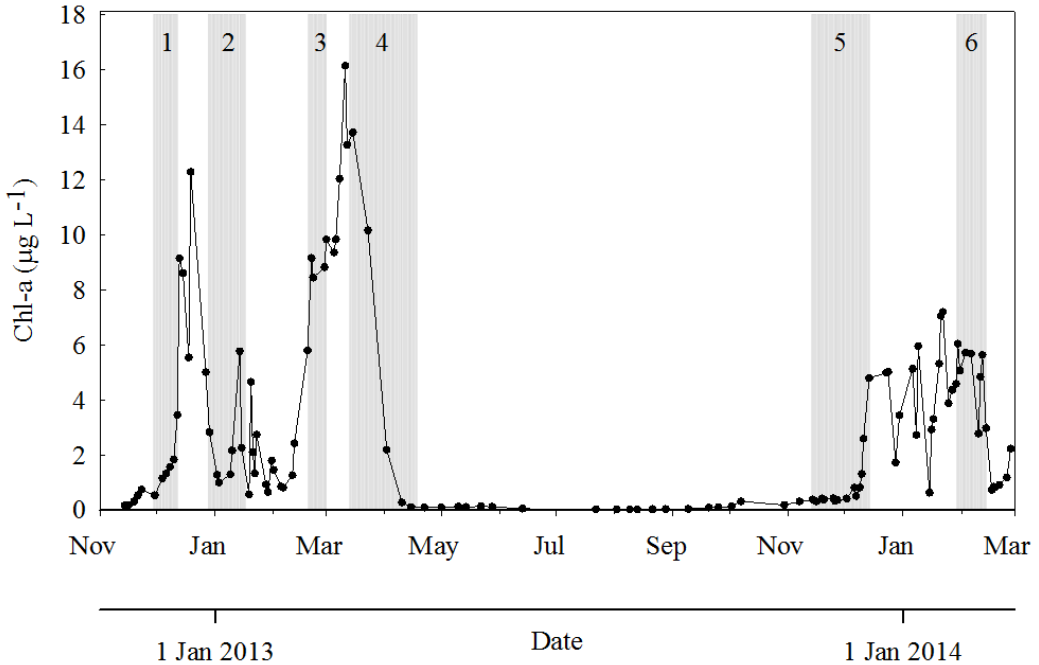
Fig. 2. Time series of chlorophyll *a* (Chl-*a*, as measured by HPLC) at 15 m depth at the sampling site in Ryder Bay. Dashed lines separate time periods of: Summer 1 (S1) from 23rd November 2012 to 18th April 2013; Winter (W) from 19th April 2013 to 13th November 2013 and Summer 2 (S2) from 14th November 2013 to 21st February 2014. Shaded areas (grey) represent time periods of vertical migration events 1 – 6 as indicated by numbers (1 – 6) at the top of the chart.

migration event (VME 1) of S1 and post winter dormancy termination. The increase in shallow female abundance coincided with a decline in numbers of females inhabiting deep waters (deep females, from 44 to 4 ind 100 m^{-3}) at the same time as rapidly increasing Chl-*a* concentrations (from 0.5 to 3.5 µg L^{-1}, Fig. 2). Following the decline of the initial phytoplankton bloom at the beginning of January in S1 (Fig. 2), shallow female numbers began to decline at the same time as a rise in the number of deep females (0 to 18 ind 100 m^{-3}, Fig. 3a), and deep CVs (0 to 9 ind 100 m^{-3}, Fig. 3c), indicating VME 2 (29 Dec to 17 Jan) and the descent of individuals to deep water (dormancy initiation). The number of deep females continued to increase until a steep decline between 20 Feb and 2 Mar (from 30 to 8 ind 100 m^{-3}, Fig. 3a) alongside a brief increase in shallow female abundance (from 8 to 33 ind 100 m^{-3}, Fig. 3b) and indicated a third VME (VME 3) and the second ascent of females in S1
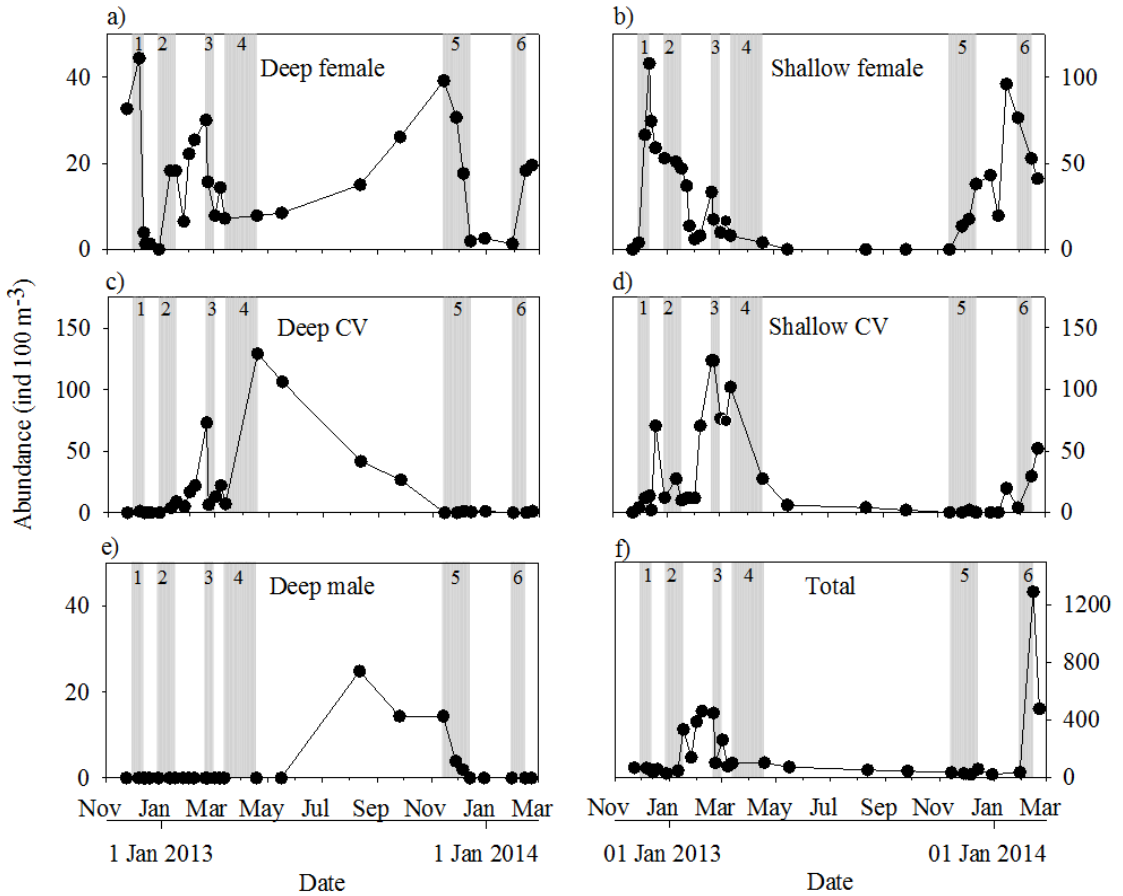
Fig. 3. Temporal dynamics of *C. acutus* abundance (ind 100 m^{-3}). Deep refers to individuals collected between 500 – 200 m depth and shallow between 200 – 0 m. Shaded areas (grey) represent time periods of vertical migration events 1 – 6. (a) the abundance of deep females, (b) the abundance of shallow females, (c) the abundance of deep CVs, (d) the abundance of shallow CVs, (e) the abundance of deep males and (f) total population abundance (stages CI – CVI). Note: different Y-axis scales between subplots.

(dormancy termination). Chlorophyll *a* concentrations had been increasing for 2 weeks prior to VME 3 (from 0.81 to 5.79 µg L^{-1}) and a high biomass phytoplankton bloom (max = 16 µg Chl-*a* L^{-1}) developed over a period of 2 months (Fig. 2). Copepodite stage CV was, overall, the second most dominant life-cycle stage contributing on average 22 ± 27 % *n* = 28 to total numbers. At the beginning of S1, CVs were absent from net hauls (Fig. 3c, d) and numbers remained relatively low until a rapid increase in the abundance of CVs inhabiting shallow waters (shallow
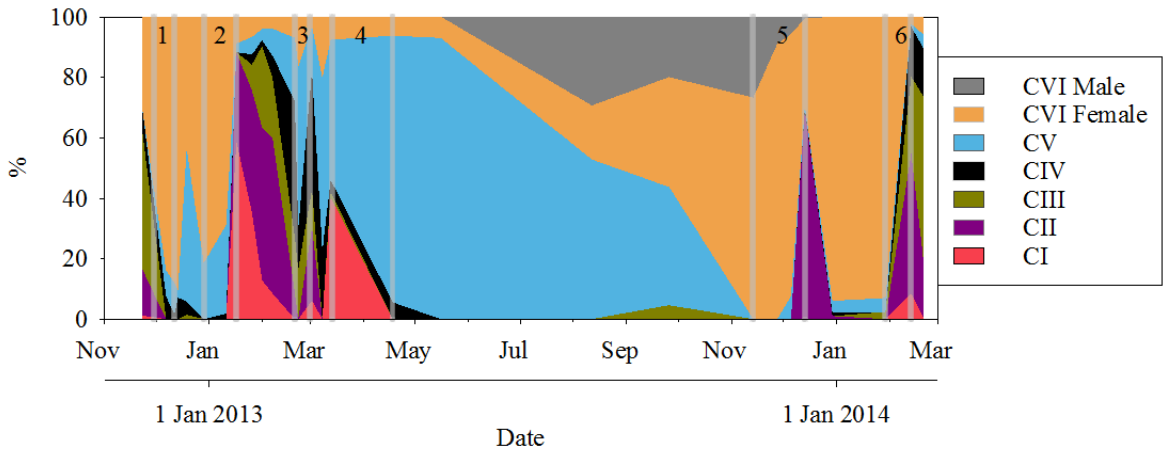
Fig. 4. Relative abundance of stage separated *C. acutus* (CI – CVI), with shallow and deep individuals combined, over the study period at the sampling site in Ryder Bay. Grey lines represent time periods (beginning and end) of vertical migration events 1 – 6, indicated at the top of the chart.

CVs) between 1 and 20 Feb (from 12 to 123 ind 100 m^{-3}, Fig. 2d), 7 - 10 weeks after the peak in abundance of shallow females during VME 1. Numbers of shallow CVs remained high until 13 Mar (Fig. 3d) and declined at the same time as increasing numbers of CVs found in deep water (deep CVs, from 7 to 129 ind 100 m^{-3}, Fig. 3c) indicating a fourth VME (VME 4, 13 Mar to 18 Apr) and the start of the CV overwintering period (dormancy initiation). Chlorophyll *a* concentrations during this late season diatom bloom peaked on 12 Mar and declined thereafter, until low concentrations on 15 Apr (Fig. 2) indicated the end of the phytoplankton productive season.

At the beginning of the winter dormancy period (18 Apr) CVs contributed 88 % to total population abundance (Fig. 4). A steady decline in the number of deep CVs was observed until 14 Nov (down to 0 ind 100 m^{-3}, Fig. 3c), at the same time as a steady rise in the number of deep females (up to 39 ind 100 m^{-3}, Fig. 3a) and indicates the maturation of copepodites from CV to CVI stages. The greatest change in ratio of CV : CVI occurred between 16 May and 12 Aug (from 13 to 1) with relatively more males in deep nets on 12 Aug (30 %) than females (18 %, Fig. 4). Male abundance remained high (and only observed in deep water) until 14 Nov and declined thereafter to zero by mid- Dec in S2 (Fig. 3e). A 68 % decline in population

abundance over winter indicates that (in retrospect) each female at VME 1 needed to contribute a minimum of 3 (CV) individuals to the population at the start of the overwintering period (VME 4) to maintain population numbers (at VME 5 compared to VME 1) and offset losses during winter. This suggests that generally, even low numbers of females can reconstitute the numbers required to ensure the population long-term viability.

At the beginning of S2 (2013 – 2014), phytoplankton biomass began to slowly increase during Nov and rapidly increased from 0.4 to 4.8 µg L^{-1} between 2 and 14 Dec (Fig.2). One extended period of increased Chl-*a* concentrations followed (2 Dec – 14 Feb) with the phytoplankton community continually dominated by diatoms (83 ± 15 %, of Chl-*a*, *n* = 32; Biggs et al. 2019). Between 14 Nov and 14 Dec, a sharp decline in deep females (39 to 2 ind 100 m^{-3}, Fig. 3a) and increase in shallow females (0 to 38 ind 100 m^{-3}, Fig. 3b) indicated a 5th VME (VME 5) and post winter dormancy termination. Shallow female abundance peaked on 17 Jan (96 ind 100 m^{-3}, Fig. 3b) and declined until the end of S2 (41 ind 100 m^{-3}), however, the number of deep females remained low until an increase between 30 Jan and 14 Feb (from 1 to 18 ind 100 m^{-3}, Fig. 3a) at the same time as declining surface Chl-*a* concentrations (from 5.6 to 0.7 µg L^{-1} between 12 to 17 Feb, Fig. 2). This indicates a 6th VME (VME 6, 30 Jan – 14 Feb) and the descent of females at the end of S2 (dormancy initiation). CVs were absent during S2 until an increase in shallow CVs on 17 Jan (20 ind 100 m^{-3}; Fig. 3d) that continued until the end of the season (52 ind 100 m^{-3} by 21 Feb).

When examining the population dynamics of all *C. acutus* copepodite stages (CI - CVI), a period of increased abundance occurred in S1 between 17 Jan and 2 Mar 2013 (304 ± 144 ind 100 m^{-3}, *n* = 7, Fig. 3f). At the initial increase on 17 Jan (333 ind 100 m^{-3}), a rapid rise in the share of CIs was observed (59 %, Fig. 4) occurring 5 weeks after the peak in shallow females at the beginning of S1 (Fig. 3b). A second rapid increase in the share of CIs occurred on 13 Mar (40 % of total, Fig. 4) when total abundance was lower (97 ind 100 m^{-3}) and 3 weeks after the second peak in numbers of shallow females (33 ind 100 m^{-3}, Fig. 3) on 20 Feb. This indicates 2 rounds of spawning occurred during S1. During S2, population abundance remained

low until a sharp increase on 14 Feb 2014 (1291 ind 100 m^{-3}, Fig. 3f). Only one sharp rise in CI abundance was captured in the dataset during S2 (Fig.4) with 3106 CI - CIV 100 m^{-3} on 14 Feb in S2 (data not shown) appearing one month later than the initial CI increase in S1.

Lipids, wax esters and fatty acids

Wax esters are often the main type of storage lipid in dormancy inducing copepods and generally dominate total lipid (TL) profiles. In this study, the % of TL contained as wax esters was ~ 80% in both females and CVs confirming that WE were the main storage lipid of *C. acutus* individuals (Fig. S1). The TL FA profiles of females were dominated by 20:1(n-9) (18%), 20:5(n-3) (16 %), 20:3(n-3) (11 %), 16:1(n-7)

Table 1. Temporal dynamics of adult female *C. acutus* fatty acids (FA %) per copepod.

	CVI female FA %: Mean (*n* = 29)																	
Month-year	Dec-2012		Jan-2013	Feb-2013	Mar-2013		Apr-2013	May-2013	Aug-2013	Sep-2013	Nov-2013		Dec-2013			Jan-2014		Feb-2014	
Day / FA	19	29	17	20	8	13	18	16	12	26	14	28	6	14	30	17	30	14	21
10:0	6.7	6.4	4.4	4.0	3.0	2.4	0.8	3.1	4.8	3.1		5.1	5.9	7.0	9.1	4.9	3.0	3.4	3.3
14:0	5.6	8.2	3.7	4.2	4.0	3.6	4.7	4.2	4.5	4.0		5.6	5.1	5.5	6.1	3.8	3.5	3.3	3.7
15:0	0.0	0.0	2.6	2.2	2.8	3.2	0.0	2.3	0.0	0.0		0.0	0.0	0.0	0.0	2.5	2.7	3.2	2.0
16:0	4.8	13.1	4.9	4.8	4.3	4.1	9.9	4.5	3.7	4.5		6.1	5.7	5.4	6.2	4.7	4.0	3.7	4.5
16:1(n-7)	8.1	5.7	12.5	13.1	11.4	12.4	9.7	12.4	10.3	8.5		9.7	8.2	8.7	10.7	10.5	8.6	8.6	9.9
16:4(n-1)	0.0	1.7	5.1	3.7	3.5	3.6	1.0	2.0	0.0	0.0		0.0	0.0	0.0	0.0	5.1	4.9	5.5	4.8
17:0	0.0	0.0	2.8	1.5	2.5	3.5	0.0	2.9	0.0	0.0		0.0	0.0	0.0	0.0	2.4	2.7	2.8	2.1
18:1(n-9)	3.9	4.3	4.4	4.5	4.3	4.3	4.6	4.8	4.3	4.8		4.1	4.5	4.9	4.0	3.4	3.9	4.0	4.8
18:1(n-7)	0.2	0.0	0.0	2.2	1.0	1.9	2.7	2.4	0.0	1.9		2.2	1.0	0.0	0.0	0.0	0.0	0.0	0.0
18:4(n-3)	0.0	1.4	4.3	3.6	3.4	4.0	3.5	3.7	0.0	2.0		0.0	0.0	0.0	0.0	3.8	3.7	3.3	3.6
20:1(n-9)	30.2	17.2	14.9	15.5	16.9	14.1	12.3	16.0	26.4	23.8		21.1	24.9	26.5	26.4	12.5	13.1	13.2	15.2
20:3(n-3)	13.2	0.0	6.4	9.0	11.7	12.2	3.8	11.4	13.7	11.1		12.3	13.9	9.7	5.8	12.0	13.4	12.9	9.6
20:4(n-3)	0.0	2.8	1.3	1.0	1.9	2.0	0.0	2.0	2.0	2.4		0.0	0.0	0.0	0.0	2.0	2.2	2.2	1.5
22:1(n-11)	10.1	18.6	6.9	7.3	7.7	6.3	15.9	6.9	11.4	10.5		10.4	10.2	13.1	12.7	6.2	6.2	6.1	6.5
20:5(n-3)	13.4	14.5	18.4	16.1	15.6	15.5	22.6	14.2	13.6	16.8		14.6	13.3	13.0	12.4	19.6	20.5	20.5	21.7
22:6(n-3)	3.8	6.0	7.4	7.4	6.1	6.9	8.5	7.1	5.3	6.6		8.8	7.1	6.1	6.6	6.6	7.5	7.2	6.9
Saturated	17.1	27.7	18.4	16.7	16.6	16.9	15.4	17.1	13.1	11.5		16.8	16.8	17.9	21.4	18.3	16.0	16.3	15.6
Monounsaturated	52.5	45.8	38.7	42.7	41.3	38.9	45.2	42.5	52.4	49.6		47.5	48.9	53.3	53.8	32.7	31.9	32.0	36.3
Polyunsaturated	30.5	26.5	42.8	40.6	42.1	44.2	39.4	40.4	34.6	38.9		35.8	34.3	28.9	24.8	49.0	52.2	51.7	48.1

7

Table 2. Temporal dynamics of pre-adult stage CV *C. acutus* fatty acids (FA %) per copepod.

| CV FA % : Mean ($n = 53$) | | | | | | | | | | | | | | | | | | | |
| Month-year | Dec-2012 | | Jan-2013 | Feb-2013 | Mar-2013 | | Apr-2013 | May-2013 | Aug-2013 | Sep-2013 | Nov-2013 | | Dec-2013 | | | Jan-2014 | | Feb-2014 | |
Day / FA	19	29	17	20	8	13	18	16	12	26	14	28	6	14	30	17	30	14	21
10:0				1.0	2.4	2.2	2.5	2.8	3.8	4.1									
14:0				3.6	2.7	2.8	2.1	2.8	3.6	3.6									
15:0				3.1	1.6	0.0	1.7	0.0	0.0	0.0									
16:0				5.8	4.1	4.0	4.3	6.4	6.3	4.7									
16:1(n-7)				8.2	5.5	5.7	3.6	4.1	5.4	4.8									
16:4(n-1)				4.2	5.1	5.0	5.4	5.9	2.2	0.0									
17:0				3.0	2.8	0.0	2.8	0.0	0.0	2.7									
18:1(n-9)				4.3	3.4	4.0	4.4	3.5	4.3	4.3									
18:1(n-7)				3.0	1.0	1.0	0.7	0.0	0.0	0.0									
18:4(n-3)				4.0	3.7	3.7	3.8	3.7	2.8	0.0									
20:1(n-9)				13.4	15.8	19.2	17.7	27.3	21.7	25.0									
20:3(n-3)				9.0	13.0	11.9	9.5	2.7	7.4	16.0									
20:4(n-3)				1.3	2.1	1.3	0.0	2.4	0.0	0.0									
22:1(n-11)				6.3	7.3	8.6	7.2	7.5	11.4	10.4									
20:5(n-3)				19.1	21.2	22.6	24.4	24.2	22.2	16.6									
22:6(n-3)				10.7	8.3	7.9	10.2	6.8	9.0	7.7									
Saturated				16.5	13.5	9.1	13.3	12.0	13.7	15.2									
Monounsaturated				35.2	33.1	38.6	33.5	42.3	42.7	44.5									
Polyunsaturated				48.3	53.4	52.3	53.3	45.7	43.6	40.3									

Table 3. Temporal dynamics of adult male *C. acutus* fatty acids (FA %) per copepod.

| CVI male FA % : Mean ($n = 6$) | | | | | | | | | | | | | | | | | | | |
| Month-year | Dec-2012 | | Jan-2013 | Feb-2013 | Mar-2013 | | Apr-2013 | May-2013 | Aug-2013 | Sep-2013 | Nov-2013 | | Dec-2013 | | | Jan-2014 | | Feb-2014 | |
Day / FA	19	29	17	20	8	13	18	16	12	26	14	28	6	14	30	17	30	14	21
10:0											12.9	2.5	7.2						
14:0											6.4	4.5	5.1						
15:0											0.0	0.0	0.0						
16:0											7.7	10.7	6.8						
16:1(n-7)											7.3	3.0	3.5						
16:4(n-1)											0.0	0.0	0.0						
17:0											0.0	0.0	0.0						
18:1(n-9)											2.3	3.3	3.6						
18:1(n-7)											0.0	0.0	0.0						
18:4(n-3)											0.0	0.0	0.0						
20:1(n-9)											13.0	22.0	31.4						
20:3(n-3)											8.6	0.0	0.0						
20:4(n-3)											0.0	0.0	0.0						
22:1(n-11)											8.3	11.8	13.0						
20:5(n-3)											12.0	17.8	14.5						
22:6(n-3)											21.4	24.3	14.9						
Saturated											27.1	17.8	19.1						
Monounsaturated											30.9	40.1	51.5						
Polyunsaturated											42.0	42.1	29.4						

(11 %) and 22:1(n-11) (9 %) (Table 1) with CV FA dominated by 20:5(n-3) (21 %), 20:1(n-9) (19 %), 20:3(n-3) (12 %), 22:6(n-3) (9 %) and 22:1(n-11) (8 %) (Table 2). Male FA profiles were mainly composed of 20:1(n-9) (22 %), 22:6(n-3) (19 %), 20:5(n-3) (14 %), 22:1(n-11) (11 %), 10:0 (9 %) and 16:0 (8 %) (Table 3). FA were grouped into poly-unsaturated fatty acids (PUFA) and saturated and mono-unsaturated fatty acids (SMUFA) to investigate seasonal unsaturation dynamics in FA data. Of total PUFA, 20:5(n-3) and 20:3(n-3) accounted for the largest share (42 and 26 % respectively) whilst 20:1(n-9), 22:1(n-11) and 16:1(n-7) accounted for the majority of SMUFA (33, 15 and 16 %, respectively). When the FA data is combined for CV and CVI stages, linear regressions indicated the concentration of 20:5(n-3) (μg ind^{-1}) significantly related to total PUFA ($p < 0.0001$, $r^2 = 0.99$, $n = 18$, Fig. 5a) as did % 20:5(n-3) to % of poly-unsaturated wax esters (PUWE, $p < 0.0001$, $r^2 = 0.84$, $n = 18$, Fig. 5b). Although concentrations of 22:6(n-3) and 20:3(n-3) significantly related to total PUFA ($p < 0.0001$, $r^2 = 0.88$ and 0.77 respectively, $n = 18$, Fig. 5c, e), no significant relationship was observed between % PUWE and both % 22:6(n-3) ($p = 0.061$, $r^2 = 0.20$, $n = 18$, Fig. 5d) and % 20:3(n-3) ($p = 0.63$, $r^2 = 0.01$, $n = 18$, Fig. 5f). Of the dominant SMUFA, the sum of 20:1(n-9) and 22:1(n-11) FA strongly related to concentrations of total SMUFA (μg ind^{-1}, $p < 0.0001$, $r^2 = 0.91$, $n = 18$, Fig. 5g) and negatively related to %PUWE ($p < 0.0001$, $r^2 = 0.61$, $n = 18$; Fig.5h). When both % 20:1(n-9) and % 22:1(n-11) were compared to PUWE, both had a significant negative linear relationship ($p = 0.0002$, $r^2 = 0.60$ and $p = 0.0032$, $r^2 = 0.43$, $n = 18$), however, no significant relationship was observed between % 16:1(n-7) and % PUWE ($p = 0.83$, $r^2 = 0.003$, $n = 18$). The FA dataset indicates that the unsaturation dynamics of WE are primarily determined by the accumulation of 20:5(n-3) during the summer and selective utilization of 20:5(n-3) combined with the retention of both 20:1(n-9) and 22:1(n-11) FA during winter.

The TL content of females at the beginning of S1 (23 Nov) was 112 μg ind^{-1} (Fig. 6a) and 28 % unsaturation of WE (Fig. 7a). Total lipid content and WE unsaturation separated by depth and stage is available in supplementary material online (Fig. S2 and S3). During dormancy termination (VME 1, 30 Nov – 12 Dec), female TL
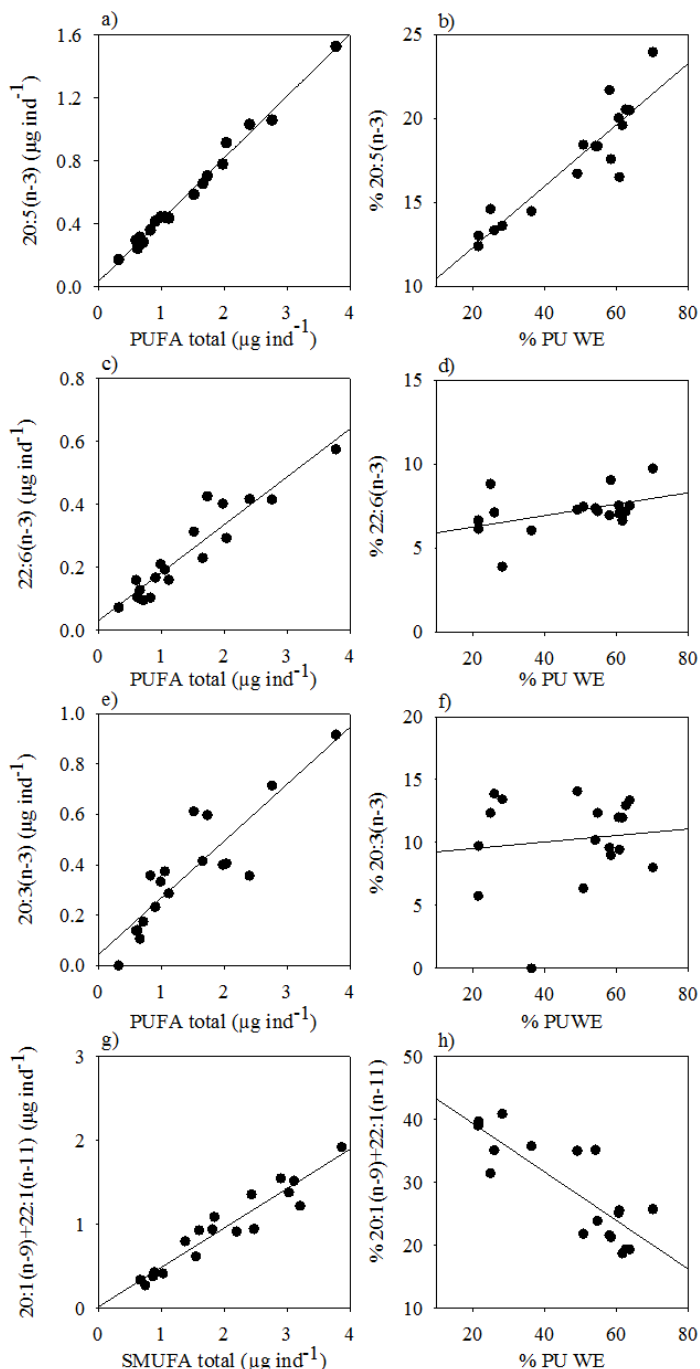
7

Fig. 5. Linear regressions of copepod fatty acids (FA) and % poly-unsaturation of total wax ester (% PUWE) for (a) concentrations of 20:5(n-3) FA vs poly-unsaturated fatty acid total (PUFA total), (b) % 20:5(n-3) vs % PUWE, (c) concentrations of 22:6(n-3) FA vs PUFA total, (d) % 22:6(n-3) vs % PUWE, (e) concentrations of 20:3(n-3) FA vs PUFA total, (f) % 20:3(n-3) vs % PUWE, (g) concentrations of 20:1(n-9) + 22:1(n-11) vs saturated and mono-unsaturated fatty acids (SMUFA total) and (h) % 20:1(n-9) + 22:1(n-11) vs % PUWE. NOTE: y axis scales differ between plots.
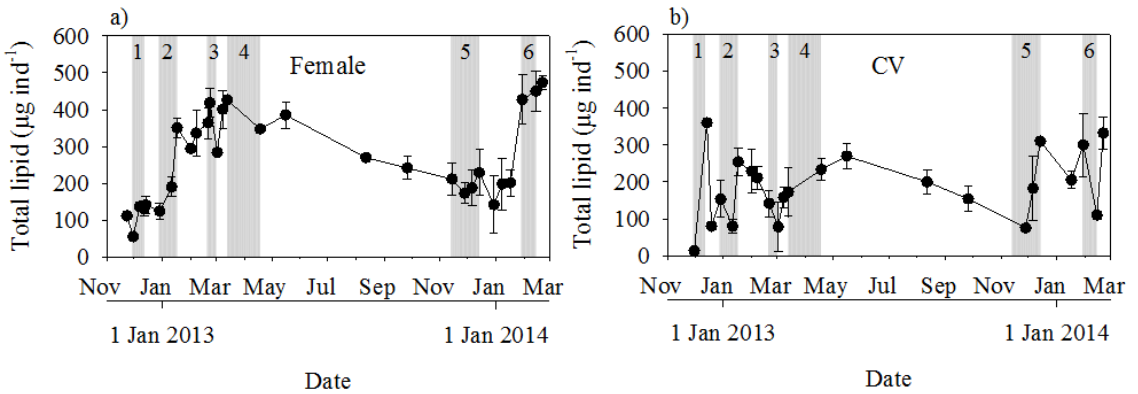
Fig. 6. Time series of total lipid (TL) content per copepod ($\mu g\ ind^{-1}$) for (a) female *C. acutus* and (b) CV *C. acutus*. Shaded areas (grey) represent time periods of vertical migration events 1 – 6. Error bars represent $\pm$ 1 standard error.
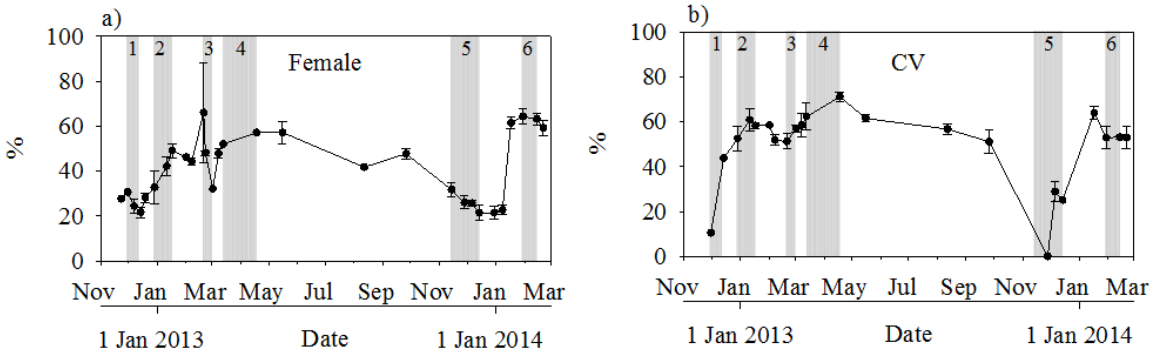
Fig. 7. Time series documenting changes in wax ester unsaturation (%) in (a) females and (b) CVs. Shaded areas (grey) represent time periods of vertical migration events 1 – 6. Error bars represent $\pm$ 1 standard error.

increased slightly to 136.8 $\mu g\ ind^{-1}$ and remained relatively constant throughout (131.5 – 141.4 $\mu g\ ind^{-1}$, Fig. 6a), however, WE unsaturation declined from 31 to 22 % (Fig. 7a). During VME 2 (dormancy initiation), female TL increased from 124 to 350 $\mu g\ ind^{-1}$ (Fig. 6a) and WE unsaturation increased from 33 to 49 % (Fig. 7a). At the beginning of VME 3 (second diapause termination in S1), female TL peaked at 419 $\mu g\ ind^{-1}$ on 22 Feb and declined to 284 $\mu g\ ind^{-1}$ at the end (2 Mar, Fig. 6a) and female WE unsaturation declined from 66 to 32 % (20 Feb – 3 Mar, Fig. 7a). This suggests lipid utilization by females during VME 3. Although abundances were low, the highest TL content of females during S1 occurred at the start of VME 4 (13 Mar, 426 $\mu g\ ind^{-1}$, Fig. 6a), however, unsaturation continued to increase until the end (57

235

% on 18 Apr, Fig. 7a) at the same time as peak unsaturation of CV WE (71 %, Fig. 7b).

Similar to females, CV TL content (Fig. 6b) and WE unsaturation (Fig. 7b) was low (12 µg ind^{-1} and 11 %, respectively) at the beginning of S1 (similar to abundances) and increased to 254 µg ind^{-1} on 17 Jan (Fig. 6b) and 61 % on 11 Jan (Fig. 7b), respectively. A decline in CV TL followed between 17 Jan and 2 Mar (down to 78 µg ind^{-1}) and coincided with the appearance of greater numbers of CIII and CIV stages, however, WE unsaturation remained relatively high (> 51 %) during this time (Fig. 7b). Wax ester unsaturation of both CVs and females peaked on 18 Apr (71 and 57 %, respectively, Fig. 7b) at the end of VME 4, however, the TL content of CVs continued to increase until 16 May (to 270 µg ind^{-1}, Fig. 6b), at the same time as a quantitatively similar rise in female TL (Fig. 6a). Prior to overwintering, female unsaturation increased to 57 % on 18 Apr and declined to 32 % on 14 Nov, a 25 % decrease during dormancy (Fig. 7a). Although female TL (in S1) peaked on 13 Mar at the start of VME 4 (426 µg ind^{-1}, Fig. 6a), TL was lower at the end of VME 4 on 18 Apr (347 µg ind^{-1}), increased to 385 µg ind^{-1} on 16 May and declined to 212 µg ind^{-1} on 14 Nov (start of VME 5). This corresponds to a decrease of 174 µg TL ind^{-1} (16 May to 14 Nov) and 130 µg ind^{-1} of poly-unsaturated WE. CVs were absent in net hauls on 14 Nov therefore winter CV lipid utilization estimates cannot be calculated.

At the end of the main overwintering period, male numbers were still relatively high (9 ind 100 m^{-3} on 14 Nov, Fig. 3e), however, their TL content (27 µg ind^{-1}, Fig. S2e) and WE unsaturation (12 %, Fig. S3e) was low and remained low (TL 20 - 30 µg ind^{-1}, unsaturation $21 - 25$ %) until male abundance declined to zero after 7 Dec (Fig. 3e). Females dominated the population at the beginning of S2 and, similar to S1, TL remained relatively constant during dormancy termination (VME 5, 173 - 229 µg ind^{-1}, Fig. 6a) unlike WE unsaturation that declined from 32 to 21 % (Fig. 7a). The TL content of females at the start of S2 (VME 5) was higher than at the start of S1 (VME 1, 137 - 132 µg, ind^{-1}), however, declines in WE unsaturation were highly similar between seasons (from 31 to 22 % in VME 1). At the start of VME 6 (female

dormancy initiation in S2), the TL content of females had rapidly increased to 427 µg ind^{-1} with 64 % unsaturation (Fig. 6a and 7a, respectively). Although female WE unsaturation of 49 % at VME 2 (Fig. 7a) suggests this level was sufficient for dormancy, the second high biomass diatom bloom of S1 (Fig. 2) allowed females to increase their TL content and unsaturation at the end of the productive season (VME 4, 426 µg ind^{-1} and 57 %, respectively), similar to those of females in S2 (at VME 6, Fig. 6 and 7).

Discussion

Chlorophyll *a* and vertical migration events

Although patchiness in time and space may theoretically have influenced the results, duplicate net hauls were comparable (slope of linear regression = 0.92, r^2 = 0.84, *p* < 0.0001, Fig. S4) and deep mixed layer depths (MLD) due to storm events were rare (maximum MLD of 112 m during winter 2013, data not shown) indicating that mixing events did not affect the vertical distribution of individuals (Clarke et al. 2008; Dong et al. 2008).

In this study, the timing of ontogenetic vertical migration events (VMEs) suggests that dormancy was initiated by females as soon as sufficient stores of TL and PUWE were accumulated. This could have consequences for predators of copepods in surface waters as lipid rich females were only available for ~ 2 weeks during the first half of Jan in S1 and 2 – 4 weeks in S2 (from mid-Jan to mid-Feb), after which females migrated to below the base of the thermocline (~ 200 m) and a portion of carbon stored as lipids was sequestered to the deep ocean as a consequence of respiration during dormancy (Jónasdóttir et al. 2015).

Vertical migration events were linked to the seasonal dynamics of Chl-*a*, i.e. the frequency and duration of phytoplankton blooms. Dormancy termination was timed to coincide with high biomass blooms that consisted both of micro-sized (VME 1) and nano-sized (VME 3 and 5) diatoms (Biggs et al. 2019). *Calanoides acutus* is primarily herbivorous with a short reproductive period that was timed to coincide with high phytoplankton food availability (Atkinson 1998; Pasternak and Schnack-

7

Schiel 2001a). Furthermore, the second ascent of females in S1 (VME 3) indicated that the high biomass diatom bloom provided a strong cue for ascent (Dezutter et al. 2019) even though female levels of total lipid (TL, 364 - 419 µg L^{-1}) and unsaturation (66 – 48 %) were still high, and only 34 – 64 days (VME 2 to 3) after the initial descent (VME 2). VME 3 represented the mass movement of carbon from deep to shallow water and may have allowed surface dwelling predators access to an additional peak in abundance of lipid rich copepods. Prior to dormancy initiation (VME 2, 4 and 6), it is likely individuals can directly sense reducing/low phytoplankton food concentrations (Bautista and Harris 1992; Perissinotto 1992; Atkinson 1994; Pasternak and Schnack-Schiel 2001a; Garrido et al. 2013), however, at dormancy depths (500 – 200 m) signals of phytoplankton biomass (at the surface) must be transmitted through the water column and is likely related to sedimentation of organic matter (Annett et al. 2010; Ducklow et al. 2012; Turner 2015). During winter, when Chl-*a* concentrations are low, increased proportions of smaller flagellated phytoplankton are observed (Rozema et al. 2017) and the shift to a high biomass, diatom dominated period (at VME 1 and 5) most likely promoted a more herbivorous diet with reduced coprophagy / coprorhexy (Pasternak and Schnack-Schiel 2001a, b; Turner 2002, 2015) and (at the same time as increased stratification during VME 1 and 5; Biggs et al. 2019) increased the load and sinking speed of fecal pellets (FP) in the water column. Similarly, a relatively low biomass, flagellate dominated period (Biggs et al. 2019) was observed prior to the second high biomass diatom bloom in S1, and the second ascent of females (VME 3). Fecal pellets produced from flagellated phytoplankton diets have been observed to sink almost 10 times slower than diatom fed pellets (Ploug et al. 2008), likely related to mineral ballasting by biogenic silica (Voss 1991). Diatoms also produce transparent exopolymer particles (TEP) in abundance and are a major component of diatom aggregates (Passow 2002). TEP production combined with organic material released from melting sea ice (and increased stratification) may produce further deposition resulting in a rain of organic material at depth. Rapidly sinking fecal pellets (>300 m d^{-1}) (Ploug et al. 2008; Atkinson et al. 2012a) would enable organic material to

reach the overwintering population of *C. acutus* (500 – 200 m) within 1 – 2 days and pigment degradation products, characteristic of the phytoplankton community, can be detected in FP (Nelson 1989). Microbial degradation of sedimenting organic matter may leak solutes into the surrounding water (Turner 2015), which, through chemosensory mechanisms and probably hormonally mediated, may trigger the ascent (Irigoien 2004).

Losses

Declines in abundance over the winter period (a 68 % reduction between Apr and Nov 2013, VME 4 to 5, Fig. S5) suggests the 64 ind 100 m^{-3} at the start of S1 (total population abundance at VME 1) each needed to contribute ~ 3 offspring (total of 192 ind 100 m^{-3} required on 18 Apr 2013) to balance losses during winter. At dormancy initiation (VME 4), population numbers were 48 % less (100 ind 100 m^{-3} captured on 18 Apr 2013) representing (in retrospect) a minimum total requirement of ~ 6 ind female^{-1}, over S1 and winter combined, to maintain the population over an annual cycle. This indicates during S1 either loss rates were twice as high (to maintain the population) or egg production twice as low. Low egg production may be related to relatively lower TL stores at the start of S1, compared to S2 (VME 1, 137 $\pm$ 5 µg ind^{-1}, $n = 3$; VME 5, 200 $\pm$ 25 µg ind^{-1}, $n = 4$) as well as reduced CI - CV recruitment (959 ind 100 m^{-3} at CI peaks in S1 and 3106 ind 100 m^{-3} in S2). Whilst the large amounts of lipid and high unsaturation alone could have triggered entrance into dormancy at VME 2 and 6, lower total lipid and unsaturation were observed at VME 2 compared to VME 6 (Fig. 6 and 7). Eggs, nauplii, copepodites and potentially even adults of *C. acutus* are within the potential prey range for many of the large zooplankton species that were often observed during both seasons, such as *Metridia gerlachei, Rhincalanus gigas*, (*Para*)*euchaeta antarctica*, euphausids, polychaetes and arrow worms. The one month earlier increase in larger-sized zooplankton abundance (> 200 µm) in S1 than S2 (Fig. S6) matched the one month earlier descent of female *C. acutus* which may imply that enhanced predation pressure affects the initial decision of females to descend. The combination of

7

increased numbers of larger-sized zooplankton and reducing/low Chl-*a* concentrations (January S1) may have resulted in even higher predation pressure on smaller zooplankton (including nauplii and copepodites) by larger omnivorous individuals (Pasternak and Schnack-Schiel 2001a) and contribute to high losses over S1.

The nano-sized cells during the second high biomass diatom bloom in S1 (Biggs et al. 2019) likely represented a suitable prey size for copepodites (Perissinotto 1992) as they mature and attempt to increase lipid stores at the end of the productive season, however, relatively low TL content of CVs was observed (270 µg ind^{-1}) at diapause initiation (VME 4). The biomass dominant phytoplankton population during this bloom (11 µm Ø diatom) was subjected to high rates of viral lysis (Chapter 3) which may have reduced food availability during a crucial time of lipid accumulation prior to diapause. Increased substrate availability (due to the viral shunt) could explain the S1 peak in bacteria abundance mid-March (Chapter 3) which likely benefitted micro-zooplankton grazers (Azam et al. 1991). Although considered primarily herbivorous, low phytoplankton abundance could stimulate carnivorous grazing (Pasternak and Schnack-Schiel 2001a) by late season recruits and explain why CV TL increased between 18 Apr to 16 May (from 233 to 270 µg ind^{-1}) whilst WE unsaturation declined (from 71 to 61 %). Reduced lipid stores combined with a relatively shallow diapause depth (< 500 m) could be related to high winter mortality as deeper depths may allow females to better take advantage of the lipid phase transition effects of a highly unsaturated (~50 %) lipid store (Pond and Tarling 2011). If neutral buoyancy cannot be achieved then high rates of lipid utilization and mortality may be due to additional energetic costs associated with swimming to maintain an optimum position in the water column. At the same time, predation pressures may be higher in the top 500 m than below (Yamaguchi et al. 2004; Harper and Peck 2016) and individuals close to bottom depth, where phase transition of WEs may occur, would be more concentrated and exposed to the benthic community. The relatively high unsaturation of CVs (compared to females) at the time of overwintering (71 – 61 %) and low TL (233 – 270 µg ind^{-1} representing 132 - 140 µg ind^{-1} of polyunsaturated

WE and ~ 32 – 34 µg ind^{-1} EPA) suggests increased unsaturation was prioritized when TL was increased. The data of Pond and Tarling (2011) also indicates that at depths below 500 m, WE phase transition occurred at higher temperatures and was more pronounced at higher levels of unsaturation (70 %). The greater increase in unsaturation of CV WE prior to diapause may have been a mechanism to compensate for lower TL stores and take advantage of energetic savings at higher temperatures as lipid stores become increasingly dense with depth.

Diapause mechanisms and lifecycle

The level of unsaturation of the WE lipid store, rather than the total amount (TL), is potentially a key mechanism influencing the dormancy behaviour of calanoid copepods (Pond and Tarling 2011; Pond et al. 2012). In our study, unsaturation levels peaked at the start of the main dormancy period (VME 4) and declined over the winter. Dynamics were determined by the retention of FA 20:1(n-9) and 22:1(n-11) (during winter) and the selective accumulation (during summer) and utilization (during winter) of 20:5(n-3) (Eicosapentaenoic acid or EPA). Changes in unsaturation were often not mirrored by changes in TL indicating a more functional role of FA composition. EPA is a precursor of eicosanoids which are locally acting 'tissue hormones' and may influence functions such as reproduction, ion and water transport (Persson and Vrede 2006). The WE of many herbivorous copepods are also characterized by considerable amounts of long-chain mono-unsaturated fatty alcohols (20:1(n-9) and 22:1(n-11)) which are not present in significant amounts in their phytoplankton diet (Albers et al. 1996; Lee et al. 2006; Pond et al. 2012). This biosynthesis of fatty alcohols and esterification with FA to WE resulted in rapid lipid accumulation since there is both de novo synthesis and incorporation of dietary lipids (Graeve et al. 2005). During increases in unsaturation (summer), stores of 20:1(n-9) and 22:1(n-11) (retained during winter) are likely reduced to fatty alcohols (Kattner et al. 1994; Pond et al. 2012) and esterified to 20:5(n-3) acquired from dietary sources. Unsaturation level of the entire lipid store was therefore determined by synergistic changes in 'pools' of 20:1(n-9) + 22:1(n-11) and 20:5(n-3), rather than

7

unsaturation dynamics determined solely by 20:5(n-3). This action has a double impact on unsaturation levels (+1 PUFA, -1 MUFA), as FA are converted to fatty alcohols (and vice versa), likely providing a stable signal regarding changes in unsaturation state. The physiological impact of selective EPA utilization during dormancy may further act as a biological timer (Häfker et al. 2017, 2018) and, combined with increased buoyancy (due to reducing unsaturation and phase transition), could stimulate ascent. In relatively deep waters of the Scotia sea, late stage *C. acutus* individuals that typically diapause between 500 and 1000 m or deeper, were observed with a tri-modal vertical distribution at one site (< 100, 400 – 600 and 800 – 1000 m) and concentrated in the 300 – 500 m depth range at another (Pond et al. 2012). One explanation for this is that individuals had ascended from deeper waters to an intermediate depth to await the initiation of the 'Spring' bloom (Pond et al., 2012). This initial 'intermediate' migration is potentially triggered by reduced levels of unsaturation, however, in coastal and relatively shallow shelf sea areas such as Ryder Bay, bottom depth (520 m) is similar to this intermediate depth therefore signals of reduced unsaturation and increased phytoplankton standing stock may combine to initiate ascent.

The late season high biomass diatom bloom of S1 coincided with the second ascent of females (VME 3) at the same time as lipids appear to be utilized (TL decreased from 419 to 284 µg ind^{-1} and WE unsaturation from 66 to 32 %). The second S1 spawning event coincided with a decline in total female abundance over VME 3 (from 31 to 9 ind 100 m^{-3}, Fig. S5a) and suggests the ascending females that spawned expired after a one-year lifecycle. In contrast during S2, a singular but prolonged high biomass bloom (Fig. 2) resulted in a singular spawning event and a 1-month delay in dormancy initiation of (most likely 'new') females. Chlorophyll-*a* concentrations were relatively low between 21 Feb to 15 Apr post S2 (1.5 ± 0.7 µg L^{-1}, *n* = 8) and these females likely remained in dormancy to complete a two year lifecycle. Such a mechanism could explain why some studies suggest the overwintering stages of *C. acutus* complete their life cycle in 1 year (Marin 1988; Quetin et al. 1996; Atkinson et al. 1997) and others that they re-enter diapause and

survive an extra year (Hagen and Schnack-Schiel 1996; Tarling et al. 2004). The late season phytoplankton bloom in S1 was associated with higher temperature (Biggs et al. 2019), similar to novel autumn blooms observed in the Arctic (Ardyna et al. 2014), and suggests that global warming could influence the lifespan of vertically migrating copepods and promote a one year, rather than a two year lifecycle.

Although two spawning events were observed in S1, the abundance of CI – IV in shallow water on 2 Mar 2013 (initial peak of 531 ind 100 m^{-3}) was similar to 17 Jan 2013 (735 ind 100 m^{-3}). Maturing copepodites from the late season spawning event would likely benefit from reduced predation pressure due to lower numbers of larger-sized zooplankton and an abundance of phytoplankton food (Pasternak and Schnack-Schiel 2001a), and could explain the similarity in CI – CIV numbers even though peak shallow female abundance was 3-fold higher during VME 1 (108 ind 100m^{-3}) than VME 3 (33 ind 100m^{-3}). Conversely, copepodites from the early season spawning event would have matured during times of low Chl-*a* (food availability) with increased proportions of cryptophytes (preference of diatoms as food type, Verity and Smayda, 1989; Head and Harris, 1994) and high numbers of larger-sized zooplankton (high predation pressure, Pasternak and Schnack-Schiel, 2001a). An early season mismatch and late season match, between peaks of Chl-*a*, new *C. acutus* recruits and higher trophic predators (Durant et al. 2013), likely resulted in a relatively greater contribution of individuals from the late season spawning event to annual reproductive success. This flexible dormancy strategy would enable females to maximize phytoplankton food availability and reproductive capability whilst reducing predation risk.

It is likely that multiple internal and external factors combine, such as a lipid modulated endogenous clock (Johnson et al. 2008; Häfker et al. 2018); TL content (to support reproductive maturation and winter survival; Hagen and Schnack-Schiel 1996; Rey-Rassat et al. 2002); WE unsaturation (buoyancy regulation; Pond et al. 2012); and food availability (Friedland et al. 2016) to serve as a timing mechanism to determine ontogenetic vertical migration behaviour.

7

Conclusions

The dormancy behaviour of *C. acutus* CV and CVI stages appears coupled to the frequency and duration of phytoplankton blooms. Dormancy termination post winter coincided with reduced unsaturation (~ 30 %) and increased phytoplankton standing stock. Once sufficient lipid stores were accumulated after the initial phytoplankton bloom period (350 µg TL ind^{-1} with ~ 49 % unsaturation), dormancy was initiated when Chl-*a* concentrations declined. An early S1 increase in larger-sized zooplankton numbers (compared to S2) likely contributed to increased losses and early dormancy initiation. A late summer diatom bloom, driven by higher temperatures, stimulated ascent and spawning of dormant females for a second time in S1 and the resulting late season copepodites would benefit from reduced predation (low numbers of larger-sized zooplankton) and high phytoplankton food availability, i.e. a match between peaks of Chl-*a*, new *C. acutus* recruits and higher trophic predators. The loss of females during dormancy termination (VME 3) suggests that individuals expire after two main 'spawning events'. Furthermore, the timing of these events is regulated by the frequency and duration of phytoplankton blooms which has consequences for the lifespan of *C. acutus* females, either 1 or 2 years. This flexible strategy would enable females to maximize phytoplankton food availability and reduce the likelihood of predation, thereby increasing reproductive capability while promoting survival of produced offspring via reduced mortality rates. As such, dormancy behaviour and copepod lifespan, and thus zooplankton's role in the biological carbon pump, are intimately linked to the structure and dynamics of the Southern Ocean food web.

Stefan Schouten at the Royal Netherlands Institute for Sea Research (NIOZ) for his expertise and support. Furthermore, we wish to thank Dr. Amber Annett, Zoi Farenzena and Dorien Verheyen for their help and support during the field campaign as well as Santiago Gonzalez and Anna Noordeloos for their technical support at the NIOZ.

References

Albers CS, Kattner G, Hagen W (1996) The compositions of wax esters, triacylglycerols and phospholipids in Arctic and Antarctic copepods: Evidence of energetic adaptations. Mar Chem 55:347–358. doi: 10.1016/S0304-4203(96)00059-X

Annett AL, Carson DS, Crosta X, et al (2010) Seasonal progression of diatom assemblages in surface waters of Ryder Bay, Antarctica. Polar Biol 33:13–29. doi: 10.1007/s00300-009-0681-7

Ardyna M, Babin M, Gosselin M, et al (2014) Recent Arctic Ocean sea ice loss triggers novel fall phytoplankton blooms. Geophys Res Lett 41:6207–6212. doi: 10.1002/2014GL061047

Atkinson A (1994) Diets and feeding selectivity among the epipelagic copepod community near South Georgia in summer. Polar Biol 14:551–560. doi: 10.1007/BF00238225

Atkinson A (1998) Life cycle strategies of epipelagic copepods in the Southern Ocean. J Mar Syst 15:289–311. doi: 10.1016/S0924-7963(97)00081-X

Atkinson A, Schmidt K, Fielding S, et al (2012a) Variable food absorption by Antarctic krill: Relationships between diet, egestion rate and the composition and sinking rates of their fecal pellets. Deep Res Part II Top Stud Oceanogr 59–60:147–158. doi: 10.1016/j.dsr2.2011.06.008

Atkinson A, Schnack-Schiel S, Ward P, Marin V (1997) Regional differences in the life cycle of *Calanoides acutus* (Copepoda: Calanoida) within the Atlantic sector of the Southern Ocean. Mar Ecol Prog Ser 150:99–111. doi: 10.3354/meps150099

Atkinson A, Ward P, Hunt BP V., et al (2012b) An overview of Southern Ocean zooplankton data: Abundance, biomass, feeding and functional relationships. CCAMLR Sci 19:171–218

Azam F, Smith DC, Hollibaugh JT (1991) The role of the microbial loop in Antarctic pelagic ecosystems. Polar Res 10:239–244. doi: 10.1111/j.1751-8369.1991.tb00649.x

Baumgartner MF, Tarrant AM (2017) The physiology and ecology of diapause in marine copepods. Ann Rev Mar Sci 9:387–411. doi: 10.1146/annurev-marine-010816-060505

Bautista B, Harris R (1992) Copepod gut contents, ingestion rates and grazing impact on phytoplankton in relation to size structure of zooplankton and phytoplankton during a spring bloom. Mar Ecol Prog Ser 82:41–50. doi: 10.3354/meps082041

Beardsley RC, Limeburner R, Brechner Owens W (2004) Drifter measurements of surface currents near Marguerite Bay on the western Antarctic Peninsula shelf during austral summer and fall, 2001 and 2002. Deep Res Part II Top Stud Oceanogr 51:1947–1964. doi: 10.1016/j.dsr2.2004.07.031

Biggs TEG, Alvarez-Fernandez S, Evans C, et al (2019) Antarctic phytoplankton community composition and size structure: Importance of ice type and temperature as regulatory factors. Polar Biol 42:1997–2015. doi: 10.1007/s00300-019-02576-3

Budge SM, Iverson SJ, Koopman HN (2006) Studying trophic ecology in marine ecosystems using fatty acids: A primer on analysis and interpretation. Mar Mammal Sci 22:759–801. doi: 10.1111/j.1748-7692.2006.00079.x

Clark KAJ, Brierley AS, Pond DW (2012) Composition of wax esters is linked to diapause behavior of *Calanus finmarchicus* in a sea loch environment. Limnol Oceanogr 57:65–75. doi: 10.4319/lo.2012.57.1.0065

Clarke A, Meredith MP, Wallace MI, et al (2008) Seasonal and interannual variability in temperature, chlorophyll and macronutrients in northern Marguerite Bay, Antarctica. Deep Res Part II Top Stud Oceanogr 55:1988–2006. doi: 10.1016/j.dsr2.2008.04.035

7

Dezutter T, Lalande C, Dufresne C, et al (2019) Mismatch between microalgae and herbivorous copepods due to the record sea ice minimum extent of 2012 and the late sea ice break-up of 2013 in the Beaufort Sea. Prog Oceanogr 173:66–77. doi: 10.1016/j.pocean.2019.02.008

Dong S, Sprintall J, Gille ST, Talley L (2008) Southern Ocean mixed-layer depth from Argo float profiles. J Geophys Res 113:C06013. doi: 10.1029/2006JC004051

Drits A V., Pasternak AF, Kosobokova KN (1994) Physiological characteristics of the antarctic copepod *Calanoides acutus* during late summer in the Weddell Sea. Hydrobiologia 292–293:201–207. doi: 10.1007/BF00229942

Ducklow H, Clarke A, Dickhut R, et al (2012) The marine system of the Western Antarctic Peninsula. In: Rogers AD, Johnston NM, Murphy EJ, Clarke A (eds) Antarctic Ecosystems: An Extreme Environment in a Changing World. Blackwell Publishing Ltd., pp 121–159

Durant J, Hjermann D, Falkenhaug T, et al (2013) Extension of the match-mismatch hypothesis to predator-controlled systems. Mar Ecol Prog Ser 474:43–52. doi: 10.3354/meps10089

Falk-Petersen S, Hagen W, Kattner G, et al (2000) Lipids, trophic relationships, and biodiversity in Arctic and Antarctic krill. Can J Fish Aquat Sci 57:178–191. doi: 10.1139/f00-194

Falk-Petersen S, Mayzaud P, Kattner G, Sargent JR (2009) Lipids and life strategy of Arctic *Calanus*. Mar Biol Res 5:18–39. doi: 10.1080/17451000802512267

Friedland KD, Record NR, Asch RG, et al (2016) Seasonal phytoplankton blooms in the North Atlantic linked to the overwintering strategies of copepods. Elem Sci Anthr 4:000099. doi: 10.12952/journal.elementa.000099

Garrido S, Cruz J, Santos AMP, et al (2013) Effects of temperature, food type and food concentration on the grazing of the calanoid copepod *Centropages chierchiae*. J Plankton Res 35:843–854. doi: 10.1093/plankt/fbt037

Graeve M, Albers C, Kattner G (2005) Assimilation and biosynthesis of lipids in Arctic Calanus species based on feeding experiments with a 13C labelled diatom. J Exp Mar Bio Ecol 317:109–125. doi: 10.1016/j.jembe.2004.11.016

Graeve M, Kattner G, Hagen W (1994) Diet-induced changes in the fatty acid composition of Arctic herbivorous copepods: Experimental evidence of trophic markers. J Exp Mar Bio Ecol 182:97–110. doi: 10.1016/0022-0981(94)90213-5

Häfker NS, Meyer B, Last KS, et al (2017) Circadian clock involvement in zooplankton diel vertical migration. Curr Biol 27:2194-2201.e3. doi: 10.1016/j.cub.2017.06.025

Häfker NS, Teschke M, Last KS, et al (2018) *Calanus finmarchicus* seasonal cycle and diapause in relation to gene expression, physiology, and endogenous clocks. Limnol Oceanogr 63:2815–2838. doi: 10.1002/lno.11011

Hagen W, Kattner G, Graeve M (1993) *Calanoides acutus* and *Calanus propinquus*, Antarctic copepods with different lipid storage modes via wax esters or triacylglycerols. Mar Ecol Prog Ser 97:135–142. doi: 10.3354/meps097135

Hagen W, Schnack-Schiel SB (1996) Seasonal lipid dynamics in dominant Antarctic copepods: Energy for overwintering or reproduction? Deep Res Part I Oceanogr Res Pap 43:139–158. doi: 10.1016/0967-0637(96)00001-5

Harper EM, Peck LS (2016) Latitudinal and depth gradients in marine predation pressure. Glob Ecol Biogeogr 25:670–678. doi: 10.1111/geb.12444

Head EJH, Harris LR (1994) Feeding selectivity by copepods grazing on natural mixtures of phytoplankton determined by HPLC analysis of pigments. Mar Ecol Prog Ser 110:75–84. doi: 10.3354/meps110075

Heath MR, Boyle PR, Gislason A, et al (2004) Comparative ecology of over-wintering *Calanus finmarchicus* in the northern North Atlantic, and implications for life-cycle patterns. ICES J Mar Sci 61:698–708. doi: 10.1016/j.icesjms.2004.03.013

Hopkins TL, Torres JJ (1989) Midwater food web in the vicinity of a marginal ice zone in the western Weddell Sea. Deep Sea Res Part A Oceanogr Res Pap 36:543–560. doi: 10.1016/0198-0149(89)90005-8

Huisman J, van Oostveen P, Weissing FJ (1999) Critical depth and critical turbulence: Two different mechanisms for the development of phytoplankton blooms. Limnol Oceanogr 44:1781–1787. doi: 10.4319/lo.1999.44.7.1781

Huntley M, Escritor F (1991) Dynamics of *Calanoides acutus* (Copepoda: Calanoida) in Antarctic coastal waters. Deep Sea Res Part A, Oceanogr Res Pap 38:1145–1167. doi: 10.1016/0198-

0149(91)90100-T

Irigoien X (2004) Some ideas about the role of lipids in the life cycle of *Calanus finmarchicus*. J Plankton Res 26:259–263. doi: 10.1093/plankt/fbh030

Johnson CL, Leising AW, Runge JA, et al (2008) Characteristics of *Calanus finmarchicus* dormancy patterns in the Northwest Atlantic. ICES J Mar Sci 65:339–350. doi: 10.1093/icesjms/fsm171

Jónasdóttir SH, Visser AW, Richardson K, Heath MR (2015) Seasonal copepod lipid pump promotes carbon sequestration in the deep North Atlantic. Proc Natl Acad Sci 112:12122–12126. doi: 10.1073/pnas.1512110112

Kattner G, Graeve M, Hagen W (1994) Ontogenetic and seasonal changes in lipid and fatty acid/alcohol compositions of the dominant Antarctic copepods *Calanus propinquus*, *Calanoides acutus* and *Rhincalanus gigas*. Mar Biol 118:637–644. doi: 10.1007/BF00347511

Kattner G, Hagen W (2009) Lipids in marine copepods: Latitudinal characteristics and perspective to global warming. In: Kainz M, Brett M, Arts M (eds) Lipids in Aquatic Ecosystems. Springer New York, pp 257–280

Lee RF, Hagen W, Kattner G (2006) Lipid storage in marine zooplankton. Mar Ecol Prog Ser 307:273–306. doi: 10.3354/Meps307273

Ma S, Tao Z, Yang X, et al (2014) Estimation of marine primary productivity from satellite-derived phytoplankton absorption data. IEEE J Sel Top Appl Earth Obs Remote Sens 7:3084–3092. doi: 10.1109/JSTARS.2014.2298863

Maps F, Record NR, Pershing AJ (2014) A metabolic approach to dormancy in pelagic copepods helps explaining inter- and intra-specific variability in life-history strategies. J Plankton Res 36:18–30. doi: 10.1093/plankt/fbt100

Maps F, Runge JA, Leising A, et al (2012) Modelling the timing and duration of dormancy in populations of *Calanus finmarchicus* from the Northwest Atlantic shelf. J Plankton Res 34:36–54. doi: 10.1093/plankt/fbr088

Marin V (1988) Qualitative models of the life cycles of *Calanoides acutus, Calanus propinquus*, and *Rhincalanus gigas*. Polar Biol 8:439–446. doi: 10.1007/BF00264720

Marrari M, Daly KL, Timonin A, Semenova T (2011) The zooplankton of Marguerite Bay, Western Antarctic Peninsula-Part I: Abundance, distribution, and population response to variability in environmental conditions. Deep Res Part II Top Stud Oceanogr 58:1599–1613. doi: 10.1016/j.dsr2.2010.12.007

Moffat C, Beardsley RC, Owens B, van Lipzig N (2008) A first description of the Antarctic Peninsula Coastal Current. Deep Sea Res Part II Top Stud Oceanogr 55:277–293. doi: 10.1016/j.dsr2.2007.10.003

Nelson J (1989) Phytoplankton pigments in macrozooplankton feces: Variability in carotenoid alterations. Mar Ecol Prog Ser 52:129–144. doi: 10.3354/meps052129

Passow U (2002) Transparent exopolymer particles (TEP) in aquatic environments. Prog Oceanogr 55:287–333. doi: 10.1016/S0079-6611(02)00138-6

Pasternak AF, Schnack-Schiel SB (2001a) Seasonal feeding patterns of the dominant Antarctic copepods *Calanus propinquus* and *Calanoides acutus* in the Weddell Sea. Polar Biol 24:771–784. doi: 10.1007/s003000100283

Pasternak AF, Schnack-Schiel SB (2001b) Feeding patterns of dominant Antarctic copepods: An interplay of diapause, selectivity, and availability of food. Hydrobiologia 453–454:25–36. doi: 10.1023/A:1013147413136

Pepin P, Head EJH (2009) Seasonal and depth-dependent variations in the size and lipid contents of stage 5 copepodites of *Calanus finmarchicus* in the waters of the Newfoundland Shelf and the Labrador Sea. Deep Res Part I Oceanogr Res Pap 56:989–1002. doi: 10.1016/j.dsr.2009.01.005

Perissinotto R (1992) Mesozooplankton size-selectivity and grazing impact on the phytoplankton community of the Prince Edward Archipelago (Southern Ocean). Mar Ecol Prog Ser 79:243–258

Persson J, Vrede T (2006) Polyunsaturated fatty acids in zooplankton: Variation due to taxonomy and trophic position. Freshw Biol 51:887–900. doi: 10.1111/j.1365-2427.2006.01540.x

Pervushin AS (1968) Observations of the behaviour and feeding of whalebone whales in the area of the Crozet Islands. Oceanology 8:110–115

Ploug H, Iversen MH, Fischer G (2008) Ballast, sinking velocity, and apparent diffusivity within marine snow and zooplankton fecal pellets: Implications for substrate turnover by attached bacteria. Limnol Oceanogr 53:1878–1886. doi: 10.4319/lo.2008.53.5.1878

7

Pond D, Watkins J, Priddle J, Sargent J (1995) Variation in the lipid content and composition of Antarctic krill *Euphausia superba* at South Georgia. Mar Ecol Prog Ser 117:49–58

Pond DW, Tarling G a. (2011) Phase transitions of wax esters adjust buoyancy in diapausing *Calanoides acutus*. Limnol Oceanogr 56:1310–1318. doi: 10.4319/lo.2011.56.4.1310

Pond DW, Tarling GA, Mayor DJ (2014) Hydrostatic pressure and temperature effects on the membranes of a seasonally migrating marine copepod. PLoS One 9:. doi: 10.1371/journal.pone.0111043

Pond DW, Tarling GA, Ward P, Mayor DJ (2012) Wax ester composition influences the diapause patterns in the copepod *Calanoides acutus*. Deep Res Part II Top Stud Oceanogr 59–60:93–104. doi: 10.1016/j.dsr2.2011.05.009

Quetin LB, Ross RM, Frazer TK, Haberman KL (1996) Factors affecting distribution and abundance of zooplankton, with an emphasis on Antarctic krill, *Euphausia superba*. In: Foundations for Ecological Research West of the Antarctic Peninsula (eds R.M. Ross, E.E. Hofmann and L.B. Quetin). pp 357–371

Record NR, Ji R, Maps F, et al (2018) Copepod diapause and the biogeography of the marine lipidscape. J Biogeogr 45:2238–2251. doi: 10.1111/jbi.13414

Rey-Rassat C, Irigoien X, Harris R, Carlotti F (2002) Energetic cost of gonad development in *Calanus finmarchicus* and *C. helgolandicus*. Mar Ecol Prog Ser 238:301–306. doi: 10.3354/meps238301

Rozema PD, Venables HJ, van de Poll WH, et al (2017) Interannual variability in phytoplankton biomass and species composition in northern Marguerite Bay (West Antarctic Peninsula) is governed by both winter sea ice cover and summer stratification. Limnol Oceanogr 62:235–252. doi: 10.1002/lno.10391

Sartoris FJ, Thomas DN, Cornils A, Schnack-Schiel SB (2010) Buoyancy and diapause in Antarctic copepods: The role of ammonium accumulation. Limnol Oceanogr 55:1860–1864. doi: 10.4319/lo.2010.55.5.1860

Schnack-Schiel SB, Hagen W, Mizdalski E (1991) Seasonal comparison of *Calanoides acutus* and *Calanus propinquus* (Copepoda: Calanoida) in the southeastern Weddell Sea, Antarctica. Mar Ecol Prog Ser 70:17–27. doi: 10.3354/meps070017

Shreeve RS, Tarling GA, Atkinson A, et al (2005) Relative production of *Calanoides acutus* (Copepoda: Calanoida) and *Euphausia superba* (Antarctic krill) at South Georgia, and its implications at wider scales. Mar Ecol Prog Ser 298:229–239. doi: 10.3354/meps298229

Smetacek V, Nicol S (2005) Polar ocean ecosystems in a changing world. Nature 437:362–368. doi: 10.1038/nature04161

Sommer U, Lengfellner K (2008) Climate change and the timing, magnitude, and composition of the phytoplankton spring bloom. Glob Chang Biol 14:1199–1208. doi: 10.1111/j.1365-2486.2008.01571.x

Stevens CJ, Deibel D, Parrish CC (2004) Incorporation of bacterial fatty acids and changes in a wax ester-based omnivory index during a long-term incubation experiment with *Calanus glacialis* Jaschnov. J Exp Mar Bio Ecol 303:135–156. doi: 10.1016/j.jembe.2003.11.008

Sverdrup H (1953) On conditions for the vernal blooming of phytoplankton. J du Cons 18:287–295. doi: 10.4319/lom.2007.5.269

Tarling GA, Shreeve RS, Ward P, et al (2004) Life-cycle phenotypic composition and mortality of *Calanoides acutus* (Copepoda: Calanoida) in the Scotia Sea: A modelling approach. Mar Ecol Prog Ser 272:165–181. doi: 10.3354/meps272165

Turner JT (2002) Zooplankton fecal pellets, marine snow and sinking phytoplankton blooms. Aquat Microb Ecol 27:57–102. doi: 10.3354/ame027057

Turner JT (2015) Zooplankton fecal pellets, marine snow, phytodetritus and the ocean's biological pump. Prog Oceanogr 130:205–248. doi: 10.1016/j.pocean.2014.08.005

Verity PG, Smayda TJ (1989) Nutritional value of *Phaeocystis pouchetii* (Prymnesiophyceae) and other phytoplankton for *Acartia* spp. (Copepoda): Ingestion, egg production, and growth of nauplii. Mar Biol 100:161–171. doi: 10.1007/BF00391955

Visser AW, Jónasdóttir SH (1999) Lipids, buoyancy and the seasonal vertical migration of *Calanus finmarchicus*. Fish Oceanogr 8:100–106. doi: 10.1046/j.1365-2419.1999.00001.x

Voronina N. (1998) Comparative abundance and distribution of major filter-feeders in the Antarctic pelagic zone. J Mar Syst 17:375–390. doi: 10.1016/S0924-7963(98)00050-5

Voss M (1991) Content of copepod faecal pellets in relation to food supply in Kiel Bight and its effect

on sedimentation rate. Mar Ecol Prog Ser 75:217–225. doi: 10.3354/meps075217

Yamaguchi A, Ikeda T, Watanabe Y, Ishizaka J (2004) Vertical distribution patterns of pelagic copepods as viewed from the predation pressure hypothesis. Zool Stud 43:475–485
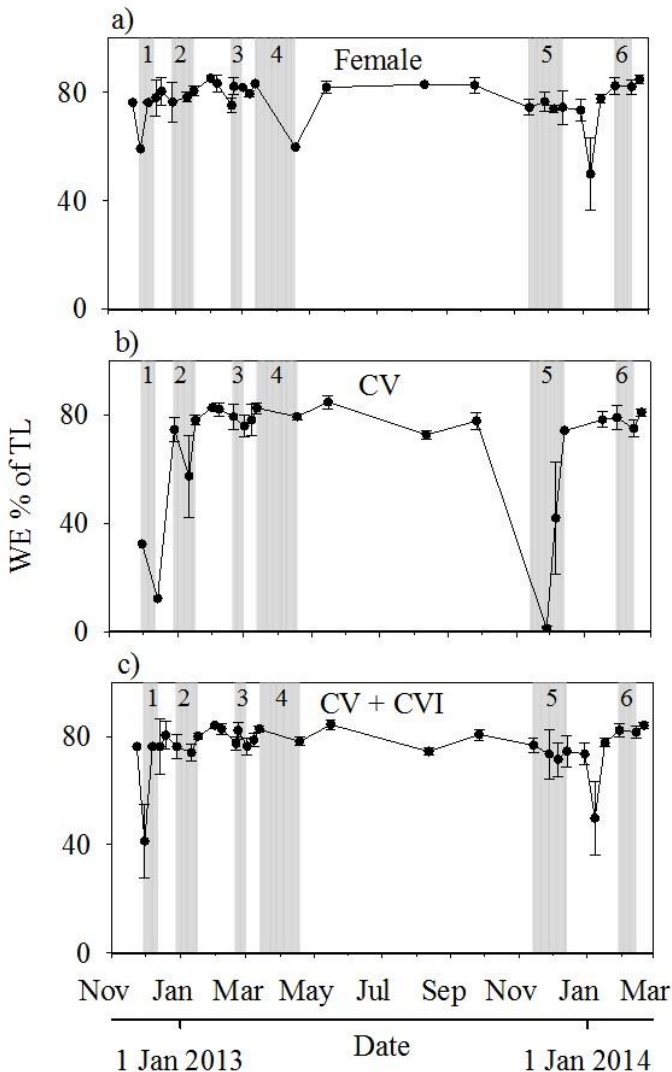
Supplementary Figures

Fig. S1. Seasonal dynamics in the proportion of wax ester (%) to total lipid (TL) of (a) females, (b) CVs and (c) CV and CVI combined. Shaded areas (grey) represent time periods of vertical migration events 1 – 6. Error bars represent ± 1 standard error.
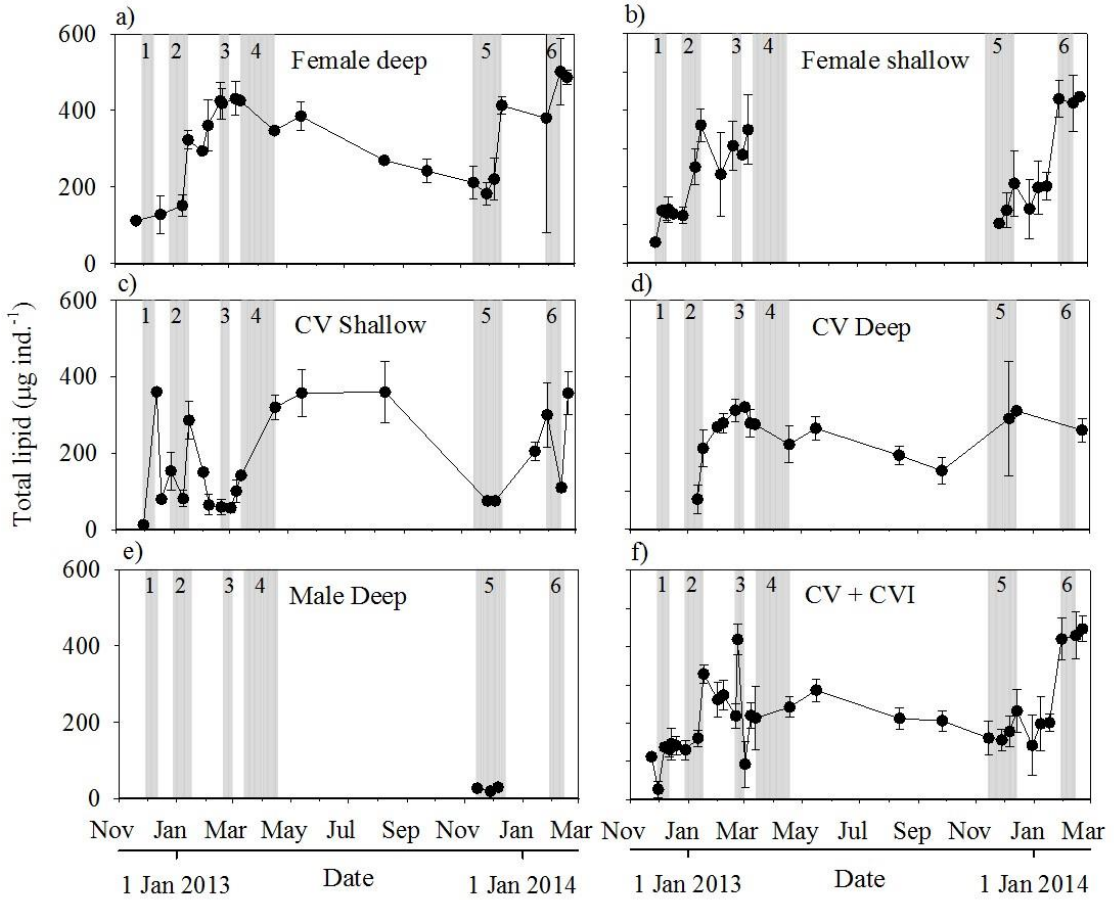
Fig. S2. Time series of total lipid content (TL) per copepod (μg ind^{-1}) for (a) deep females (b) shallow females, (c) shallow CVs, (d) deep CVs, (e) deep males and (f) CV and CVI stages combined. Shaded areas (grey) represent time periods of vertical migration events 1 – 6. Error bars represent ± 1 standard error.
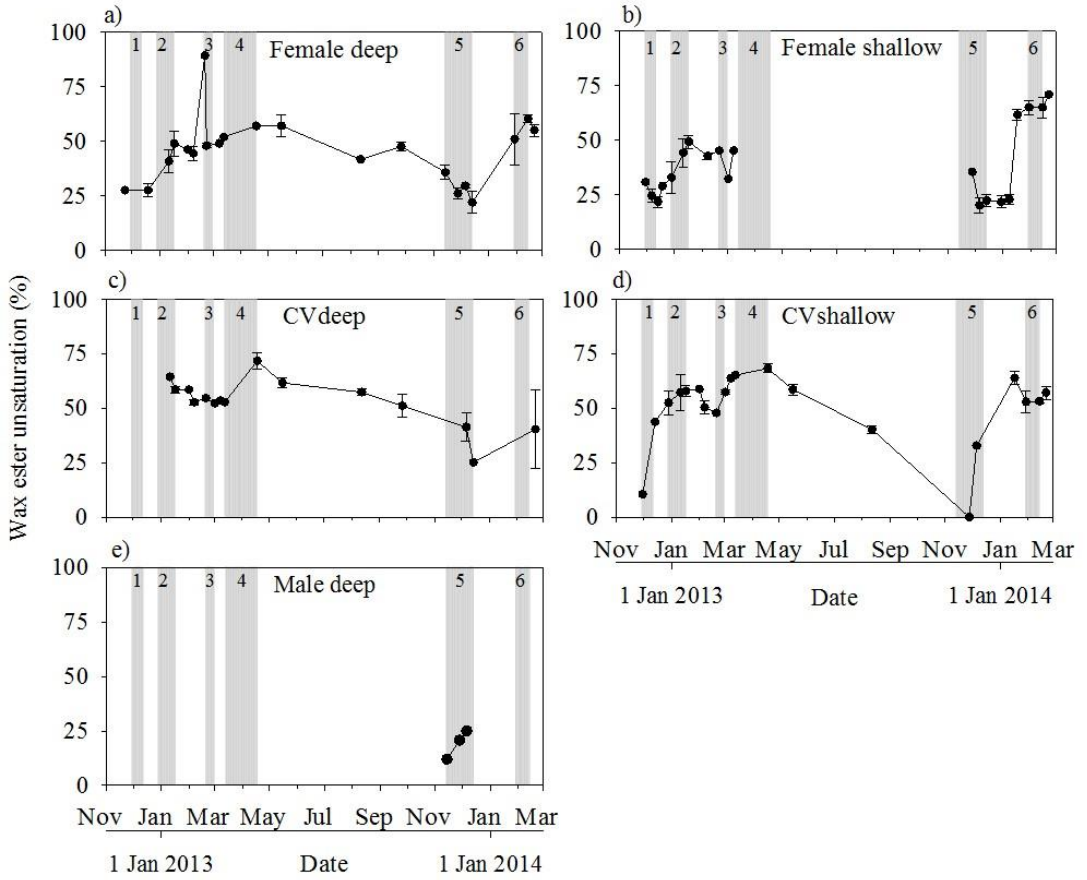
Fig. S3. Temporal dynamics of wax ester unsaturation (%) in (a) deep females, (b) shallow females, (c) deep CVs (d) shallow CVs and (e) deep males. Shaded areas (grey) represent time periods of vertical migration events 1 – 6. Error bars represent ± 1 standard error.
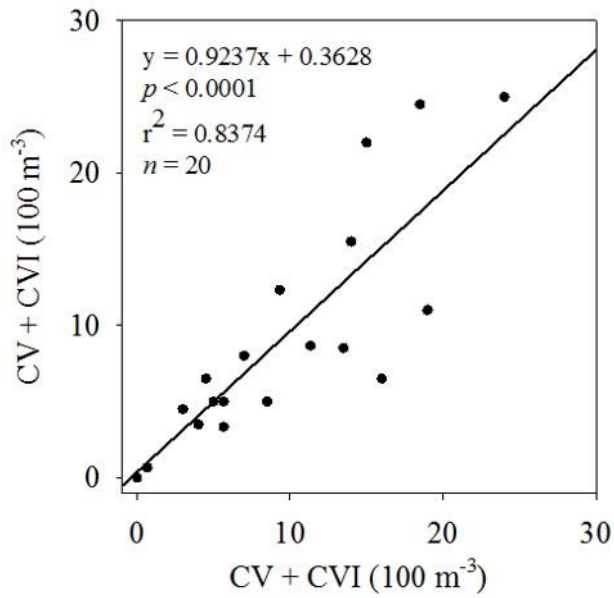
Fig. S4. Duplicate comparison (linear regression) of CV and CVI abundance from shallow water (200 versus 500 µm mesh width) and deep water net hauls (500 versus 500 µm mesh width).
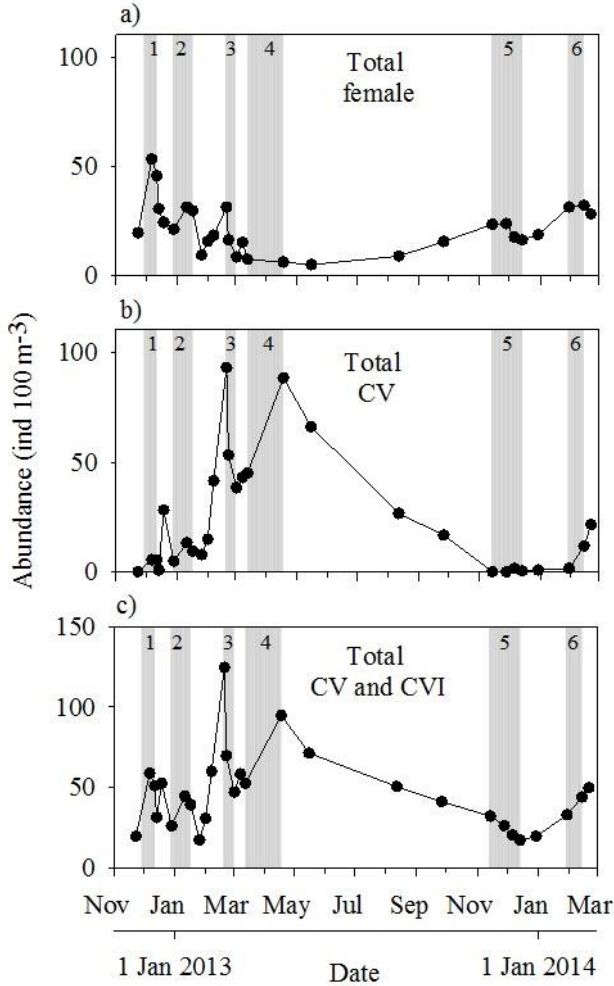
Fig. S5. Temporal dynamics of *C. acutus* abundance (ind 100 m^{-3}) from net hauls at the sampling site in Ryder Bay. (a) indicates total female abundance (shallow + deep), (b) total CVs and (c) total CV and CVI. Shaded areas (grey) represent time periods of vertical migration events 1 – 6.
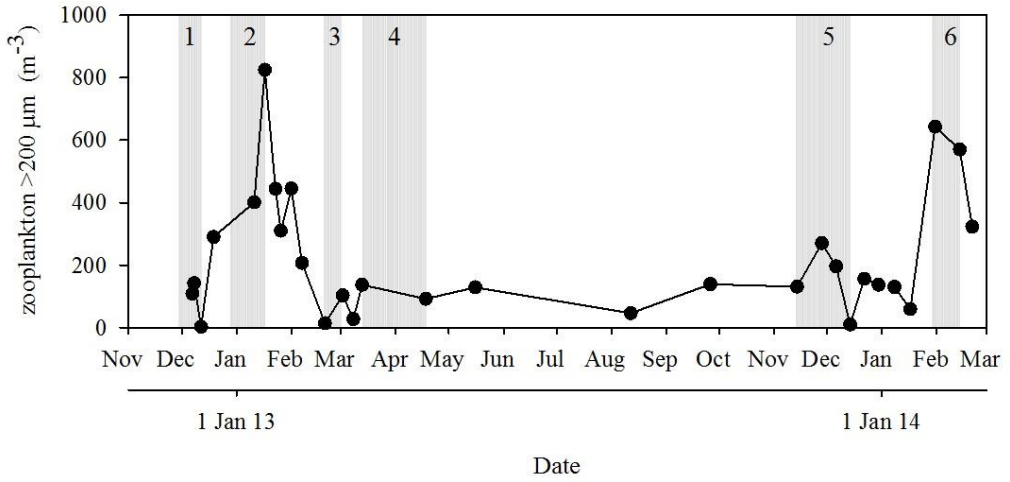
7

Fig. S6. Temporal dynamics of larger-sized zooplankton abundance (> 200 µm) from shallow water (200 – 0 m) net hauls at the study site. Shaded areas (grey) represent time periods of vertical migration events 1 – 6.

Chapter 8

Thesis Synthesis

The polar regions are semi-pristine environments (with little direct anthropogenic influence) subjected to extreme seasonality in primary and secondary production. Our understanding of their complex trophic interactions is limited, partly due to the remote location and difficult working conditions and partly because not all factors are fully considered. For example, losses due to viral lysis are still most often excluded in polar phytoplankton studies, and even the factors that may regulate dormancy behaviour of traditionally acknowledged important zooplankton predators (such as copepods) are not always examined. An improved description of the structuring role of environmental factors would benefit our perception of the links between trophic levels. Especially light availability and temperature are of interest, considering the current and future impact of potential climate change on polar marine ecosystems (Sommer and Lengfellner 2008; Marinov et al. 2010; Collins et al. 2013; Rozema et al. 2017).

This multi-trophic level study targeted both bottom-up and top-down regulatory factors of phytoplankton to provide a more complete understanding of naturally complex microbial community dynamics and interactions. Seasonal studies of phytoplankton growth, losses (viral lysis and grazing) and predator concentrations were combined with phytoplankton growth bioassays (in relation to ecologically relevant light intensities) and an experimental laboratory study of novel algal viruses (in relation to the effect of temperature).

The use of flow cytometry to provide a high-resolution description of the phytoplankton community provided a large amount of quantitative (rate) data crucial for the identification of relationships between environmental factors, phytoplankton growth, grazing and viral lysis rates. Moreover, the combination of flow cytometry, chemical taxonomy and size structure was vital for a more detailed description of the different ecologically relevant taxonomic groups (Chapters 2-5). For example, various diatom populations could be identified, varying in size between 4.5 and 20 μm cell diameter (Chapter 2). Diatoms are responsible for ~ 25% of total carbon fixed on earth (Leblanc et al. 2012) and up to 75% of primary production in the

Southern Ocean (Treguer et al. 1995). In both Arctic and Antarctic waters diatoms often dominate the 'spring' phytoplankton bloom (in Marguerite Bay the 'spring' bloom frequently occurs in summer) where they represent an important source of essential fatty acids (e.g. eicosapentaenoic acid or 20:5ω-3) for both small and large zooplankton. Diatom production is therefore one of the key drivers of secondary production in high latitude ecosystems (Kattner and Hagen 2009; Duarte et al. 2012). Diatoms are also an important contributor of particulate organic carbon to the deeper ocean (the biological carbon pump) for multiple reasons i.e. (i) diatom species differ in cell size (Chapter 2) and degree of silicification (biogenic silica skeleton) and thus sinking rate, in particular dead cells (Miklasz and Denny 2010; Assmy et al. 2013; Boyd 2013; Petrou et al. 2019), (ii) depending on growth conditions they can form relatively heavy resting spores (Rembauville et al. 2018), (iii) they can aggregate depending on their physiological conditions, amount of extracellular carbon release and cell abundance (Thornton 2002), and (iv) as prey of zooplankton (copepods and krill) they ballast their large faecal pellets (Voss 1991; Tréguer et al. 2018). Although the larger-sized diatoms typically contribute most to total chlorophyll *a* (especially during high biomass phytoplankton blooms; Rozema et al. 2017), the smaller diatoms (≤ 20 µm cell diameter) should not be ignored (Chapter 2) as they are highly diverse (Chapter 2-5; Tréguer et al. 2018) and globally overlooked (Leblanc et al. 2018). Chapter 2 shows indeed that nano-sized diatoms can dominate high biomass phytoplankton blooms and highlights their importance (especially Phyto IX and X) for efficient transfer of photosynthetically fixed carbon. Additionally, prymnesiophytes *Phaeocystis* Phyto III and cryptophytes Phyto IV could be identified, both important taxonomic groups in the Arctic and Southern Ocean (Garibotti et al. 2005; Assmy et al. 2017; Park et al. 2017). The combination of methods furthermore allowed the identification of pico-sized phytoplankton groups that are difficult to quantify using microscopy and pigment-based methods. Picoeukaryotic phytoplankton are numerically important in polar marine waters and there is evidence that picophytoplankton based systems may increase under global warming, especially in the Arctic (Li et al. 2009; Tremblay and Gagnon 2009;

8

Ardyna et al. 2011). Global warming is expected to strengthen stratification and increase seasonal light availability (more so in the Arctic Ocean), with an overall shift from diatoms to smaller-sized phytoplankton predicted to cause a trophic switch in copepod diet (Stibor et al. 2019). This will directly impact zooplankton communities as well as food web efficiency and organic carbon export (Williams et al. 2016).

Although seasonal light availability largely governs the length of the productive period, and phytoplankton are known to acclimate to their light environment (Dubinsky and Stambler 2009; Alderkamp et al. 2013), the mechanisms that regulate phytoplankton bloom dynamics, as well as the response of natural phytoplankton populations to low light, still require a better understanding. Extended periods of low light may occur during dense phytoplankton blooms (Vernet et al. 2008; Venables and Moore 2010; Park et al. 2017) where efficient acclimation to low light would be advantageous (Schofield et al. 2015). Using the natural light intensity and phytoplankton biomass data from Chapter 2, a negative exponential relationship was found for both S1 and S2 (Fig. 1) inferring high phytoplankton biomass was found at low light intensities and that indeed phytoplankton biomass had a large influence on the natural light environment during summer.

Seasonality in the initial slope of light response curves (α; Sloughter et al. 2019), i.e. a switch between modes of high and low growth, allows phytoplankton to take advantage of low light availability either side of mid-winter as well as under sea ice. The inclusion of α seasonality in phytoplankton models has only recently been suggested for Arctic phytoplankton (Sloughter et al. 2019) with the authors highlighting a need for experimentation to test this theoretical result. Chapter 5, focussing on phytoplankton growth responses under different light levels, provides experimental data in support of the idea that natural communities can indeed switch between different modes of growth and identified a potential boundary (4 – 7 µmol quanta m^{-2} s^{-1}) around which these changes may occur. The different light levels tested for the growth bioassays in Chapter 5 were based on climatological estimates
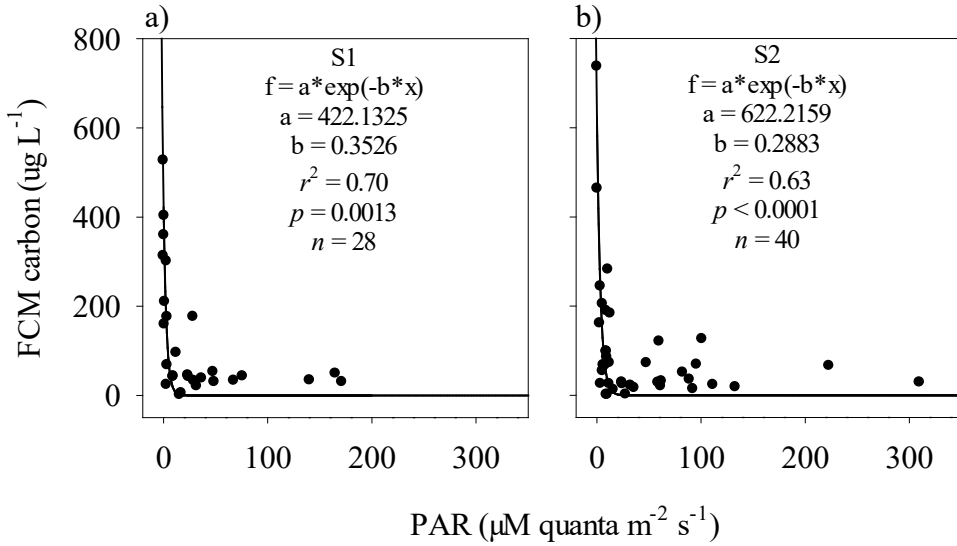
Fig. 1. Negative exponential regression analysis of natural PAR and flow cytometry estimated carbon standing stock (FCM carbon) at 15 m depth for (a) S1 and (b) S2.

from the Rothera Time Series (RaTS) and are therefore relevant to the natural phytoplankton blooms that fuel the ecosystem in this coastal environment. In contrast to what might be expected, the ability to switch to a low growth mode during summer can thus provide a distinct advantage. Although this phenomenon was documented for multiple phytoplankton populations, the highest growth rates under low light were achieved by nano-sized diatoms (Phyto IX), allowing this group (and size class) to become a recurrent feature of bloom climax. As such, the ability of phytopankton populations to switch between modes of growth during summer has consequences for bloom phenology, magnitude and trophic transfer efficiency (Chapters 2 and 5). A recent modeling study in the Amundsen Sea Polygna, an area often dominated by *P. antarctica* (Oliver et al. 2019), also suggests dense blooms become limited by low light soon after initiation. Therefore the capability to switch between modes of growth over relatively short time scales is likely an important feature for both diatoms and *Phaeocystis*.

Although light is an ecologically important variable to study as it strongly varies during the season, interactions with temperature can also influence phytoplankton

8

physiology (Raven and Geider 1988). Cryptophytes were associated with high temperature and high light environments (Chapter 2) and the only incubation experiment in S2 with significantly higher cryptophyceae net growth (at high and mid light, compared to low light intensity) was INC 5, when *in-situ* temperature rose above 1℃ (Chapter 5). Average growth (and viral lysis rates) of cryptophytes (Phyto IV) were also much higher during the warmer S1 (0.64 d^{-1}) than the colder S2 (0.16 d^{-1}, Chapter 4), agreeing with Chapter 2 and 5. A study by Mendes et al. (2017) also associated natural populations of cryptophytes in the WAP with temperature (rather than salinity; Buma et al. 1992; Moline et al. 1997, 2004; Mendes et al. 2013), however, other studies suggest mixotrophy is likely more important (Schofield et al. 2017; van Leeuwe et al. 2020). Still, cryptophyte dominance was stated as a feature of mid-summer when temperature and light intensity were highest (van Leeuwe et al. 2020). Unlike diatoms and *Phaeocystis*, both cryptophyceae and prasinophyceae contain mixotrophic species (Bell and Laybourn-Parry 2003; Stoecker and Lavrentyev 2018) with Chapter 2 indicating a stronger association of cryptophytes with temperature and prasinophytes with light. Chapter 2 also suggests selective grazing (on large diatoms) by large zooplankton may be involved in the transition from a diatom to a cryptophyte dominated community, as suggested previously for the Western Atlantic Peninsula (Kopczynska 1992). More research is required to better comprehend the importance of mixotrophy for cryptophyte populations and the interactive effects of temperature and light. Temporal variation in loss factors, for example cryptophytes were subjected to high rates of viral lysis in S1 (0.42 d^{-1}) compared to relatively low rates in the colder S2 (0.11 d^{-1}), as well as prey availability (bacteria and picoeukaryotes), will also influence their seasonal and inter-annual dynamics.

Phytoplankton standing stock is the net result of gross growth minus losses (Behrenfeld and Boss 2018) such as viral lysis and zooplankton grazing (Atkinson et al. 2012; Mojica et al. 2016). The type of loss factor and the size class of the grazer community determines the efficiency of carbon and nutrient flow through the

ecosystem (Suttle 2007; Brussaard et al. 2008b; Stibor et al. 2019), hence, studies that quantify specific viral lysis and grazing rates, and their functional significance throughout the productive season are greatly warranted. Most knowledge on phytoplankton-virus interactions is from temperate oceans and coastal waters, whereas very little is known about the extent to which viral losses may affect phytoplankton populations in cold productive polar waters and there are no seasonal studies (Brussaard et al. 2008a, 2013; Evans and Brussaard 2012). Chapters 3 and 4 show that all major taxonomic groups of Antarctic phytoplankton (e.g., diatoms, cryptophytes and prymnesiophytes) were subjected to viral lysis and highlights that even in cold polar waters, virus-induced mortality is an important loss factor. This suggests that energy and nutrient transfer through polar pelagic food webs is less efficient than previously believed, as half of primary production is shunted by viruses towards the microbial loop where lysed labile cellular components stimulate bacterial production (Chapters 3 and 4) and increase community respiration. Moreover, Chapters 3 and 4 represent the first detailed intra-seasonal studies of viral lysis and grazing rates in polar marine systems. Also for non-polar waters only a handful of studies comparing viral lysis and grazing rates have been published (Mojica et al. 2016 and references within) and no inter-seasonal comparisons. The inclusion of losses due to viral lysis was found critical for the closure of the seasonal mass balance (Chapters 3 and 4), independent of the seasonal average temperature. The importance of cell size is clear when converting abundance to cellular carbon and large portions of seasonal phytoplankton production were shunted towards the microbial loop in relatively short time periods. This finding calls for a reconsideration of the efficiency of the biological carbon pump in this climate sensitive region.

The average seasonal microzooplankton grazing rates were lower in the colder S2 (< 0°C, compared to S1 with average temperature > 0°C; Chapter 2), whilst viral lysis rates were comparable. Consequently, viral lysis in the colder S2 made up for a greater share of the phytoplankton cell losses. Although this suggests that the Antarctic marine coastal food web is relatively more regenerative during colder

8

summers, the seeding of fast growing, larger nano-sized diatoms from mobile sea ice (that can account for large portions of seasonal carbon production; Chapter 2, 4 and 5) provides large zooplankton with direct access to primary production and would (partly) counteract the reduction in trophic transfer efficiency (Sommer et al. 2005). More specifically during seasonal bloom dynamics, both productive seasons revealed a distinct shift in the share of loss factors with more viral lysis during the phytoplankton accumulation phase and more grazing during bloom decline. This trend occurred over a wide range of growth, with the tipping point in the share of loss factors related to the seasonal average growth (lower in S2 than S1). These results provide a mechanistic insight, indicating a shift in the share of losses could be an inherent feature of phytoplankton blooms, especially in eutrophic coastal waters where light availability becomes a primary driver of phytoplankton net growth (Chapter 2 and 5; Vernet et al. 2008; Park et al. 2017; Oliver et al. 2019). Subsequently, reduced growth at bloom climax (Chapter 2-5) likely prompted reduced virus production (Chapter 6; Piedade et al. 2018; Gann et al. 2020).

These results show that viruses are an important cause of phytoplankton mortality and should be included in ecosystem models. Modeling is a critical tool to investigate the potential impact of climate change on ecosystems and biogeochemical cycles, however, models are restricted by a lack of quantitative data in the literature to describe key processes and evaluate predictions (Gruber and Doney 2009; Mateus 2017). Those that incorporate phytoplankton losses usually accredit zooplankton grazing as the dominant loss factor and frequently exclude viruses in marine ecosystem models (Mateus 2017). The addition of particle sorting and molecular identification of both virus and host would further advance our understanding of the regulatory role of viruses. Still, bringing new viruses and their hosts into culture for characterization and detailed experimental studies is greatly warranted to improve our insight in virus-host diversity, interactions, and how they are affected by environmental stressors. *Micromonas* is a genus of flagellated picophytoplankton with a worldwide distribution, including both Arctic and Antarctic waters (Worden and Not 2008; Simmons et al. 2015). We isolated and characterised the first polar

algal viruses, *Micromonas polaris* MpoVs (Chapter 6). At the same time, we also investigated temperature related differences between the various strains of both virus and host (Chapter 6). Our results show that polar MpoVs can withstand freezing, highlighting the potential for seeding of both virus and host populations from melting sea ice in spring and summer. As temperature can vary both within and between productive seasons, host and virus-specific responses are likely to promote strain diversity and allow different (sub)populations to coexist (Chapter 4 and 6). The ecological impact of temperature on virus-host dynamics is complex, for example, the combination of host RCC2258 with virus MpoV-45T displayed at higher temperature (7 compared to 3˚C) a shorter viral latent period and higher burst size, while TX-01 with MpoV-45T produced more progeny viruses with an unchanged latent period. At the same time, infectivity of MpoV-45T was lowest at 7℃ (compared to 0℃) whilst that of virus strain MpoV-47T remained stable over the range of temperature tested and virus strain MpoV-44T was most infective at the warmest temperature. A subsequent study by Piedade et al. (2018) investigated the impact of both temperature and light on polar host-virus interactions (RCC2257 and 2258 with MpoV-45T). Similar to Chapter 6, at higher temperature and non-limiting light levels, the latent period was reduced, burst size increased and infectivity reduced. However, under low light conditions (5 µmol quanta m^{-2} s^{-1}) the latent period was extended and temperature made no additional difference to the latent period or burst size. At the same time infectivity was drastically reduced under all temperatures. This suggests that as low light limits phytoplankton growth at bloom climax, reduced virus production and reduced infectivity combine to drastically reduce losses due to viral lysis and initiate the shift to more grazing whilst preventing the decimation of host populations. These findings demonstrate the ecological importance of temperature and light as factors controlling polar phytoplankton host-virus-grazing interactions. As these factors vary both within and between productive seasons, such host and virus strain-specific responses are likely to promote strain diversity and allow different (sub)populations to coexist (Chapter 4 and 6). Longer term eco-evolutionary dynamics experiments with different host and virus stains are

8

recommend to shed light on how global warming may selectively force phytoplankton host and virus dynamics over short evolutionary time scales.

Temperature has far reaching effects, as also demonstrated by faster maturation rates of *Calanoides acutus* nauplii and an earlier increase in larger-sized zooplankton in the warm Antarctic summer of S1 (Chapter 7). Pelagic food webs are highly size-structured (Sommer et al. 2018) and increased numbers of larger-sized zooplankton provide an additional grazing pressure on larger nano-sized diatoms (Atkinson 1994; Sommer and Stibor 2002; Sommer and Sommer 2006; Chapter 2 and 7). Combined with losses due to viral lysis and microzooplankton grazing (Chapter 3 and 4), this likely shortened the 'spring' bloom (S1) and extended the post bloom period. A greater importance of carnivorous grazing by larger-sized zooplankton could increase predation pressure on the population of *C. acutus* as a whole and combined with low Chl-*a* concentrations, initiate early overwintering behaviour (Chapters 2 and 7). If the post bloom period (high light, high temperature and relatively low nutrients) extends into late summer and restricts the accumulation of smaller-sized diatoms (e.g. Phyto V and VI, highly grazed by microzooplankton; Chapter 3), it could prevent an increase of the larger Phyto IX that prevails in dense blooms with low light conditions (Chapter 2 and 5). Under future conditions of increased stratification strength resulting from global warming (especially in the Arctic; Collins et al. 2013), late season blooms of Phyto IX could disappear. A greater share of smaller-sized diatoms (Phyto V and VI) and flagellated phytoplankton (Phyto III and IV, and likely Phyto I) could be a feature of warm Antarctic summers with early ice melt, matching predictions in the literature (Petrou et al. 2016, 2019). This could cause a trophic switch in the diet of primarily herbivorous copepods, from large diatoms to microzooplankton (Sommer et al. 2005), increasing the length of the food chain and potentially contributing to population decline of *C. acutus* (Chapter 7). A trophic switch in copepod diet could be intensified by viral lysis of suitably sized cells. This could have severe consequences for ecosystems dynamics in polar food webs with a high lipid demand.

At the time of dormancy termination in both seasons (December and February), *Phaeocystis* Phyto III and diatoms Phyto VI, VIII and IX contributed most to carbon lysed (> 90%; Chapter 2-5 and 7). Yamada and colleagues (2018) showed that viral lysis of the diatom *Chaetoceros tenuissimus* induced aggregation and sedimentation, resulting in rapidly sinking particles ($35 – 113$ m d^{-1}). The potential to induce sinking of organic matter that is usually considered to remain suspended (Suttle 2007), implies that viral lysis could contribute positively to the biological pump (Brussaard et al. 2008b). Lysis derived aggregates would have a different stoichiometry (Yamada et al. 2018), and thus nutritional quality, than those derived from zooplankton grazing. The suggestion that sticky lysis products may induce sedimentation during phases of phytoplankton accumulation should be investigated further in natural (coastal) communities as well as in areas with a deeper average mixed layer depth during summer. This thesis suggests that global warming will enhance rates of phytoplankton growth, resulting in greater contributions by smaller-sized cells and potentially a greater importance of lysis induced sinking of organic matter.

Sedimentation may initiate dormancy termination of large herbivorous copepods (by providing a signal of food availability above) and ultimately regulate the lifecycle of this key herbivorous grazer. Copepod studies often center around a singular event in a particular life stage and there is a need for studies that span entire lifecycles (Mitra et al. 2014). Even the lifespan of an important Antarctic species such as *C. acutus* is still not certain. Chapter 7 presents previously unreported flexibility in behaviour of a key copepod species that potentially resolves the discrepancy between estimations of lifespan, i.e. either one year or two. Similar to the phytoplankton blooms documented in S1 (Chapter 2), higher temperatures have been linked to novel late season phytoplankton blooms in the Arctic (Ardyna et al. 2014). This suggests that dormancy inducing copepods may already be transitioning from a two- to a one-year lifecycle and a reorganisation of Arctic food webs could already be underway, highlighting the critical need for further research.

8

Dormancy behaviour was linked to bottom-up and top-down factors as well as the composition of internal lipid reserves (Chapter 2 and 7). The potential synergistic relationship between lipid pools of monounsaturated (22:1ω-11 and 20:1ω-9) and polyunsaturated (20:5ω-3) fatty acids suggests the long chain alcohols within wax esters may represent a store of 22:1ω-11 and 20:1ω-9 fatty acids as well as having a direct biophysical role. Alternatively, this could also be a mechanism to achieve extremely high wax ester unsaturation values critical for phase transition of the (CV) lipid store, especially when overwintering with relatively low concentrations of total lipid. More seasonal investigations are needed, especially over time scales relevant to the lifecycle of key trophic links, to better understand the complex interactions of microbes and bridge the modelling gap between biogeochemical cycles and fish (Mitra et al. 2014).

Climate change in the Antarctic is difficult to predict, however, a recent (and also future predicted; Turner et al. 2009) trend of positive Southern Annular Mode (SAM) events (Fig. 2; Marshall and Staff 2018) suggests that in the near future more Southern parts of the Western Antarctic Peninsula may potentially experience more cold summers similar to S2, whereas more Northern parts may experience more warmer summers similar to S1. However, shallow water temperatures will be influenced by differences in ice cover, average mixed layer depth and the frequency of storm events, as well as the influence of relatively cold Weddell Sea water to the North and intrusions of relatively warm circumpolar deep water in the Marguerite Bay area (Huneke et al. 2016; Moffat and Meredith 2018). The timing and frequency of wind-induced mixing played an important role in temporal temperature dynamics (Chapter 2) and consequently phytoplankton growth, cell size and taxonomy. Therefore the state of SAM could potentially also influence the share of viral lysis and grazing during the most productive time of the year (Chapter 3 and 4).
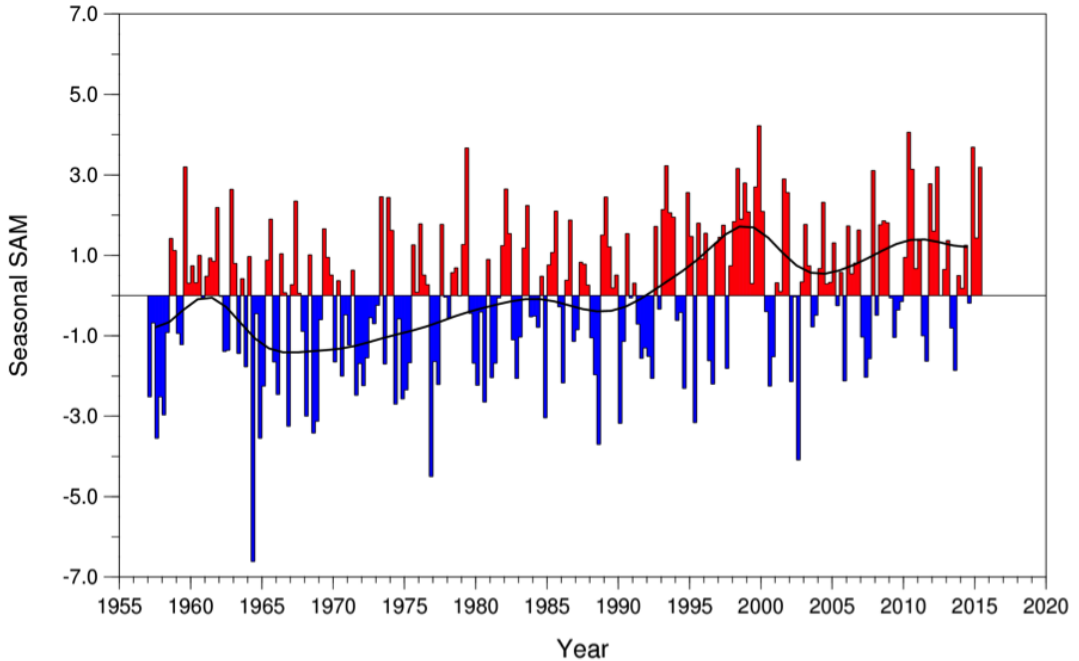
Fig. 2. Seasonal values of Peninsula observation-based Southern Annular Mode (SAM) index, whereby the smooth black curve shows decadal variations (copied from Marshall and Staff 2018). A positive SAM phase (with a greater influence during the warmer summer months; Clem et al. 2016) is linked to cooling, more storms and more sea ice in the Southern part of the Western Antarctic Peninsula (WAP) area, related to meridional winds flowing South along the WAP as well as a shift in the storm track towards the Antarctic continent. However, effects of SAM are not geographically consistent with an opposing trend (i.e. global warming and reduced sea ice) in the Northern part of the WAP, where stronger zonal winds advect sea ice out of the area and cross over the WAP resulting in leeside adiabatic warming (Clem et al. 2016).

References

Alderkamp A, Mills M, van Dijken G, Arrigo K (2013) Photoacclimation and non-photochemical quenching under in situ irradiance in natural phytoplankton assemblages from the Amundsen Sea, Antarctica. Mar Ecol Prog Ser 475:15–34. doi: 10.3354/meps10097

Ardyna M, Babin M, Gosselin M, et al (2014) Recent Arctic Ocean sea ice loss triggers novel fall phytoplankton blooms. Geophys Res Lett 41:6207–6212. doi: 10.1002/2014GL061047

Ardyna M, Gosselin M, Michel C, et al (2011) Environmental forcing of phytoplankton community structure and function in the Canadian high Arctic: Contrasting oligotrophic and eutrophic regions. Mar Ecol Prog Ser 442:37–57. doi: 10.3354/meps09378

Assmy P, Fernández-Méndez M, Duarte P, et al (2017) Leads in Arctic pack ice enable early phytoplankton blooms below snow-covered sea ice. Sci Rep 7:1–9. doi: 10.1038/srep40850

Assmy P, Smetacek V, Montresor M, et al (2013) Thick-shelled, grazer-protected diatoms decouple ocean carbon and silicon cycles in the iron-limited Antarctic Circumpolar Current. Proc Natl Acad Sci U S A 110:20633–20638. doi: 10.1073/pnas.1309345110

8

Atkinson A (1994) Diets and feeding selectivity among the epipelagic copepod community near South Georgia in summer. Polar Biol 14:551–560. doi: 10.1007/BF00238225

Atkinson A, Ward P, Hunt BP V., et al (2012) An overview of Southern Ocean zooplankton data: Abundance, biomass, feeding and functional relationships. CCAMLR Sci 19:171–218

Behrenfeld MJ, Boss ES (2018) Student's tutorial on bloom hypotheses in the context of phytoplankton annual cycles. Glob Chang Biol 24:55–77. doi: 10.1111/gcb.13858

Bell EM, Laybourn-Parry J (2003) Mixotrophy in the Antarctic phytoflagellate, *Pyramimonas gelidicola* (Chlorophyta: Prasinophyceae). J Phycol 39:644–649. doi: 10.1046/j.1529-8817.2003.02152.x

Boyd PW (2013) Diatom traits regulate Southern Ocean silica leakage. Proc Natl Acad Sci U S A 110:20358–20359. doi: 10.1073/pnas.1320327110

Brussaard CPD, Noordeloos AAM, Witte H, et al (2013) Arctic microbial community dynamics influenced by elevated CO_2 levels. Biogeosciences 10:719–731. doi: 10.5194/bg-10-719-2013

Brussaard CPD, Timmermans KR, Uitz J, Veldhuis MJW (2008a) Virioplankton dynamics and virally induced phytoplankton lysis versus microzooplankton grazing southeast of the Kerguelen (Southern Ocean). Deep Sea Res Part II Top Stud Oceanogr 55:752–765. doi: 10.1016/j.dsr2.2007.12.034

Brussaard CPD, Wilhelm SW, Thingstad F, et al (2008b) Global-scale processes with a nanoscale drive: The role of marine viruses. ISME J 2:575–578. doi: 10.1038/ismej.2008.31

Buma AGJ, Gieskes WWC, Thomsen HA (1992) Abundance of Cryptophyceae and chlorophyll b-containing organisms in the Weddell-Scotia Confluence area in the spring of 1988. Polar Biol 12:43–52. doi: 10.1007/BF00239964

Clem KR, Renwick JA, McGregor J, Fogt RL (2016) The relative influence of ENSO and SAM on Antarctic Peninsula climate. J Geophys Res Atmos 121:9324–9341. doi: 10.1002/2016JD025305

Collins M, Knutti R, Arblaster J, et al (2013) Long-term climate change: Projections, commitments, and irreversibility. Cambridge University Press, United Kingdom and New York, NY, USA,

Duarte CM, Agustí S, Wassmann P, et al (2012) Tipping elements in the Arctic marine ecosystem. Ambio 41:44–55. doi: 10.1007/s13280-011-0224-7

Dubinsky Z, Stambler N (2009) Photoacclimation processes in phytoplankton: Mechanisms, consequences, and applications. Aquat Microb Ecol 56:163–176. doi: 10.3354/ame01345

Evans C, Brussaard CPD (2012) Viral lysis and microzooplankton grazing of phytoplankton throughout the Southern Ocean. Limnol Oceanogr 57:1826–1837. doi: 10.4319/lo.2012.57.6.1826

Gann ER, Gainer PJ, Reynolds TB, Wilhelm SW (2020) Influence of light on the infection of *Aureococcus anophagefferens* CCMP 1984 by a "giant virus." PLoS One 15:e0226758. doi: 10.1371/journal.pone.0226758

Garibotti IA, Vernet MM, Ferrario ME, et al (2005) Annually recurrent phytoplanktonic assemblages during summer in the seasonal ice zone west of the Antarctic Peninsula (Southern Ocean). Deep Res Part I Oceanogr Res Pap 52:1823–1841. doi: 10.1016/j.dsr.2005.05.003

Gruber N, Doney SC (2009) Ocean biogeochemistry and ecology, modeling of. In: Encyclopedia of Ocean Sciences. Elsevier, pp 89–104

Huneke WGC, Huhn O, Schröeder M (2016) Water masses in the Bransfield Strait and adjacent seas, austral summer 2013. Polar Biol 39:789–798. doi: 10.1007/s00300-016-1936-8

Kattner G, Hagen W (2009) Lipids in marine copepods: Latitudinal characteristics and perspective to global warming. In: Kainz M, Brett M, Arts M (eds) Lipids in Aquatic Ecosystems. Springer New York, pp 257–280

Kopczynska EE (1992) Dominance of microflagellates over diatoms in the Antarctic areas of deep vertical mixing and krill concentrations. J Plankton Res 14:1031–1054. doi: 10.1093/plankt/14.8.1031

Leblanc K, Arístegui J, Armand L, et al (2012) A global diatom database- Abundance, biovolume and biomass in the world ocean. Earth Syst Sci Data 4:149–165. doi: 10.5194/essd-4-149-2012

Leblanc K, Quéguiner B, Diaz F, et al (2018) Nanoplanktonic diatoms are globally overlooked but play a role in spring blooms and carbon export. Nat Commun 9:1–12. doi: 10.1038/s41467-018-03376-9

Li WKW, McLaughlin FA, Lovejoy C, Carmack EC (2009) Smallest algae thrive as the arctic ocean freshens. Science (80-) 326:539. doi: 10.1126/science.1179798

Marinov I, Doney SC, Lima ID (2010) Response of ocean phytoplankton community structure to climate change over the 21st century: Partitioning the effects of nutrients, temperature and light. Biogeosciences 7:3941–3959. doi: 10.5194/bg-7-3941-2010

Marshall G, Staff NC for AR (2018) The climate data guide: Marshall Southern Annular Mode (SAM) index (station-based). https://climatedataguide.ucar.edu/climate-data/marshall-southern-annular-mode-sam-index-station-based. Accessed 18 Jul 2020

Mateus MD (2017) Bridging the gap between knowing and modeling viruses in marine systems—An upcoming frontier. Front Mar Sci 3:1–16. doi: 10.3389/fmars.2016.00284

Mendes CRB, Tavano VM, Dotto TS, et al (2017) New insights on the dominance of cryptophytes in Antarctic coastal waters: A case study in Gerlache Strait. Deep Sea Res Part II Top Stud Oceanogr 149:161–170. doi: 10.1016/j.dsr2.2017.02.010

Mendes CRB, Tavano VM, Leal MC, et al (2013) Shifts in the dominance between diatoms and cryptophytes during three late summers in the Bransfield Strait (Antarctic Peninsula). Polar Biol 36:537–547. doi: 10.1007/s00300-012-1282-4

Miklasz KA, Denny MW (2010) Diatom sinking speeds: Improved predictions and insight from a modified Stoke's law. Limnol Oceanogr 55:2513–2525. doi: 10.4319/lo.2010.55.6.2513

Mitra A, Castellani C, Gentleman WC, et al (2014) Bridging the gap between marine biogeochemical and fisheries sciences; configuring the zooplankton link. Prog Oceanogr 129:176–199. doi: 10.1016/j.pocean.2014.04.025

Moffat C, Meredith M (2018) Shelf–ocean exchange and hydrography west of the Antarctic Peninsula: a review. Philos Trans R Soc A Math Phys Eng Sci 376:20170164. doi: 10.1098/rsta.2017.0164

Mojica KDA, Huisman J, Wilhelm SW, Brussaard CPD (2016) Latitudinal variation in virus-induced mortality of phytoplankton across the North Atlantic Ocean. ISME J 10:500–513. doi: 10.1038/ismej.2015.130

Moline MA, Claustre H, Frazer TK, et al (2004) Alteration of the food web along the Antarctic Peninsula in response to a regional warming trend. Glob Chang Biol 10:1973–1980. doi: 10.1111/j.1365-2486.2004.00825.x

Moline MA, Prezelin BB, Schofield OM, Smith RC (1997) Temporal dynamics of coastal Antarctic phytoplankton: Environmental driving forces and impact of a 1991/92 summer diatom bloom on the nutrient regimes. In: Battaglia B, Valencia H, Walton DWH (eds) Antarctic communities: Species, structure and survival. Cambridge University Press, pp 67–72

Oliver H, St-Laurent P, Sherrell RM, Yager PL (2019) Modeling iron and light controls on the summer *Phaeocystis antarctica* bloom in the Amundsen Sea Polynya. Global Biogeochem Cycles 2018GB006168. doi: 10.1029/2018GB006168

Park J, Kuzminov FI, Bailleul B, et al (2017) Light availability rather than Fe controls the magnitude of massive phytoplankton bloom in the Amundsen Sea polynyas, Antarctica. Limnol Oceanogr 62:2260–2276. doi: 10.1002/lno.10565

Petrou K, Baker KG, Nielsen DA, et al (2019) Acidification diminishes diatom silica production in the Southern Ocean. Nat Clim Chang 9:781–786. doi: 10.1038/s41558-019-0557-y

Petrou K, Kranz SA, Trimborn S, et al (2016) Southern Ocean phytoplankton physiology in a changing climate. J Plant Physiol 203:135–150. doi: 10.1016/j.jplph.2016.05.004

Piedade GJ, Wesdorp EM, Borbolla EM, Maat DS (2018) Influence of irradiance and temperature on the virus MpoV-45T infecting the Arctic picophytoplankter *Micromonas polaris*. Viruses 1–17. doi: 10.3390/v10120676

Raven JA, Geider RJ (1988) Temperature and algal growth. New Phytol 110:441–461. doi: 10.1111/j.1469-8137.1988.tb00282.x

Rembauville M, Blain S, Manno C, et al (2018) The role of diatom resting spores in pelagic–benthic coupling in the Southern Ocean. Biogeosciences 15:3071–3084. doi: 10.5194/bg-15-3071-2018

Rozema PD, Venables HJ, van de Poll WH, et al (2017) Interannual variability in phytoplankton biomass and species composition in northern Marguerite Bay (West Antarctic Peninsula) is governed by both winter sea ice cover and summer stratification. Limnol Oceanogr 62:235–252. doi: 10.1002/lno.10391

Schofield O, Miles T, Alderkamp A-C, et al (2015) In situ phytoplankton distributions in the Amundsen Sea Polynya measured by autonomous gliders. Elem Sci Anthr 3:000073. doi: 10.12952/journal.elementa.000073

Schofield O, Saba G, Coleman K, et al (2017) Decadal variability in coastal phytoplankton community

8

composition in a changing West Antarctic Peninsula. Deep Res Part I Oceanogr Res Pap 124:42–54. doi: 10.1016/j.dsr.2017.04.014

Simmons MP, Bachy C, Sudek S, et al (2015) Intron invasions trace algal speciation and reveal nearly identical Arctic and Antarctic *Micromonas* populations. Mol Biol Evol 32:2219–2235. doi: 10.1093/molbev/msv122

Sloughter TM, Banas NS, Sambrotto RN (2019) Seasonal variation in light response of polar phytoplankton. J Mar Syst 191:64–75. doi: 10.1016/j.jmarsys.2018.12.003

Sommer U, Charalampous E, Scotti M, Moustaka-Gouni M (2018) Big fish eat small fish: Implications for food chain length? Community Ecol 19:107–115. doi: 10.1556/168.2018.19.2.2

Sommer U, Hansen T, Blum O, et al (2005) Copepod and microzooplankton grazing in mesocosms fertilised with different Si:N ratios: No overlap between food spectra and Si:N influence on zooplankton trophic level. Oecologia 142:274–283. doi: 10.1007/s00442-004-1708-y

Sommer U, Lengfellner K (2008) Climate change and the timing, magnitude, and composition of the phytoplankton spring bloom. Glob Chang Biol 14:1199–1208. doi: 10.1111/j.1365-2486.2008.01571.x

Sommer U, Sommer F (2006) Cladocerans versus copepods: The cause of contrasting top–down controls on freshwater and marine phytoplankton. Oecologia 147:183–194. doi: 10.1007/s00442-005-0320-0

Sommer U, Stibor H (2002) Copepoda - Cladocera - Tunicata: The role of three major mesozooplankton groups in pelagic food webs. Ecol Res 17:161–174. doi: 10.1046/j.1440-1703.2002.00476.x

Stibor H, Stockenreiter M, Nejstgaard JC, et al (2019) Trophic switches in pelagic systems. Curr Opin Syst Biol 13:108–114. doi: 10.1016/j.coisb.2018.11.006

Stoecker DK, Lavrentyev PJ (2018) Mixotrophic plankton in the polar seas: A pan-Arctic review. Front Mar Sci 5:. doi: 10.3389/fmars.2018.00292

Suttle CA (2007) Marine viruses — major players in the global ecosystem. Nat Rev Microbiol 5:801–812. doi: 10.1038/nrmicro1750

Thornton DCO (2002) Diatom aggregation in the sea: mechanisms and ecological implications. Eur J Phycol 37:S0967026202003657. doi: 10.1017/S0967026202003657

Tréguer P, Bowler C, Moriceau B, et al (2018) Influence of diatom diversity on the ocean biological carbon pump. Nat Geosci 11:27–37. doi: 10.1038/s41561-017-0028-x

Treguer P, Nelson DM, Van Bennekom AJ, et al (1995) The silica balance in the world ocean: A reestimate. Science (80-) 268:375–379. doi: 10.1126/science.268.5209.375

Tremblay J-É, Gagnon J (2009) The effects of irradiance and nutrient supply on the productivity of Arctic waters: A perspective on climate change. In: Nihoul JCJ, Kostianoy AG (eds) Influence of Climate Change on the Changing Arctic and Sub-Arctic Conditions. Springer Netherlands, Dordrecht, pp 73–93

Turner J, Bindschadler R, Convey P, et al (2009) Antarctic climate change and the environment. Sci Comm Antarct Res 555

van Leeuwe MA, Webb AL, Venables HJ, et al (2020) Annual patterns in phytoplankton phenology in Antarctic coastal waters explained by environmental drivers. Limnol Oceanogr 1651–1668. doi: 10.1002/lno.11477

Venables H, Moore CM (2010) Phytoplankton and light limitation in the Southern Ocean: Learning from high-nutrient, high-chlorophyll areas. J Geophys Res 115:C02015. doi: 10.1029/2009JC005361

Vernet M, Martinson D, Iannuzzi R, et al (2008) Primary production within the sea-ice zone west of the Antarctic Peninsula: I—Sea ice, summer mixed layer, and irradiance. Deep Sea Res Part II Top Stud Oceanogr 55:2068–2085. doi: 10.1016/j.dsr2.2008.05.021

Voss M (1991) Content of copepod faecal pellets in relation to food supply in Kiel Bight and its effect on sedimentation rate. Mar Ecol Prog Ser 75:217–225. doi: 10.3354/meps075217

Williams CM, Dupont AM, Loevenich J, et al (2016) Pelagic microbial heterotrophy in response to a highly productive bloom of *Phaeocystis antarctica* in the Amundsen Sea Polynya, Antarctica. Elem Sci Anthr 4:000102. doi: 10.12952/journal.elementa.000102

Worden AZ, Not F (2008) Ecology and diversity of picoeukaryotes. In: Kirchman DL (ed) Microbial Ecology of the Oceans. John Wiley & Sons, Inc., Hoboken, NJ, USA, pp 159–205

Yamada Y, Tomaru Y, Fukuda H, Nagata T (2018) Aggregate formation during the viral lysis of a marine diatom. Front Mar Sci 5:. doi: 10.3389/fmars.2018.00167

Summary

Summary

The polar oceans play a pivotal role in global climate regulation, are key areas for global pCO_2 drawdown and are particularly sensitive to global climate change. Ocean climate models predict further warming of ocean surface waters combined with increased fresh water input at high latitudes that will affect the structure and functioning of polar phytoplankton (unicellular algae) communities. The key processes that regulate phytoplankton community dynamics are currently understudied in polar marine waters and the lack of a 'baseline' against which to compare, inhibits predictions of potential ecosystem changes and ultimately the carrying capacity of polar marine food webs.

Due to extreme seasonality at high latitudes, polar marine phytoplankton experience strong variation in temperature, sea ice cover, light intensity and photoperiod, yet, the precise role of these so called 'bottom-up' factors on polar phytoplankton growth, peak biomass and seasonal phytoplankton dynamics is not fully understood. Furthermore, global climate change is linked to greater contributions by smaller-sized phytoplankton and a reduction in micro-sized diatoms in polar seas. Detailed seasonal phytoplankton field data is limited in polar waters and therefore the drivers behind shifts in phytoplankton remain largely unclear.

Not only the sum but also the size class, taxonomy and the timing of phytoplankton production can influence the flow of energy and matter and hence the potential of polar regions to serve as a long-term sink for atmospheric CO_2. Phytoplankton abundances are also controlled by 'top-down' predation factors, traditionally accredited to zooplankton grazers. More recently viral lysis has been shown as a significant mortality factor of phytoplankton, thereby shunting photosynthetically fixed particulate matter away from higher trophic levels to the pool of dissolved and detrital organic matter. Zooplankton grazing and viral lysis have very different effects on trophic transfer efficiency and organic carbon export to the deep sea (biological pump), yet viral lysis as a loss factor of Antarctic phytoplankton is still seriously understudied. Moreover, no temporal studies have been published thus far, nor polar algal virus-host model systems brought into culture for more detailed

analysis under controlled conditions. Besides grazing by smaller zooplankton, larger lipid-rich zooplankton (such as copepods) are important predators and a key trophic link in polar marine ecosystems. Nevertheless, there are very few seasonal and multi-factor studies of copepod behaviour in the literature (i.e. those that study bottom-up and top-down factors as well as abundance and lipid dynamics), let alone for polar ecosystems.

The main aim of this thesis was to better understand the seasonal dynamics of polar phytoplankton in relation to viruses and zooplankton predators, which translated into the following research objectives: (A) Investigate the environmental factors responsible for structuring polar phytoplankton communities (Chapter 2) and examine more specifically how changing light and temperature affect phytoplankton net growth (Chapter 5) and polar virus-host interactions (Chapter 6), (B) Determine the importance of viral lysis compared to grazing over seasonal cycles (Chapter 3 and 4) and (C) Study how phytoplankton dynamics influence lipid accumulation and dormancy behaviour of key copepod grazers (Chapter 7).

To better determine the main environmental variables shaping the phytoplankton community at a productive coastal site in the Western Antarctic Peninsula (WAP), flow cytometry, size fractionation and chemical taxonomy were combined in **Chapter 2** and analysed alongside physicochemical factors by multivariate analysis. Ice type was important during the 'spring' bloom period, not only seeding different sized diatoms (i.e. brash ice seeded nano-sized cells and fast ice micro-sized diatoms) but also light availability due to shading. During the relatively warm Antarctic summer (season 1, S1), post 'spring' bloom seasonal succession by cryptophytes was linked to high temperature and high light and potentially encouraged by selective grazing on large diatoms by large zooplankton. Small-sized diatoms (average 4.5 µm cell diameter) became dominant later in the season, associated with high temperature, high light and high nutrient concentrations until reduced PAR and nutrients (due to high phytoplankton biomass) resulted in

succession by relatively larger nano-sized diatoms (11.5 µm). A prolonged period of stratification in the colder season 2 (S2), due to delayed sea ice melt, resulted in large numbers of *Phaeocystis* (3.1 µm, associated with high light and low salinity) and increasing contributions by micro-sized diatoms linked to increased (i.e. non-limiting) light availability and periodic mixing (but high stratification strength). Chapter 2 furthermore suggests that rising temperatures in this area will promote greater contributions by smaller-sized cells (<10 µm, diatoms, cryptophytes and prymnesiophytes). Under conditions of strengthened vertical stratification due to rising temperatures and ice melt (resulting in reduced nutrient flux from deep to surface waters), the post-bloom period may extend into later summer and the absence of nano-sized diatom blooms will have severe consequences for populations of larger-sized zooplankton such as copepods due to a trophic switch in diet (Chapter 7).

In **Chapters 3 and 4** the importance of viral lysis (compared to grazing) for various key Antarctic phytoplankton populations is examined over two productive seasons. Our results show that even in cold polar waters all phytoplankton populations and taxonomically important groups displayed substantial rates of viral lysis, responsible for roughly half of phytoplankton losses and essential to explain the coupling of growth and mortality. Viral lysis bridged-the-gap between phytoplankton production and grazing losses to close the seasonal mass balance in both seasons. In the light of global climate change, it is important to study temporal as well as inter-seasonal dynamics to understand how environmental variation influences these important loss processes and to provide 'baseline' estimates. The inter-annual comparison in Chapter 4 shows that the seasonal average viral lysis rates of phytoplankton were comparable for both years studied (0.22 and 0.29 d^{-1} for S2 and S1, respectively), despite reduced gross growth rates during the colder S2 (0.41 versus 0.61 d^{-1} in S1). In contrast, lower seasonal temperature resulted in significantly reduced grazing rates (0.21 d^{-1} in S2 versus 0.31 d^{-1} in S1). Furthermore, a greater share of viral lysis during bloom accumulation, when gross growth rates were largest, indicates a closer relationship between viruses and phytoplankton rates of gross growth than found for

grazing (higher during bloom decline). These results show a far greater proportion of phytoplankton biomass is diverted towards the microbial loop than previously considered, thereby reducing trophic level transfer efficiency and calling for a reconsideration of the biological carbon pump in this climate sensitive region.

The results of Chapter 2 showed that light was correlated with phytoplankton accumulation. The effects of different light intensities on phytoplankton net growth and community composition was investigated in more detail in **Chapter 5** using growth bioassays during S1 and S2. The results illustrate that low light was the primary factor limiting net growth and peak phytoplankton biomass. Furthermore, efficient acclimation to low light (4-7 µmol quanta m^{-2} s^{-1}) allowed nano-sized diatoms (Phyto IX) to dominate bloom climax and seasonal carbon flow (Chapter 2-5). Whilst the smaller diatom Phyto VI (4.5 µm) and large diatom Phyto X (20 µm) consistently exhibited highest growth at high and medium light (150-200 and 30-50 µmol quanta m^{-2} s^{-1}), *Phaeocystis* Phyto III also displayed relatively high growth under low light. The low light levels used in Chapter 5 were based on climatological estimates and therefore could represent an important boundary around which phytoplankton 'switch' between modes of high and low growth, directly influencing bloom phenology (size class) and magnitude. These results suggest that if smaller-sized diatoms (such as Phyto V and VI) are a feature of warm (nutrient replete) Antarctic summers, blooms of Phyto IX will become crucial for efficient carbon flow (Chapter 2-5) and the nutritional health of polar ecosystems.

Chapter 6 reports the first isolation of algal viruses from polar marine waters. These phycoviruses (MpoVs) infecting the picophytoplankter *Micromonas polaris* were characterised as Prasinoviruses, with double stranded genome sizes of around 200 Kb and containing a lipid membrane. The genus *Micromonas* has a bi-polar distribution and is ecologically important, especially in the Arctic Ocean. As a result of global warming-induced strengthening of vertical stratification and subsequent enhancement of nutrient limitation, *Micromonas* spp. are predicted to thrive even more during the Arctic summer. Temperature not only affected the virus latent period and burst size, it also strongly influenced the infectivity of the different MpoV virus

strains. However, results varied for the various different virus-host combinations. Seasonal dynamics in water temperature and global warming are thus likely to induce shifts in virus (and host) strain diversity. In combination with expected alterations in phytoplankton community composition (Chapter 2) as well as the relative importance of the different loss factors (Chapters 3 and 4), the implications of these results are crucial to the functioning of the polar marine pelagic ecosystem.

Chapter 7 reports the summer-winter-summer abundance and lipid profiles of Antarctic *Calanoides acutus* in relation to phytoplankton and larger zooplankton dynamics. The results show that the flexibility of copepods allows them to modulate their life-cycle strategy in response to bottom-up and top-down conditions, enabling individuals to optimize their probability of reproductive success in the very variable environment intrinsic to polar regions. The unsaturation value of the lipid store, combined with chlorophyll-*a* concentrations and numbers of large zooplankton, determined ontogenetic vertical migration behaviour. This study implies that the frequency and duration of high biomass phytoplankton blooms had consequences for the lifespan of *C. acutus* females (either 1 or 2 years) that we suggest is limited by a total of two main spawning 'events'. Late summer recruits, generated by a second inter-season spawning event, likely benefitted from lower predation pressure and high phytoplankton food availability. Combining the data from Chapters 2-4 and 7 suggests that high losses due to viral lysis during the accumulation phase of the late summer diatom bloom, may have stimulated sedimentation of organic matter that initiated early dormancy termination and a second spawning event. However, biomass-large lysis events of suitably sized phytoplankton cells could have restricted food availability, contributing to relatively low levels of (CV) total lipid prior to overwintering and the observed population decline after the warm Antarctic summer. Overall, the results of this multi-trophic level thesis provide new insights in polar phytoplankton dynamics by elucidating (i) viral lysis as a major and critical loss factor for all Antarctic phytoplankton taxonomic groups, including diatoms, (ii) ice type can influence the size class of ice-associated diatoms, (iii) the efficiency of acclimation to low light intensities influences bloom phenology and magnitude, (iv)

temperature is a regulator of phytoplankton and zooplankton growth rates as well as viral infectivity, production and virus-host strain composition, and (v) the combined effects influence copepod lipid content, behaviour, lifecycle and annual reproductive success. The findings of this thesis improve the comprehension of multifaceted effects of environmental variables, combined with the impact of various top-down factors, regulate changes in the phytoplankton community which feeds through to ecosystem productivity and the biological carbon pump. This thesis exemplifies the significance of an integrative approach for an improved understanding of the various key processes and underlying mechanisms related to polar phytoplankton community dynamics. Complementary approaches such as this are highly recommended to advance our understanding of the impact of global climate change in highly productive polar coastal waters, as well as the Southern and Arctic Ocean.

Summary

Samenvatting

Samenvatting

De pooloceanen spelen een cruciale rol in de wereldwijde klimaatregulering, zijn sleutelgebieden voor de wereldwijde afname van pCO_2 en zijn bijzonder gevoelig voor klimaatverandering. Oceaanklimaatmodellen voorspellen een verdere opwarming van de bovenste waterlaag in combinatie met een verhoogde toevoer van zoetwater op hoge breedtegraden, wat de structuur en het functioneren van de polaire fytoplankton (eencellige algen) gemeenschappen zal beïnvloeden. De belangrijkste processen die de dynamiek van de fytoplanktongemeenschap in polaire mariene wateren reguleren wordt momenteel onvoldoende bestudeerd. Het ontbreken van een 'basislijn' ter vergelijk, remt voorspellingen van mogelijke ecologische veranderingen en uiteindelijk de draagkracht van polaire mariene ecosystemen.

Vanwege extreme seizoensinvloeden op hoge breedtegraden, ervaart de polaire mariene fytoplankton sterke variaties in temperatuur, zee-ijsbedekking, lichtintensiteit en fotoperiode, maar het precieze effect van deze zogenaamde 'bottom-up' factoren op de groei van polaire fytoplankton, piekbiomassa en seizoensgebonden fytoplankton-dynamiek wordt nog niet volledig begrepen. Bovendien is de wereldwijde klimaatverandering gekoppeld aan grotere bijdragen van kleine fytoplankton en een vermindering van grotere diatomeeën (kiezelwieren) in de poolzeeën. Gedetailleerde seizoensgebonden gegevens van fytoplankton dynamiek in poolwateren zijn beperkt en daarom blijven de drijvende krachten achter verschuivingen in fytoplankton grotendeels onduidelijk.

Niet alleen de som, maar ook de grootteklasse, taxonomie en de timing van de fytoplanktonproductie kunnen de stroom van energie en materie beïnvloeden en daarmee het potentieel van pooloceanen om op lange termijn te dienen als een opslag voor atmosferische CO_2. Fytoplankton concentraties worden medebepaald door 'top-down' predatiefactoren, vanouds toegeschreven aan zoöplankton begrazing. Recentelijk is aangetoond dat sterfte door virusinfecties (virale lysis) ook een belangrijke oorzaak is van fytoplankton celsterfte. Hierdoor wordt organisch algen celmateriaal (gefixeerd door fotosynthese) omgeleid van hogere trofische niveaus naar de microbiële voedselketen. Ondanks dat begrazing door zoöplankton en sterfte

door virale lysis zeer verschillende effecten hebben op de trofische overdrachtsefficiëntie en de export van organische koolstof naar de diepzee (biologische pomp), virale lysis als een verliesfactor van Antarctisch fytoplankton is nog steeds ernstig onderbelicht. Er tot dusver geen seizoensstudies gepubliceerd, noch polaire algenvirus-host modelsystemen in cultuur gebracht voor meer gedetailleerde analyse onder gecontroleerde omstandigheden. Ook zijn er zeer weinig seizoensstudies naar de grotere lipidenrijke zoöplankton (zoals copepoden, ofwel roeipootkreeftjes) gepubliceerd, terwijl dit belangrijke predatoren zijn van de grotere diatomeeën en daardoor een belangrijke trofische schakel in de (huidige) polaire mariene ecosystemen.

Het belangrijkste onderzoeksdoel van dit proefschrift was om de seizoensgebonden dynamiek van polaire fytoplankton in relatie tot virussen en zoöplankton beter te begrijpen. Dit vertaalt zich in de volgende onderzoeksvragen:

(A) Welke omgevingsfactoren zijn verantwoordelijk voor het structureren van polaire fytoplanktongemeenschappen (Hoofdstuk 2) en daarbij, meer specifiek, hoe veranderen lichtintensiteiten en temperatuur de netto groei van fytoplankton en de interacties tussen polaire fytoplankton gastheer en virus (Hoofdstuk 5 en 6)?

(B) Hoe belangrijk is virale lysis van de verschillende fytoplanktongroepen is ten opzichte van begrazing, gedurende twee productieseizoenen (Hoofdstuk 3 en 4)?

(C) Hoe beïnvloedt de seizoensdynamiek van fytoplankton de accumulatie van lipiden en de winterrust van belangrijke copepoden?

Om de belangrijkste omgevingsvariabelen die de fytoplanktongemeenschap in de productieve kustwateren van het West-Antarctisch Schiereiland (WAP) vormgeven beter te kunnen bepalen, werden flowcytometrie, grootefractionering en chemische taxonomie gecombineerd in **Hoofdstuk 2** en de data geanalyseerd met behulp van multivariate analyse. Tijdens de lente bloeiperiode van primaire productie was ijstype de belangrijkste structurende factor; niet alleen verantwoordelijk voor het vrijkomen van diatomeeen van verschillende celgrootte uit smeltende licht drijfijs

en landvast ijs (respectievelijk nanometer en micrometer cel diameter), maar ook de beschikbaarheid van licht in de waterkolom onder het ijs. De taxonomische groep cryptofyten aan het eind van de lentebloei dijdens de relatief warme Antarctische zomer van het eerste seizoen (S1) kon worden toegeschreven aan de relatief hoge temperaturen,veel licht en mogelijk selectieve begrazing op grote diatomeeën door copepoden. Kleine diatomeeën (Phyto VI, gemiddelde celdiameter van 4,5 µm) domineerden de algengemeenschap later in het seizoen bij hoge temperatuur, veel licht en hoge nutriëntenconcentraties, totdat afname van licht en nutriënten (door hoge fytoplanktonbiomassa) leidde tot de opvolging van een specifieke groep van middelgrote diatomeeën (Phyto IX, 11,5 µm celdiameter). Een langdurige periode van stratificatie in het koudere tweede seizoen (S2) als gevolg van een vertraagd smelten van het zeeijs, resulteerde in grote aantallen *Phaeocystis* (Phyto III, 3,1 µm, gecorreleerd met hoge lichtintensiteit en lage saliniteit). Periodieke menging (zonder aanzienlijk verlies van stratificatiesterkte) in combinatie met voldoende licht, zorgde voor een toenemende bijdrage van grotere diatomeeën. Hoofdstuk 2 impliceert tevens dat stijgende temperaturen in dit gebied leidt tot grotere bijdragen van kleinere cellen (<10 µm, diatomeeën, cryptofyten en prymnesiofyten). Onder omstandigheden van versterkte verticale stratificatie, als gevolg van stijgende temperaturen en smeltend ijs (resulterend in een verminderde nutriëntenstroom van diep naar oppervlaktewater), kan de post-bloei periode zich uitstrekken tot later in de zomer en zal de afwezigheid van bloeien van de middelgrote diatomeeën ernstige gevolgen hebben voor populaties van grotere zoöplankton zoals copepoden als gevolg van een trofische verandering in het dieet (Hoofdstuk 7).

In **Hoofdstukken 3 en 4** is het belang van virale lysis (in vergelijking met begrazing) voor verschillende belangrijke Antarctische fytoplanktonpopulaties onderzocht gedurende twee productieseizoenen. Onze resultaten laten zien dat zelfs in koude poolwateren alle fytoplanktonpopulaties en taxonomisch belangrijke groepen aanzienlijke virale lysis ondergaan. Virale lysis bleek verantwoordelijk voor ongeveer de helft van de fytoplanktonverliezen en essentieel om de koppeling van groei en mortaliteit te verklaren. Virale lysis sluit de seizoensgebonden massabalans

in beide seizoenen en overbrugt zo de kloof tussen de productie van fytoplankton en de verliezen door begrazing. In het kader van de wereldwijde klimaatverandering is het belangrijk om zowel de seizoensdynamiek als de jaar-tot-jaarvariatie te bestuderen om zo beter te begrijpen hoe omgevingsvariatie deze belangrijke verliesprocessen beïnvloedt en om 'basislijn' schattingen te maken. Hoofdstuk 4 laat zien dat de seizoensgemiddelde van de specifieke virale lysis sterftesnelheden van fytoplankton vergelijkbaar was voor beide jaren S1 en S2 (respectievelijk 0,29 en 0,22 d^{-1}), ondanks lagere bruto groeisnelheden tijdens het koudere seizoen S2 (0,41 versus 0,61 d^{-1} in S1). Daarentegen resulteerde een lagere seizoenstemperatuur in significant lagere begrazing (0,21 d^{-1} in S2 versus 0,31 d^{-1} in S1). Bovendien duidt een groter aandeel van virale lysis tijdens de bloeiaccumulatie, wanneer de bruto groeisnelheden het grootst waren, op een nauwere relatie tussen virussen en bruto groei van fytoplankton dan bij begrazing (hoger tijdens bloeidaling). Deze resultaten tonen aan dat een veel groter deel van de fytoplanktonbiomassa wordt omgeleid naar het microbiële voedselweb dan eerder werd aangenomen, waardoor de overdrachtsefficiëntie van trofisch niveau wordt verminderd en een heroverweging van de biologische koolstofpomp in deze klimaatgevoelige regio nodig is.

De resultaten van Hoofdstuk 2 toonden aan dat licht gecorreleerd was met accumulatie van fytoplankton. De effecten van verschillende lichtintensiteiten op de netto groei van fytoplankton en de samenstelling van de gemeenschap werden in meer detail onderzocht in **Hoofdstuk 5** met behulp van bioassays tijdens S1 en S2. De resultaten illustreren dat lage lichtintensiteit de belangrijkste limiterende factor was voor netto groei en de maximale fytoplanktonbiomassa. Bovendien zorgde efficiënte acclimatisatie aan weinig licht (4-7 µmol quanta m^{-2} s^{-1}) ervoor dat middelgrote diatomeeën (Phyto IX) verantwoordelijk waren voor de bloei maxima en de seizoensgebonden koolstofstroom (Hoofdstuk 2-5). Terwijl de kleinere en grote diatomeeën Phyto VI (4,5 µm) en Phyto X (20 µm) consequent de hoogste groei vertoonden bij hoog en gemiddeld lichtintensiteit (150-200 en 30-50 µmol quanta m^{-2} s^{-1}), vertoonde *Phaeocystis* Phyto III ook een relatief hoge groei bij weinig licht. De lage lichtintensiteit die in Hoofdstuk 5 werd gebruikt, was gebaseerd

op klimatologische schattingen en zou daarom een belangrijke grens kunnen vormen waarrond fytoplankton 'schakelt' tussen modi van hoge en lage groei, wat weer een directe invloed heeft op de fenologie (grootteklasse) en omvang van de fytoplanktonbloei. Deze resultaten suggereren dat als kleinere diatomeeën (zoals Phyto V en VI) een kenmerk zijn van warme (niet nutrient gelimiteerde) Antarctische zomers, bloeien van Phyto IX cruciaal zal worden voor een efficiënte koolstofstroom (Hoofdstuk 2-5) en de nutritionele waarde van polaire ecosystemen.

Hoofdstuk 6 beschrijft de eerste isolatie van algenvirussen uit polaire mariene wateren. Deze algenvirussen (MpoV) die de picofytoplankton *Micromonas polaris*, werden gekarakteriseerd als Prasinovirussen, met dubbelstrengs genoomgroottes van ongeveer 200 kb en met een lipidemembraan. Het geslacht *Micromonas* heeft een bipolaire verspreiding en is ecologisch belangrijk, vooral in de Noordelijke IJszee. Door klimaatverandering zal de verticale stratificatie versterken waardoor nutrientlimitatie toeneemt en *Micromonas* spp. naar verwachting nog meer zal gedijen tijdens de poolzomer. Temperatuur beïnvloedde niet alleen de latente periode van het virus en het aantal virussen geproduceerd per gelyseerde gastheercel (burst-grootte), maar ook de infectiviteit van de verschillende MpoV virussen. De resultaten varieerden echter voor de verschillende virus-gastheercombinaties. Seizoensgebonden dynamiek in de watertemperatuur en de opwarming van de aarde zullen dus waarschijnlijk leiden tot verschuivingen in de diversiteit van virussen (en gastheer). In combinatie met verwachte veranderingen in de samenstelling van de fytoplanktongemeenschap (Hoofdstuk 2) en het relatieve belang van de verschillende verliesfactoren (Hoofdstukken 3 en 4), zijn de implicaties van deze resultaten cruciaal voor het functioneren van het polaire mariene pelagische ecosysteem.

Hoofdstuk 7 rapporteert de zomer-winter-zomer concentraties en lipidenprofielen van Antarctische *Calanoides acutus* in relatie tot fytoplankton en grotere zoöplankton populatie dynamiek. De resultaten laten zien dat de flexibiliteit van de copepods hen in staat stelt om hun levenscyclusstrategie te moduleren in reactie op bottom-up en top-down omstandigheden, waardoor individuen hun kans op

reproductief succes kunnen optimaliseren in de zeer variabele omgeving die inherent is aan poolgebieden. De onverzadigingswaarde van de lipidenopslag, gecombineerd met chlorofyl-a concentraties en aantallen van grote zoöplankton, bepaalde het ontogenetisch verticaal migratiegedrag. Deze studie impliceert dat de frequentie en duur van fytoplanktonbloei met hoge biomassa gevolgen had voor de levensduur van *C. acutus*-vrouwtjes (1 of 2 jaar) waarvan we suggereren dat deze beperkt is door in totaal twee hoofd paaigebeurtenissen. Rekruten in de late zomer, voortgebracht uit een tweede inter-seizoen paaigebeurtenis, profiteerden waarschijnlijk van een lagere predatiedruk en een hoge beschikbaarheid van fytoplanktonvoedsel. Uit de combinatie van gegevens uit de Hoofdstukken 2-4 en 7 volgt dat grote verliezen van diatomeeën als gevolg van virale lysis tijdens de accumulatiefase van de late zomerbloei waarschijnlijk de sedimentatie van organisch materiaal heeft gestimuleerd, waardoor een vroege stopzetting van de rustperiode en een tweede paaigebeurtenis kon ontstaan. Echter, grote verliezen door virale lysis beperkt het aanbod van (fytoplankton) prooi, wat kan bijdragen aan de relatief lage niveaus van (CV) totaal lipide voorafgaand aan overwintering en de waargenomen populatie-afname na de warme Antarctische zomer.

De resultaten van dit proefschrift bieden nieuwe inzichten in de dynamiek van polaire fytoplankton:(i) virale lysis is een uiterst belangrijke verliesfactor voor alle Antarctische fytoplanktontaxonomische groepen, inclusief diatomeeën, (ii) het ijstype beïnvloedt de grootteklasse van ijs-geassocieerde diatomeeën, (iii) de efficiëntie van acclimatisering aan lage lichtintensiteiten beïnvloedt bloeifenologie en omvang, (iv) temperatuur reguleert de groeisnelheden van fytoplankton en zoöplankton, evenals virale infectiviteit, productie en virus-gastheerstam samenstelling, en (v) de gecombineerde effecten beïnvloeden het lipidengehalte, het gedrag, de levenscyclus en het jaarlijkse reproductieve succes van copepoden. De bevindingen van dit proefschrift verbeteren het begrip van de veelzijdige effecten van omgevingsvariabelen die, gecombineerd met de impact van verschillende top-down factoren, veranderingen in de fytoplanktongemeenschap reguleren die doorwerken in de productiviteit van ecosystemen en de biologische koolstofpomp.

Samenvatting

Dit proefschrift illustreert het belang van een geïntegreerde aanpak om zo tot een beter inzicht te komen van de verschillende sleutelprocessen en onderliggende mechanismen die verband houden met de dynamiek van de polaire fytoplanktongemeenschap. Aanvullende benaderingen zoals deze worden sterk aanbevolen om ons begrip van de gevolgen van klimaatverandering in de zeer productieve polaire kustwateren, evenals in de Zuidelijke en Arctische Oceaan, te vergroten.

Author Contributions

Chapter 2: C.P.D.B. initiated the research and had the project oversight. T.E.G.B., C.P.D.B. and C.E. were responsible for research design. T.E.G.B. performed the research and laboratory analyses. P.D.R. ran the CHEMTAX analysis. T.E.G.B. and S.A-F. performed the multivariate analysis and K.D.A.M. contributed to statistical analysis. C.E., H.J.V. and D.W.P. provided their expertise and advise. T.E.G.B. and C.P.D.B. took the lead and all authors contributed to the writing of the paper.

Chapter 3: C.P.D.B. initiated the research and had the project oversight. T.E.G.B. and C.P.D.B. were responsible for research design and data analysis. T.E.G.B. performed the research and laboratory analysis and J.H. contributed to statistical analysis. T.E.G.B. and C.P.D.B. took the lead writing the paper and all authors contributed to results interpretation and the final writing of the paper.

Chapter 4: C.P.D.B. initiated the research and had the project oversight. T.E.G.B. and C.P.D.B. were responsible for research design and data analysis. T.E.G.B. performed the research, sample and statistical analysis. C.E. provided her expertise and advise. T.E.G.B. and C.P.D.B. took the lead writing the paper and all authors contributed to the final version of the paper.

Chapter 5: C.P.D.B. initiated the research and had the project oversight; T.E.G.B., C.E., and C.P.D.B. designed the study. T.E.G.B. performed the research, sample and statistical analysis. K.R.T. provided funding for some of the sample analysis and P.D.R. ran the CHEMTAX analysis. C.E., K.R.T., H.J.V. and D.W.P. provided their expertise and advise. T.E.G.B. and C.P.D.B. analysed the data and wrote the paper and all authors commented on the final version.

Chapter 6: C.P.D.B. initiated the research. C.E. and D.S.M. isolated the MpoVs and D.S.M. isolated the host *M. polaris* TX-01. D.S.M., T.E.G.B., C.E. and C.P.D.B. performed the virus characterizations and N.N.W. was responsible for TEM analysis. T.E.G.B. and D.S.M. designed and performed the experiments. D.S.M., T.E.G.B. and C.P.D.B. analyzed the data and wrote the paper, with D.S.M. and T.B. joint first authors. All authors contributed to the writing of the paper and commented on the final version.

Chapter 7: C.P.D.B has initiated the research, T.E.G.B., C.P.D.B. and D.W.P. have designed the study, and D.W.P. had the project oversight. T.E.G.B. performed the research, sample and statistical analysis, with C.P.D.B. providing scientific support, and C.E. and H.J.V. provided their expertise and advise. T.E.G.B. and D.W.P. analysed the data. T.E.G.B., C.P.D.B. and D.W.P. wrote the paper and all authors commented on the final version.

Acknowledgements

After a long long journey the time has finally arrived, even though on many occasions I thought I would never make it to the end. I have shared many emotions with friends and colleagues who have come and gone along the way. Even though I may never see some of you again, and may not mention some of you here, you will always be a part of my experience.

I am extremely grateful to my supervisor and promoter Corina Brussaard, who probably never imagined our journey would be like this. You have always provided support and encouragement when it was needed. Even though we did not always see eye to eye you have moulded me into the scientist and person I am today. You always pushed for the best of me and I appreciate my development more and more each day. Also my co-promoter David Pond who taught me a lot about copepods and lipids! Stefan Schouten, I appreciate your wisdom and support, it really helped to pull me to the finish line.

To the students who helped me in the lab, Wessel Jellema and Ryan Sewbaransingh, we shared some long days and late nights but you kept on going and taught me a lot about supervising. I am grateful to the technical staff at the NIOZ: Richard Doggen, Swier Oosterhuis, Anna Noordeloos, Kirsten Kooijman, Santiago Gonzalez, Harry Witte and Alma Lamers. Also my awesome office mate Didier De Bakker.

Spending two summers in the Antarctic was an unreal experience. I have many amazing memories both out on the boat and back in the container labs alongside Zoi Farenzena and Dorien Verheyen. I will never forget either of you and without your dedication to the fieldwork we would not have such an amazing dataset.

I am grateful to have shared this experience alongside others within the Dutch science programme, Jacqueline, Maria, Desiree, Nikki, Patrick (Laan) and Patrick (Rozema), Hein, Libby, Anita, Amber, Mairi, Pim, Ronald and Johann. Also the occasional penguin and elephant seal who would listen to my late night rants! Especially Johann, we shared a lot of experiences from boating through ice bergs

and avoiding whales, late nights in the lab and back in our 4 person room listening to the snores of the other people. Thanks for putting up with my snooze alarm!

There were many other scientists and staff that made the great atmosphere both in the Bonner and Gerritsz Lab (Rothera) as well as around the base. The success of the field campaigns would not have been possible without the fantastic support from the British Antarctic Survey, from the lab managers to the marine assistants, boatmen, base commanders, carpenters, electricians, mechanics and logistical support. And of course the excellent facilities and staff at the NIOZ. A huge thank you.

Completing a PhD is not just about work. I feel lucky to have met some awesome people and great friends with whom I shared many experiences. Yvonne Lipsewers, Andreas Waser, Jenni Welsh, Niamh McSweeney, Nikki Clargo, Santi Alvarez, Johann Bown, I hope we all stay in touch.

Maram Ghadban, my wife, has been there by my side through it all, a real roller coaster ride. We have moved from one country to the next together, got married and had two beautiful girls along the way. You have felt my stress and kept us all together, you are amazing, I love you.

To my parents, Linda and Richard. You have both been there with us, moving us from place to place without question, squeezing furniture into vans, around corners and into tiny places. You always provided me with encouragement to follow my dreams and making all this possible. My mum especially has always put up with my stress time and time again. You are such a strong and capable person and I am so proud you are my mother.

To my other parents, Czeslaw and Margaret, you always look on the positive side of life, encouraged me to follow my heart and do what makes me happy. Without this my life and even my family would be different. I love you all.

It's now time to enter another phase, thank you everyone and I hope to see many of you there!